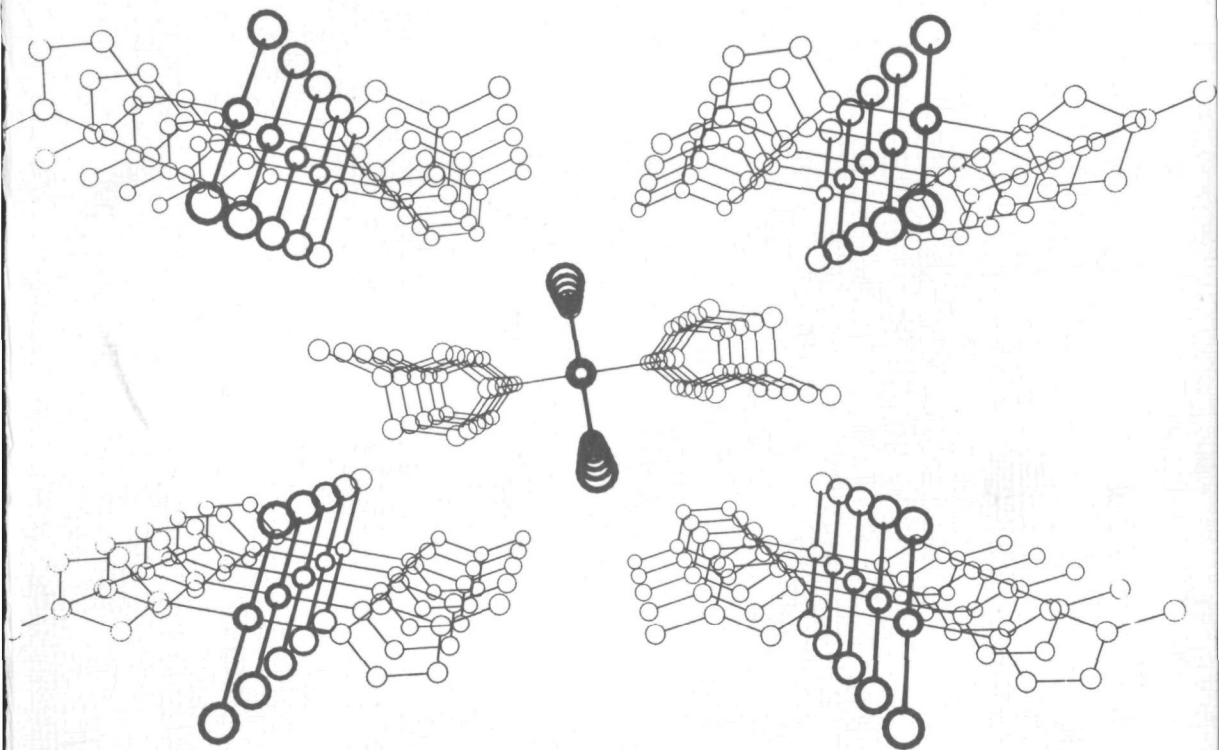


# RELATIONS BETWEEN MAGNETIC AND STRUCTURAL PARAMETERS IN POLYNUCLEAR TRANSITION METAL COORDINATION COMPOUNDS



1152 5095

J. A. C. VAN OOIJEN

RELATIONS BETWEEN MAGNETIC AND STRUCTURAL PARAMETERS IN  
POLYNUCLEAR TRANSITION METAL COORDINATION COMPOUNDS



BIBLIOTHEEK TU Delft  
P 1152 5095



C

274768



# RELATIONS BETWEEN MAGNETIC AND STRUCTURAL PARAMETERS IN POLYNUCLEAR TRANSITION METAL COORDINATION COMPOUNDS

## PROEFSCHRIFT

ter verkrijging van de graad van doctor in de technische  
wetenschappen aan de Technische Hogeschool Delft,  
op gezag van de rector magnificus Prof. Dr. Ir. F. J. Kievits,  
voor een commissie aangewezen door het college van dekanen  
te verdedigen op woensdag 18 april 1979 te 16.00 uur

door

**Johannes Adrianus Cornelis van Ooijen**

scheikundig doctorandus  
geboren te Leerdam

1152 5095



Dit proefschrift is goedgekeurd door de promotor:

Lector Dr. J. Reedijk

*For this world's wisdom  
is foolishness with God.*

*De wijsheid dezer wereld  
is dwaasheid bij God.*

*(I. Cor. 3:19)*

aan mijn ouders

aan Petra

Het in dit proefschrift beschreven onderzoek werd voor het grootste deel uitgevoerd in het gebouw voor Scheikundige Propadeuse en verder op het Laboratorium voor Anorganische en Fysische Chemie van de Technische Hogeschool Delft.

Aan allen, die op enigerlei wijze hebben bijgedragen aan de totstandkoming van dit proefschrift, betuig ik hierbij mijn dank.

Met name dank ik in het bijzonder de heren Drs. P.J. van der Put, Drs. G.A. Korteweg en Ir. C.G. van Kralingen, die mij steeds met raad en ook daad terzijde hebben gestaan.

Voor de uitvoering van de kristalstrukturbepalingen ben ik veel dank verschuldigd aan de heren J.C. Jansen, Dr. H. van Koningsveld, Dr. A.L. Spek (Rijks Universiteit Utrecht), E.J. Sonneveld en Drs. J.W. Visser (beiden Technisch Fysische Dienst, TNO/TH).

Ik dank de heren Dr. A.M. van der Kraan en Dr. P.C.M. Gubbens (beiden Interuniversitair Reactor Instituut) voor de uitvoering van en discussies over de Mössbauer-effect metingen en de heren Dr. A.J. van Duyneveldt, Drs. H.A. Groenendijk, Dr. L.J. de Jongh, Drs. J. Smit en Drs. D.W. Engelfriet (allen Rijks Universiteit Leiden) voor de uitvoering van magnetische metingen beneden 4.2K en de hulp bij de interpretatie daarvan.

Ik bedank de stichtingen "Younger Research Workers Interchange Scheme" en "Deutscher Akademische Austauschdienst" voor de reisbeurzen waardoor het mogelijk was enige laboratoria in Engeland en West Duitsland te bezoeken.

De reprografische Dienst van het Gebouw voor Scheikunde en de heren J. van Willigen en J.C. Ruis wil ik bedanken voor hun bijdragen aan de verwerking van de resultaten.

Ik dank de heer J.C. Jansen voor het ontwerpen van de figuur voor de omslag.

Voor de verzorging van de tekeningen en de foto's daarvan, ben ik veel dank verschuldigd aan de heer P. Dullaert.

# RELATIONS BETWEEN MAGNETIC AND STRUCTURAL PARAMETERS IN POLYNUCLEAR TRANSITION METAL COORDINATION COMPOUNDS

## CONTENTS

I.	GENERAL INTRODUCTION AND SURVEY	1
1.	Motivation	1
2.	Theory	1
3.	Survey	2
4.	References	4
II.	HALOGEN-BRIDGED COMPOUNDS	6
1.	Introduction	6
2.	Crystal and Molecular Structure of <i>catena</i> -di- $\mu$ -bromobis(N-methylimidazole)Copper(II)	9
3.	Crystal and Molecular Structure of <i>catena</i> -di- $\mu$ -bromobis(3,5-dimethylpyridine)Copper(II)	12
4.	Linear-chain Antiferromagnetism and Spectroscopy of Compounds $\text{CuX}_2\text{L}_2$ , with $\text{X}=\text{Cl}$ , Br and $\text{L}=(\text{substituted})\text{-pyridine}$	16
5.	Magnetic Exchange and Spectroscopy in some polynuclear Compounds of Cu(II) with azole Ligands	28
6.	Alternating Antiferromagnetism in the one-dimensional Compound <i>catena</i> -di- $\mu$ -bromobis(N-methylimidazole)Copper(II)	38
7.	Magnetic Superexchange in single-chlorine bridged Copper(II) Chains	41
8.	Linear-chain Ferromagnetism and Spectroscopy of the Compounds $\text{CoCl}_2(\text{pyrazole})_2$ and $\text{CoCl}_2(\text{indazole})_2$	46
9.	Compressed tetragonal Geometry in Cu(II)-doped dichlorobis(pyrazole)Cadmium(II)	51
10.	Magnetism and Mössbauer Spectroscopy of dichlorobis(pyrazole)Iron(II)	55
11.	General Discussion and Conclusions	58
12.	References	63
III.	OXALATO- AND SQUARATO-BRIDGED COMPOUNDS	66
1.	Introduction	66
2.	Crystal and Molecular Structure of <i>catena</i> - $\mu$ -oxalato- <i>cis</i> -bis(2-methylimidazole)Zinc(II). $\frac{1}{2}$ -water	68
3.	Magnetic Exchange and Spectroscopy in Compounds of Ni(II), Co(II) and Zn(II), with oxalato Anions as symmetric tetradentate bridging Ligands	73
4.	Magnetic Susceptibility Measurements and Mössbauer Spectroscopy on Fe(II) oxalato-bridged chain Compounds	86

5.	Crystal and Molecular Structure of diaquobis-(imidazole)- <i>catena</i> - $\mu$ -((1,3)-squarato)Nickel(II)	90
6.	Spectroscopy and Magnetism of diaquobis(imidazole)- <i>catena</i> - $\mu$ -((1,3)-squarato)Nickel(II)	96
7.	Conclusions	101
8.	References	103
IV.	HALOGEN-BRIDGED DIMERIC AND TETRAMERIC COMPOUNDS	105
1.	Introduction	105
2.	Crystal and Molecular Structure of di- $\mu$ -chlorodi-chlorobis(bis(3,5-dimethylpyrazolyl)methane)diNickel(II)	106
3.	Magnetic Superexchange Interactions in five-coordinated chlorine-bridged dimeric Ni(II) Compounds	111
4.	Magnetic Superexchange Interactions in dimeric and tetrameric fluorine-bridged Co(II) Compounds	115
5.	References	121
V.	EXPERIMENTAL PROCEDURES	122
1.	Spectroscopy and chemical Analysis	122
2.	Magnetic Susceptibility	123
3.	References	123
VI.	APPENDIX	124
1.	Magnetism and Structure of Copper(II) coordination Compounds. Crystal and Molecular Structure of <i>trans</i> -dichlorobis(N-methylimidazole)Copper(II)	124
2.	Acoustic Emission during the Preparation of dichloro(pyrazine)Zinc(II)	132
	SUMMARY	134
	SAMENVATTING	136
	FREQUENTLY USED ABBREVIATIONS, SYMBOLS AND UNITS	138
	<i>Curriculum Vitae</i>	

*The present investigations have been carried out under the auspices of the Netherlands Foundation for Chemical Research (SON) with financial aid from the Netherlands Organisation for the advancement of Pure Research (ZWO).*

## I. GENERAL INTRODUCTION AND SURVEY

### I.1. Motivation

For several years, experimentalists and theoreticians, both physicists and chemists, have been studying magnetic superexchange interactions that occur in an infinite ensemble of paramagnetic metal centers<sup>1,2</sup>. At present, unfortunately, it is not yet possible to predict in a quantitative way the magnitude and kind (antiferromagnetic or ferromagnetic) of interaction even in the simplest systems, like *e.g.* the dimeric  $S=\frac{1}{2}$  system.

The main goal of the research described in this thesis is to investigate the structural factors that govern the magnetic superexchange interactions.

Practically, coordination chemistry plays an important rôle by supplying model systems in which the paramagnetic metal ions and the dimensionality of the interactions can be varied. From spectroscopic and X-ray diffraction measurements the structure of the model compounds can be determined and if necessary the systems can be modified by taking slightly-different organic ligands (alkyl, halogen substituted ligands or isomers).

To study the magnetic superexchange interactions in model systems one has to know the structural details as precise as possible to interpret the magnetic susceptibility measurements. For an X-ray structure determination in most cases single crystals are needed. "Normal" coordination compounds generally can be prepared as single crystals, however, those compounds having chain structures very often cannot be prepared as single crystals.

### I.2. Theory

The theoretical interest in the magnetic superexchange mechanism has resulted in a number of models which can be used for the interpretation of thermodynamic data as a function of temperature<sup>1,2</sup>. The interactions between the electrons generally can be represented by the interaction Hamiltonian:

$$H = -2J \sum_{i,j} \{a(S_i^x \cdot S_j^x + S_i^y \cdot S_j^y) + b(S_i^z \cdot S_j^z)\}$$

where  $J$  is the superexchange parameter between nearest neighbours, the summation is over pairs of ions and  $S^x$ ,  $S^y$  and  $S^z$  are the components of spin



angular momentum operator. The  $a/b$  ratio is an anisotropy parameter. Each model is further characterized by the so-called spin dimensionality,  $\underline{D}$  (not the zero-field splitting parameter), and the lattice dimensionality,  $\underline{d}$ . The spin dimensionality is affected by the crystal field which can introduce an anisotropy in the coupling, whereas the lattice dimensionality is dependent on the direction of the coupling through the crystal. For the fully-isotropic case,  $a=b=1$ , one has the Heisenberg model<sup>3</sup> ( $D=3$ ;  $d=1,2,3$ ). There exist two anisotropic limits, *i.e.*  $a=0$ ,  $b=1$  representing the Ising model<sup>4</sup> ( $D=1$ ;  $d=1,2,3$ ) and  $a=1$ ,  $b=0$ , which represents the XY model<sup>5</sup> ( $D=2$ ,  $d=1,2,3$ ). Of course, all intermediate possibilities between these extreme models can occur in practice.

For only two cases, *i.e.*  $D=1$ ,  $d=1$ ,  $S=\frac{1}{2}$  and  $D=2$ ,  $d=1$ ,  $S=\frac{1}{2}$ , exact solutions of the general Hamiltonian are available. For all other cases approximate techniques are required to estimate the thermodynamical behaviour, *e.g.* the magnetic susceptibility as a function of temperature, of the infinite system.

### I.3. Survey

Here the synthesis, structure, spectroscopy and magnetism of compounds, which in most cases can be treated theoretically with the available theories on magnetic properties of exchange-coupled paramagnetic transition metal ions, are presented; furthermore, the relationships between the structural and magnetic parameters are investigated.

Chapter II deals with halogen-bridged chain compounds. Two X-ray crystal structures are reported; one of these structure determinations results from powder data only, which is not a usual procedure in coordination chemistry. The ligand-field, electron spin resonance, (far)-infrared spectroscopy and magnetism of these and related infinite chain compounds are described. The interpretation of the magnetic susceptibility data was carried out using different models, *i.e.* the Heisenberg, Ising and dimer model (Bleaney-Bowers<sup>6</sup>). Further, several -more or less experimentally obtained- susceptibility equations are used in the fitting procedures. One of the compounds, *i.e.* *catena-di-μ-bromobis(N-methylimidazole)Copper(II)*, could be described using an alternating chain model; both the magnetic susceptibilities and magnetization data are interpreted with the theoretical results of Bonner and Blöte<sup>7</sup>. In hydroxo-bridged  $\text{Cu(II)}$  dimers the bridging  $\text{Cu-O-Cu}$  angle was found to be the determining factor for the exchange ( $J$ -value)<sup>8</sup>. Contrary to this it is demonstrated here that in single-chlorine bridged copper chain compounds, the brid-

ging Cu-Cl-Cu angle is not the most important factor, that determines the J-value; in this latter system the long Cu-Cl distance influences the magnitude of the superexchange interaction.

Two ferromagnetic Co(II) chain compounds, which could be described within the Ising model, are presented; the interactions are influenced apparently by the rotational position of the organic ligand. Furthermore, it was noticed that by taking more bulky organic ligands, the one-dimensional character does not necessarily increase.

A Jahn-Teller<sup>9</sup> distorted system, showing a "reversed" Cu(II) ESR spectrum, which is seldomly found in coordination compounds, is described.

In the final part of this chapter the magnetism and Mössbauer-effect spectroscopy of the linear chain compound dichlorobis(pyrazole)Iron(II) are reported; the effects of three-dimensional ordering, originating from spin-spin interaction or spin-lattice relaxation, are found to occur.

In chapter III, two new types of chain compounds are presented, *i.e.* zig-zag oxalato- and linear squarato- bridged transition metal compounds. Both new types have been confirmed by single-crystal X-ray diffraction analyses. The infrared and Raman data have been interpreted using symmetry considerations and are consistent with the observed tetradentate coordinated planar oxalate groups. The magnetic susceptibility measurements of the Ni(II) compounds are interpreted with the results of recent calculations that include both exchange interaction and zero-field splitting. Furthermore, the one-dimensionality of the Fe(II) chain compounds has been investigated with Mössbauer-effect spectroscopy.

In chapter IV halogen-bridged dimeric and tetrameric compounds are described. The synthesis, X-ray structure determination and magnetism of the first ferromagnetic five-coordinated dimeric Ni(II) compound are presented. The ferromagnetic interaction observed, apparently, is due to the small differences in the geometry around the Ni(II) ions and is not influenced by comparable changes in the bridge geometries. The magnetic susceptibility data and magnetization measurements of a new class of fluorine-bridged dimeric and tetrameric Co compounds are presented. Because of strong crystal-field effects no quantitative interpretation of the data was possible.

In chapter V, the general experimental procedures and instrumentation used are summarized, whereas the synthetical procedures and X-ray diffraction data are given in the appropriate parts.

In appendix VI.1, the single-crystal X-ray structure determination of a Cu(II) compound, which was thought to belong to the compounds described in

chapter II, is reported. The structure is built up of monomeric molecules instead of chains; it is noticed that structure proposals based on ESR data can only be tentative, which is illustrated with several examples.

Finally, in appendix VI.2, a so far unknown phenomenon is presented, *i.e.* the acoustic emission during the preparation of dichloro(pyrazine)Zinc(II). A definite explanation cannot yet be given.

The major part of this thesis has been published, submitted or is in press<sup>10-26</sup>.

#### I.4. References

- (1) L.J. de Jongh and A.R. Miedema, *Adv. Phys.*, **23**, 1 (1974).
- (2) R.L. Carlin and A.J. van Duyneveldt, "Magnetic Properties of Transition Metal Compounds", Springer Verlag, New York (1977).
- (3) J.C. Bonner and M.E. Fisher, *Phys. Rev.*, **A135**, 640 (1964).
- (4) M.E. Fisher, *J. Math. Phys.*, **4**, 124 (1963).
- (5) S. Katsura, *Phys. Rev.*, **127**, 1508 (1962).
- (6) B. Bleaney and K.D. Bowers, *Proc. Roy. Soc.*, **A214**, 451 (1952).
- (7) J.C. Bonner and H.J. Blöte, private communication.
- (8) V.H. Crawford, H.W. Richardson, J.R. Wasson, D.J. Hodgson and W.E. Hatfield, *Inorg. Chem.*, **15**, 2107 (1976).
- (9) A. Abragam and B. Bleaney, "EPR of Transition Metal Ions", Oxford University Press, London (1970).
- (10) J.C. Jansen, H. van Koningsveld and J.A.C. van Ooijen, *Cryst. Struct. Comm.*, **7**, 637 (1978).  
"Crystal and Molecular Structure of *catena*-di- $\mu$ -bromobis(N-methylimidazole)Copper(II)"
- (11) J.A.C. van Ooijen, J. Reedijk, E.J. Sonneveld and J.W. Visser, *Transition Met. Chem.*, in press.  
"One-dimensional Magnetism and Crystal Structure of *catena*-di- $\mu$ -bromobis(3,5-dimethylpyridine)Copper(II)"
- (12) J.A.C. van Ooijen and J. Reedijk, *Inorg. Chim. Acta*, **25**, 131 (1977).  
"Linear-Chain Antiferromagnetism and Spectroscopy of Compounds  $\text{CuX}_2\text{L}_2$ , with  $\text{X}=\text{Cl}$ ,  $\text{Br}$  and  $\text{L}=(\text{substituted})\text{-pyridine}$ "
- (13) J.A.C. van Ooijen and J. Reedijk, *J. Chem. Soc. Dalton*, 1170 (1978).  
"Magnetic Exchange in some Polynuclear Bis(azole)dihalogenocopper(II) Complexes"
- (14) J.C. Bonner, L.J. de Jongh, J.A.C. van Ooijen, J. Reedijk and J. Smit, *Physica*, submitted.  
"Antiferromagnetic  $S=\frac{1}{2}$  alternating chain Model applied to *catena*-di- $\mu$ -bromobis(N-methylimidazole)Copper(II)"
- (15) J.A.C. van Ooijen and J. Reedijk, *Solid State Comm.*, submitted.  
"Magnetic Superexchange and Structure in single-chlorine bridged  $\text{Cu(II)}$  chain Compounds"

- (16) J.A.C. van Ooijen and J. Reedijk,  
*J. of Magn. & Magn. Mat.*, in press.  
"Linear-chain Ferromagnetism in the one-dimensional Compounds  $\text{CoCl}_2\text{L}_2$ ,  
with L=pyrazole, indazole"
- (17) J.A.C. van Ooijen, P.J. van der Put and J. Reedijk,  
*Chem. Phys. Letters*, 51, 380 (1977).  
"Compressed tetragonal Geometry in Cu(II)-doped dichlorobis(pyrazole)-  
Cadmium(II)"
- (18) P.C.M. Gubbens, A.M. van der Kraan, J.A.C. van Ooijen and J. Reedijk,  
*Solid State Comm.*, submitted.  
"Magnetism and Mössbauer-effect Spectroscopy of the one-dimensional  
Compound dichlorobis(pyrazole)Iron(II)"
- (19) J.C. Jansen, H. van Koningsveld and J.A.C. van Ooijen,  
*Cryst. Struct. Comm.*, in press.  
"Crystal and Molecular Structure of *catena*- $\mu$ -oxalatobis(2-methyl-  
imidazole)Zinc(II). $\frac{1}{2}$ -water"
- (20) C.G. van Kralingen, J.A.C. van Ooijen and J. Reedijk,  
*Transition Met. Chem.*, 3, 90 (1978).  
"Polymeric Coordination Compounds of Nickel(II), Cobalt(II) and Zinc(II)  
with Oxalato Ions as symmetric tetradentate bridging Ligands"
- (21) P.C.M. Gubbens, A.M. van der Kraan, J.A.C. van Ooijen and J. Reedijk,  
*J. de Phys.*, in press.  
"Mössbauer-effect Study of oxalato-bridged Fe(II) chain Compounds"
- (22) J.A.C. van Ooijen, J. Reedijk and A.L. Spek,  
*Inorg. Chem.*, in press.  
"Crystal and Molecular Structure, Spectroscopy and Magnetism of diaquo-  
bis(imidazole)*catena*- $\mu$ -((1,3-)squarato)Nickel(II). A one-dimensional  
Polymer"
- (23) J.C. Jansen, H. van Koningsveld, J.A.C. van Ooijen and J. Reedijk,  
*Inorg. Chem.*, submitted.  
"Structure and Magnetic Exchange in di- $\mu$ -chloro bridged Ni(II) Dimers.  
Crystal and Molecular Structure of di- $\mu$ -chlorodichlorobis(bis(3,5-di-  
methylpyrazolyl)methane)-diNickel(II)"
- (24) L.J. de Jongh, J.A.C. van Ooijen, J. Reedijk and J. Smit,  
*Physica*, submitted.  
"Susceptibility and Magnetization of dimeric and tetrameric fluorine-  
bridged Co(II) Compounds"
- (25) J.A.C. van Ooijen, J. Reedijk and A.L. Spek,  
*J. Chem. Soc. Dalton*, in press.  
"Magnetism and Structure of Copper(II) coordination Compounds.  
Crystal and Molecular Structure of *trans*-dichlorobis(N-methyl-  
imidazole)Copper(II)"
- (26) J.A.C. van Ooijen, E. van Tooren and J. Reedijk,  
*J. Am. Chem. Soc.*, 100, 5569 (1978).  
"Acoustic Emission during the Preparation of dichloro(pyrazine)Zinc(II)"

## II. HALOGEN-BRIDGED COMPOUNDS

### II.1. Introduction

In coordination chemistry several systems having halogen bridging ligands between metal ions are known. Among them, chain-type compounds have been observed frequently, especially in combination with first-row transition metal ions.

Copper(II) ions arranged in linear chains can be regarded as good examples of one-dimensional  $S=\frac{1}{2}$  systems and because these systems have been examined theoretically, for the present study such a chain system was chosen. For comparison also some corresponding Co(II) and Fe(II) compounds were studied. Two types of chains were studied, *i.e.* the double-halogen bridged and the single-halogen bridged compounds. Double-halogen bridged compounds have been the subject of several spectroscopic, magnetic and crystallographic studies<sup>1-9</sup>. For the single-halogen bridged compounds much less examples are known<sup>18-21</sup> and only very few magnetic data have been reported<sup>6,6</sup>.

Single-crystal structure determinations of some of the compounds<sup>1-5</sup> have shown that by varying the ligands the double-halogen bridged chain structure remains, whereas only small changes in bridge geometry (angles and distances) occur, which influence the magnetic superexchange interactions within the chains; how they influence these interactions is hardly understood.

To investigate the influence of small changes in the ligand molecule (*e.g.* different substituents and different hydrogen-bonding properties) on the exchange constant,  $J$ , detailed far-IR, ESR and magnetic susceptibility measurements have been carried out.

Single-crystal analyses of  $\text{CuCl}_2(\text{pyridine})_2$  (CPC)<sup>1</sup>,  $\text{CuBr}_2(\text{pyridine})_2$  (CPB)<sup>2</sup>,  $\text{CuCl}_2(4\text{-ethylpyridine})_2$ <sup>3</sup>,  $\text{CuCl}_2(4\text{-vinylpyridine})_2$ <sup>4</sup> and  $\text{CuCl}_2(\text{thiazole})_2$ <sup>5</sup>, have shown that the metal ions are surrounded by a distorted elongated octahedron of four halogen ions and two ligands. The octahedra share edges of halogen ions to form linear chains of copper ions, separated by the unidentate non-bridging ligands. Although the structure of CPB is not completely isomorphous with the CPC structure, the coordination around copper is similar<sup>6</sup>. Hatfield, Hodgson and coworkers<sup>5,7-9</sup> investigated the above-mentioned compounds and calculated the  $J$ -values. Here this class of

compounds is studied in greater detail in order to:

- a) have a larger number of comparisons,
- b) find out how the structural parameters (*e.g.* bridge angles and distances) influence the J-value, and
- c) compare and hopefully improve existing theories in describing linear-chain systems of the  $S=\frac{1}{2}$  type.

Two X-ray structure determinations on the compounds  $\text{CuBr}_2(\text{N-methylimidazole})_2$  (II.2) and  $\text{CuBr}_2(3,5\text{-dimethylpyridine})_2$  (II.3) are presented, whereas the physical measurements of these and related compounds are described in II.4 and II.5. In these latter chapters also the calculation of the J-values is described. For the interpretation of powder magnetic susceptibility data, only the Heisenberg<sup>10</sup> (isotropic coupling) and Ising<sup>11</sup> (anisotropic coupling) models can be used, because for the XY model<sup>12</sup> (anisotropic coupling) only the perpendicular susceptibility is known. Within the Ising model the theoretical parallel and perpendicular susceptibilities have been published by Katsura<sup>11</sup>, but within the Heisenberg model no exact expressions are known and only numerical approximations are available<sup>10</sup>. Recently, Jotham<sup>13</sup> discussed the problems concerning the description of magnetic data of Cu(II) chains and proposed an empirical susceptibility formula; he also gave a closed-form expression for the Heisenberg model in the form of a polynomial. In chapter II.5, in particular, attempts were made to fit the susceptibility data to these latter models, together with the Bleaney-Bowers equation<sup>14</sup> for dimeric Cu(II) compounds. The obtained J-values are discussed together with the available structure parameters with regard to the theories on superexchange interactions proposed by Anderson *et al*<sup>15</sup>.

In chapter II.6 the susceptibility and magnetization data on *catena*-di- $\mu$ -bromobis(N-methylimidazole)Copper(II) (CNIMB) are described within the alternating chain model presented some time ago by Duffy and Barr<sup>16</sup>. Bonner and Blöte<sup>17</sup> also calculated the magnetization and susceptibility curves down to much lower temperatures; the present data are interpreted with these results.

Chapter II.7 describes the magnetic study on the structurally-established single-chlorine bridged compounds dichlorobis(dimethylsulphoxide)Copper(II)<sup>18</sup>, dichlorobis(imidazole)Copper(II)<sup>19</sup>, aquacaffeinedichloroCopper(II)<sup>20</sup>, and dichloro(2-(2-methylaminoethyl)pyridine)Copper(II)<sup>21</sup>. The main goal of this study is to find out relationships between the value of the superexchange integral and the bridge geometry of the superexchange

path; the bridge angle in these compounds varies between  $114^\circ$  and  $145^\circ$ .

In almost all copper chain compounds the superexchange interactions are antiferromagnetic in nature. In order to find out what happens in case of ferromagnetic compounds on changing the ligands, several cobalt linear chain compounds, which frequently show ferromagnetic interactions, have been studied. In chapter II.8, the susceptibility and ESR data on the compounds  $\text{CoCl}_2(\text{pyrazole})_2$  and  $\text{CoCl}_2(\text{indazole})_2$  are interpreted using the Ising model, allowing comparison with the structural and magnetic data of the known pyridine analogue<sup>22-24</sup>. The factors determining the exchange constant are discussed, by considering in detail the superexchange paths, connecting the metal ions.

In chapter II.9, ESR and ligand-field data on a doped chain compound, *i.e.*  $\text{Cu}_{0.02}\text{Cd}_{0.98}\text{Cl}_2(\text{pyrazole})_2$  are presented. Dealing with octahedra, the Jahn-Teller effect in most cases introduces an elongation along the tetragonal axis. Thus far, a tetragonal compression in coordination compounds has been demonstrated only in one compound, *i.e.*  $\text{Cu(II)}$  doped in  $(\text{NH}_4)_2(\text{Zn}(\text{NH}_3)_2(\text{CrO}_4)_2)^{25}$ , although the spectrum at liquid-nitrogen temperature appears to be quite rhombic. The  $\text{Cu(II)}$  ions in this compound have compressed tetragonal geometry, which could be deduced from the ESR spectroscopic  $g_{//}$ -value of ca. 2.00 and from the fact that  $g_{\perp} > g_{//}$ <sup>26</sup>. During the present study on antiferromagnetic copper chains,  $\text{Cu(II)}$  dopes in the corresponding  $\text{Cd(II)}$  chain compounds were also investigated. For the above-mentioned doped compound the ESR spectrum reveals that in this system the geometry around copper is tetragonally compressed.

Finally, in chapter II.10, the magnetic susceptibilities of the linear chain compound  $\text{FeCl}_2(\text{pyrazole})_2$  are described. The Mössbauer spectra at different temperatures show the occurrence of three-dimensional ordering effects. This chapter ends with some general conclusions, about the possible relations between structure of and superexchange interaction within the chain.

## II.2. Crystal and Molecular Structure of *catena*-di- $\mu$ -bromobis(N-methylimidazole)Copper(II).

### II.2.1. Experimental

Single crystals of  $\text{CuBr}_2(\text{N-methylimidazole})_2$ , abbreviated CNIMB, were prepared by mixing alcoholic solutions of the hydrated copper(II) bromide and N-methylimidazole in a ratio slightly less than 1:2. For dehydration an excess of triethylorthoformate was added to the solution. The slowly-formed crystals were filtered off, washed several times with ethanol and diethylether, and finally dried *in vacuo* at room temperature.

### II.2.2. Crystal and intensity data, structure determination and refinement

From single-crystal diffractometry ( $\text{MoK}\alpha_1 = 0.70926 \text{ \AA}$ ) the following data were obtained:  $a = 4.130(1)$ ,  $b = 13.899(4)$ ,  $c = 10.529(3) \text{ \AA}$ ,  $\beta = 99.00(4)^\circ$ , space group  $\text{P2}_1/\text{c}$ ,  $D_m = 1.1 \text{ g/cm}^3$ ,  $D_c = 1.08 \text{ g/cm}^3$ , and  $Z = 2$ .

Intensities of 1173 independent reflections above background ( $I > 2.85\sigma(I)$ ) were collected from a crystal with dimensions *ca.*  $0.2 \times 0.1 \times 0.2 \text{ mm}$  using a computer-controlled NONIUS single-crystal diffractometer with a graphite monochromator and Mo-radiation.

The crystal structure was solved by the heavy-atom method and refined by full-matrix least-squares calculations, using programs of the XRAY system<sup>27</sup>. The form factors for Cu, Br, C and N were taken from Cromer and Mann<sup>28</sup> and

TABLE II.2.1. FINAL PARAMETERS WITH E.S.D.'s IN PARENTHESES. THE FRACTIONAL ATOMIC COORDINATES ( $\times 10^5$  FOR Br,  $\times 10^4$  FOR THE OTHER NON-HYDROGEN ATOMS AND  $\times 10^3$  FOR THE HYDROGEN ATOMS) WITH THE ANISOTROPIC THERMAL PARAMETERS ( $\text{\AA}^2 \times 10^4$  FOR THE NON-HYDROGEN ATOMS) AND ISOTROPIC THERMAL PARAMETERS ( $\text{\AA}^2 \times 10^3$  FOR THE HYDROGEN ATOMS). THE  $U_{ij}$  COEFFICIENTS ARE GIVEN BY THE EXPRESSION:

$$\text{EXP}(-2\pi^2(U_{11}h^2a^{*2} + U_{22}k^2b^{*2} + U_{33}l^2c^{*2} + U_{12}h.k.a^*b^* + U_{13}h.l.a^*c^* + U_{23}k.l.b^*c^*))$$

ATOM	x/a	y/b	z/c	$U_{11}/U$	$U_{22}$	$U_{33}$	$U_{12}$	$U_{13}$	$U_{23}$
Cu	0 <sup>x</sup>	0 <sup>x</sup>	0 <sup>x</sup>	694(10)	122(5)	527(9)	-27(5)	-344(8)	31(5)
Br	43994(17)	2436(5)	18830(7)	388(3)	290(9)	304(3)	-23(3)	-9(2)	6(3)
N1	-158(16)	1385(4)	-317(6)	548(39)	191(24)	396(33)	-6(25)	-156(28)	4(24)
N2	-1095(15)	2922(4)	-91(5)	479(34)	224(25)	281(28)	5(24)	30(25)	28(20)
C1	-1398(21)	2037(5)	369(8)	526(48)	296(34)	424(43)	-94(32)	30(35)	58(29)
C2	-2256(29)	3811(6)	408(12)	784(81)	285(41)	703(68)	84(43)	116(57)	-51(40)
C3	445(20)	2825(5)	-1148(8)	523(45)	311(34)	413(42)	-8(32)	28(34)	99(29)
C4	1028(22)	1880(6)	-1274(8)	598(52)	350(38)	462(47)	81(36)	59(39)	-27(34)
H1	-280(21)	189(6)	84(6)	46 <sup>x</sup>					
H3	78(20)	343(6)	-170(8)	52 <sup>x</sup>					
H4	146(21)	154(6)	-190(9)	54 <sup>x</sup>					

<sup>x</sup>PARAMETER WAS HELD FIXED



Final positional and thermal parameters are listed in table II.2.1.

Bond lengths and bond angles of CNIMB are shown in figure II.2.1. The geometry around copper is best described as square planar, with two bromide ions and two nitrogen atoms of N-methylimidazole, forming the basal plane. The axial sites are occupied by two more distant bromide ions belonging to two neighbouring molecules, completing a distorted octahedron. The bromide ions are thus shared by adjacent copper ions which parallel the  $a$ -axis as shown in figure II.2.2. All angles around copper and within the bridge are very close to  $90.0^{\circ}$ , as found in  $\text{CuBr}_2(\text{pyridine})_2$ , abbreviated CPB<sup>6</sup>. The only differences in the bridge geometry between CPB and CNIMB are the Cu-Br bond lengths, *i.e.* 2.451(1), 3.240(1) and 2.494(1), 3.291(1) Å, resp.

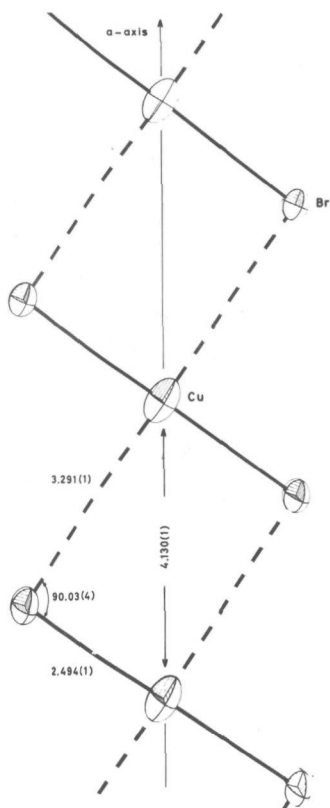


Fig. II.2.2. Geometry of the copper bromine chains, which parallel the  $a$ -axis. The nitrogen atoms are below and above the bridge plane.

The methyl protons could not be uniquely located in a Fourier-difference map, and were, therefore, left out of the refinement.

The packing of the chains in the crystal is shown in figure II.2.3. The front page shows a view of the chains along the  $a$ -axis.

The chains are held together by van der Waals contacts of the ligands.

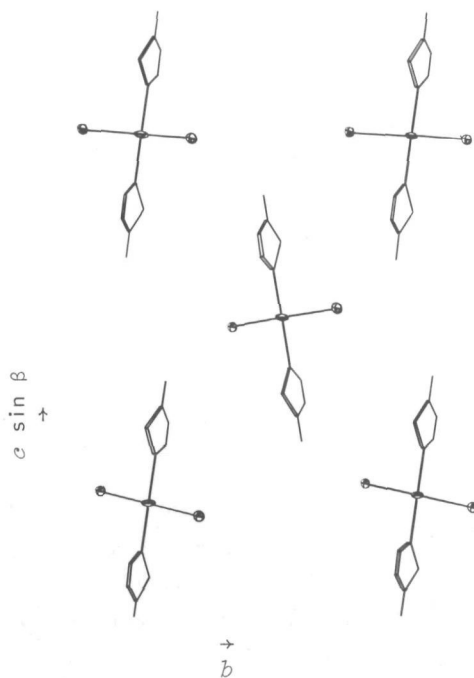


Fig. II.2.3. Packing of the chains in the crystal projected along the chain direction ( $a$ -axis).

### II.3. Crystal and Molecular Structure of *catena*-di- $\mu$ -bromobis(3,5-dimethylpyridine)Copper(II).

#### II.3.1. Experimental

The compound  $\text{CuBr}_2(3,5\text{-dimethylpyridine})_2$ , abbreviated CLB, was prepared by mixing alcoholic solutions of the hydrated copper(II) bromide and 3,5-dimethylpyridine in a ratio slightly less than 1:2, in order to prevent the formation of the tetra-adduct  $\text{CuL}_4\text{Br}_2$ . For dehydration an excess of triethylorthoformate was added to the solution. The immediately-obtained precipitate was filtered off, washed several times with ethanol and diethylether, and finally dried *in vacuo* at room temperature.

#### II.3.2. X-ray data collection and structure determination

Guinier-Johansson powder photographs were made at room temperature using  $\text{Cu-K}\alpha_1$  radiation. Special care was given at the specimen preparation: to avoid preferred orientation of the needle-like particles, the powder was sprinkled onto the specimen plane. To account for film shrinkage and displacement of the specimen or the film, the pattern was calibrated with silicon as an internal standard. With a microdensitometer the optical density of the powder photograph was measured in steps of  $0.01^\circ$  of  $2\theta$ . From this set of density data, the intensities of the individual powder lines were determined with the use of the computer program PEAK<sup>31</sup>. The intensity data were corrected for absorption and oblique incidence. The complete powder pattern was sent to the JCPDS- International Center for Diffraction Data<sup>32</sup>.

With an indexing computer program<sup>33</sup> the unit cell of CLB was determined from the powder pattern. The values of the unit-cell parameters after refinement on the  $2\theta$ -values of the 148 observed powder lines are:  $a = 13.900(2)$ ,  $b = 14.416(2)$ ,  $c = 4.097(1)$  Å,  $\beta = 93.49(2)^\circ$ , space group  $P2_1/a$ , and  $Z = 2$ . The space group  $P2_1/a$  was derived from the systematic extinctions in the pattern. The number of formula units CLB per unit cell, was derived from a comparison of the volume of the unit cell with that of a formula unit. An approximation of the crystal structure, which proved to be accurate enough for refinement of the structural parameters has been derived. The following considerations may illustrate this derivation.

- 1) Since  $Z = 2$ , the space group  $P2_1/a$  requires the Cu ions to be at centers of symmetry.
- 2) From similar compounds<sup>6,34</sup> it is known that they crystallize in a chain

structure, consisting of formula units  $\text{CuBr}_2\text{L}_2$ . Since CLB exhibits a fibrous character, and moreover one of the cell parameters,  $c$ , is in good agreement with the repetition distance in the chain (which is  $ca. 4 \text{ \AA}$ ), it is assumed that the structure consists of these chains along  $c$ .

- 3) Since  $a$  and  $b$  are almost equal, one should expect the N-atom of the ligand as well as the bromide ion to be not far from the bisector plane between the  $ac$  and  $bc$  planes.
- 4) The plane of the ligand is assumed to be approximately in the  $ab$  plane, as is almost true for  $\text{CuBr}_2(\text{pyridine})_2$ , abbreviated CPB<sup>6</sup>.
- 5) The  $z$ -coordinate of the bromide ion is assumed to be approximately equal to the value observed in CPB<sup>6</sup>.

In the subsequent refinement of the structure, the 3,5-dimethylpyridine group was considered as a fixed group, in order to reduce the number of positional parameters. The geometry of this group was derived from the structure determination of similar compounds. The pyridine ring was considered as a regular hexagon, with an atom to atom distance of  $1.37 \text{ \AA}$ , which is the mean of the values observed in CPB and  $\text{CuCl}_2(\text{pyridine})_2$ , abbreviated CPC<sup>6</sup>. For the distance C-C(methyl) the value of  $1.51 \text{ \AA}$  was used, which is the mean of the values found in  $\text{CuBr}_2(2,3\text{-dimethylpyridine})_2$ <sup>35</sup>. The angles around the ring carbons have been set at  $120^\circ$ . The position and orientation of the ligand can be described with 6 parameters. In addition there are 3 positional parameters for the bromide ion, whereas the copper ion must be fixed in the origin. With one overall isotropic temperature factor and a scale factor the total number of parameters amounts to 11. The number of powder intensities used in the refinement was 95, some of them representing two or more not completely resolved but distinctly visible powder lines. The majority of the powder intensities ( $ca. 50$ ) consists of two or more reflections. The total number of reflections involved is 197.

The atomic form factors used for  $\text{Cu}^{2+}$ ,  $\text{Br}^-$ , N, C and H were those given in reference (<sup>36</sup>). The function minimized was

$$r = \frac{\sum_i w_i (I_o - I_c)_i^2}{\sum_i w_i I_o^2} \quad \text{where } w = 1/(1 + I_o/c)^2, \quad c = I_{\text{max}}/60$$

The final  $r$ -value is 0.03. The final value of the conventional  $R$ -index, calculated for 45 singly-indexed powder intensities is 0.132. The overall isotropic temperature factor amounts to  $5.5 \text{ \AA}^2$ . The structure refinement was carried out with a simplex refinement procedure<sup>37</sup>, which permits the introduction of one intensity value for several reflections together. However, since this program does not calculate standard deviations for the refined parameters, the program

TABLE II.3.1. FINAL POSITIONAL PARAMETERS OF THE NON-HYDROGEN ATOMS

ATOM	x/a	y/b	z/c
Cu	0.0	0.0	0.0
Br	-0.1016(3)	0.0949(4)	-0.378(1)
N <sup>x</sup>	0.1017(7)	0.1000(7)	0.027(3)
C1	0.1924 <sup>x</sup>	0.0829	-0.0725
C2	0.2607	0.1515	-0.0535
C21	0.3606	0.1327	-0.1628
C3	0.2383	0.2373	0.0647
C4	0.1476	0.2544	0.1639
C41	0.1229	0.3489	0.2941
C5	0.0793	0.1858	0.1450

<sup>x</sup>THE LIGAND WAS CONSIDERED AS A FIXED GROUP. THE STANDARD DEVIATIONS IN THE COORDINATES OF THE CENTER OF THE LIGAND ARE 0.0001, 0.0001 AND 0.001 FOR x, y AND z RESPECTIVELY. THE STANDARD DEVIATIONS IN THE EULERIAN ANGLES, WHICH DESCRIBE THE ORIENTATION ARE ALL 1.0°. AS DESCRIBED ABOVE, THE GEOMETRY OF THE LIGAND IS SLIGHTLY DIFFERENT FROM THE GEOMETRY AS REPORTED IN THE LITERATURE (SEE TEXT). THESE DIFFERENCES CONTRIBUTE THE LARGEST PART OF THE STANDARD DEVIATION IN THE Cu-N DISTANCE. THE GIVEN STANDARD DEVIATIONS IN THE COORDINATES OF THE N-ATOM ARE THOSE DERIVED FROM THESE DIFFERENCES.

CRYLSQ of the XRAY system<sup>27</sup>

was used for a few cycles of least-squares refinement using all singly-indexed powder intensities and all the doublets divided according to the calculated ratio, together 95 reflection intensities. The values of the positional parameters and their standard deviations are listed in table II.3.1.

### II.3.3. Results and discussion

The molecular structure around the copper(II) ion may be described as square planar with two bromide ions and two nitrogen atoms of the 3,5-dimethylpyridine ligand, forming the basal plane. The axial sites are occupied by two more distant bromide ions belonging to two neighbouring molecules, completing a distorted elongated octahedron. The structure is, as expected (see above), quite similar to that of CPB<sup>6</sup>, but the compounds are not isomorphous.

The details of the structure and the intra-molecular non-hydrogen bond lengths and angles are shown in figure II.3.1. From this figure it is observed that all angles around copper are close to 90.0° as found in CPB<sup>6</sup> and CNIMB<sup>34</sup>. The Cu-N distance (2.02(2) Å) and Cu-Br distance (2.449(7) Å) are both within experimental error similar to those observed in CPB (2.013(5) and 2.451(1) Å respectively)<sup>6</sup>.

The bromide ions are shared with adjacent copper(II) ions resulting in chains which parallel the *c*-axis, as is shown schematically in figure II.3.2. The long Cu-Br distance (3.286(7) Å) is slightly larger than in CPB (3.240(1) Å) and within experimental error equal to that in CNIMB (3.291(1) Å).

Fig. II.3.1. Drawing of CLB. Bond lengths ( $\text{\AA}$ ) and bond angles ( $^\circ$ ) are given. The values for distances and angles of the ligand are given in the text. Long Cu-Br distances and angles have been omitted for clarity.

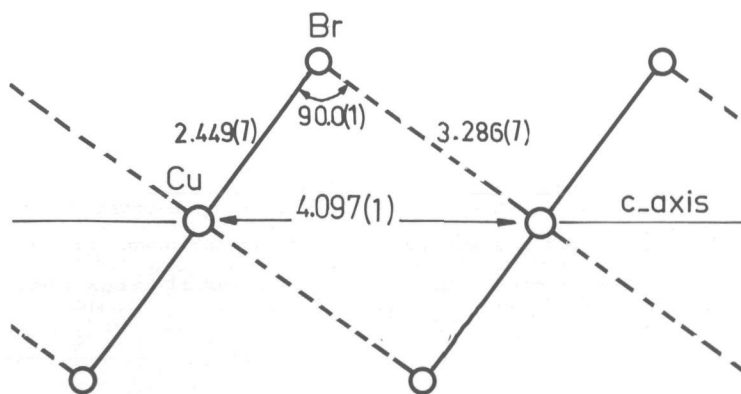
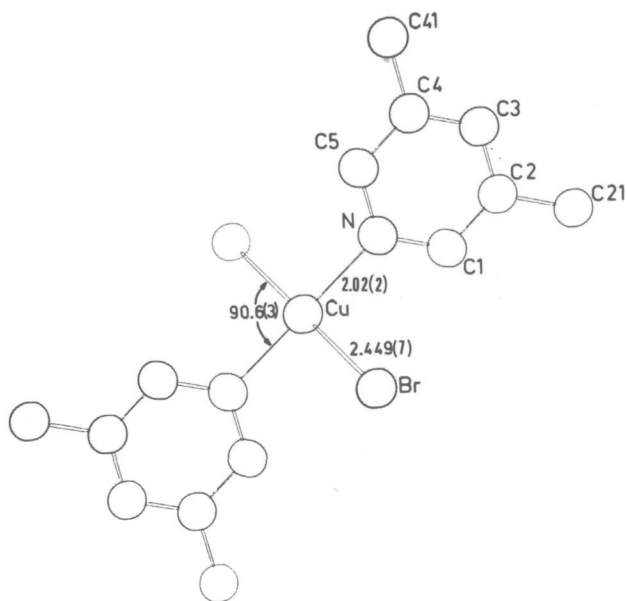


Fig.II.3.2. Geometry of the copper bromine chains along the  $c$ -axis. The nitrogen atoms are below and above the plane of the Cu-Br bonds.

## II.4. Linear-chain Antiferromagnetism and Spectroscopy of Compounds $\text{CuX}_2\text{L}_2$ , with $\text{X}=\text{Cl}$ , $\text{Br}$ and $\text{L}=(\text{substituted})\text{-pyridine}$ .

### II.4.1. Experimental

Compounds  $\text{CuX}_2\text{L}_2$  (5 mmol), with  $\text{X}=\text{Cl}$ ,  $\text{Br}$  and  $\text{L}=(\text{substituted})\text{-pyridine}$ , were prepared by mixing alcoholic solutions of the hydrated copper(II) halides and ligand in a ratio slightly less than 1:2 in order to prevent the formation of the tetra-adducts  $\text{CuL}_4\text{X}_2$ . For dehydration an excess of triethylorthoformate was added to the solution. The immediately obtained precipitates were filtered off, washed several times with ethanol and diethylether, and finally dried *in vacuo* at room temperature.

All compounds were characterized using techniques described in chapter V.

### II.4.2. Results and discussion

#### *General*

The analytical results of the compounds are listed in table II.4.1. A number of these compounds have been mentioned previously<sup>38-46</sup> and have been re-analyzed to confirm purity. The colors of the chlorides are blue, those of the bromides green, except for  $\text{CuBr}_2(3,5\text{-diClpy})_2$  which is yellow.

Infrared spectra of all compounds have been recorded to find out whether a difference occurs between the chloride and bromide complex of one ligand or not. In case of the 4-Etpy and the 4-Vipy compounds small differences in the IR spectra occur; the other pairs can be considered as isomorphous.

The IR spectra showed that water, solvent and free ligand are absent in the present compounds. X-ray powder diffraction patterns show, that the chloride and bromide compounds of the same ligand are not powder isomorphous, just as found for the pyridine compounds, although X-ray single-crystal analysis showed that details around  $\text{Cu(II)}$  are similar<sup>6</sup>. It is further seen that in the present series only two compounds exist, having almost identical X-ray powder patterns, *i.e.*  $\text{CuCl}_2(3\text{-Mepy})_2$  and  $\text{CuCl}_2(3,4\text{-diMepy})_2$ .

#### *Far-infrared spectra*

Far-infrared spectra were recorded to confirm the linear chain structure of the compounds. The observed absorptions in the  $400\text{-}50\text{ cm}^{-1}$  region are listed in table II.4.2, together with the free ligand absorptions. By comparing the spectra of the compounds with the spectra of the free ligand, a literature study

TABLE II.4.1. CHEMICAL ANALYSIS OF COMPOUNDS  $\text{CuX}_2\text{L}_2$ , WITH  $\text{X}=\text{Cl}, \text{Br}$  AND  $\text{L}=(\text{SUBSTITUTED})\text{-PYRIDINE}$

COMPOUND <sup>x</sup>	% Cu		% C		% H		% N	
	cal.	exp.	cal.	exp.	cal.	exp.	cal.	exp.
$\text{CuCl}_2(\text{py})_2^a$	21.7	21.5	41.0	41.2	3.42	3.47		
$\text{CuCl}_2(3\text{-Mepy})_2^b$	19.8	20.2	44.9	43.9	4.41	4.32	8.74	8.37
$\text{CuCl}_2(4\text{-Mepy})_2^b$	19.8	19.8	44.9	45.1	4.41	4.47	8.74	8.61
$\text{CuCl}_2(4\text{-Etpy})_2^c$	18.2	18.6	48.2	47.9	5.16	5.17	8.03	7.83
$\text{CuCl}_2(4\text{-Vipy})_2^d$	18.4	18.3	48.7	48.7	4.06	4.16		
$\text{CuCl}_2(4\text{-Acpy})_2^e$	16.9	17.0	44.6	44.5	3.72	3.64		
$\text{CuCl}_2(4\text{-Mison})_2^e$	15.5	15.5	41.1	41.4	3.43	3.64		
$\text{CuCl}_2(3,4\text{-diMepy})_2^b$	18.2	18.8	48.2	46.9	5.21	5.06	8.03	7.74
$\text{CuCl}_2(3,5\text{-diMepy})_2^b$	18.2	18.0	48.2	47.0	5.21	5.24	8.03	8.13
$\text{CuCl}_2(3,5\text{-diClpy})_2$	14.8	14.2	27.9	28.3	1.39	1.59	6.51	6.46
$\text{CuBr}_2(\text{py})_2^f$	16.7	16.6	31.4	30.9	2.62	2.63		
$\text{CuBr}_2(3\text{-Mepy})_2^g$	15.5	15.2	35.2	34.8	3.45	3.42	6.84	6.45
$\text{CuBr}_2(4\text{-Mepy})_2^h$	15.5	15.2	35.2	35.0	3.45	3.41	6.84	6.69
$\text{CuBr}_2(4\text{-Etpy})_2^i$	14.5	14.5	38.4	38.2	4.11	4.34	6.40	6.28
$\text{CuBr}_2(4\text{-Vipy})_2$	14.7	14.5	38.7	38.3	3.23	3.14		
$\text{CuBr}_2(4\text{-Acpy})_2$	13.6	13.7	36.1	36.2	3.01	3.00		
$\text{CuBr}_2(4\text{-Mison})_2$	12.8	12.9	33.8	34.2	2.81	2.86		
$\text{CuBr}_2(3,4\text{-diMepy})_2$	14.5	14.6	38.4	38.1	4.15	4.29	6.40	6.22
$\text{CuBr}_2(3,5\text{-diMepy})_2$	14.5	14.4	38.4	38.1	4.15	4.19	6.40	5.95
$\text{CuBr}_2(3,5\text{-diClpy})_2$	12.2	12.2	23.1	23.3	1.16	1.16	5.39	5.34

ABBREVIATIONS: 3-Mepy = 3-methylpyridine, 4-Mepy = 4-methylpyridine, 4-Etpy = 4-ethylpyridine, 4-Vipy = 4-vinylpyridine, 4-Acpy = 4-acetylpyridine, 4-Mison = 4-methylisonicotinate, 3,4-diMepy = 3,4-dimethylpyridine, 3,5-diMepy = 3,5-dimethylpyridine, 3,5-diClpy = 3,5-dichloropyridine.

<sup>x</sup>FIRST PREPARED BY: <sup>a</sup>LANG<sup>38</sup>, <sup>b</sup>FRANK AND ROGERS<sup>39</sup>, <sup>c</sup>BURGESS<sup>40</sup>, <sup>d</sup>AGNEW AND LARKWORTHY<sup>41</sup>, <sup>e</sup>WONG AND BREWER<sup>42</sup>, <sup>f</sup>PFEIFFER AND PIMMER<sup>43</sup>, <sup>g</sup>LAMAR<sup>44</sup>, <sup>h</sup>ALLAN et al.<sup>45</sup>, <sup>i</sup>LEVER AND RAMASWAMY<sup>46</sup>

on stretching vibrations of  $\text{CuCl}_2(\text{py})_2$ <sup>47-49</sup> and comparing the spectra of the chlorides and bromides, the Cu-X and Cu-L vibrations can be assigned.

The Cu-L vibrations are mostly interpreted as Cu-N vibrations<sup>47-49</sup>; however, one has to bear in mind, that also vibrations due to ligand waggings and ligand torsions occur, the so-called wagging vibrations<sup>50</sup>. Very recently, Rüede and Thornton<sup>49</sup> published some results for  $\text{CuCl}_2(\text{py})_2$ , in which also deuterated pyridine was used, re-assigning earlier data. These results do not completely agree with the present assignment. For the present assignment, both the chloride and bromide compounds and their deuterated analogues were prepared and their far-infrared spectra investigated.



TABLE II.4.2. FAR-INFRARED DATA OF COMPOUNDS  $\text{CuX}_2\text{L}_2$ , WITH  $\text{X}=\text{Cl}$ ,  $\text{Br}$  AND  $\text{L}=(\text{SUBSTITUTED})\text{-PYRIDINE}$ 

COMPOUND <sup>x</sup>	$\nu_{\text{Cu-Cl}}$	$\nu_{\text{Cu-Br}}$	$\nu_{\text{Cu-L}}$	LIGAND AND UNASSIGNED BANDS ( $\text{cm}^{-1}$ )	
				LIGAND (FREE)	LIGAND (COMPOUND)
$\text{CuCl}_2(3,5\text{-diClpy})_2$	302br 170m 92br		253m 200s 153m	390m 192m	399m 223w
$\text{CuBr}_2(3,5\text{-diClpy})_2$		247br 115m 67s	247br 190s 160m 147s	390m 192m	400m
$\text{CuCl}_2(4\text{-Vipy})_2$	303s 168s 75br		278s 250s 185s	220m	270sh
$\text{CuBr}_2(4\text{-Vipy})_2$		226br 127s 59s	247m 226br 174s	220m	292w 268w
$\text{CuCl}_2(\text{pyH}_5)_2$	293s 179s 78s		270s 235s 205m 196w		
$\text{CuCl}_2(\text{pyD}_5)_2$	293s 178s 78s		266s 225s 195m 186w		400s
$\text{CuBr}_2(\text{pyH}_5)_2$		254s 131s 64s <sup>a</sup>	267m 204s 195m		
$\text{CuBr}_2(\text{pyD}_5)_2$		250s 130s 64s <sup>a</sup>	264s 197s 186m		400s
$\text{CuCl}_2(4\text{-Mepy})_2$	294s 169s 69br <sup>a</sup>		284w 259s 207s	212m	
$\text{CuBr}_2(4\text{-Mepy})_2$		237s 125s 52br <sup>a</sup>	283w 257s 193s	212m	
$\text{CuCl}_2(4\text{-Etpy})_2$	289s 163s 62s		274m 249s 182s	396m 300s 152m	303s 92w
$\text{CuBr}_2(4\text{-Etpy})_2$		216br 120s 58s <sup>a</sup>	275m 246s 179s	396m 300s 152m	
$\text{CuCl}_2(3\text{-Mepy})_2$	293s 169s 74s <sup>a</sup>		265s 211m 192m	342m 219m	358m 233w
$\text{CuBr}_2(3\text{-Mepy})_2$		240s 129s 58s	270s 187s	342m 219m	358m
$\text{CuCl}_2(3,5\text{-diMepy})_2$	290br 164s 79s		284sh 247s 189w 181s	273m 205m	223w
$\text{CuBr}_2(3,5\text{-diMepy})_2$		240br 121s 65s	291s 240br 174s	273m 205m	215m
$\text{CuCl}_2(3,4\text{-diMepy})_2$	291br 164s 68s <sup>b</sup>		291br 255s 190s 145w	257m 183m	
$\text{CuBr}_2(3,4\text{-diMepy})_2$		244s 118s 59s <sup>b</sup>	294w 255m 180s 144w	257m 183m	214m
$\text{CuCl}_2(4\text{-Acpy})_2$	299s 176s 98s <sup>a</sup>		267m 242s	360m 220s 160s 90br	400w 240sh 170sh
$\text{CuBr}_2(4\text{-Acpy})_2$		232s 129m 82br <sup>b</sup>	278s 242m 166s	360m 220s 160s 90br	395m
$\text{CuCl}_2(4\text{-Mison})_2$	303s 168s 93br		266w 232br	338br 216br 167m 70s	398m 345br
$\text{CuBr}_2(4\text{-Mison})_2$		226s 124s 58s	276s 240w 212s 167s	338br 216br 167m 70s	394m 343s

ABBREVIATIONS: br=BROAD AND STRONG, s=STRONG, m=MEDIUM, w=WEAK, sh=SHOULDER; <sup>x</sup> THE LIGANDS ARE ARRANGED WITH INCREASING  $\text{pK}_a$  VALUES, EXCEPT FOR Acpy AND Mison; <sup>a</sup>=SMALL SPLITTING OBSERVED; <sup>b</sup>=STRONG SPLITTING OBSERVED

These far-infrared data are listed in table II.4.2. Examination of this table reveals that the highest Cu-L band, assigned to the Cu-L stretching vibration, shifts only  $4\text{ cm}^{-1}$  on deuteration. According to this shift the  $270\text{ cm}^{-1}$  band cannot be assigned to a Cu-Cl stretching. The other bands for  $\text{X}=\text{Cl}$  at  $235$ ,  $205$  and  $196\text{ cm}^{-1}$  shift  $3\alpha$ .  $7\text{-}10\text{ cm}^{-1}$  on deuteration and according to Adams<sup>50</sup> must be due to Cu-L bending and wagging vibrations.

Theoretical approximations using monomers do not describe the system exactly, because the halogens are also bound to adjacent copper ions. Since the X-ray structure of most of the compounds is unknown, it is impossible to take the line group symmetry, which in fact is the best approach to prediction of the vibrational spectrum<sup>51</sup>. However, especially for the Cu-L vibrations the monomer approach seems reasonable.

Theoretically the number of far-infrared vibrations for a species  $\text{CuX}_2\text{X}'\text{L}_2$  in  $\text{C}_{2h}$  symmetry can be calculated. The results are listed in table II.4.3 and are calculated according to methods outlined by Cotton<sup>52</sup>. Examination of this table reveals that 12 bands are expected in the far-infrared region ( $3\text{A}_u$  and  $9\text{B}_u$ ). It is clear that the bending vibrations in which the  $\text{X}'$  atom (the halogen at longer distance) is involved, will occur at very low frequencies. The Cu-L wagging vibrations and Cu-L bending vibrations have the same symmetry, therefore

TABLE II.4.3. DESCRIPTION OF NORMAL MODES IN  $\text{CuX}_2\text{X}'_2\text{L}_2$  UNDER  $\text{C}_{2h}$  SYMMETRY

DESCRIPTION	TOTAL DEGENERACY	SYMMETRY SPECIES			
		$A_g$	$B_g$	$A_u$	$B_u$
2 LIGANDS ( $\text{C}_5\text{H}_5\text{N}$ )	54	13	14	14	13
Cu-X STRETCHING	2	1	0	0	1
Cu-X' STRETCHING	2	1	0	0	1
Cu-L STRETCHING	2	1	0	1	0
Cu-L	9	1	2	2	4
Cu-X } BENDINGS					
Cu-X' }					
Cu-L WAGGINGS	6	1	2	0	3
TOTAL VIBRATIONAL DEGREES OF FREEDOM	75	18	18	17	22

mixing of these vibrations is expected. Therefore, it is clear that all 12 bands cannot be observed in the far-infrared region investigated here, *i.e.* above  $50\text{ cm}^{-1}$ . Neglecting bendings involving the halogen atoms at longer distance, 10 bands are expected in the far-infrared region; from these three are Cu-L wagging vibrations.

In the  $\text{CuBr}_2(\text{py})_2$  spectrum the Cu-Br and Cu-L stretching vibrations are very close to each other, giving rise to overlap and mixing of these vibrations. As expected, deuteration of the pyridine molecule did not yield strong evidence for discrimination between Cu-Br and Cu-L vibrations. The band of lowest intensity was assigned to the Cu-L stretching vibration, because in the spectrum of the chloride the Cu-L stretching vibration also has lower intensity than the Cu-Cl stretching.

It turns out that only three Cu-X vibrations can be assigned throughout this series. It is assumed that the two highest bands belong to short Cu-X vibrations and the band at lowest energy to the long Cu-X vibration.

For most compounds only three Cu-L vibrations can be assigned, being indicative of mixing between the theoretically expected Cu-L vibrations, having the same symmetry.

The effect of  $\text{pK}_a$  of the ligands has been thoroughly investigated by Wong and Brewer<sup>42</sup>. The effect of substituting electron-attracting and electron-donating groups in the pyridine ring, on the Cu-L stretching vibration is clearly seen from table II.4.2. Examination of this table reveals that with a few exceptions the Cu-L stretching vibration increases in the order:



This sequence of ligands goes parallel with the increasing  $\text{pK}_a$  values of ligands. From this sequence the Acpy and Mison compounds have been excluded, because the free ligands show a great number of absorptions, making assignments unreliable. Moreover, the bulky polar substituents in these ligands are expected to influence

the crystal packing significantly, and therefore also Cu-L vibrations. Although  $\text{CuBr}_2(4\text{-Vipy})_2$  has its Cu-L vibration within the series,  $\text{CuCl}_2(4\text{-Vipy})_2$  deviates. This may have something to do with the fact that these two compounds are not mutually infrared isomorphous (*vide supra*).

A similar sequence is found for the Cu-Cl vibrations, although the effect is smaller. Now the Cu-Cl stretching frequency increases with decreasing  $\text{pK}_a$  value of the ligands. The suggestion of Wong and Brewer<sup>42</sup> that the influence of electron-attracting and electron-donating substituents in the ligand is similar when regarding Cu-Cl vibrations, does not hold for this large class of ligands. It appears from table II.4.2 that the electrostatic ( $\sigma$ -donation) effect of the ligand is considerably larger than the  $\pi$ -back-bonding contribution, at least with respect to the Cu-Cl frequency.

A few other remarks concerning the assignments in this table should be made, since some results are different from those obtained by others<sup>46,47</sup>. The origin of these differences is the fact that discrimination between Cu-L and free ligand vibrations is difficult for many ligands, making assignments ambiguous. Even when low-temperature measurements are carried out, exact assignment is difficult. It is found that the low-temperature spectra of the present compounds did not yield much additional information, other than confirming the assignments, although most absorptions appear much sharper. The fact that reversed assignments in table II.4.2 do not allow a good comparison between the chlorides and the bromides, and between the normal and the deuterated compounds, and also yields deviations in the  $\text{pK}_a$  sequence, strengthens the present choice of Cu-X and Cu-L vibrations.

#### *Electron spin resonance and ligand-field spectra*

ESR spectra of the powdered compounds have been recorded at ambient temperature and both X- and Q-band frequencies to confirm the proposed structure and to obtain information about the geometry in the present compounds. The ESR and ligand-field data are listed in table II.4.4.

From the results in table II.4.4 it is seen that all the chloride compounds show a three g-value spectrum. Such a spectrum can be due to both a rhombic geometry and to exchange coupling between different axial or rhombic Cu(II) sites<sup>26</sup>. The g-values have been taken from the Q-band spectra, as these are better resolved than the X-band spectra. Hyperfine splittings remain unresolved, since the magnetic exchange between the Cu(II) ions is large compared to the (super)-hyperfine interactions.

The g-values of the compound  $\text{CuCl}_2(4\text{-Etpy})_2$  appear less anisotropic than

TABLE II.4.4. ESR AND LIGAND-FIELD DATA OF COMPOUNDS  $\text{CuX}_2\text{L}_2$ , WITH  $\text{X}=\text{Cl}$ ,  $\text{Br}$  AND  $\text{L}=(\text{SUBSTITUTED})\text{-PYRIDINE}$ . UNCERTAINTIES IN THE LAST DIGIT ARE IN PARENTHESES

COMPOUND	ESR DATA <sup>a</sup>			LIGAND-FIELD DATA
	$g_1$	$g_2$	$g_3$	MAXIMA (kK)
$\text{CuCl}_2(\text{py})_2$	2.23(1)	2.09(1)	2.07(1)	14.8(2)
$\text{CuCl}_2(3\text{-Mepy})_2$	2.24(1)	2.07(1)	2.04(1)	15.2(2)
$\text{CuCl}_2(4\text{-Mepy})_2$	2.24(1)	2.07(1)	2.03(1)	15.4(2)
$\text{CuCl}_2(4\text{-Etpy})_2$	2.18(1)	2.13(1)	2.03(1)	14.9(2)
$\text{CuCl}_2(4\text{-Vipy})_2$	2.26(1)	2.08(1)	2.04(1)	14.9(2)
$\text{CuCl}_2(4\text{-Acpy})_2$	2.27(1)	2.09(1)	2.04(1)	14.2(2)
$\text{CuCl}_2(4\text{-Mison})_2$	2.26(1)	2.08(1)	2.05(1)	14.4(2)
$\text{CuCl}_2(3,4\text{-diMepy})_2$	2.25(1)	2.07(1)	2.04(1)	15.9(2)
$\text{CuCl}_2(3,5\text{-diMepy})_2$	2.25(1)	2.08(1)	2.06(1)	15.4(2)
$\text{CuCl}_2(3,5\text{-diClpy})_2$	2.23(1)	2.09(1)	2.06(1)	14.1(2)
$\text{CuBr}_2(\text{py})_2$		2.13(1)		14.5(1)
$\text{CuBr}_2(3\text{-Mepy})_2$		2.12(1)		14.7(1)
$\text{CuBr}_2(4\text{-Mepy})_2$		2.11(1)		14.7(1)
$\text{CuBr}_2(4\text{-Etpy})_2$		2.12(1)		14.7(1)
$\text{CuBr}_2(4\text{-Vipy})_2$		2.12(1)		14.6(1)
$\text{CuBr}_2(4\text{-Acpy})_2$		2.13(1)		14.4(1)
$\text{CuBr}_2(4\text{-Mison})_2$		2.12(1)		14.5(1)
$\text{CuBr}_2(3,4\text{-diMepy})_2$		2.13(2) <sup>b</sup>		14.7(1)
$\text{CuBr}_2(3,5\text{-diMepy})_2$		2.13(1)		14.7(1)
$\text{CuBr}_2(3,5\text{-diClpy})_2$		2.12(1)		14.0(1)

<sup>a</sup>THE BROMINE COMPOUNDS HAVE ISOTROPIC  $g$ -VALUES; LINE WIDTHS VARY FROM 500-800 G; <sup>b</sup>THERE APPEARED TO BE A SMALL ANISOTROPY IN THE  $g$ -VALUE.

with the chlorides, whereas another reason may be the fact that the  $g$ -tensor for the bromides is less anisotropic than that of the chlorides. Theoretically isotropic spectra could be expected for several orientations of two orthorhombic  $\text{Cu(II)}$  sites that are exchange coupled; however, it is not expected that this should be the case for all the bromides.

The ligand-field maxima have been included in table II.4.4. The bromide compounds show mutually similar spectra in band width, band shape and approximate band position, in agreement with a basically-similar geometry around  $\text{Cu(II)}$ . The bands in the chloride compounds are rather weak and broad; furthermore, the compounds differ slightly in the position of the band maxima. It is well known that the position of the band maximum is a function of both the spectrochemical position of the surrounding atoms and the distortion from octahedral geometry<sup>26</sup>. The observed band maxima all fall between the 16.0 and the 14.0 kK corroborating with a distorted octahedral geometry<sup>26</sup>.

those of the other chlorides. This does not imply a different geometry, but can be solely due to the relative orientation of the exchange-coupled  $g$ -tensors in the unit cell<sup>26</sup>. As discussed by Hatfield<sup>7</sup> the site orientations might well differ in these compounds.

For the bromide compounds the X- and Q-band spectra exhibit only a single broad absorption. Due to exchange coupling between the copper(II) ions the hyperfine splittings remain also unresolved. The fact that the bromide compounds even do not show a three  $g$ -value spectrum could be caused by a larger spin-lattice coupling compared

## Magnetic susceptibility measurements

The relevant data of the susceptibility measurements are listed in table II.4.5. The values for the susceptibility are corrected for diamagnetism of constituent atoms, using Pascal's constants<sup>53</sup> and for temperature independent paramagnetism<sup>54</sup>. The appearance of a broad maximum in the susceptibility curves, provides evidence for the presence of antiferromagnetically-coupled linear chain systems.

To describe the experimental magnetic susceptibility data, a model has to be selected. Jotham<sup>55</sup> has shown, that the anisotropic Ising simplification of the Heisenberg exchange Hamiltonian<sup>10</sup> is substantially in error for the description of one-dimensional polymeric systems having large exchange interactions. In addition, a single-crystal magnetic susceptibility study<sup>56</sup> of the linear chain compound  $\text{Cu}(\text{NO}_3)_2(\text{pyrazine})_2$  has demonstrated that, for the small J-value of  $-3.7 \text{ cm}^{-1}$ , the exchange interaction is quite isotropic. The Heisenberg approximation was therefore chosen to describe the experimental magnetic data. For some compounds, however, it was not possible to describe the data within the Heisenberg model (see table II.4.5), and in those cases the Ising expression<sup>11</sup> was also tried to fit the data.

TABLE II.4.5. SUSCEPTIBILITY DATA FOR COMPOUNDS  $\text{CuX}_2\text{L}_2$ , WITH  $\text{X}=\text{Cl}, \text{Br}$  AND  $\text{L}=(\text{SUBSTITUTED})\text{-PYRIDINE}$ . UNCERTAINTIES IN THE LAST DIGIT ARE IN PARENTHESES

COMPOUND	$T_{\text{max}}$	$\chi_{\text{M max}} \cdot 10^2$	$-J^a$	$-J^b$	$g^c$	$\bar{g}^d$	HEISENBERG FIT		CURIE TEMPERATURE
	(K)	(emu/mole)	( $\text{cm}^{-1}$ )	( $\text{cm}^{-1}$ )			$-J(\text{cm}^{-1})$	$g$	
$\text{CuCl}_2(\text{py})_2$	16.6(3)	0.94(2)	9.0(2)	9.2(2)	2.10(5)	2.13(1)	9.2(2)	2.12(1)	11(2)
$\text{CuCl}_2(3\text{-Mepy})_2$	14.3(3)	1.07(2)	7.8(2)	8.0(2)	2.09(5)	2.12(1)	8.1(2)	2.14(1)	9(2)
$\text{CuCl}_2(4\text{-Mepy})_2$	14.2(3)	1.16(2)	7.7(2)	7.4(2)	2.16(5)	2.12(1)	7.3(2)	2.12(1)	7(1)
$\text{CuCl}_2(4\text{-Etpy})_2$	12.6(3)	1.30(2)	6.8(2)	6.6(2)	2.15(5)	2.11(1)	6.9(2)	2.15(1)	7(1)
$\text{CuCl}_2(4\text{-Vipy})_2$	14.8(5)	1.09(2)	8.0(2)	8.0(3)	2.13(7)	2.13(1)	8.4(2)	2.15(1)	8(1)
$\text{CuCl}_2(4\text{-Acpy})_2$	14.5(3)	1.06(2)	7.9(2)	8.2(2)	2.09(5)	2.13(1)	8.2(2)	2.13(1)	8(1)
$\text{CuCl}_2(4\text{-Mison})_2$	15.8(3)	0.98(2)	8.6(2)	8.9(2)	2.10(5)	2.13(1)	9.0(2)	2.14(1)	10(2)
$\text{CuCl}_2(3,4\text{-diMepy})_2$	14.0(3)	1.08(2)	7.6(2)	8.0(2)	2.07(5)	2.12(1)	7.9(2)	2.11(1)	9(2)
$\text{CuCl}_2(3,5\text{-diMepy})_2$	16.2(4)	0.96(2)	8.8(2)	9.1(2)	2.10(5)	2.13(1)	9.0(2)	2.11(1)	12(2)
$\text{CuCl}_2(3,5\text{-diClpy})_2$	20.0(5)	0.80(2)	10.8(4)	10.9(4)	2.12(6)	2.13(1)	11.0(2)	2.13(1)	14(2)
$\text{CuBr}_2(\text{py})_2$	32(1)	0.58(1)	17.3(6)	15.0(7)	2.3(1)	2.13(2)	16.6(3)	2.24(1)	e
$\text{CuBr}_2(3\text{-Mepy})_2$	23.0(6)	0.70(2)	12.5(4)	12.3(5)	2.14(8)	2.12(2)	f	f	40(9)
$\text{CuBr}_2(4\text{-Mepy})_2$	19.0(6)	0.72(2)	10.3(4)	11.8(5)	1.97(8)	2.11(2)	f	f	25(5)
$\text{CuBr}_2(4\text{-Etpy})_2$	23.0(6)	0.63(2)	12.5(4)	13.7(5)	2.03(8)	2.12(2)	13.0(2)	2.07(1)	30(6)
$\text{CuBr}_2(4\text{-Vipy})_2$	26(1)	0.61(1)	14.1(5)	14.1(6)	2.12(9)	2.13(2)	14.2(2)	2.13(1)	50(9)
$\text{CuBr}_2(4\text{-Acpy})_2$	32(1)	0.49(1)	17.3(7)	17.7(8)	2.10(8)	2.13(2)	17.4(3)	2.12(1)	e
$\text{CuBr}_2(4\text{-Mison})_2$	33(1)	0.47(1)	17.9(7)	18.3(8)	2.12(8)	2.12(2)	18.4(3)	2.12(1)	e
$\text{CuBr}_2(3,4\text{-diMepy})_2$	28(1)	0.60(1)	15.2(6)	14.5(7)	2.18(9)	2.13(3)	f	f	36(9)
$\text{CuBr}_2(3,5\text{-diMepy})_2$	37(1)	0.38(1)	20(1)	23(1)	2.0(1)	2.13(2)	21.3(4)	2.07(1)	e
$\text{CuBr}_2(3,5\text{-diClpy})_2$	39(2)	0.37(1)	21(1)	23(1)	2.0(1)	2.12(2)	22.7(4)	2.11(1)	e

<sup>a</sup>=FROM  $T_{\text{max}}$ ; <sup>b</sup>=FROM  $\bar{g}$ ,  $T_{\text{max}}$  and  $\chi_{\text{M max}}$ ; <sup>c</sup>=FROM  $T_{\text{max}}$  and  $\chi_{\text{M max}}$ ; <sup>d</sup>=AVERAGE ESR  $g$ -VALUE; <sup>e</sup>=COULD NOT BE OBTAINED DUE TO

NON-LINEARITY IN  $\chi_{\text{M}}^{-1}$  VERSUS  $T$  CURVE IN THE TEMPERATURE REGION INVESTIGATED; <sup>f</sup>=NO FIT COULD BE OBTAINED.

Fisher<sup>11</sup> published the closed-form expressions for the anisotropic susceptibility of one-dimensional Ising chains of  $S=\frac{1}{2}$  ions. From his expressions for the parallel susceptibility and the perpendicular susceptibility the value  $\chi_{\text{powder}} = (\chi_{\parallel} + 2\chi_{\perp})/3$  was tried to fit the magnetic data. Although closed-form expressions for the magnetic susceptibility of an isotropically-coupled linear Heisenberg chain antiferromagnet are not available, the results of Bonner and Fisher<sup>10</sup> for infinite chains make it possible to calculate the exchange constants. They calculated the antiferromagnetic susceptibilities for isotropic coupling in zero field for finite rings up to 11 spins of  $S=\frac{1}{2}$ . From these calculations they extrapolated the temperature of the maximum ( $T_{\text{max.}}$ ) and the value of the maximum susceptibility ( $\chi_{\text{M max.}}$ ) for an infinite chain<sup>10</sup>:

$$T_{\text{max.}} = 1.282 |J| / k \dots (a) \quad \chi_{\text{M max.}} = 0.07346 N g^2 \beta^2 / |J| \dots (b)$$

From these two equations two independent J-values are obtained. The first value is obtained directly from (a). The second value of J is obtained from the experimental ESR g-value, defined as:  $\bar{g} = \{(g_1^2 + g_2^2 + g_3^2)/3\}^{\frac{1}{2}}$ , and equation (b). It is also possible to calculate an experimental g-value, combining equations (a) and (b). Bonner and Fisher<sup>10</sup> also plotted an extrapolated susceptibility curve for the infinite  $S=\frac{1}{2}$  chain. The extrapolated theoretical curve was tried to fit the experimental curves graphically, yielding a third J-value.

In the high-temperature region, above ca. 50K, the present susceptibility curves obey Curie-Weiss relations, with a negative asymptotic Curie temperature, in agreement with antiferromagnetic interactions. For the chloride compounds the Curie temperatures occur in the 7-14K region, for the bromide compounds in the 25-50K region (see table II.4.5). A small rise in susceptibility at very low temperatures due to paramagnetic impurities has been found for several cases. In those cases assumption of the presence of impurities up to ca. 1% was necessary to fit the low-temperature part of the curves with the Heisenberg model. This procedure is generally accepted<sup>7</sup>.

For the chloride compounds the fits using the Heisenberg model are fair, except for the 4-Mepy compound, as illustrated in figure II.4.1. For this compound also the Ising fit was very poor, suggesting that an antiferromagnetic inter-chain interaction or an alternating chain behaviour (as described in chapter II.6) might be present. In figure II.4.2 a plot of data for 3,5-diClpy is shown; the Heisenberg fit is good.

The bromine series revealed more problems, since the compounds of 3-Mepy, 4-Mepy and 3,4-diMepy could be fitted neither with the Heisenberg model, nor

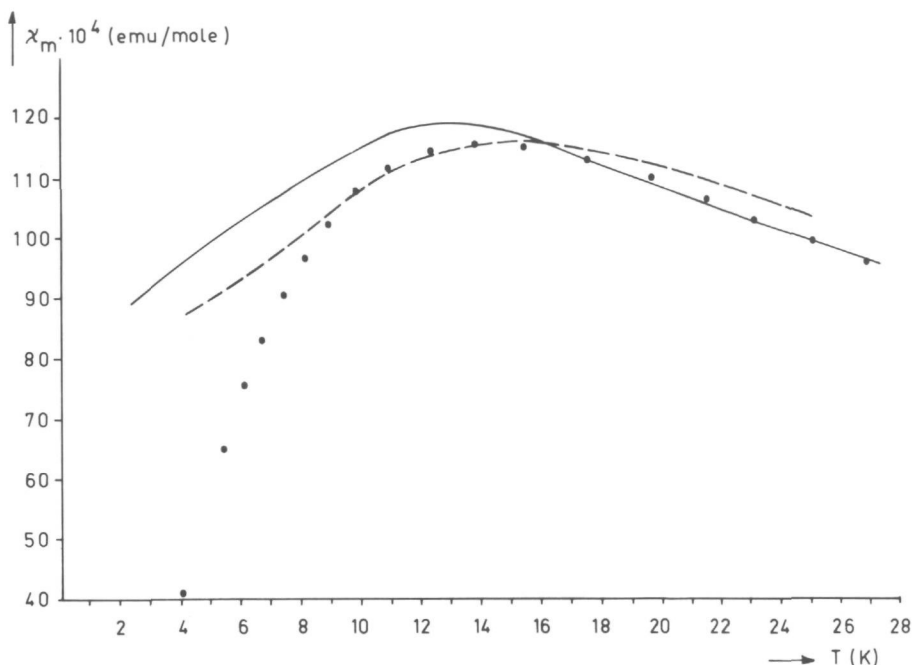


Fig. II.4.1. Molar susceptibility of  $\text{CuCl}_2(4\text{-Mepy})_2$  as a function of temperature;  $\bullet$  = experimental points. The full curve represents the fit for  $J = -7.3 \text{ cm}^{-1}$  and  $g = 2.12$  according to the results of Bonner and Fisher (Heisenberg model). The dotted curve represents the fit for  $J = -11.1 \text{ cm}^{-1}$  and  $g = 2.12$  according to Fisher's results (Ising model).

with the Ising model. These compounds exhibit an anisotropy somewhat intermediate between the two extreme models of Ising and Heisenberg. Jeter and Hatfield<sup>8</sup> found the same for  $\text{CuBr}_2(\text{py})_2$ . For this compound a reasonable fit within the Heisenberg model was found, although the obtained  $g$ -value was remarkably high ( $\bar{g} = 2.13$  and  $g_{\text{fit}} = 2.24$ ).

Examination of table II.4.5 reveals the influence of the different ligands on the exchange constant of both the chlorides and bromides. For all ligands the exchange interaction increases when the chloride is replaced by the bromide; Hatfield and coworkers<sup>7-9</sup> found a similar increase for the pyridines and also for the nicotinamide, isonicotinamide and pyrazinamide compounds. The small differences in the substituents of the pyridine molecule, cause different manners of packing of the chains and this affects bond lengths and bridge angle within the chains. In table II.4.6 the relevant structural and magnetic data of chains of the present series are listed; the  $J$ -values listed in this table are very close to those published by Hatfield and coworkers<sup>7-9</sup>. From this table a clear

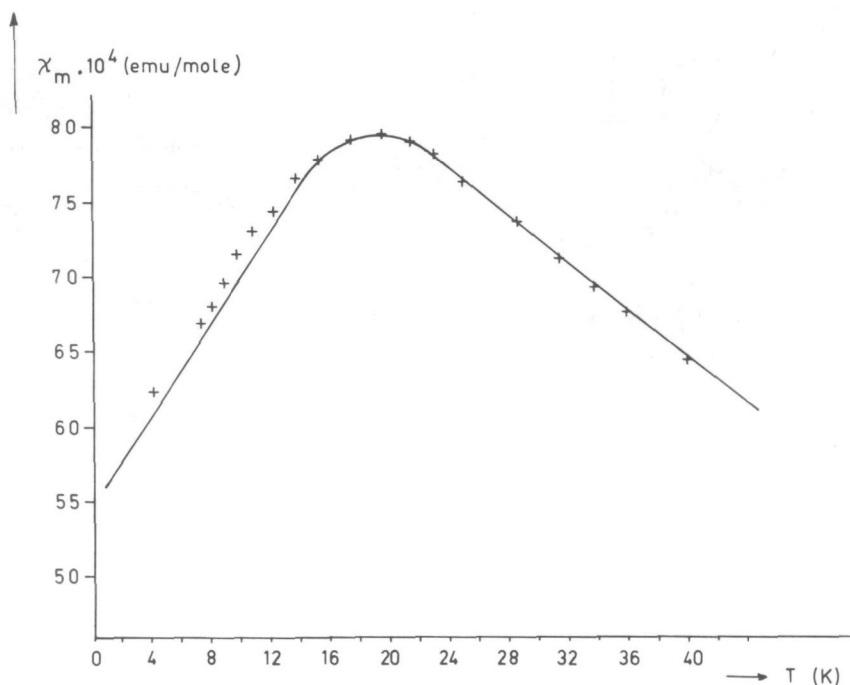


Fig. II.4.2. Molar susceptibility of  $\text{CuCl}_2(3,5\text{-diClpy})_2$  as a function of temperature; + = experimental points. The full curve represents the fit for  $J = -11.0 \text{ cm}^{-1}$  and  $g = 2.13$  according to the results of Bonner and Fisher (Heisenberg model).

correlation between the Cu-Cl-Cu angle and the  $J$ -value, similar to that observed for hydroxo-bridged dimers<sup>57</sup> seems absent.

It appears that the length of the largest Cu-X distance affects the exchange constant (see below).

Sources of the observed anisotropy are the dipolar interaction (especially between copper(II) ions in the chain) and spin-orbit coupling. For symmetry

TABLE II.4.6. MAGNETIC AND STRUCTURAL DATA OF COMPOUNDS  $\text{CuCl}_2\text{L}_2$

COMPOUND	Cu-Cl(Å)		Cu-Cu	Cu-Cl-Cu	$-J^x$	REF.
	long	short	(Å)	(°)	( $\text{cm}^{-1}$ )	
$\text{CuCl}_2(\text{py})_2$	3.026	2.299	3.848	91.5	9.2(2)	6
$\text{CuCl}_2(4\text{-Vipy})_2$	3.10	2.38	3.91	90.0	8.2(2)	4
$\text{CuCl}_2(4\text{-Etpy})_2$	3.21	2.28	4.00	92.0	6.8(2)	3

<sup>x</sup>=AVERAGED  $J$ -VALUE FROM TABLE II.4.5.



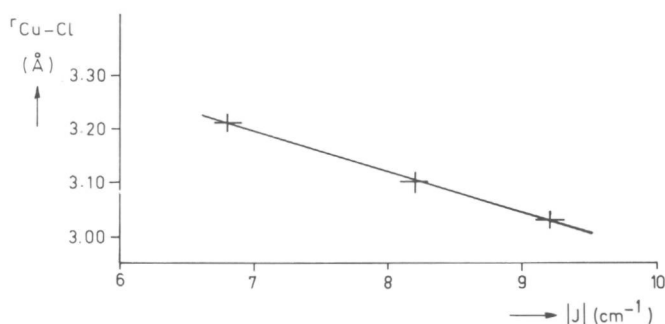


Fig. II.4.3. Plot of the long Cu-Cl bond length  $r_{\text{Cu-Cl}}$  against the  $|J|$ -value for the compounds listed in table II.4.6.

reasons anti-symmetric exchange vanishes. Within the present series the anisotropy due to dipolar interaction and spin-orbit coupling are both small compared to the isotropic  $J$ -values. However, inter-chain coupling can play an important rôle here.

Although the superexchange path goes along the chemical chain (the halogen ions), it is difficult

to deduce to what extent the non-bridging ligands play a rôle in the superexchange mechanism.

#### *Relation between structural and magnetic parameters*

Recently, Hatfield, Hodgson and coworkers<sup>57</sup> published a study of structural and magnetic properties of hydroxo-bridged dimers of copper(II); they found a linear relationship between the Cu-O-Cu bridge angle and the exchange constant. For the linear chain compounds  $\text{CuX}_2\text{L}_2$  it was tried to find out, which structural relationship would exist with the exchange constant. In the chlorine series, as has already been mentioned, three compounds having one-dimensional magnetic properties are available for which also a single-crystal structure determination has been published<sup>3,4,6</sup>. In table II.4.6 the structural data of these compounds have been collected, together with the available  $J$ -values. In figure II.4.3 the long Cu-Cl bond length is plotted against the  $J$ -value. By plotting the Cu-Cu distance instead of the long Cu-Cl distance, against the  $J$ -value a similar plot is obtained. This long Cu-Cl bond is also correlated with the lowest observed Cu-Cl vibration in the far-infrared. Clearly, the length of the bond is strongly correlated to its vibration frequency, so this frequency can be regarded as a measure of the bond length. In figure II.4.4 the averaged  $J$ -values from table II.4.5 are plotted against the long Cu-Cl vibration of the corresponding compounds. In the  $J$ -region investigated the relationship is linear. In this figure also a plot of the long Cu-Cl vibration, divided by the short Cu-Cl vibration frequency against the  $J$ -value is drawn. This was done in order to correct in some way for the influence of  $\text{pK}_a$  values on the frequency of the stretching vibrations. The 3-Mepy and 3,4-

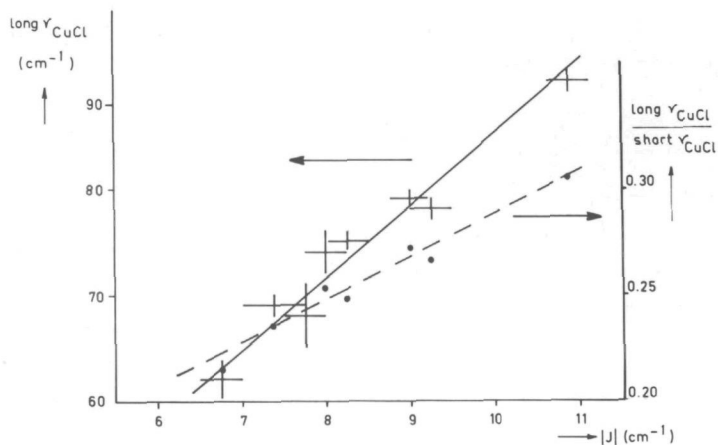


Fig. II.4.4. Plot of averaged  $|J|$ -value of some compounds  $\text{CuCl}_2\text{L}_2$  against the lowest Cu-Cl frequency (full curve) and against the lowest Cu-Cl frequency divided by the highest Cu-Cl frequency (dotted curve).

diMepy compounds fall slightly besides the curve; probably this originates from a different symmetry of these ligands compared to the others. For these compounds the long Cu-Cl band is split, and for the plot the averaged value of this doublet was used. The splitting of this band in these compounds can also be explained by assuming that in these cases chains built up from dimeric units are present, with alternating distances between the copper(II) ions within the chain. Because of the uncertainty of the Cu-Cl vibrations the Mison and Acpy compounds were not included.

Accurate  $J$ -values could not be determined for all the bromine compounds (see magnetic measurements). Furthermore, almost all compounds showed a splitting in the long Cu-Br band, making it too speculative to construct a frequency *versus*  $J$ -value plot for the bromides.

## II.5. Magnetic Exchange and Spectroscopy in some polynuclear Compounds of Cu(II) with azole Ligands.

### II.5.1. Experimental

Compounds  $\text{CuX}_2\text{L}_2$  (5mmol), with  $\text{X}=\text{Cl}$ ,  $\text{Br}$  and  $\text{L}=\text{imidazole (Iz)}$ ,  $\text{N-methyl-imidazole (NMiz)}$ ,  $\text{pyrazole (Pz)}$  and  $\text{indazole (Indz)}$ , were prepared by mixing alcoholic solutions of the hydrated copper(II) halides and ligand in a ratio slightly less than 1:2, in order to prevent the formation of the tetra-adducts  $\text{CuL}_4\text{X}_2$ . For dehydration an excess of triethylorthoformate was added to the solution. The immediately formed crystals were filtered off, washed several times with ethanol and diethylether, and finally dried *in vacuo* at room temperature.

All compounds were characterized using techniques described in chapter V.

### II.5.2. Results and discussion

#### *General*

The analytical results for the present compounds (Cu, C, H and N) are listed in table II.5.1. The compound  $\text{CuBr}_2(\text{Iz})_2$  could not be prepared pure (from an alcoholic solution), due to the formation of imidazolyl compounds for which three modifications are known<sup>60</sup>, and is excluded from the present study. Infrared spectra showed that no water, solvent, or free ligand molecules are present in the compounds. X-ray powder-diffraction patterns and IR spectra show that none of the compounds is mutually isomorphous.

In this chapter only the  $\beta$ -form of the compound  $\text{CuCl}_2(\text{NMiz})_2$  is described, whereas the details of both the  $\alpha$ - and  $\beta$ -form are reported in appendix VI.1.

TABLE II.5.1. CHEMICAL ANALYSES AND COLOR OF COMPOUNDS  $\text{CuX}_2\text{L}_2$ , WITH  $\text{X}=\text{Cl}$ ,  $\text{Br}$  AND  $\text{L}=\text{Iz}$ ,  $\text{NMiz}$ ,  $\text{Pz}$  AND  $\text{Indz}$

COMPOUND <sup>x</sup>	%Cu		%C		%H		%N		COLOR
	cal.	exp.	cal.	exp.	cal.	exp.	cal.	exp.	
$\text{CuCl}_2(\text{Iz})_2$ <sup>a</sup>	23.5	23.5	26.6	27.1	2.96	3.02	20.7	20.4	green
$\text{CuCl}_2(\text{NMiz})_2$ <sup>b</sup>	21.3	21.3	32.3	32.6	4.02	4.10	18.8	18.5	green
$\text{CuCl}_2(\text{Pz})_2$ <sup>c</sup>	23.5	23.6	26.6	27.2	2.96	2.98	20.7	20.5	green
$\text{CuCl}_2(\text{Indz})_2$	17.2	17.2	45.4	45.7	3.24	3.34	15.1	14.9	yellow
$\text{CuBr}_2(\text{NMiz})_2$ <sup>b</sup>	16.4	16.3	24.8	24.8	3.10	3.10	14.5	14.6	green
$\text{CuBr}_2(\text{Pz})_2$ <sup>c</sup>	17.7	17.7	20.0	20.9	2.23	2.26	15.6	15.6	green
$\text{CuBr}_2(\text{Indz})_2$	13.8	13.8	36.6	37.2	2.61	2.76	12.2	12.2	brown

ABBREVIATIONS: Iz=imidazole, NMiz=N-methylimidazole, Pz=pyrazole, Indz=indazole

<sup>x</sup>=FIRST PREPARED BY: <sup>a</sup>LUNDBERG<sup>19</sup>; <sup>b</sup>GOODGAME *et al*<sup>58</sup>; <sup>c</sup>REEDIJK *et al*<sup>59</sup>.

The brown color of  $\text{CuBr}_2(\text{Indz})_2$  at room temperature changes to green at ca. 250K; however, from the far-IR, ESR and ligand-field spectra, both forms are identical and probably no structural change is involved. The color change is presumably caused by a narrowing of either the d-d transition or charge-transfer bands which occur in the visible region.

#### Far-infrared spectra

Far-IR spectra were recorded ( $450\text{--}40\text{ cm}^{-1}$ ) in order to characterize the compounds with the aid of published data, to see whether the compounds show similar absorptions and to assign possible M-X and M-L vibrations. The absorptions and tentative assignments are listed in table II.5.2, together with the free-ligand data for indazole. Reedijk *et al.*<sup>59</sup> published some far-IR data for the Pz compounds. The apparatus used at present has a much better resolution and goes down to very low frequencies. Therefore, it is now possible to assign some bending vibrations by comparing the spectra of the chloride and the bromide compound.

The present data for the NMiz compounds agree with those published by Goodgame *et al.*<sup>58</sup> who only assigned the absorptions of  $\text{CuCl}_2(\text{NMiz})_2$ . The band at ca.  $310\text{ cm}^{-1}$  was reassigned; in both the chloride and bromide spectrum this band occurs and because the free ligand shows no absorptions in this region, this band can only be assigned to a Cu-L vibration. For  $\text{CuCl}_2(\text{Iz})_2$ , for which an X-ray crystal structure analysis has been published<sup>19</sup>, the far-IR spectrum is complicated, presumably due to the asymmetric coordination sphere around

TABLE II.5.2. FAR-INFRARED DATA ( $450\text{--}40\text{ cm}^{-1}$ ) OF COMPOUNDS  $\text{CuX}_2\text{L}_2$ , WITH X=Cl, Br AND L=Iz, NMiz, Pz, Indz AND OF THE LIGAND Indz

COMPOUND <sup>x</sup>	$\nu_{\text{Cu-X}}$	$\nu_{\text{Cu-L}}$	LIGAND AND UNASSIGNED BANDS
	( $\text{cm}^{-1}$ )	( $\text{cm}^{-1}$ )	( $\text{cm}^{-1}$ )
$\text{CuCl}_2(\text{Iz})_2$	278br 206s	305m 242s 160m	100br 75w 53m
$\text{CuCl}_2(\text{NMiz})_2^a$	284s 188s	314s 213m 167s	383m 265m 236w 105m 72w 62w
$\text{CuCl}_2(\text{Pz})_2^b$	282s 189s	302m 236s 201s	217m 122s 90sh 82m 70m
$\text{CuCl}_2(\text{Indz})_2$	282br 184s	282br 248s 200m	441s 425s 128s 82s
Indz			432s 401s 273s 238m 224m 104s
$\text{CuBr}_2(\text{NMiz})_2^a$	200s 128s	306s 223s 179s	376s 87s 69s
$\text{CuBr}_2(\text{Pz})_2^b$	206s 131s	304s 259s 186s	95s 65m 52s
$\text{CuBr}_2(\text{Indz})_2$	216s 123s	271s 216s 171s	429s 70s 50s

ABBREVIATIONS: br=BROAD AND STRONG, s=STRONG, m=MEDIUM, w=WEAK, sh=SHOULDER;

<sup>x</sup>=DATA ARE IN AGREEMENT WITH THOSE PUBLISHED BY: <sup>a</sup>GOODGAME *et al.*<sup>58</sup> ;

<sup>b</sup>REEDIJK *et al.*<sup>59</sup> .

the copper ions. The only spectrum available for comparison is that of the free ligand, making an assignment rather doubtful. For the Indz compounds assignments were based on those of the Pz compounds; the Cu-L vibrations are expected<sup>61</sup> to occur at lower energies because of the smaller  $pK_a$  value of the Indz ligand whereas the Cu-X vibrations are expected to occur at similar frequencies. The agreement between the chloride and bromide assignment is not very good, making the assignment at best tentative.

### Ligand-field and ESR spectra

In order to obtain information about the geometry and coordination of the compounds, the ligand-field and ESR spectra (X- and Q-band) of the powdered solids were recorded (table II.5.3). Such spectra may give evidence about the tetrahedral or octahedral geometry<sup>26</sup> and about the nature and magnitude of distortions from these symmetries.

From the results in table II.5.3 it is seen that each chloride compound shows a three g-value ESR spectrum, which is either characteristic for rhombic geometry or due to exchange coupling between different axial or rhombic Cu(II) sites<sup>26</sup>. The X-band parameters for NMiz and Pz are in agreement with those published by Goodgame *et al.*<sup>58</sup> and Reedijk *et al.*<sup>59</sup> respectively. The ESR spectra of the bromide compounds exhibit only a single absorption, as also observed in the  $\text{CuBr}_2(\text{py})_2$ -like series of compounds<sup>61</sup> (chapter II.4.2).

It is well known that the position of the band maximum in ligand-field spectra is a function of both the spectrochemical position of the surrounding atoms and the distortion from octahedral geometry<sup>26</sup>. The observed band maxima are all (except for  $\text{CuCl}_2(\text{NMiz})_2$ ) at ca. 14.0 kK; this is in agreement with a distorted octahedral geometry around the copper ions. Goodgame *et al.*<sup>58</sup> suggested

TABLE II.5.3. ESR AND LIGAND-FIELD MAXIMA OF COMPOUNDS  $\text{CuX}_2\text{L}_2$ , WITH X=Cl, Br AND L=Iz, NMiz, Pz AND Indz. UNCERTAINTIES IN THE LAST DIGIT ARE IN PARENTHESES

COMPOUND	ESR DATA AT Q-BAND FREQUENCIES				LIGAND-FIELD MAX.
	$g_1$	$g_2$	$g_3$	$\frac{x}{g}, \frac{y}{g_1}$	(kK)
$\text{CuCl}_2(\text{Iz})_2$	2.24(1)	2.09(1)	2.03(1)	2.12(2)	14.0(3)
$\text{CuCl}_2(\text{NMiz})_2$	2.27(1)	2.09(1)	2.04(1)	2.14(2)	12.4(3)
$\text{CuCl}_2(\text{Pz})_2$	2.27(1)	2.10(1)	2.03(1)	2.14(2)	14.2(3)
$\text{CuCl}_2(\text{Indz})_2$	2.27(1)	2.09(1)	2.04(1)	2.14(2)	13.9(3)
$\text{CuBr}_2(\text{NMiz})_2$				2.14(1)	12.5(4) sh 14.7(2)
$\text{CuBr}_2(\text{Pz})_2$				2.09(2) <sup>a</sup>	14.3(2) 21(1)
$\text{CuBr}_2(\text{Indz})_2$				2.13(2)	14.5(2) 21.7(5)

ABBREVIATIONS: sh=SHOULDER;  $x = ((g_1^2 + g_2^2 + g_3^2)/3)^{1/2}$ ;  $y$ =ISOTROPIC g-VALUES; <sup>a</sup>=A SMALL ANISOTROPY APPEARED TO OCCUR IN THIS g-VALUE.

that the compound  $\text{CuCl}_2(\text{NMiz})_2$  has a distorted tetrahedral configuration, since the band maximum occurred at 12.4 kK. Anyway, the ESR spectrum and magnetic data (see later) suggest that magnetic interaction might be present.

### Magnetic susceptibility measurements

Magnetic susceptibility measurements down to 4.2K have been carried out in order to determine whether the copper(II) ions are coupled and what kind of model is able to describe these measurements. The relevant data are in table II.5.4. The molar susceptibility values are corrected for diamagnetism of constituent atoms using Pascal's constants<sup>53</sup> and for temperature independent paramagnetism (t.i.p.) of  $60.10^{-6}$  emu/mole<sup>54</sup>. In order to describe the experimental susceptibility data for infinite copper(II) chain compounds the Heisenberg model for isotropic coupling is usually chosen. According to Jotham<sup>13</sup>, this model, having an effective spin-exchange Hamiltonian (1) where the symbols take their conventional meanings, best describes antiferromagnetically coupled linear chain copper(II) compounds. Bonner and Fisher<sup>10</sup> published a curve of theoretical susceptibility against temperature for the infinite Heisenberg  $S=\frac{1}{2}$  chain, whereas Jotham<sup>13</sup> published the polynomial expression (2) ( $P=kT/|J|$ ). The latter has the

$$H = -J \sum_{i,j} \vec{S}_i \cdot \vec{S}_j \quad \dots(1)$$

advantage that a fitting program can be used. However, at the lowest temperatures this polynomial is not correct, because it disobeys the third law of thermodynamics, i.e.  $\partial\chi/\partial T \rightarrow 0$  as  $T \rightarrow 0$ . Anyway, for values of  $kT/|J| > ca. 0.1$  the polynomial can be used.

$$\chi_M = (Ng^2\beta^2/|J|)(0.092281 + 0.18616P - 0.20556P^2 + 0.074679P^3 - 0.0091808P^4) \quad \dots(2)$$

advantage that a fitting program can be used. However, at the lowest temperatures this polynomial is not correct, because it disobeys the third law of thermodynamics, i.e.  $\partial\chi/\partial T \rightarrow 0$  as  $T \rightarrow 0$ . Anyway, for values of  $kT/|J| > ca. 0.1$  the polynomial can be used.

Anisotropic coupling is described by the Ising model (i.e. only coupling of the z-component of spin angular momentum). Fisher<sup>11</sup> published the theoretical parallel and perpendicular susceptibilities for the infinite  $S=\frac{1}{2}$  Ising chain (equations (3) and (4)). The expression for the powder susceptibility is (5).

$$\chi_{M//} = (Ng_{//}^2\beta^2/4kT) \cdot (\exp(J/kT)) \quad \dots(3)$$

$$\chi_{M\perp} = (Ng_{\perp}^2\beta^2/4|J|) \cdot (\tanh(|J|/2kT) + (|J|/2kT) \cdot (\text{sech}^2(|J|/2kT))) \dots(4)$$

$$\chi_p = (\chi_{//} + 2\chi_{\perp})/3 \quad \dots(5)$$

Following Jotham<sup>13</sup>, who published Monte-Carlo calculations on 100 and 101 atoms in a chain, the present data were also fitted to an empirical equation derived from Monte-Carlo calculations, which were improved by choosing a Morse function instead of a simple polynomial, i.e. as in (6) ( $P=kT/J$ )\*.

\* In the original paper of Jotham<sup>13</sup> formula (6) was incorrectly written.

$$\chi_M = \frac{Ng^2\beta^2}{|J|} \cdot \left\{ \frac{\exp(\frac{1}{2}P)}{4|P|} + 0.096\{ (1 - \exp(-3.55(|P| - 0.025)))^2 - 1 \} \right\} \dots (6)$$

Furthermore, Jotham showed experimentally that the parallel component of the Ising model very often adequately described the magnetic data of polymeric copper(II) compounds. For this reason the present data were also fitted with the parallel Ising component, *i.e.* expression (3).

Since dimeric copper compounds can be described with the Bleaney-Bowers<sup>14</sup> equation (7) and magnetochemists very often use magnetic data as a criterion

$$\chi_M = \frac{Ng^2\beta^2}{kT} \cdot \left\{ \frac{\exp(J/kT)}{1 + 3\exp(J/kT)} \right\} \dots (7)$$

of structure, *e.g.* dimeric or linear chain, the present magnetic susceptibility data were also fitted to this equation. In the above expressions  $\chi_M$  represents the molar susceptibility corrected for diamagnetism and t.i.p.

Using a least-squares technique, the magnetic susceptibility data of all the present compounds were fitted to the expressions (2)-(7), with parameters J and g, and to expression (5) with J,  $g_{//}$  and  $g_{\perp}$ . The results, from the best fit having the correct order of magnitude for the g-value, are in table II.5.4.

First, it is noticed that in none of the compounds the Ising model yielded appropriate g-values. The measurements will now be discussed, in their sequence of listing in table II.5.4. In figure II.5.1 the experimental susceptibility data for  $\text{CuCl}_2(\text{Iz})_2$  are plotted, together with the fits according to Jotham's expression (6) and the Bleaney-Bowers expression (7). The curve of susceptibility against temperature shows a maximum, indicating the presence of anti-

TABLE II.5.4. SUSCEPTIBILITY DATA FOR COMPOUNDS  $\text{CuX}_2\text{L}_2$ , WITH X=Cl, Br AND L=Iz, NMiz, Pz AND Indz. UNCERTAINTIES IN THE LAST DIGIT ARE IN PARENTHESES

COMPOUND	T <sub>max.</sub> (K)	χ <sub>M</sub> <sub>max.</sub> · 10 <sup>2</sup> (emu/mole)	MODELS USED IN THE DESCRIPTION OF THE SUSCEPTIBILITY								C (emu.K/mole)	θ (K)
			JOTHAM		BLEANEY-BOWERS		PARALLEL ISING		HEISENBERG			
			g	J (cm <sup>-1</sup> )	g	J (cm <sup>-1</sup> )	g	J (cm <sup>-1</sup> )	g	J (cm <sup>-1</sup> )		
CuCl <sub>2</sub> (Iz) <sub>2</sub>	7.0(3)	3.29(2)	2.19(1)	-5.36(4)	2.12(1)	-7.00(8)					0.41(2)	-1.8(3)
CuCl <sub>2</sub> (NMiz) <sub>2</sub>			2.36(2)	-2.88(8)			2.46(4)	-2.7(2)			0.42(2)	-0.5(3)
CuBr <sub>2</sub> (NMiz) <sub>2</sub>	12.8(5)	1.49(1)	2.15(1)	-11.7(1)	2.05(1)	-14.3(2)					0.41(2)	-6.8(5)
CuCl <sub>2</sub> (Pz) <sub>2</sub>			2.35(7)	-1.2(3)	2.18(2)	-1.3(3)					0.40(2)	-0.2(3)
CuBr <sub>2</sub> (Pz) <sub>2</sub>	15.0(8)	0.96(1)							2.063(5)	-19.0(1) <sup>a</sup>	0.40(3) <sup>b</sup>	-10(1) <sup>b</sup>
CuCl <sub>2</sub> (Indz) <sub>2</sub>					2.10(2)	+5.2(2)	2.21(2)	+0.9(1)			0.41(2)	+1.7(3)
CuBr <sub>2</sub> (Indz) <sub>2</sub>	17.5(5)	0.87(1)							2.06(1)	-18.7(1)	0.39(3) <sup>b</sup>	-18(2) <sup>b</sup>

<sup>a</sup> DATA HAVE BEEN FITTED INCLUDING AN IMPURITY CORRECTION, BEHAVING AS C/T; <sup>b</sup> THESE VALUES ARE NOT ACCURATE, BECAUSE ONLY A FEW POINTS OBEYED THE CURIE-WEISS LAW.

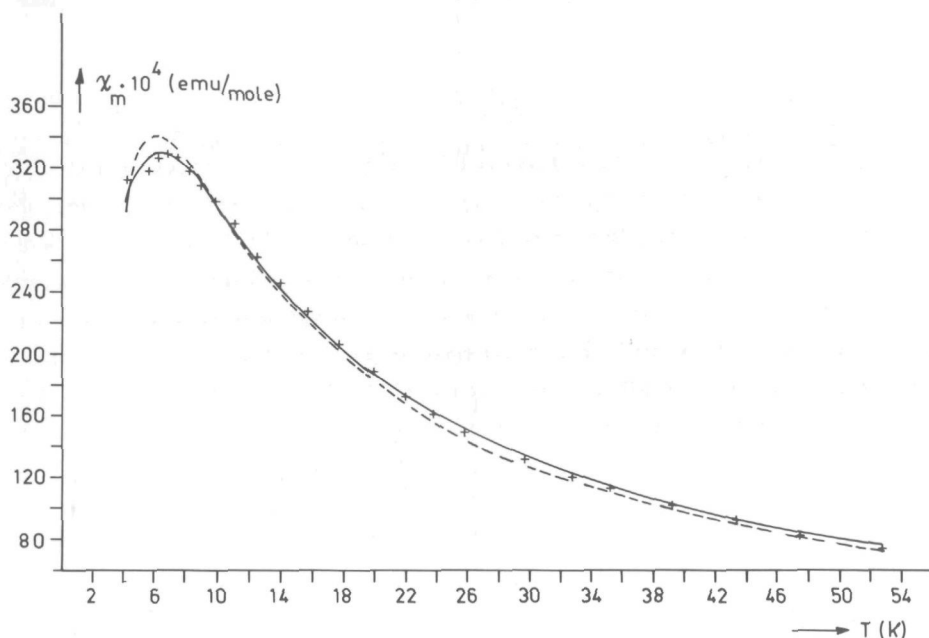


Fig. II.5.1. Molar susceptibility of  $\text{CuCl}_2(\text{Iz})_2$  as a function of temperature; (+) experimental points; the fit for  $J = -5.36 \text{ cm}^{-1}$  and  $g = 2.19$  according to the Jotham expression (full curve); the fit for  $J = -7.00 \text{ cm}^{-1}$  and  $g = 2.12$  according to the Bleaney-Bowers expression (dotted curve).

ferromagnetic coupling. The data can be described with both expressions (6) and (7) yielding acceptable  $g$ -values. While crystallographic studies on  $\text{CuCl}_2(\text{Iz})_2$  show it to be a linear chain compound<sup>19</sup>, the magnetic susceptibility data may be described not only by the Jotham (infinite chain) expression but also by the Bleaney-Bowers (dimeric) equation. This shows that in using magnetic data as a criterion for structure determination great care must be taken; to fit the data at least several models have to be tried. The magnetic behaviour cannot be described by the Heisenberg model. While the Ising model yielded a reasonable fit, the magnitude of the  $g$ -values did not agree well with those obtained from ESR spectra.

The molar susceptibility of  $\text{CuCl}_2(\text{Iz})_2$  at 4.2K seemed to be slightly dependent on the magnetic-field strength; increasing the field strength yielded a slightly increased susceptibility. Furthermore, at *ca.* 6.2K there is a discontinuity in the susceptibility-temperature curve, which becomes more obvious at lower fields and can be ascribed to long-range interchain interactions. A similar effect was found in  $\text{CuCl}_2(\text{py})_2$ <sup>62</sup>. Above *ca.* 15K the susceptibility



data obey the Curie-Weiss relation with a negative  $\theta$  value, indicative of anti-ferromagnetic coupling.

In order to determine the differences in magnetic properties on going from the Iz to the NMiz compound (in compounds of NMiz no hydrogen bridges are present) the susceptibility of  $\text{CuCl}_2(\text{NMiz})_2$  was measured. Down to 4.2K no maximum was found; however, the Curie-Weiss law was obeyed over the whole temperature region investigated, yielding a small negative  $\theta$  value. From these data it is concluded that only a small degree of exchange is present between the copper(II) ions in this compound. The data are best described with the Jotham expression (6), but this results in a too large g-value. The parallel Ising component (3) also fitted the data, but the fit was worse than the one obtained from expression (6). The observed exchange is so small that it is not possible to discriminate between

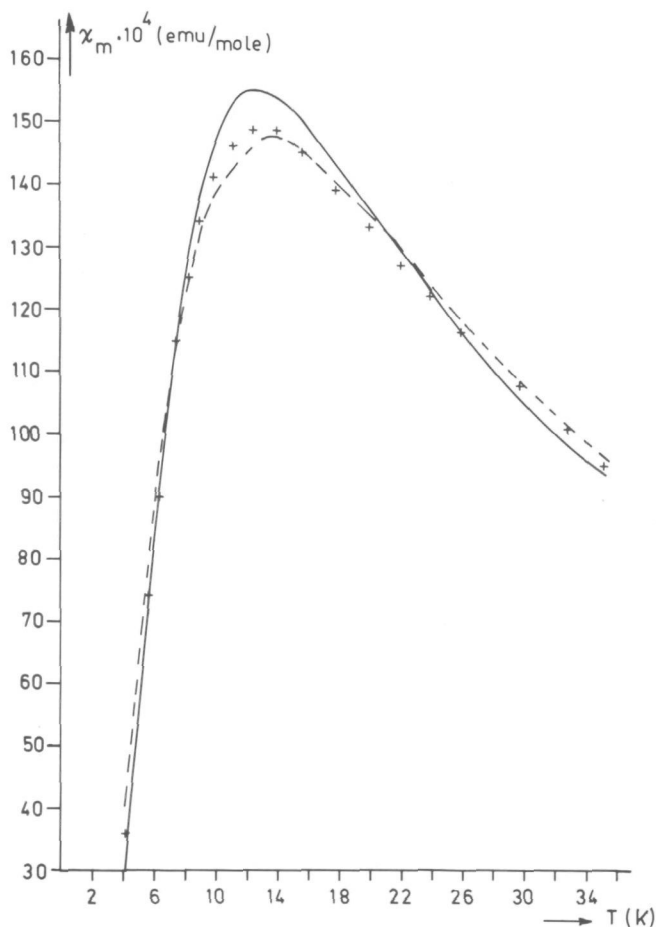


Fig. II.5.2. Molar susceptibility of  $\text{CuBr}_2(\text{NMiz})_2$  as a function of temperature; (+) experimental points; the fit for  $J = -14.3 \text{ cm}^{-1}$  and  $g = 2.05$  according to the Bleaney-Bowers expression (full curve); the fit for  $J = -11.7 \text{ cm}^{-1}$  and  $g = 2.15$  according to the Jotham expression (dotted curve).

exchange "through space" or exchange *via* a chloride bridge. The rather large difference in exchange constants between the Iz and NMiz compounds indicates that the structure of the compounds must be quite different, suggesting that the hydrogen bonding in the Iz compound is responsible for the remarkable bridge structure. (see also appendix VI.1)

The bromo analogue, *i.e.*  $\text{CuBr}_2(\text{NMiz})_2$ , showed a broad maximum in the susceptibility curve. Above *ca.* 35K the susceptibility data obey the Curie-Weiss relation with a rather large negative  $\theta$  value, indicating that the copper(II) ions are antiferromagnetically coupled. Both expressions (6) and (7) give reasonable fits (figure II.5.2), the former being the better description. The Jotham g-value of 2.15 agrees more closely with the average g-value calculated from the ESR spectrum than does the Bleaney-Bowers value of 2.05. In chapter II.6 the susceptibility data are interpreted with the alternating chain model, together with magnetization data performed at very low temperatures (1-4K).

The susceptibility curve of the compound  $\text{CuCl}_2(\text{Pz})_2$  did not show a maximum down to 4.2K. Again the susceptibility data obey the Curie-Weiss relation with a  $\theta$  value of -0.2K. From this value it is concluded that if a chain structure is present, the exchange must be very small. The Jotham and Bleaney-Bowers models both yielded good fits of equal quality and gave the same values for the parameters. From the parameters it is concluded that if this compound has a chemical chain structure it would be very interesting to determine it in order to find out what kind of bridge geometry (Cu-Cl-Cu angle and Cu-Cl distances) would lead to a net exchange equal to zero. However, it was not possible to prepare suitable single crystals.

The bromo analogue shows a very broad maximum in the susceptibility curve, but at low temperatures the susceptibility increases indicating the presence of a paramagnetic impurity. Fitting these data was only successful for the Heisenberg model including an impurity correction that behaves like a Curie law. The fit so obtained was of good quality and the agreement with calculated and experimental data indicated that this compound is a very good example of a Heisenberg chain. Since the superexchange path goes *via* bromide ions and the exchange is isotropic, this is a good example of a linear bromine-bridged chain with isotropic exchange<sup>8,61</sup>.

The compound  $\text{CuCl}_2(\text{Indz})_2$  did not show a maximum in the susceptibility curve. The data obey the Curie-Weiss relation over the whole temperature region investigated, having  $\theta = +1.7\text{K}$ . A measurement of  $\theta$  in the region 90-280K, carried out at Queen Mary College in London with a Faraday balance, agreed with the above positive value. Such a value is indicative of ferromagnetic coupling. The

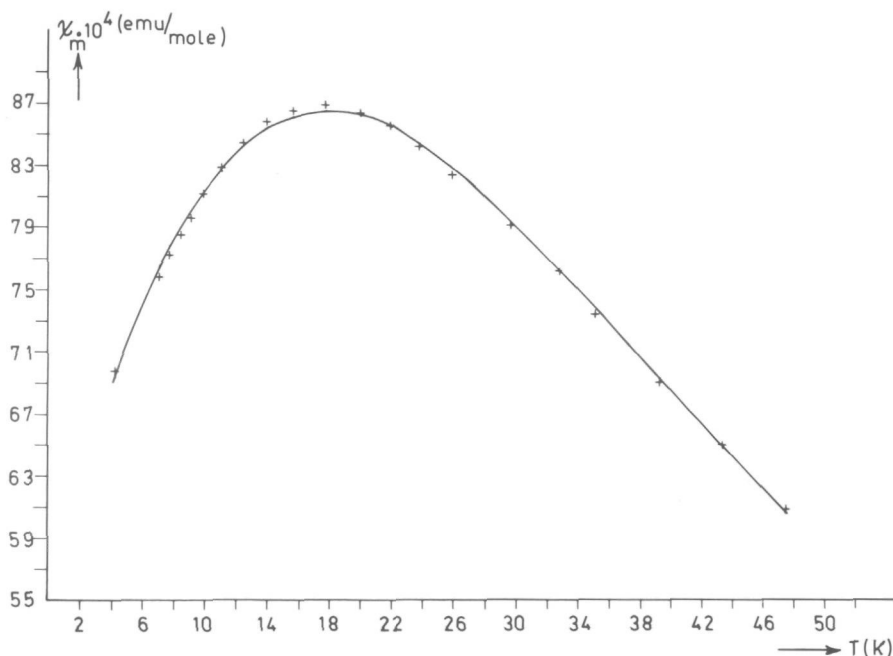


Fig. II.5.3. Molar susceptibility of  $\text{CuBr}_2(\text{Indz})_2$  as a function of temperature; (+) experimental points; the fit for  $J=-18.7 \text{ cm}^{-1}$  and  $g=2.06$  according to the Heisenberg polynomial (full curve).

data could be fitted equally well with both the parallel Ising component (3) and the Bleaney-Bowers equation (7), which differed only in  $J$  and  $g$ -values obtained. Because of this small positive exchange constant it is not possible to distinguish between a dimeric or linear chain structure from magnetic susceptibility measurements at  $> 4.2\text{K}$ ; however, it remains interesting that there is a positive  $J$ -value here. Substitutions on C atoms in the aromatic ring of the ligands mostly do not greatly affect the structures of the compounds and only small changes in bridging geometries occur, resulting in different magnetic behaviour<sup>61</sup>. For these reasons and the assumption that  $\text{CuCl}_2(\text{Pz})_2$  has a chain structure (see above) it is likely that  $\text{CuCl}_2(\text{Indz})_2$  is a ferromagnetically-coupled chain compound. Such an exchange has not been found before in  $\text{CuCl}_2(\text{ligand})_2$  chain compounds. A single crystal X-ray structure determination is required to resolve the structure. Unfortunately, thus far it was not possible to prepare single crystals.

The bromo analogue showed a very broad maximum in the susceptibility curve. A plot of the data together with the Heisenberg fit is illustrated in figure

II.5.3. At  $> ca. 35K$  the data obey the Curie-Weiss relation with a rather large and negative  $\theta$  value. The susceptibility curve can be fitted only with the Heisenberg polynomial (2); the excellent agreement between theory and experiment is shown in figure II.5.3. Again a linear chain compound having bromine bridges is described by the Heisenberg model of isotropic coupling and, as already mentioned, a good fit has seldomly been found. So, from the magnetic measurements it is concluded that the compounds  $CuBr_2(Pz)_2$  and  $CuBr_2(Indz)_2$  have similar structures.

## II.6. Alternating Antiferromagnetism in the one-dimensional Compound *caterina*-di- $\mu$ -bromobis(N-methylimidazole)Copper(II).

### II.6.1. Experimental

Single crystals of the title compound, abbreviated CNIMB, were prepared as described in chapter II.2.

Magnetic susceptibility measurements on ground single crystals were performed down to liquid-helium temperature as described in chapter V.

Magnetization measurements were performed up to very high magnetic fields (300 kG). The applied field with a duration of 17.5 ms was obtained by discharging a condenser of 30.000  $\mu$ F, 3.5 kV, across a magnet-coil with an inner diameter of 2 cm. This installation produces a sinusoidal magnetic field *vs.* time curve, with a pulse duration of 17.5 ms. Further details of the instrumentation used are described elsewhere<sup>63</sup>.

### II.6.2. Results and discussion

#### *Magnetic susceptibility measurements*

The magnetic susceptibility measurements of CNIMB are described in

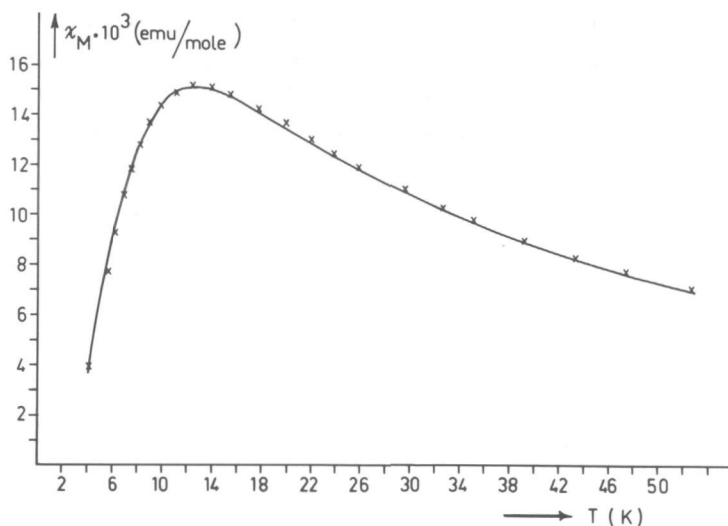


Fig. II.6.1. Molar susceptibility (x) for CNIMB as a function of temperature. The full curve with  $J = -7.2 \text{ cm}^{-1}$ ,  $\alpha = 0.4$  and  $g = 2.13$  are results of Bonner/Blöte<sup>17</sup>

chapter II.5.2. The data were interpreted with Jotham's model and the Bleaney-Bowers equation for dimeric compounds. Although the description of the magnetic data was reasonably good for the dimer model, the fact that at room temperature the compound is crystallographically a linear chain<sup>34</sup>, could not be ignored. Because recent magnetization studies (see below) pointed at an alternating magnetic exchange, the data are reinterpreted with an alternating chain model<sup>16,17</sup>.

An alternating chain is described by the following Hamiltonian:

$$H = -2J \sum_{i=1}^{n/2} (\vec{S}_{2i} \cdot \vec{S}_{2i+1} + \alpha (\vec{S}_{2i} \cdot \vec{S}_{2i-1})) - g\beta (\sum \vec{H} \cdot \vec{S})$$

Duffy and Barr<sup>16</sup> reported results on calculations using  $S=\frac{1}{2}$  down to temperatures for which  $kT/J = 0.3$  and chains, containing up to 10 spins. Very recently, Bonner and Blöte<sup>17</sup> have calculated the magnetic susceptibility as a function of temperature down to much lower temperatures for chains up to 13 spins.

In figure II.6.1 the experimental susceptibilities are shown, together with a best fit to the latter results, using calculations within the alternating chain model<sup>17</sup>. The parameters obtained are  $J = -7.2(3) \text{ cm}^{-1}$ ,  $\alpha=0.4$  and  $g=2.13(3)$ .

#### *Magnetization measurements*

One-dimensional magnetic systems show a characteristic magnetic-field dependence of their zero-temperature magnetization<sup>64</sup>. For a dimer ( $\alpha=0$ ) the magnetization is marked by a vertical increase to saturation at  $g\beta H/|J|$ , whereas in the other limit ( $\alpha=1$ ), which represents the regular  $S=\frac{1}{2}$  chain, the magnetization increases gradually to saturation. For systems with  $\alpha \neq 0$  two critical magnetic fields  $H_{c1}$  and  $H_{c2}$  can be defined. For  $T=0$ , below  $H_{c1}$ , the magnetization is zero while above  $H_{c2}$  it is saturated.

In figure II.6.2 the magnetization curves at 4.2K and 1.2K are shown, together with the best fits. The best fit has been obtained for  $J=-8.1(5) \text{ cm}^{-1}$ , and  $\alpha=0.4$ . It is clear that the experimental curve is characteristic for the alternating chain model. The agreement between the parameter values independently obtained from the magnetic susceptibility and those of the magnetization measurements is very good.

The crystal structure determination at room temperature shows the compound CNIMB to consist of linear chains, therefore at a temperature below 300K a phase transition is expected to occur, to explain the observed dimerization below ca. 50K. This phase transition could be in the form of the so-called Spin-Peierls transition<sup>65</sup>. In that case the interaction between the magnetic energy and the lattice leads to a spontaneous dimerization of the magnetic chain below

a certain temperature, and thus to alternating chain behaviour. However, neither differential thermal analysis in the 100-300K region, nor magnetic susceptibility measurements in the 4.2-100K region,<sup>\*</sup> gave evidence for a phase transition. This observation makes the magnetic properties of CNIMB even more interesting. However, to be sure that no phase transition has occurred, a crystal-structure determination at liquid-helium temperature would be most welcome.

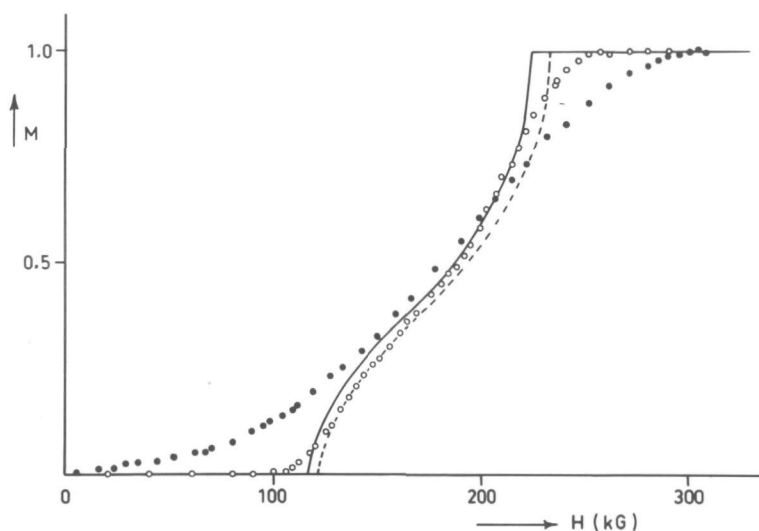


Fig. II.6.2. Relative magnetization of CNIMB as a function of the magnetic field; (o)  $T=1.15\text{K}$  and ( $\bullet$ )  $T=4.23\text{K}$ . The full curve with  $\alpha=0.4$ ,  $g=2.14$  and  $J=-7.9\text{ cm}^{-1}$  and the dotted curve with  $\alpha=0.4$ ,  $g=2.14$  and  $J=-8.1\text{ cm}^{-1}$  are the results at  $T=0\text{K}$  of Bonner/Blöte<sup>17</sup>.

<sup>\*</sup>Dr. J. Bartolomé, University of Zaragoza, Spain.

## II.7. Magnetic Superexchange in single-chlorine bridged Copper(II) Chains

### II.7.1. Experimental

Crystals of the compound  $\text{CuCl}_2(\text{Iz})_2$  were prepared as described in chapter II.5. Crystals of the compound  $\text{CuCl}_2(\text{DMSO})_2$  were prepared according to a method described in literature<sup>18</sup>. Single crystals of the compound  $\text{CuCl}_2(\text{CAF})(\text{H}_2\text{O})$  were kindly provided by Prof. Dr. M.B. Cingi\*.

The magnetic susceptibility data on  $\text{CuCl}_2(\text{MAEP})$  were obtained from Prof. Dr. W.E. Hatfield\*\*.

Abbreviations of the ligands are shown in table II.7.1.

The magnetic susceptibility data on powdered samples were performed as described in chapter V.

### II.7.2. Results and discussion

The chain structure of the present compounds is shown schematically in figure II.7.1. In all compounds the coordination around the Cu(II) centers is

approximately tetragonal pyramidal, the base being formed by two atoms of the non-chlorine atoms and two chlorides, while the axial site is occupied by another chloride. The chain is propagated through the axial chloride, which is part of the base of the adjacent tetragonal pyramid. The base is not exactly planar in none of the compounds and the distortion increases in the sequence

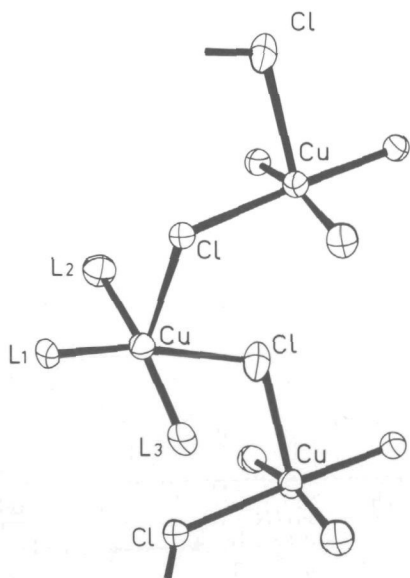


Fig. II.7.1. Schematic illustration of the single-chlorine bridged Cu(II) chains.  $L_1$ ,  $L_2$  and  $L_3$  represent the non-bridging ligands and chlorides.

\* University of Parma, Italy

\*\* University of North Carolina, Chapel Hill, U.S.A.



$\text{CuCl}_2(\text{Iz})_2$ ,  $\text{CuCl}_2(\text{MAEP})$ ,  $\text{CuCl}_2(\text{CAF})(\text{H}_2\text{O})$ ,  $\text{CuCl}_2(\text{DMSO})_2$ . In all compounds the chloride ions in the base are *trans* coordinated except in  $\text{CuCl}_2(\text{MAEP})$  in which they are in the *cis* position. Some relevant interatomic distances, angles and magnetic parameters are listed in table II.7.1.

Magnetic susceptibility measurements down to 4.2K have been carried out in order to find out the type of exchange interaction and to obtain a value for the superexchange integral, J. Hatfield *et al.*<sup>66</sup> have reported the magnetic data on the compound  $\text{CuCl}_2(\text{DMSO})_2$ . The magnetic susceptibility *vs.* temperature curve shows a broad maximum at *ca.* 14K, which is indicative for the presence of antiferromagnetically coupled Cu(II) ions. The data were described within the Ising model<sup>11</sup>. The data obtained here are in reasonable agreement with those of Hatfield *et al.*<sup>66</sup>, but are interpreted within the Heisenberg model of isotropic coupling<sup>10</sup>. The Hamiltonian used was  $H = -2J \sum S_i \cdot S_j$ , in which the symbols have their usual meaning<sup>10</sup>. Since no exact susceptibility expressions are known within the Heisenberg model, the analytical equation published by Jotham<sup>13</sup> was used. As mentioned in chapter II.5, this equation

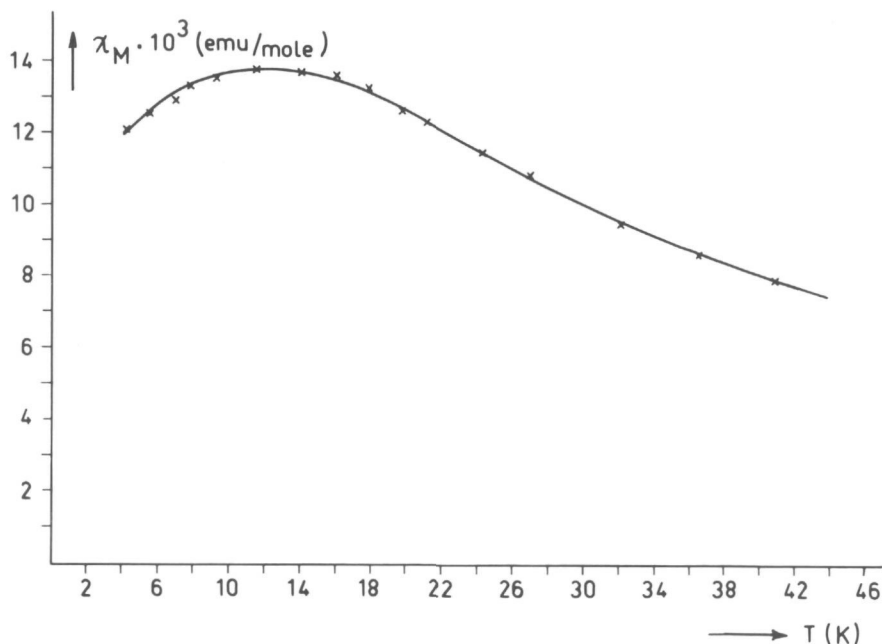


Fig. II.7.2. Molar susceptibility ( $\chi$ ) of  $\text{CuCl}_2(\text{DMSO})_2$  as a function of temperature. The full curve represents the theoretical susceptibility for a chain within the Heisenberg model with parameters,  $J = -6.2 \text{ cm}^{-1}$  and  $g = 2.11$ .

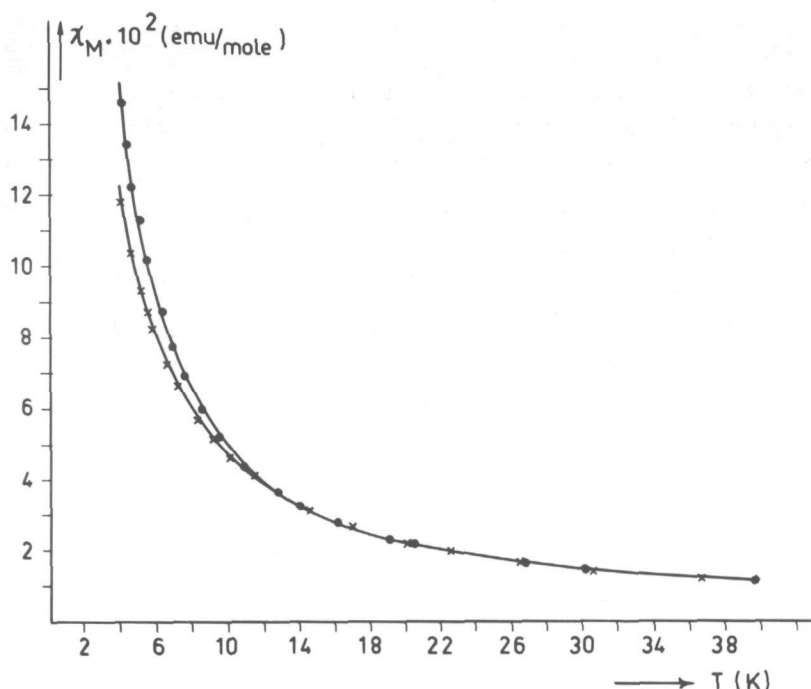


Fig. II.7.3. Molar susceptibility of  $\text{CuCl}_2(\text{MAEP})$  (●) and of  $\text{CuCl}_2(\text{CAF})(\text{H}_2\text{O})$  (x). The full curves represent the susceptibilities obtained from the parallel expression of the Ising model with parameters  $J=+1.1 \text{ cm}^{-1}$ ,  $g=2.16$  and  $J=+0.31 \text{ cm}^{-1}$ ,  $g=2.18$  for respectively  $\text{CuCl}_2(\text{MAEP})$  and  $\text{CuCl}_2(\text{CAF})(\text{H}_2\text{O})$ .

describes the results of Bonner and Fisher<sup>10</sup> very well at not too low temperatures; the advantage of such an analytical polynomial is that the fitting procedure is possible by using a computer program, which is less easy if the data must be fitted graphically. The susceptibilities fitted to this polynomial, *i.e.* expression (2) of chapter II.5, in which  $J$  is substituted for  $2J$ , yielded  $J$  and  $g$  parameters of  $-6.2(3) \text{ cm}^{-1}$  and  $g=2.11(3)$  respectively. The results are presented in figure II.7.2. From this figure it is clear that the Heisenberg model describes the magnetism of this linear  $\text{Cu(II)}$  chain very well.

In  $\text{CuCl}_2(\text{Iz})_2$  the  $\text{Cu(II)}$  ions are also coupled antiferromagnetically; however, as pointed out in chapter II.5, neither the Heisenberg, nor the Ising model described the magnetic data. An additional problem arises because of the fact that the magnetic moment of the  $\text{Cu(II)}$  ion is slightly field dependent

at 4.2K; the higher the applied field, the higher the magnetic moment. The equation presented by Jotham yielded a reasonably good fit, which was described in chapter II.5.

In figure II.7.3 the theoretical and experimental results are shown for the compounds  $\text{CuCl}_2(\text{CAF})(\text{H}_2\text{O})$  and  $\text{CuCl}_2(\text{MAEP})$ . So far no exact results are available within the Heisenberg model in the case of an infinite chain in which the interactions are ferromagnetic. However, to obtain a  $J$ -value, the data were interpreted with the parallel susceptibility expression from the Ising model (expression (3) of chapter II.5, in which  $J$  is substituted for  $2J$ ), which has shown (chapter II.5) to give a good description in the case of ferromagnetically-coupled  $\text{Cu(II)}$  ions. Fitting to this expression yielded two very good fits, shown in figure II.7.3, with parameters  $J=+1.1(1) \text{ cm}^{-1}$ ,  $g=2.16(1)$  and  $J=+0.31(4) \text{ cm}^{-1}$ ,  $g=2.18(2)$  for  $\text{CuCl}_2(\text{MAEP})$  and  $\text{CuCl}_2(\text{CAF})(\text{H}_2\text{O})$  respectively.

If one tries to correlate  $J$ -values calculated with different models it is necessary to bear in mind that these values are dependent upon the model. Therefore, the  $J$ -values obtained in the present study cannot be compared quantitatively, since three different models were used in the calculations, *i.e.* the Heisenberg model ( $\text{CuCl}_2(\text{DMSO})_2$ ), the Ising model ( $\text{CuCl}_2(\text{MAEP})$  and  $\text{CuCl}_2(\text{CAF})(\text{H}_2\text{O})$ ) and the Bleaney-Bowers equation ( $\text{CuCl}_2(\text{Iz})_2$ ). Qualitatively, however, the  $J$ -values give a clear picture of the superexchange interactions that occur in the four different compounds. In figure II.7.4 the  $\mu_{\text{eff.}}$  (defined as  $(8\chi_M \cdot T)^{\frac{1}{2}}$ ) *vs.* temperature curves for the compounds under study are shown, indicating the different exchange properties involved.

To find out which structural parameters govern the superexchange interactions in this type of single-chlorine bridged  $\text{Cu(II)}$  compounds, table II.7.1 has been constructed.

TABLE II.7.1. STRUCTURAL AND MAGNETIC PARAMETERS IN SINGLE-CHLORINE BRIDGED  $\text{Cu(II)}$  CHAIN COMPOUNDS

COMPOUND	$J$	$\text{Cu-Cl}_{b,l}^a$	$\text{Cu-Cl}_{b,s}^b$	$\text{Cu-Cu}$	$\text{Cl}_{b,s}-\text{Cu-Cl}_{b,l}$	$\text{Cu-Cl}_b-\text{Cu}$	REF.
	( $\text{cm}^{-1}$ )	( $\text{\AA}$ )	( $\text{\AA}$ )	( $\text{\AA}$ )	( $^\circ$ )	( $^\circ$ )	
$\text{CuCl}_2(\text{DMSO})_2$	-6.2(3)	2.702(2)	2.290(2)	4.757(2)	112.67(5)	144.6(1)	18
$\text{CuCl}_2(\text{Iz})_2$	-2.7(2)	2.751(6)	2.365(4)	4.37(1)	97.1(1)	117.0(9)	19
$\text{CuCl}_2(\text{CAF})(\text{H}_2\text{O})$	+0.31(4)	2.788(2)	2.319(2)	4.597(2)	89.5(1)	128.1(9)	20
$\text{CuCl}_2(\text{MAEP})$	+1.1(1)	2.785(2)	2.300(2)	4.263(2)	93.97(4)	113.58(5)	21

ABBREVIATIONS: DMSO=dimethylsulphoxide, Iz=imidazole, CAF=caffeine, MAEP=2-(2-methylaminoethyl)pyridine;

$^a = \text{Cu-Cl}_{b,l}$  IS THE LONG COPPER CHLORINE BRIDGE DISTANCE;

$^b = \text{Cu-Cl}_{b,s}$  IS THE SHORT COPPER CHLORINE BRIDGE DISTANCE.

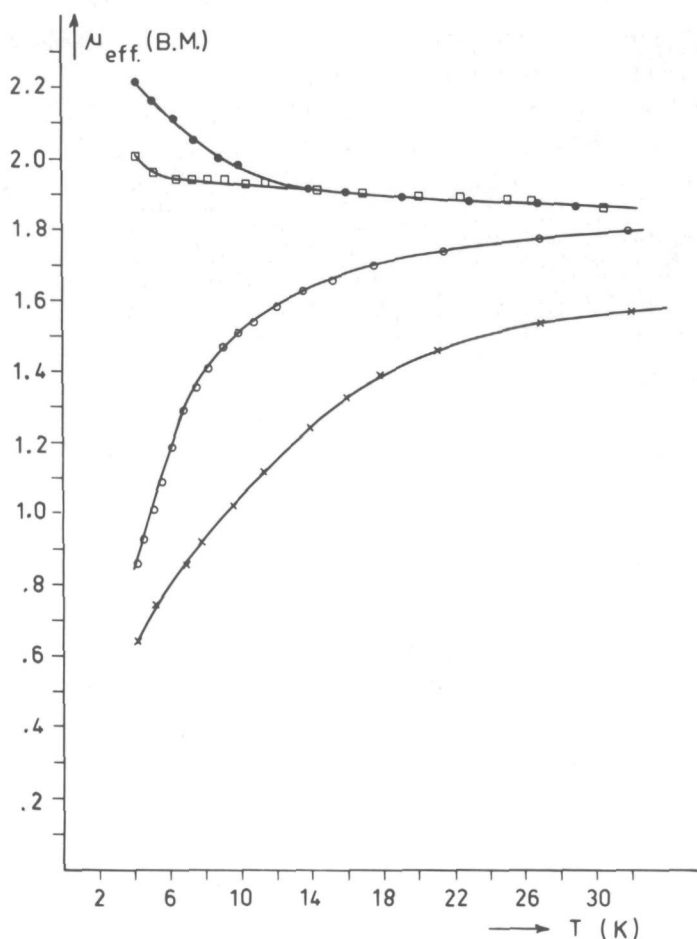


Fig. II.7.4. Effective magnetic moment per Cu(II) ion as a function of temperature for the compounds  $\text{CuCl}_2(\text{MAEP})$  ( $\bullet$ ),  $\text{CuCl}_2(\text{CAF})(\text{H}_2\text{O})$  ( $\square$ ),  $\text{CuCl}_2(\text{Iz})_2$  ( $\circ$ ) and  $\text{CuCl}_2(\text{DMSO})_2$  ( $\times$ ).

From this table it is clear that no linear relationship between the  $J$ -value and the Cu-Cl-Cu angle exists as found for dimeric hydroxo-bridged Cu(II) dimers<sup>57</sup>. It is assumed that several exchange pathways are involved; a more detailed description of these pathways is given in chapter II.11.

## II.8. Linear-chain Ferromagnetism and Spectroscopy of the Compounds



### II.8.1. Experimental

The compounds  $\text{CoCl}_2\text{L}_2$ , with L=pyrazole (Pz) and indazole (Indz), were prepared by mixing ethanol/diethylether solutions (1:1) of the hydrated Co(II) chloride and the ligand. The used ratio was slightly less than 1:2, to prevent the formation of the monomeric compound  $\text{CoL}_4\text{Cl}_2$ . For dehydration an excess of triethylorthoformate was added to the solution. The immediately-formed polycrystalline powder was filtered, washed several times with ethanol and diethylether and finally dried *in vacuo* at room temperature.

The compounds were characterized using techniques described in chapter V.

### II.8.2. Results and discussion

#### General

In table II.8.1 analytical results, X-ray types, ESR, ligand-field and far-IR data are collected. The analytical results of the compounds under study are in agreement with their chemical formulae. The IR spectra did not show the presence of either free ligand, solvent molecules, or water. For each ligand the corresponding compounds reveal similar X-ray powder patterns. The far-IR spectra all reveal a similar pattern. For the Pz compound, recently the far-IR data have been published by Barvinok *et al.*<sup>67</sup>. They found the same absorptions although a systematic error may account for a positive shift of *ca.* 5  $\text{cm}^{-1}$  for all vibrations. They tentatively assign the bands at 269 and 257  $\text{cm}^{-1}$  to M-N

TABLE II.8.1. SOME X-RAY TYPES, LIGAND-FIELD, ESR AND FAR-IR DATA OF COMPOUNDS  $\text{CoCl}_2\text{L}_2$ , WITH L=Pz, Indz AND Py

COMPOUND	X-RAY <sup>a</sup>	LIGAND-FIELD (kK) AND ESR PARAMETERS <sup>b</sup>	FAR-IR BANDS ( $\text{cm}^{-1}$ ) <sup>c</sup>
$\text{CoCl}_2(\text{Pz})_2$ <sup>d</sup>	A	6.1 9.4 15.9 19.5	269s 257s 196s <u>168br</u> 136m
$\text{CdCl}_2(\text{Pz})_2$ (1% Co)	A	$g_1=6.96$ $g_2=2.66$ $g_3=1.99$ ; $A_1=134\text{G}$ $A_2=60\text{G}$ $A_3=55\text{G}$	e
$\text{CoCl}_2(\text{Indz})_2$ <sup>d</sup>	B	6.3 9.3 16.1 19.4	236s 225s <u>165br</u>
$\text{CdCl}_2(\text{Indz})_2$ (1% Co)	B	$g_1=5.97$ $g_2=4.06$ $g_3=2.28$ ; $A_1=110\text{G}$ $A_2=60\text{G}$ $A_3=45\text{G}$	e
$\text{CoCl}_2(\text{Py})_2$	C	6.1 9.1 16.1 19.2	243sh 236s 228m <u>178br</u> <sup>f</sup>
$\text{CdCl}_2(\text{Py})_2$ (1% Co)	C	$g_1=6.39$ $g_2=4.04$ $g_3=2.74$ ; $A_1=113\text{G}$ $A_2=63\text{G}$ $A_3=40\text{G}$	e

ABBREVIATIONS: Pz=pyrazole, Indz=indazole, Py=pyridine; br=BROAD AND STRONG, s=STRONG, m=MEDIUM AND sh=SHOULDER.

<sup>a</sup>=ONLY VERY SMALL DIFFERENCES OCCURRED WITHIN THE LINE PATTERNS A,B,C; <sup>b</sup>=ESD'S ARE 0.1kK, 0.01 FOR THE g-VALUES AND 2G FOR THE A-VALUES; ESD'S IN ESTIMATED A-VALUES ARE ABOUT 10G; <sup>c</sup>=THE UNDERLINED VIBRATIONS ARE ASSIGNED TO Co-Cl VIBRATIONS, WHEREAS THE OTHERS BELONG TO Co-L VIBRATIONS; <sup>d</sup>=Pz: %Co=22.4 (cal. 22.2), %N=21.5 (cal. 21.2) %C=27.9 (cal. 27.1), %H=3.12 (cal. 3.01); Indz: %Co=16.4 (cal. 16.1), %N=15.2 (cal. 15.3), %C=46.0 (cal. 45.9). %H=3.33 (cal. 3.28); <sup>e</sup>=FOR THE Cd COMPOUNDS A BROAD MULTIPLET BETWEEN ABOUT 220 AND 150  $\text{cm}^{-1}$  IS OBSERVED, INCLUDING BOTH Cd-Cl AND Cd-L VIBRATIONS; <sup>f</sup>=REPORTED BY FERRARO<sup>78</sup>.

stretching vibrations, by comparing the spectra of the chloride and bromide. The present assignment is based on the comparison of the Pz, Indz and pyridine (py)<sup>78</sup> spectra, in which the only differences are expected to be the M-L vibration bands, just as found for the corresponding copper(II) compounds<sup>61,68</sup>.

The ligand-field spectra show very similar patterns for the Pz, Indz and py compounds; again indicative for a similar geometry around the Co(II) ion. The observed absorption bands, listed in table II.8.1, are in agreement with a distorted octahedral geometry around the Co(II) ions. Both the near-infrared and the visible band is split, indicative for the distortion of the regular octahedron<sup>69</sup>. On the high-energy side of the bands at *ca.* 19.4 kK (the  ${}^4T_{1g}(P) \leftarrow {}^4T_{1g}(F)$  transition, assuming octahedral geometry) several poorly-resolved bands are observed, which can be assigned to additional spin-forbidden transitions<sup>69</sup>.

In table II.8.1 the X-band parameters of the ESR spectra, recorded at 4.2K,

of the 1% Co(II) doped Cd analogues are also listed. From these parameters it is concluded that the geometry is tetragonally distorted with a rhombic component. In figure II.8.1 the spectra are plotted. The magnetically concentrated materials showed very broad (*ca.* 3000G) unresolved bands. From

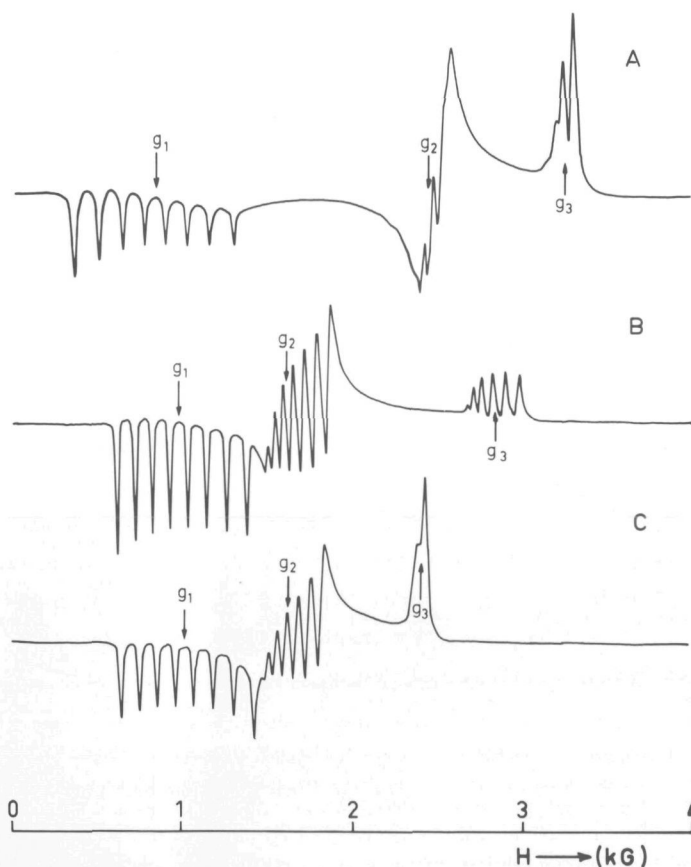


Fig. II.8.1. ESR derivative spectra of the 1% Co(II) doped compounds  $CdCl_2(Pz)_2$  (A),  $CdCl_2(Indz)_2$  (B) and  $CdCl_2(py)_2$  (C) at 4.2K at X-band frequencies.

figure II.8.1 it is clear that the Pz compound shows the smallest splitting of the  $g_2$ - and  $g_3$ - values. The spectrum of the Cu(II) doped compound<sup>70</sup> also showed the rhombicity, however, much less clear as observed for the Co(II) doped compound. These data once again show the strong dependence of the g-values on geometrical differences for the Co(II) ion.

According to Abragam and Price<sup>71</sup> a relationship exists between structural and spectral parameters, *i.e.* the g-values are very sensitive to small changes of the geometry around the Co(II) ion. With this in mind one expects that the three compounds under study should have quite large differences in the ESR spectra, just as observed. From calculations of g-values using the angular overlap model<sup>72,73</sup> it became clear, that the g-values are indeed strongly dependent on both the geometry and the choice of the angular overlap parameters, *e.g.* the  $e_g$ - and  $e_\pi$ -parameters. Hence, one has to be careful in predicting structure differences from ESR g-values only. In the present case, it seems (see II.11) that the difference in g-values for the Pz and py compounds cannot be interpreted by assuming only structural differences, since also the  $\pi$ -bond contributions to the Co-N bond are expected to be different.

The observed hyperfine values (A) for the Co(II) nucleus, are all in the range usually found for this type of compounds<sup>74</sup>.

#### *Magnetic measurements*

It is observed that the increase of the magnetic susceptibility with decreasing temperature is much larger than expected for Curie behaviour. This is indicative for the presence of ferromagnetic coupling. In addition magnetization measurements showed the occurrence of saturation effects at 4.2K, in agreement with the proposed ferromagnetism. Complete magnetic saturation could not be achieved in magnetic fields up to 18 kG, which is consistent with anisotropic interactions, similar as observed for  $\text{CoCl}_2(\text{py})_2$ <sup>75</sup>.

Since octahedral Co(II) ions behave as  $S=\frac{1}{2}$  ions below *ca.* 30K, due to the large energy gap between the ground state doublet and the first excited Kramers doublet, only those data collected at temperatures below 25K can be used in the fitting procedure within the  $S=\frac{1}{2}$  limit (see also chapter III.3). Because of saturation effects the data below *ca.* 10K could not be used in the fitting procedure.

For the description of magnetic susceptibility data of superexchange coupled  $S=\frac{1}{2}$  ions, one may use the Heisenberg<sup>10</sup>, Ising<sup>11</sup> or XY<sup>12</sup> model. The XY model (anisotropic coupling in the xy-plane only) cannot be used for the interpretation of powder data, since no theoretical expressions for the powder

susceptibility are available. Because the coupling of Co(II) ions is mostly anisotropic<sup>76</sup>, as seen also from the highly anisotropic  $g$ -values (with  $g_{//} > g_{\perp}$ ), the data are interpreted assuming the Ising spin interaction Hamiltonian  $H = -2J \sum_i S_i^z \cdot S_j^z$ , where all symbols have their usual meaning<sup>11</sup> and the summation is over nearest neighbours only. For the  $S=\frac{1}{2}$  case, the principal theoretical susceptibility expressions were given in chapter II.5 ( $J$  is substituted for  $2J$ ). Fitting the powder expression to the experimental data, yielded a very good fit for the compound  $\text{CoCl}_2(\text{Pz})_2$ , whereas for  $\text{CoCl}_2(\text{Indz})_2$  a slightly worse fit was obtained. The parameters are  $J=+7.2(6) \text{ cm}^{-1}$ ,  $g_{//}=7.9(7)$ ,  $g_{\perp}=4.6(9)$  and  $J=+7.4(9) \text{ cm}^{-1}$ ,  $g_{//}=10.8(9)$ ,  $g_{\perp}=3(1)$  for respectively the Pz and Indz compound. The obtained  $g$ -values are too large compared with the ESR results, but agree with the expected anisotropy in the interaction, *i.e.*  $g_{//} > g_{\perp}$ . The experimental data are plotted in figure II.8.2, together with the theoretical

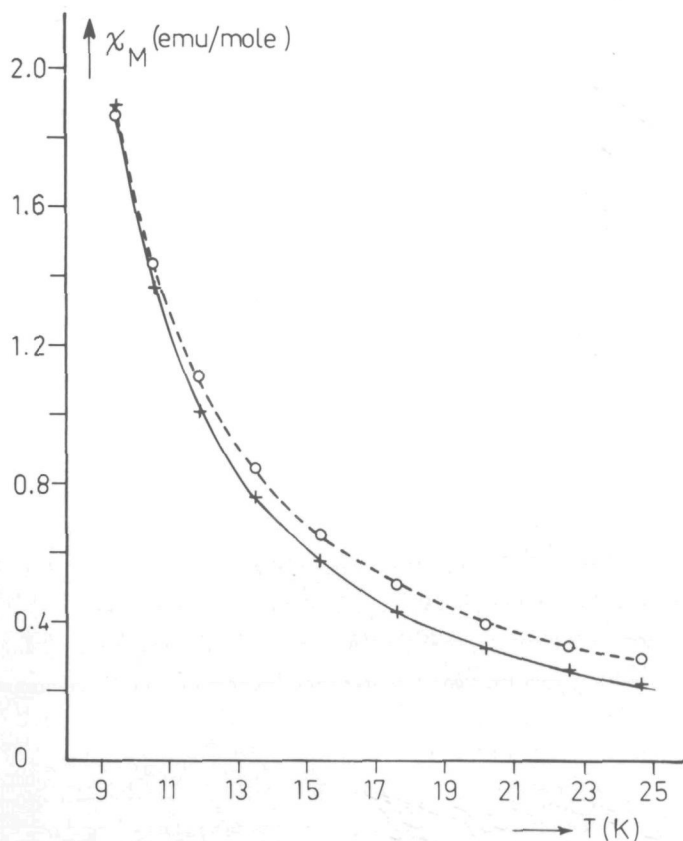


Fig. II.8.2. Molar susceptibility of  $\text{CoCl}_2(\text{Pz})_2$  (+) and  $\text{CoCl}_2(\text{Indz})_2$  (o) as a function of temperature. The full curve represents the fit (in the 9-25K region) for  $J=+7.2 \text{ cm}^{-1}$ ,  $g_{//}=7.9$  and  $g_{\perp}=4.6$  according to the Ising model. The dotted curve has parameters,  $J=+7.4 \text{ cm}^{-1}$ ,  $g_{//}=10.8$  and  $g_{\perp}=3.0$ .



fits. It is noticed that the Pz data agree very well with the calculated susceptibility values; however, the fit on the Indz data was less good. Perhaps the larger rhombicity of the g-tensor is responsible for this.

Up till now, many workers have used a single powder g-value in the fitting procedure within the Ising model. However, it is stated here, that assuming an Ising type of interaction implies the use of a parallel and a perpendicular g-value, because these will always be very different and therefore, affect the powder susceptibility unequally. The g-values from the fit agree only qualitatively with those calculated from the ESR spectra, although quantitatively the agreement is less good. Several reasons can be mentioned for the differences. First, the ESR parameters are from the Co(II) ion in the lattice of the isomorphous Cd(II) compound. In the pure cobalt lattice, distances, angles and probably g-values, could be slightly different. Groenendijk and van Duyneveldt<sup>77</sup> measured the zero-field susceptibility of  $\text{CoCl}_2(\text{Indz})_2$  between 1.2 and 4.2K. Their data showed the presence of a small ferromagnetic moment, which could be a second reason for the high g-values obtained from the present fitting results.

Groenendijk and van Duyneveldt<sup>77</sup> determined the three-dimensional ordering temperature and found it to occur at 3.8(1)K. In  $\text{CoCl}_2(\text{py})_2$  this temperature amounts to 3.2K<sup>75</sup>. Despite of the more bulky ligand, the one-dimensionality of  $\text{CoCl}_2(\text{Indz})_2$  is not as high as in the pyridine compound; this might indicate that an interchain exchange path does go *via* a hydrogen bridge (Co-Cl---H-N-N-Co), which is absent in the pyridine compound.

Recently, the data of Haseda *et al.*<sup>23</sup> were reinterpreted<sup>24</sup> with the Ising model including interchain coupling and a fit was obtained with parameters  $J=+3.8 \text{ cm}^{-1}$ ,  $g_{\parallel}=7.0$  and  $g_{\perp}=5.0$ . Neglecting interchain interactions, Haseda<sup>23</sup> earlier obtained a J-value of  $+3.5 \text{ cm}^{-1}$  with an isotropic g-value of 5.49. From the present results it is clear that the ferromagnetic coupling in the Pz and Indz compounds is stronger than the coupling in the pyridine compound. A possible reason is that the orientation of the d-orbitals in the Pz and py compounds is different; a relatively largest difference in the structure is the angle between the ligand plane and the N-Co-Cl plane. In chapter II.11 a detailed analysis of the possible relationship between exchange and structure is given.

## II.9. Compressed tetragonal Geometry in Cu(II)-doped dichlorobis-(pyrazole)Cadmium(II).

### II.9.1. Experimental

The compound  $\text{Cu}_{0.02}\text{Cd}_{0.98}\text{Cl}_2(\text{Pz})_2$ , abbreviated CCCP, (5 mmol) was prepared by mixing alcoholic solutions of the hydrated  $\text{Cu}_{0.02}/\text{Cd}_{0.98}$  chlorides and ligand in a ratio 1:2. For dehydration an excess of triethylorthoformate was added to the solution. The obtained precipitate was filtered off, washed several times with ethanol and diethylether, and finally dried *in vacuo* at room temperature.

The pure compounds  $\text{CuCl}_2(\text{Pz})_2$  and  $\text{CdCl}_2(\text{Pz})_2$  were prepared as the compounds described in chapter II.5.

The compounds were characterized using techniques described in chapter V. The copper content in the doped compound was determined from atomic absorption spectroscopy (AAS).

### II.9.2. Results and discussion.

The chemical analyses of the compounds all agree with the formula  $\text{MCl}_2(\text{Pz})_2$ . Infrared spectra and X-ray diffraction patterns of the compounds  $\text{MCl}_2(\text{Pz})_2$ , with  $\text{M}=\text{Mn}$ ,  $\text{Cd}$ ,  $\text{Cu}$  and  $\text{Cu}_{0.02}\text{Cd}_{0.98}$  have been recorded to find out whether they are isomorphous or not. The compounds having  $\text{M}=\text{Mn}$ ,  $\text{Cd}$  and  $\text{Cu}_{0.02}\text{Cd}_{0.98}$  were mutually

isomorphous according to their X-ray powder pattern and almost identical IR spectrum; the only difference being a small shift in frequency, which occurs

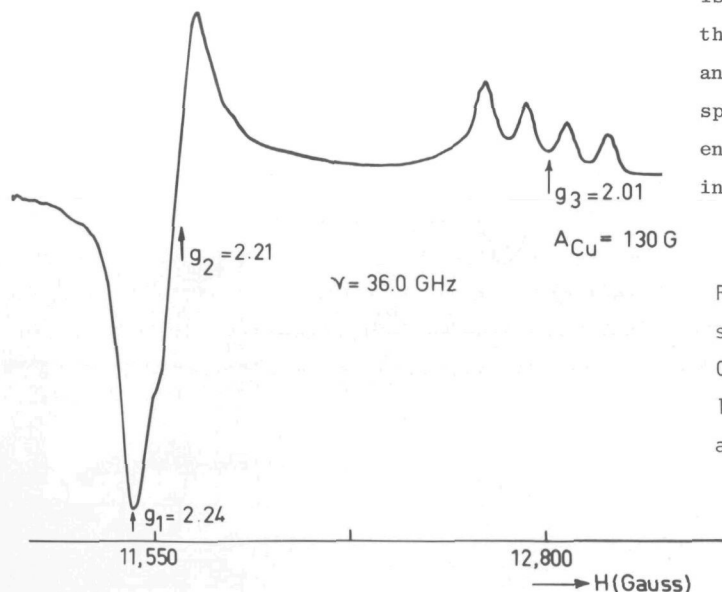


Fig. II.9.1. Q-band ESR spectrum of the compound  $\text{Cu}_{0.02}\text{Cd}_{0.98}\text{Cl}_2(\text{Pz})_2$  at liquid-nitrogen temperature.

at  $3310\text{ cm}^{-1}$  for  $M=\text{Cu}$  and at  $3340\text{ cm}^{-1}$  for the other compounds. These data suggest that the doped copper ions do not distort the Cd lattice by imposing their own preferred geometry.

The X- and Q-band ESR spectra of the compounds  $\text{CuCl}_2(\text{Pz})_2$  and CCCP were recorded at both room and liquid-nitrogen temperature. In figure II.9.1 the Q-band ESR spectrum of the compound CCCP obtained at liquid-nitrogen temperature, is illustrated. It is clearly seen from this spectrum, that  $g_{//} < g_{\perp}$ , and  $g_{//}$  is close to the free-electron  $g$ -value of 2.00. This means that the copper(II) ground state is  $d_{z^2}^{79}$ , indicating that the geometry around the copper ion in this complex is tetragonally compressed, which is very unusual for a six-coordinated Cu(II) ion.

The superhyperfine splitting on the parallel hyperfine absorption is shown in figure II.9.2. It is noticed that the hyperfine line splits into five lines having distances of *ca.* 14.6G. This pattern agrees with the theoretically expected hyperfine splitting of two equivalent N atoms. All four

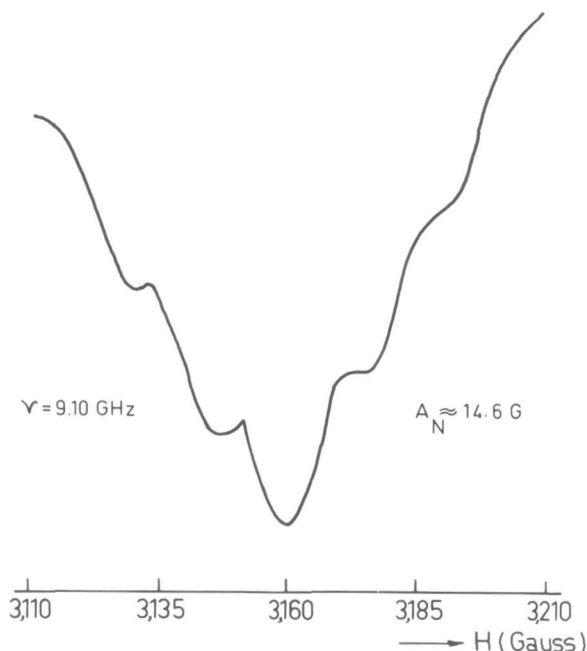


Fig. II.9.2. X-band ESR parallel hyperfine line at liquid-nitrogen temperature.

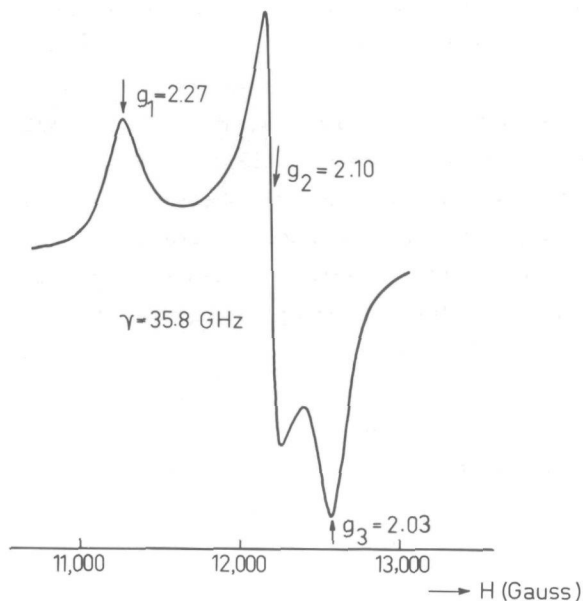


Fig. II.9.3. Q-band ESR spectrum of the compound  $\text{CuCl}_2(\text{Pz})_2$  at room temperature.

copper parallel lines ( $M_{\text{I}(\text{Cu})} = 3/2$ ) show the nitrogen splitting.

Finally, the Q-band ESR spectrum obtained at room temperature of the compound  $\text{CuCl}_2(\text{Pz})_2$  is shown in figure II.9.3.

The ligand-field spectrum of the compound  $\text{CuCl}_2(\text{Pz})_2$  showed only one very broad and intensive absorption at ca. 14.2 kK, as frequently observed in distorted octahedral  $\text{Cu}(\text{II})$  compounds<sup>59</sup>. The ligand-field spectrum of the compound CCCP shows two absorptions, i.e. at 13.5 kK a strong one and at ca. 8.9 kK a broader and weaker one. The theoretically-expected number of three absorptions in the tetragonally-compressed octahedron, were not observed; perhaps the  ${}^2\text{B}_{1g} \leftarrow {}^2\text{A}_{1g}$  and  ${}^2\text{E}_g \leftarrow {}^2\text{A}_{1g}$  transitions are not resolved in the powder reflection spectrum.

The assignment is consistent with the measured g-values, which yield an orbital reduction factor  $\lambda = \zeta_{\text{obs.}} / \zeta_{\text{free-ion}} = 0.62$ ;  $\zeta_{\text{obs.}}$  is the spin-orbit coupling parameter derived from the observed g-perpendicular value and  $\zeta_{\text{free-ion}}$  is the free-ion spin-orbit coupling parameter, being equal to  $829 \text{ cm}^{-179}$ . The hyperfine coupling constant  $A_{\text{Cu}} = 0.0113 \text{ cm}^{-1}$  then indicates that the empirical parameters determining the hyperfine coupling constants are  $P \approx 0.02$  and  $|\kappa| < 0.05$ ; the upper limit of  $\kappa$  is determined by the fact that the perpendicular Cu lines are not resolved. The fact that here  $\kappa$  is much less than 0.3 and may be negative

is additional evidence for a copper(II) ion having the unpaired hole in an  $a_{1g}$  orbital<sup>80</sup>.

The reason that in the present compound the compressed distortion is energetically more favourable compared with the compounds having the same kind of ligands without an  $\alpha$ -nitrogen proton, could be the occurrence of intra-molecular hydrogen bonding. In the X-ray powder isomorphous compound  $MnCl_2(Pz)_2$  this intra-molecular hydrogen bonding had been proven to be significant<sup>81</sup>. The ESR spectra of some other Cu(II) doped compounds  $CdCl_2L_2$ , with L=(substituted)-pyridine, imidazole or pyrazole, showed several remarkable features. Two different sites seemed to be present frequently, having  $g_{//}$ -values (both hyperfine split) of *ca.* 2.22 and 2.00 respectively. The analysis of these data will not be discussed here.

## II.10. Magnetism and Mössbauer Spectroscopy in dichlorobis(pyrazole)iron(II).

### II.10.1. Experimental

The compound  $\text{FeCl}_2(\text{pyrazole})_2$  was prepared by mixing alcoholic solutions of the hydrated  $\text{Fe(II)Cl}_2$  and pyrazole in a ratio 1:2. The immediately-formed yellow powder was washed several times with ethanol and diethylether, filtered off and finally dried *in vacuo* at room temperature.

The compound is characterized using techniques described in chapter V.

### II.10.2. Results and discussion

#### *General*

The analytical results for the present compound (C/H/N) are in agreement with the chemical formula  $\text{FeCl}_2(\text{pyrazole})_2$ . The X-ray powder pattern is rather similar to that found for  $\text{MnCl}_2(\text{pyrazole})_2$  (see also chapter II.9) which means that the structure is built up of double-chlorine bridged Fe(II) chains.

#### *Magnetism*

Magnetic susceptibility measurements down to 4.2K have been carried out in order to find out whether the Fe(II) ions are coupled magnetically or not. At low temperatures the magnetic data show a rapidly increasing magnetization per Fe(II) ion with increasing field. For applied magnetic fields above ca. 2 kG the magnetization increases gradually and no saturation occurs even in the highest field, *i.e.* 18 kG.

The use of a vibrating-sample magnetometer for molar susceptibility measurements requires that the observed moment is linearly dependent on the applied external magnetic field. Since in the present compound the moments were not linearly dependent on this field strength, it was not possible to measure the magnetic susceptibility below ca. 10K (lowest applied magnetic field that can be reached is ca. 150 G, where the data become field dependent).

The observed susceptibility values in the temperature region 10-80K do not obey Curie-Weiss relations; the magnetic data increase much stronger with decreasing temperature as is the case for a normal paramagnetic compound. It is evident that in the present system quite strong ferromagnetic intrachain interactions occur. At 4.2K also strong hystereses occurs, which is also indicative for the presence of a ferromagnetic material.

Since theoretical models for the description of ferromagnetically-coupled one-dimensional  $S=2$  systems are not available, the data could not be analyzed

in a quantitative way. Qualitatively, it seems that the system resembles  $\text{FeCl}_2(\text{bipyridyl})$ <sup>82</sup> and  $\text{FeCl}_2(\text{pyridine})_2$ <sup>75,83,84</sup>. In the latter compound the iron ions are also arranged in double-chlorine bridged chains (see *e.g.* figure II.2.2) in which the bridges are symmetric; at lower temperatures a phase transition occurs, presumably resulting in a chain structure with asymmetric bridges, just as found in the corresponding copper<sup>6</sup> and cobalt<sup>22</sup> compounds. This phase transition in  $\text{FeCl}_2(\text{py})_2$  could be followed with Mössbauer-effect measurements; however, such a phase transition was not observed in the present compound (see further).

#### Mössbauer spectroscopy

The Mössbauer spectrum of the compound  $\text{FeCl}_2(\text{pyrazole})_2$  consists of a single quadrupole doublet from 300K down to *ca.* 15K, as is illustrated in

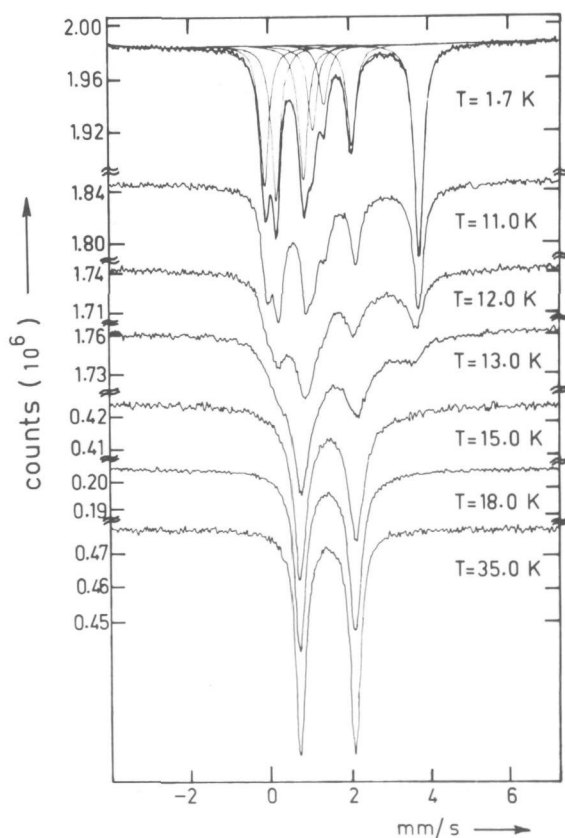


figure II.10.1. As the temperature is decreased below 15K the spectrum is observed to split into magnetic hyperfine components, indicating the onset of long-range magnetic order. The positions of the absorption lines are determined by a least-squares fitting procedure of Lorentzian lines. From the line positions the different parameters are calculated using the program of van Dongen Torman *et al.*<sup>85</sup> and Kündig<sup>86</sup>.

Fig. II.10.1. Mössbauer spectra of  $\text{FeCl}_2(\text{pyrazole})_2$  at different temperatures.

At 4.2K the spectrum is compatible with the following parameters: quadrupole splitting,  $\Delta E_q = +1.39(3)$  mm/sec, asymmetry parameter,  $\eta = 1.00(5)$ , effective hyperfine field  $H_{\text{eff.}} = 101(2)$  kG, whereas  $\theta$ , the angle between the principal component of the electric field gradient tensor and the magnetic hyperfine field, amounts to  $0(3)^\circ$ . By assuming that the principal axis  $V_{zz}$  coincides with that of the *trans* pyrazole nitrogen atoms, one can note that a value for  $\theta$  of  $0^\circ$  indicates spin alignment along the N-Fe-N axis. The isomer shift,  $IS = 1.47(3)$  mm/sec, is as expected for high spin  $Fe^{2+}$  ions in an octahedral environment.

A structural phase transition as found in  $FeCl_2(py)_2$ <sup>84</sup> is not observed in the present compound; presumably, the intramolecular hydrogen bonds between the bridging chloride ions and the hydrogen atom of the non-bonding nitrogen of the pyrazole ring, are responsible for this<sup>81</sup>.

Figure II.10.1 shows that at temperatures above the magnetic transition temperature,  $T_N$ , rather strong line broadening occurs. This effect can be explained by assuming spin-lattice relaxation, as found in  $FeCl_2(5,5'-(CH_3)_2\text{-bipy})$ <sup>82</sup>. The observed value for  $T_N$  may be influenced by this spin-lattice relaxation process; a more precise value for  $T_N$  can be obtained from specific heat measurements.



## II.11. General Discussion and Conclusions.

The results of this study support the suggestion that most polymeric compounds  $\text{CuX}_2\text{L}_2$  exhibit considerable interaction within the chains. The magnetic interactions are antiferromagnetic in nature (except for  $\text{CuCl}_2(\text{Indz})_2$  in which ferromagnetic interactions occur) and the magnitude is dependent on the type and number of substituents in the organic ligand.

This study also confirms the suggestion made by several magnetochemists (see *e.g.* Jotham<sup>13</sup> and references therein) that the Ising model cannot be used to describe the magnetic susceptibility of antiferromagnetically-coupled  $\text{Cu(II)}$  ions, although it describes very well the magnetism of exchange-coupled  $\text{Co(II)}$  ions in the low-temperature region. As is evident from the observed ESR  $g$ -values, in  $\text{Cu(II)}$  systems the exchange is almost isotropic, whereas for the octahedrally-surrounded  $\text{Co(II)}$  ions the anisotropic exchange follows from their highly anisotropic ESR  $g$ -values.

A comparison of the copper chloride and bromide compounds shows that bromide ions generally give rise to stronger coupling (higher  $|J|$  values) than chloride ions do.

To study the structural parameters that influence or determine the superexchange interactions, table II.11.1 has been constructed. In figure II.11.1 some relevant parameters are defined (it is noticed that the  $\text{M-X-M}$  bridge angle is equal to  $(180 - \alpha)^\circ$ ). Apart from the  $\text{M-M}$  and  $\text{M-X}$  distances and the  $\text{M-X-M}$  angle, the orientation of the ligand with respect to the bridge  $\text{MX}_2\text{M}$  is considered. The least-squares planes through the ligand atoms and  $\text{M}$  are almost perpendicular to the  $\text{MX}_2\text{M}$  plane, but the projection of the former plane on the latter plane makes different angles with  $\text{M-X}$  for the different compounds. Comparing  $\text{CoCl}_2(\text{Pz})_2$  and  $\text{CoCl}_2(\text{py})_2$  is only possible by taking the structural data from  $\text{MnCl}_2(\text{Pz})_2$ <sup>81</sup>. After a correction for the difference in ionic radii between  $\text{Co(II)}$  and  $\text{Mn(II)}$ , (*ca.*  $0.1 \text{ \AA}$ <sup>87</sup>) the structural differences in bond lengths are very small for the  $\text{py}$  and  $\text{Pz}$  compounds; the bridge geometry is also very similar. In fact the only difference between  $\text{CoCl}_2(\text{py})_2$  and  $\text{MnCl}_2(\text{Pz})_2$  is the ligand rotational position. The rotational position is expressed by the angle  $\beta$  (see figure II.11.1). In the pyridine compounds this angle amounts to  $58\text{--}62^\circ$ , *i.e.* a position of the ligand in between the two anions. In theazole compounds this angle is *ca.*  $72^\circ$ , *i.e.* a position much closer to one of the halide ions.

Now several explanations for the observed differences of  $J$ -values in the

TABLE II.11.1. MAGNETIC AND STRUCTURAL DATA OF SOME HALOGEN-BRIDGED CHAIN COMPOUNDS  $MX_2L_2$ 

COMPOUND	J	$\alpha^b$	$\beta^b$	$\gamma^b$	$M-X_1^c$	$M-X_2^c$	$M-M^c$	REF.
	( $cm^{-1}$ )	( $^\circ$ )	( $^\circ$ )	( $^\circ$ )	( $\text{\AA}$ )	( $\text{\AA}$ )	( $\text{\AA}$ )	
$CuCl_2(py)_2$	-9.2(2)	88.5	58.1	51.8	2.299	3.026	3.848	6
$CuCl_2(4-Etpy)_2$	-6.8(2)	88.0	61.9	53.5	2.28	3.21	4.00	3
$CuCl_2(Thia)_2$	-3.8 <sup>d</sup>	88.1	58.9	51.0	2.322	2.998	3.853	5
$CuBr_2(py)_2$	-16(1)	90.4	58.7	53.2	2.451	3.240	4.050	6
$CuBr_2(3,5-diMepy)_2$	-21(2)	90.0	61.2	53.3	2.449	3.286	4.097	II.3.
$CuBr_2(NMiz)_2$	-5.8(1)	90.0	73.8	52.8	2.494	3.291	4.130	II.2.
$CoCl_2(py)_2$	+3.8	86.7	57.6	44.2	2.435	2.507	3.593	22
$CoCl_2(Pz)_2^a$	+7.2(6)	87.1	21.7 <sup>e</sup>	43.4	2.592	2.594	3.761	a

ABBREVIATIONS: py=pyridine, 4-Etpy=4-ethylpyridine, Thia=thiazole, 3,5-diMepy=3,5-dimethylpyridine, NMiz=N-methylimidazole and Pz=pyrazole;

<sup>a</sup>=STRUCTURAL DATA WERE TAKEN FROM THE ISOMORPHOUS Mn COMPOUND (SEE TEXT); <sup>b</sup>= THE ANGLES ARE DEFINED IN FIG. II.11.1; <sup>c</sup>= $M-X_1$  IS SHORT METAL-HALOGEN DISTANCE,  $M-X_2$  IS LONG METAL-HALOGEN DISTANCE AND  $M-M$  IS METAL-METAL DISTANCE ALONG THE CHAIN; <sup>d</sup>=MAGNETICALLY THIS COMPOUND IS BEST DESCRIBED AS TWO-DIMENSIONAL; <sup>e</sup>=SINCE IN THIS CASE THE BRIDGE IS ALMOST SYMMETRIC, AN EQUALLY-USEFUL VALUE FOR  $\beta$  IS  $71.2^\circ$ .

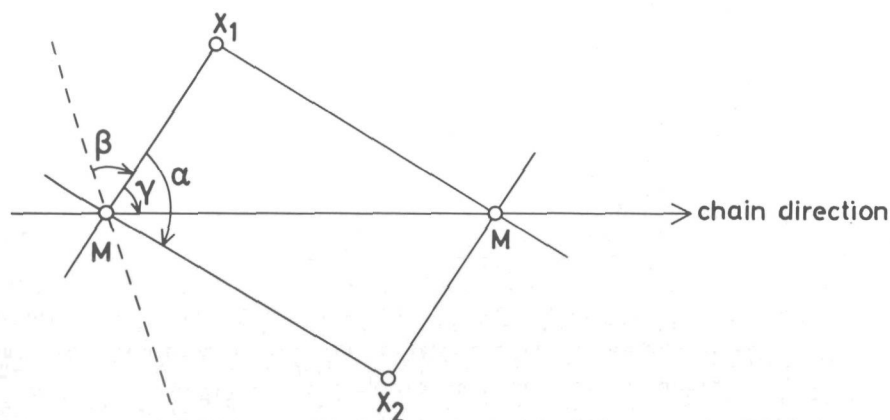


Fig. II.11.1. Definition of angles and distances used in table II.11.1.

The dotted line is the projection of the ligand plane on the MXM bridge plane.  $X=Cl, Br$ , and  $M=Cu, Co$ ; the  $M-X$  lines are the projections of the  $NMX$  planes on the bridge  $MXM$  plane, assuming the  $N-M-X_1$  and  $N-M-X_2$  angles are  $90^\circ$  what is almost the case in all compounds.

double-halogen bridged compounds will be discussed.

Firstly, there is a difference in bonding properties between the pyridine ligands and the azole ligands, influencing the ground state of the metal ion. A dramatic effect of such a ground-state dependence on the superexchange interactions has been reported by Hendrickson *et al.*<sup>88</sup> for Cu(II) dimers with several different types of ligands. However, in view of the small differences in ligand-field spectra, this contribution to the differences in the present J-values is assumed to be small. Secondly, the different rotational positions of the ligands will influence the orientation of the metal d-electrons. Therefore, the orientation of the unpaired d-electron density may vary on going from the pyridine compounds to the azole compounds. As a result the magnitude of the superexchange interactions will vary too. Kahn *et al.*<sup>89,90</sup> reported several compounds in which this orbital orientation determined the magnetic properties; in these systems the magnetic orbitals on adjacent metal ions were orthogonal, giving rise to ferromagnetic coupling. A third reason can be a contribution of the ligand to the superexchange. If direct ligand-ligand interaction *via, e.g.* the  $\pi$ -clouds, would contribute to the exchange, it is evident that a different rotational position of the ligand has a strong influence upon the J-value.

Because the number of structural data of this type of compounds is still too small, it is not yet possible to distinguish between the possibilities mentioned here.

In the present discussion the chemically one-dimensional compound  $\text{CuCl}_2(\text{thiazole})_2$  is not included, since this compound exhibits two-dimensional magnetic behaviour<sup>5</sup>.

Finally, it is noticed that in the corresponding py and Pz compounds with  $\text{M}=\text{Mn(II)}$  and  $\text{Ni(II)}$ , the interactions are antiferromagnetic and ferromagnetic respectively<sup>91,92</sup>. Furthermore, the interactions in both the py and Pz compounds are of similar magnitude, contrary to those in the Cu(II) (chapter II.4 and II.5), Co(II)<sup>75</sup> (chapter II.8) and Fe(II) compounds<sup>84</sup> (chapter II.10). These differences and the facts that the Ni, Co and Fe compounds are ferromagnetic and the Cu and Mn compounds antiferromagnetic, are not understood. The effect of zero-field splitting and different number of interacting electrons are possible origins for the occurrence of different superexchange interactions in these compounds. However, due to the limited number of structural data no quantitative discussion can be given at the moment.

For the single-chlorine bridged chain compounds table II.7.1 has already been given; the compounds are listed in a sequence in which the J-values vary

from antiferromagnetic to ferromagnetic. The bridging Cu-Cl-Cu angle varies between 144.6 and 113.6°.

According to Anderson's theory on magnetic superexchange interactions<sup>15</sup>, J-values are mainly dependent on the two possible ways of interaction for electrons. Firstly, overlap of magnetic orbitals couples the spins antiparallel and secondly, orthogonality of the magnetic orbitals couples the spins parallel, giving rise to either antiferromagnetic or ferromagnetic interactions respectively. Therefore, one has to know the orientation of the d-electrons on the metal centers. However, an additional problem arises, *i.e.* the orientation of the d-electrons on neighbouring Cu(II) ions is also different. This implies that it is very difficult to predict the amount of overlap and/or orthogonality of the magnetic orbitals involved in the superexchange paths, which makes it impossible to describe quantitatively the magnetic exchange properties in relation with the structural parameters.

From table II.7.1 it is evident that the Cu-Cl-Cu angle hardly affects the J-value, which presumably means that the differences in the interactions must be caused by the exchange contribution through the s-orbitals of the chloride ions. Assuming that the unpaired electron is within the plane in which the four shortest copper-ligand bonds occur, the different orientation of the d-electron on adjacent Cu(II) sites implies that for all compounds there will be several ferromagnetic pathways. As stated above, the antiferromagnetic pathways will be over s-orbitals of the chloride ion and therefore, will depend on the Cu-Cl distances within the bridge. As shown in table II.7.1 the long Cu-Cl bond indeed decreases on going from ferromagnetic to antiferromagnetic interactions. However, much more structural and magnetic data of compounds that differ only in small structural details are needed to find out which structural parameters determine the magnetic superexchange interactions, occurring in one-dimensional single-halogen bridged chain compounds.

A few final remarks concerning the structural and magnetic data should be made here. Experiments by Gazo *et al.*<sup>93</sup>, have demonstrated that several Cu(II) compounds occur in two so-called distortion isomers. These isomers differ slightly in their geometry around the Cu(II) ion resulting in different physical properties for each isomer. In view of the present findings (see also appendix VI.1, concerning the two forms of  $\text{CuCl}_2(\text{NMIz})_2$ ) and the occurrence of two distortion isomers for the compounds  $\text{CuCl}_2(\text{py})_2$  and  $\text{CuCl}_2(4\text{-Mepy})_2$  as recently reported by Gazo *et al.*<sup>94</sup>, it is evident that throughout the presently-investigated series of Cu(II) compounds these effects could occur also. However, since

magnetic susceptibility measurements and other spectroscopic measurements were carried out on the same samples, it is not expected that wrong conclusions were made, in those cases where structure-exchange relations have been studied.

It is further noticed that due to a lowering of temperature also the occurrence of another phase could be introduced; this was initially thought to happen in the compound  $\text{CuBr}_2(\text{NMIz})_2$  since this compound shows to consist of linear Cu(II) chains at room temperature (chapter II.2) and behaves as a magnetic alternating Cu(II) chain at temperatures below ca. 50K. However, because in no case a discontinuity in susceptibility vs. temperature curves up to ca. 100K was observed and ESR data at liquid-nitrogen temperature and room temperature for all compounds are identical, it is assumed that in the present series of compounds it is unlikely that this latter effect occurs.

## II.12. References

- (1) J.D. Dunitz, *Acta Crystallogr.*, **10**, 307 (1957).
- (2) V. Kupcik and S. Durovic, *Czech. J. Phys.*, **10**, 182 (1960).
- (3) M. Laing and G. Carr, *J. Chem. Soc. A*, 1141 (1971).
- (4) M. Laing and E. Horsfield, *J. Chem. Soc. Chem. Comm.*, 735 (1968).
- (5) W.E. Estes, D.P. Gavel, W.E. Hatfield and D.J. Hodgson, *Inorg. Chem.*, **17**, 1415 (1978).
- (6) B. Morosin, *Acta Crystallogr.*, **B31**, 632 (1975).
- (7) V.H. Crawford and W.E. Hatfield, *Inorg. Chem.*, **16**, 1336 (1977).
- (8) D.Y. Jeter and W.E. Hatfield, *J. Inorg. Nucl. Chem.*, **34**, 3055 (1972).
- (9) R.P. Eckberg and W.E. Hatfield, *J. Chem. Soc. Dalton*, 1364 (1975).
- (10) J.C. Bonner and M.E. Fisher, *Phys. Rev.*, **135A**, 640 (1964).
- (11) M.E. Fisher, *J. Math. Phys.*, **4**, 124 (1963).
- (12) S. Katsura, *Phys. Rev.*, **127**, 1508 (1962).
- (13) R.W. Jotham, *J. Chem. Soc. Dalton*, 266 (1977).
- (14) B. Bleaney and K.D. Bowers, *Proc. Roy. Soc.*, **A214**, 451 (1952).
- (15) A.P. Ginsberg, *Inorg. Chim. Acta Rev.*, **5**, 45 (1971).
- (16) W. Duffy and K. Barr, *Phys. Rev.*, **165**, 647 (1968).
- (17) J.C. Bonner and H.J. Blöte, private communication.
- (18) R.D. Willett and K'un Chang, *Inorg. Chim. Acta*, **4**, 447 (1970).
- (19) B.K.S. Lundberg, *Acta Chem. Scand.*, **26**, 3977 (1972).
- (20) G. Bandoli, M.C. Biagini, D.A. Clemente and G. Rizzardi, *Inorg. Chim. Acta*, **20**, 71 (1976).
- (21) R.A. Bream, E.D. Estes and D.J. Hodgson, *Inorg. Chem.*, **14**, 1672 (1975).
- (22) P.J. Clarke and H.L. Milledge, *Acta Crystallogr.*, **B31**, 1543 (1975).
- (23) K. Takeda, S. Matsukawa and T. Haseda, *J. Phys. Soc. Japan*, **30**, 1330 (1971).
- (24) A. Pires and D. Hone, *J. Phys. Soc. Japan*, **44**, 43 (1978).
- (25) J. Chandrasekhar and S. Subramanian, *J. Magn. Res.*, **16**, 82 (1974).
- (26) B.J. Hathaway and D.E. Billing, *Coord. Chem. Rev.*, **5**, 143 (1970).
- (27) X-ray system -version of June 1972- technical report TR-192 of the computer science center, University of Maryland, June (1972).
- (28) D.T. Cromer and J.B. Mann, *Acta Crystallogr.*, **A24**, 321 (1968).
- (29) R.F. Stewart, E.R. Davidson and W.T. Simpson, *J. Phys. Chem.*, **42**, 3175 (1965).
- (30) C.K. Johnson, ORTEP, report ORNL-3794 (1965).
- (31) E.J. Sonneveld and J.W. Visser, *J. Appl. Cryst.*, **8**, 1 (1975).
- (32) JCPDS, 1601 Parklane, Swarthmore, PA, USA.
- (33) J.W. Visser, *J. Appl. Cryst.*, **2**, 89 (1969).
- (34) J.C. Jansen, H. van Koningsveld and J.A.C. van Ooijen, *Cryst. Struct. Comm.*, **7**, 637 (1978).
- (35) W. Stählin and H.R. Oswald, *Acta Crystallogr.*, **B27**, 1368 (1971).
- (36) International Tables of Crystallography, part IV, table 2.2B (1974).
- (37) J.A. Nelder and R. Mead, *Comput. J.*, **8**, 308 (1965).
- (38) W. Lang, *Chem. Ber.*, **21**, 1578 (1888).
- (39) C.W. Frank and L.B. Rogers, *Inorg. Chem.*, **5**, 615 (1966).
- (40) J. Burgess, *Spectrochim. Acta*, **24A**, 277 (1968); 1645 (1968).
- (41) N.H. Agnew and L.F. Larkworthy, *J. Chem. Soc.*, 4669 (1965).
- (42) P.T.T. Wong and D.G. Brewer, *Can. J. Chem.*, **46**, 131 (1968).
- (43) V. Pfeiffer and V. Pimmer, *Z. Anorg. Allg. Chem.*, **48**, 49 (1906).
- (44) G.N. LaMar, *Inorg. Chem.*, **6**, 1939 (1967).
- (45) J.R. Allan, D.H. Brown, R.H. Nuttal and D.W.A. Sharp, *J. Chem. Soc. A*, 1031 (1966).
- (46) A.B.P. Lever and B.S. Ramaswamy, *Can. J. Chem.*, **51**, 1582 (1973).
- (47) P.T.T. Wong and D.G. Brewer, *Can. J. Chem.*, **46**, 139 (1968).
- (48) R.J.H. Clark and C.S. Williams, *Inorg. Chem.*, **4**, 351 (1965).

- (49) J.E. Rüede and D.A. Thornton, *J. Mol. Struct.*, **34**, 75 (1976).
- (50) D.M. Adams and W.R. Trumble, *J. Chem. Soc. Dalton*, **30** (1975).
- (51) M. Goldstein, *Inorg. Chim. Acta*, **31**, L425 (1978).
- (52) F.A. Cotton "Chemical Applications of Group Theory", Wiley-Interscience, New York (1971).
- (53) E. König, "Magnetic Properties of Coordination and Organometallic Transition Metal Complexes", Springer Verlag, Berlin (1966).
- (54) E.P. Maarschal, A.C. Botterman, S. Vega and A.R. Miedema, *Physica*, **41**, 473 (1969).
- (55) R.W. Jotham, *J. Chem. Soc. Chem. Comm.*, **178** (1973).
- (56) H.W. Richardson and W.E. Hatfield, *J. Am. Chem. Soc.*, **98**, 835 (1976).
- (57) V.H. Crawford, H.W. Richardson, J.R. Wasson, D.J. Hodgson and W.E. Hatfield, *Inorg. Chem.*, **15**, 2107 (1976).
- (58) D.M.L. Goodgame, M. Goodgame and G.W.R. Canham, *Inorg. Chim. Acta*, **3**, 406 (1969).
- (59) J. Reedijk, J.C.A. Windhorst, N.H.M. Ham and W.L. Groeneveld, *Rec. Trav. Chim.*, **90**, 234 (1971).
- (60) M. Inoue and M. Kubo, *Coord. Chem. Rev.*, **21**, 1 (1976).
- (61) J.A.C. van Ooijen and J. Reedijk, *Inorg. Chim. Acta*, **25**, 131 (1977).
- (62) K. Andres, S. Darack and S.L. Holt, *Solid State Comm.*, **15**, 1087 (1974).
- (63) H.A. Jordaan, R. Wolf and D. de Klerk, *Phys. Letters*, **44A**, 381 (1973).
- (64) L.S.J.M. Henkens, K.M. Diederix, T.O. Klaassen and N.J. Poullis, *Physica (Utrecht)*, **B81**, 259 (1976).
- (65) I.S. Jacobs, J.W. Bray, H.R. Hart jr., L.V. Interrante, J.S. Kaspers, D.E. Prober and J.C. Bonner, *Phys. Rev.*, **B14**, 3036 (1976).
- (66) N.T. Watkins, D.Y. Jeter, W.E. Hatfield and S.M. Horner, *Trans. Faraday Soc.*, 2431 (1971).
- (67) M.S. Barvinok and L.G. Lukina, *Russ. J. Inorg. Chem.*, **22**, 1173 (1977).
- (68) J.A.C. van Ooijen and J. Reedijk, *J. Chem. Soc. Dalton*, **1170** (1978).
- (69) A.B.P. Lever, "Inorganic Electronic Spectroscopy", Elsevier Publishing Company, Amsterdam (1968).
- (70) J.A.C. van Ooijen, P.J. van der Put and J. Reedijk, *Chem. Phys. Letters*, **51**, 380 (1977).
- (71) A. Abragam and M.H.L. Price, *Proc. Roy. Soc.*, **A206**, 173 (1951).
- (72) C.E. Schäffer, *Structure and Bonding*, **5**, 68 (1968).
- (73) P.J. van der Put, private communication.
- (74) P.J. van der Put and J.A.C. van Ooijen, unpublished results.
- (75) S. Foner, R.B. Frankel, W.M. Reiff, H. Wong and G.J. Long, *J. Chem. Phys.*, **68**, 4781 (1978).
- (76) L.J. de Jongh and A.R. Miedema, *Adv. Phys.*, **23**, 1 (1974).
- (77) A.J. van Duynveldt and H.A. Groenendijk, private communication.
- (78) J.R. Ferraro, "Low Frequency Vibrations of Inorganic and Coordination Compounds", Plenum Press, New York (1971).
- (79) A. Abragam and B. Bleaney, "EPR of Transition Ions", Oxford University Press, London (1970).
- (80) P.A. Narayana and K.V.L.N. Sastry, *J. Chem. Phys.*, **57**, 3266 (1972).
- (81) S. Gorter, A.D. van Ingen Schenau and G.C. Verschoor, *Acta Crystallogr.*, **B30**, 1867 (1974).
- (82) W.M. Reiff, B. Dockum, M.A. Weber and R.B. Frankel, *Inorg. Chem.*, **14**, 800 (1975).
- (83) G.J. Long, D.L. Whitney and J.E. Kennedy, *Inorg. Chem.*, **10**, 1406 (1971).
- (84) B.F. Little and G.J. Long, *Inorg. Chem.*, **17**, 3401 (1978).
- (85) J. van Dongen Torman, R. Jagannathan and J.M. Trooster, *Hyperfine Int.*, **1**, 135 (1975).
- (86) W. Kündig, *Nucl. Instr. and Meth.*, **48**, 219 (1967).
- (87) J.E. Huheey, "Inorganic Chemistry: principles of Structure and Reactivity", Harper & Row Publishers, New York (1972).

- (88) M.S. Haddat and D.N. Hendrickson, *Inorg. Chem.*, 17, 2622 (1978).
- (89) O. Kahn, R. Claude and H. Coudanne, *J. Chem. Soc. Chem. Comm.*, 1012 (1978).
- (90) O. Kahn, P. Tola, J. Galy and H. Coudanne, *J. Am. Chem. Soc.*, 100, 3931 (1978).
- (91) H.T. Witteveen, B. Nieuwenhuyse and J. Reedijk, *J. Inorg. Nucl. Chem.*, 36, 1535 (1974).
- (92) H.T. Witteveen, W.L.C. Rutten and J. Reedijk, *J. Inorg. Nucl. Chem.*, 37, 913 (1975).
- (93) J. Gazo, I.B. Bersuker, J. Garaj, M. Kabesová, J. Kohout, H. Langfelderová, M. Melnik, M. Serátor and F. Valach, *Coord. Chem. Rev.*, 19, 253 (1976).
- (94) H. Langfelderová, L. Macásková, M. Melnik, M. Kabesová and J. Gazo, *Z. Anorg. Allg. Chem.*, 445, 233 (1978).



### III. OXALATO- AND SQUARATO-BRIDGED COMPOUNDS

#### III.1. Introduction

In this chapter the magnetic superexchange interactions that occur in chain compounds having relatively large organic molecules as a bridging unit instead of halogen ions, are discussed.

Firstly, the chain compounds having oxalato dianions as the bridging unit are prepared and investigated. Thus far only two similar chain compounds have been reported, *i.e.*  $\text{FeOx}(\text{H}_2\text{O})_2$ <sup>1</sup> and  $\text{CuOx}(\text{NH}_3)_2$ <sup>2</sup>. For the compound  $\text{FeOx}(\text{H}_2\text{O})_2$  two independent X-ray structure determinations have been reported<sup>3,4</sup>. The structure is shown schematically in figure III.1.1. Each Fe(II) ion is located at the center of a distorted octahedron, having axial positions occupied by the oxygen atoms of the two water molecules, whereas the equatorial positions are occupied by four coplanar oxygens belonging to two different oxalate ( $\text{Ox}$ ) groups. Barros and Friedberg<sup>5</sup> showed that a rather strong interchain interaction exists in the compound  $\text{FeOx}(\text{H}_2\text{O})_2$ . In order to eliminate this interchain interaction, a series of compounds having the general formula  $\text{MOxL}_2$ , with  $\text{M}=\text{Ni}(\text{II})$ ,  $\text{Co}(\text{II})$ ,  $\text{Fe}(\text{II})$  and  $\text{Zn}(\text{II})$  and  $\text{L}=(\text{substituted})\text{-imidazole}$ , have been prepared.

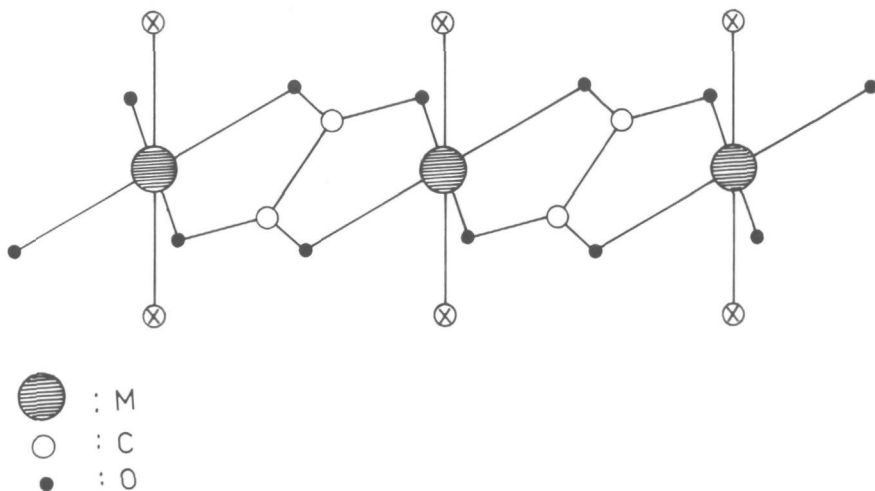


Fig. III.1.1. Schematic representation of polymeric  $\text{FeOx}(\text{H}_2\text{O})_2$  and  $\text{CuOx}(\text{NH}_3)_2$ ;  $\otimes$  is  $\text{O}(\text{H}_2\text{O})$  and  $\text{N}(\text{NH}_3)$ , respectively.

In addition the compounds having  $L=H_2O$ , were investigated for comparison.

In chapter III.2 the results of a single-crystal X-ray structure analysis on one of these new oxalate compounds, *i.e.*  $ZnOx(2\text{-methylimidazole})_2 \cdot \frac{1}{2}\text{-water}$ , are presented.

In chapter III.3 the physical (IR, far-IR, Raman, ligand-field and ESR) and magnetic susceptibility measurements in the region 4.2-100K are interpreted. For the Ni(II) compounds the magnetic susceptibility data are fitted to the results of Weng<sup>6</sup> and de Neef<sup>7</sup>. De Neef included in his calculations an axial zero-field splitting, which in most cases cannot be neglected for octahedrally-coordinated Ni(II) ions. The susceptibility data on the Co(II) compounds are interpreted with the anisotropic Ising model.

In order to study the interchain coupling interactions, Mössbauer-effect measurements on the isomorphous Fe(II) compounds have been performed down to 1.7K. The results of this study are presented in chapter III.4.

The magnetic superexchange interactions *via* the oxalato dianions appeared to be quite large, *i.e.* in the order of *ca.*  $-10\text{ cm}^{-1}$ . Dimeric oxalato-bridged compounds have been investigated thoroughly and interactions of similar magnitudes were found<sup>8</sup>. Within the dimeric compounds it is known, that the magnetic superexchange interactions strongly reduce on substitution of the oxalato anions by squarato anions<sup>8</sup>. A further aim of the present investigation, therefore is to obtain a squarato-bridged chain compound and find out how the superexchange interactions are influenced. To explain the small value of the superexchange constant,  $J$ , obtained from the interpretation of the magnetic susceptibility data in the region 1.8-100K, a structural and spectroscopic study of  $Ni(\text{squarate})(\text{imidazole})_2(H_2O)_2$  was undertaken.

The results of the single-crystal X-ray structure determination are presented in chapter III.5, whereas the spectroscopy and magnetism are described in chapter III.6.

This chapter ends with a few general conclusions about the effects of size and structure of the ligand bridge on the magnetic superexchange interaction.

## III.2. Crystal and Molecular Structure of *catena-μ-oxalato-cis-bis*(2-methylimidazole)Zinc(II). $\frac{1}{2}$ -water.

### III.2.1. Experimental

Single crystals of  $\text{ZnOx}(2\text{-methylimidazole})_2 \cdot \frac{1}{2}\text{-water}$  were prepared as described in chapter III.3.

### III.2.2. Crystal and intensity data, structure determination and refinement

From single-crystal diffractometry ( $\text{MoK}\alpha_1 = 0.70926 \text{ \AA}$ ) the following data were obtained:  $a = 13.767(5)$ ,  $b = 11.959(5)$ ,  $c = 16.993(6) \text{ \AA}$ ,  $\beta = 103.34(4)^\circ$ , space group  $\text{P}2_1/c$ ,  $D_m = 1.6 \text{ g/cm}^3$ ,  $D_c = 1.59 \text{ g/cm}^3$ , and  $Z = 8$ .

Intensities of 4149 reflections above background ( $I > 2.85\sigma(I)$ ) were collected from a nearly octahedrally-shaped crystal (approximate edge 0.4 mm) using a computer-controlled NONIUS single-crystal diffractometer with a graphite monochromator and Mo-radiation.

The crystal structure was solved by the heavy-atom method and refined by (blocked) full-matrix

least-squares calculations, using programs of the XRAY system<sup>9</sup>.

The form factors used for Zn, O, N and C were obtained from Cromer and Mann<sup>10</sup> and those for H from Stewart *et al.*<sup>11</sup>. No absorption correction has been applied ( $\mu_{\text{MoK}\alpha_1} = 18.8 \text{ cm}^{-1}$ ). The structure was solved with anisotropic thermal parameters for the non-hydrogen atoms. The assigned isotropic temperature factors of the remaining hydrogen atoms were not refined. The

TABLE III.2.1. FINAL FRACTIONAL ATOMIC COORDINATES ( $\times 10^5$  FOR THE Zn ATOMS,  $\times 10^4$  FOR THE OTHER NON-HYDROGEN ATOMS AND  $\times 10^3$  FOR THE HYDROGEN ATOMS). ESTIMATED STANDARD DEVIATIONS ARE IN PARENTHESES

ATOM	x/a	y/b	z/c	ATOM	x/a	y/b	z/c
Zn(1)	-2613(5)	19786(5)	8369(4)	C(22)	10740(5)	1602(6)	2580(4)
Zn(2)	58305(5)	31517(5)	-6285(4)	C(23)	10744(6)	1821(7)	3349(4)
C(111)	7952(5)	3164(5)	94(3)	C(24)	8551(6)	3371(7)	2294(5)
C(112)	7564(4)	2009(5)	290(3)	H(2)	980(5)	276(6)	365(4)
O(111)	6650(3)	1823(3)	39(2)	H(22)	1116(4)	115(5)	235(4)
O(112)	8191(3)	1350(3)	691(3)	H(23)	1116(5)	153(6)	382(4)
O(113)	8860(3)	3337(3)	320(3)	N(3)	4526(4)	2241(4)	-783(3)
O(114)	7308(3)	3843(3)	-267(2)	N(32)	3108(5)	1416(6)	-1236(4)
C(121)	201(4)	-290(4)	408(3)	C(31)	3728(5)	2251(6)	-1366(5)
O(121)	270(3)	275(3)	1028(2)	C(32)	4427(6)	1373(6)	-274(5)
O(122)	9572(3)	1304(3)	-378(2)	C(33)	3555(6)	881(6)	-562(5)
C(141)	5097(4)	4729(4)	423(3)	C(34)	3501(6)	3043(9)	-2068(5)
O(141)	5556(3)	3820(3)	514(2)	H(3)	271(5)	136(7)	-162(4)
O(142)	5207(3)	4752(3)	-961(2)	H(32)	468(5)	115(6)	28(4)
N(1)	1072(4)	2740(4)	752(3)	H(33)	321(5)	23(6)	-38(4)
N(12)	2173(4)	3993(5)	623(4)	N(4)	6084(4)	2921(4)	-1778(3)
C(11)	1300(5)	3825(5)	807(4)	N(42)	5984(4)	2332(5)	-3013(3)
C(12)	1853(5)	2228(6)	519(5)	C(41)	5922(5)	2038(5)	-2266(4)
C(13)	2540(5)	2988(6)	439(5)	C(42)	6279(5)	3775(6)	-2247(4)
C(14)	730(6)	4748(6)	1082(4)	C(43)	6224(6)	3443(7)	-2997(4)
H(1)	245(5)	456(5)	64(4)	C(44)	5732(7)	861(6)	-2028(5)
H(12)	185(5)	142(6)	44(4)	H(4)	576(4)	189(5)	-348(4)
H(13)	316(4)	295(5)	26(4)	H(42)	643(5)	448(5)	-207(4)
N(2)	9949(4)	2118(4)	2078(3)	H(43)	629(5)	377(5)	-344(4)
N(22)	9942(5)	2483(5)	3323(3)	O(51)	1368(4)	285(5)	-1887(3)
C(21)	9471(5)	2659(5)	2555(4)				

hydrogen atoms of the water molecule and of the methyl groups could not be located, properly due to thermal motion.

The final conventional R-value for the 4149 contributing reflections is 0.050.

The final positional parameters are listed in table III.2.1.

### III.2.3. Results and discussion

The molecular structure is shown in figure III.2.1. The 2-methylimidazole ligands are *cis*-coordinated, resulting in a rather complicated zig-zag Zn(II) chain with tetradentate bridging oxalato anions, as is illustrated in figure III.2.2.

Bond distances are listed in table III.2.2, whereas the angles are listed in table III.2.3.

In figure III.2.2 also the packing of the chains in the crystal is shown. The short interchain contacts are given in table III.2.4. The contacts *via* the water molecule are added because they play an important rôle during

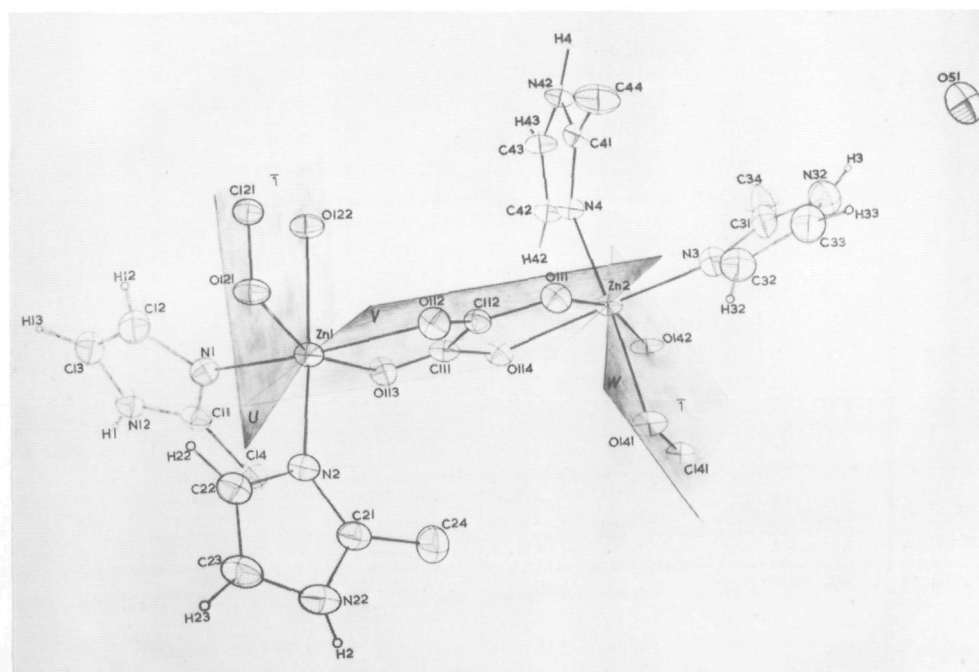


Fig. III.2.1. ORTEP<sup>44</sup> drawing of  $\text{ZnOx}(\text{2Mlz})_2 \cdot \frac{1}{2}(\text{H}_2\text{O})$ .

TABLE III.2.2. INTERATOMIC DISTANCES ( $\text{\AA}$ )

COORDINATION OF Zn(1)	RING I
Zn(1) - O(112) 2.218(5)	N(1) - C(11) 1.333(7)
Zn(1) - O(113) 2.094(4)	N(1) - C(12) 1.373(10)
Zn(1) - O(121) 2.164(4)	C(11) - C(14) 1.491(10)
Zn(1) - O(122) 2.179(4)	C(11) - N(12) 1.326(10)
Zn(1) - N(1) 2.083(5)	N(12) - C(13) 1.368(9)
Zn(1) - N(2) 2.068(5)	C(12) - C(13) 1.341(10)
COORDINATION OF Zn(2)	N(12) - H(1) 0.77(7)
Zn(2) - O(111) 2.120(4)	C(12) - H(12) 0.98(6)
Zn(2) - O(114) 2.150(4)	C(13) - H(13) 0.98(8)
Zn(2) - O(141) 2.210(4)	RING II
Zn(2) - O(142) 2.121(4)	N(2) - C(21) 1.325(9)
Zn(2) - N(3) 2.064(5)	N(2) - C(22) 1.366(8)
Zn(2) - N(4) 2.080(5)	C(21) - C(24) 1.505(10)
OXALATE SPECIAL I <sup>a</sup>	C(21) - N(22) 1.334(8)
C(121)- O(121) 1.237(6)	N(22) - C(23) 1.351(11)
C(121)- O(122) <sup>b</sup> 1.256(6)	C(22) - C(23) 1.332(10)
C(121)- C(121) <sup>b</sup> 1.535(7)	N(22) - H(2) 0.71(7)
OXALATE SPECIAL II <sup>a</sup>	C(22) - H(22) 0.93(7)
C(141)- O(141) 1.250(7)	C(23) - H(23) 0.94(6)
C(141)- O(142) <sup>b</sup> 1.254(7)	RING III
C(141)- C(141) <sup>b</sup> 1.543(7)	N(3) - C(31) 1.300(8)
OXALATE GENERAL <sup>c</sup>	N(3) - C(32) 1.377(9)
C(112)- O(111) 1.252(7)	C(31) - C(34) 1.500(12)
C(112)- O(112) 1.250(6)	C(31) - N(32) 1.363(10)
C(112)- C(111) 1.545(8)	N(32) - C(33) 1.333(10)
C(111)- O(113) 1.238(7)	C(32) - C(33) 1.325(11)
C(111)- O(114) 1.254(7)	N(32) - H(3) 0.75(6)
RING IV	C(32) - H(32) 0.97(6)
N(4) - C(41) 1.328(8)	C(33) - H(33) 1.00(7)
N(4) - C(42) 1.359(8)	C(42) - C(43) 1.321(10)
C(41) - C(44) 1.505(10)	N(42) - H(4) 0.95(6)
C(41) - N(42) 1.339(9)	C(42) - H(42) 0.90(6)
N(42) - C(43) 1.368(10)	C(43) - H(43) 0.86(7)

<sup>a</sup>=OXALATE SPECIAL I AND OXALATE SPECIAL II ARE HALF OXALATE IONS BETWEEN A Zn IN GENERAL POSITION AND AN INVERSION CENTER AS IS SHOWN IN FIGURE III.2.1; <sup>b</sup>=RELATED BY THE INVERSION CENTER; <sup>c</sup>=OXALATE GENERAL IS SITUATED BETWEEN THE TWO Zn ATOMS IN GENERAL POSITION.

TABLE III.2.3. BOND ANGLES ( $^{\circ}$ )

COORDINATION OF Zn(1)				COORDINATION OF Zn(2)				OXALATE			
O(112) - Zn(1) - O(113)	76.7(2)	O(111) - Zn(2) - O(114)	77.5(1)	O(113) - C(111) - O(114)	126.3(5)						
O(112) - Zn(1) - O(121)	88.9(1)	O(111) - Zn(2) - O(141)	88.8(2)	O(113) - C(111) - C(112)	117.2(5)						
O(112) - Zn(1) - O(122)	83.1(2)	O(111) - Zn(2) - O(142)	162.2(2)	O(114) - C(111) - C(112)	116.4(5)						
O(112) - Zn(1) - N(1)	168.2(2)	O(111) - Zn(2) - N(3)	90.7(2)	O(111) - C(112) - O(112)	126.0(5)						
O(112) - Zn(1) - N(2)	92.6(2)	O(111) - Zn(2) - N(4)	102.7(2)	O(111) - C(112) - C(111)	117.1(5)						
O(113) - Zn(1) - O(121)	159.4(2)	O(114) - Zn(2) - O(141)	87.3(1)	O(112) - C(112) - C(111)	116.9(5)						
O(113) - Zn(1) - O(122)	88.0(2)	O(114) - Zn(2) - O(142)	91.5(1)	Zn(1) - O(113) - C(111)	116.4(4)						
O(113) - Zn(1) - N(1)	93.7(2)	O(114) - Zn(2) - N(3)	167.7(2)	Zn(1) - O(112) - C(112)	111.9(4)						
O(113) - Zn(1) - N(2)	107.3(2)	O(114) - Zn(2) - N(4)	88.1(2)	Zn(1) - O(121) - C(121)	115.5(3)						
O(121) - Zn(1) - O(122)	75.6(1)	O(141) - Zn(2) - O(142)	76.5(1)	Zn(2) - O(111) - C(112)	114.7(3)						
O(121) - Zn(1) - N(1)	98.6(2)	O(141) - Zn(2) - N(3)	89.0(2)	Zn(2) - O(114) - C(111)	113.9(4)						
O(121) - Zn(1) - N(2)	87.7(2)	O(141) - Zn(2) - N(4)	166.4(2)	Zn(2) - O(141) - C(141)	113.0(3)						
O(122) - Zn(1) - N(1)	89.9(2)	O(142) - Zn(2) - N(3)	99.0(2)								
O(122) - Zn(1) - N(2)	162.8(2)	O(142) - Zn(2) - N(4)	90.8(2)								
N(1) - Zn(1) - N(2)	96.7(2)	N(3) - Zn(2) - N(4)	98.1(2)								
RING I		RING II		RING III		RING IV					
Zn(1) - N(1) - C(11)	128.2(4)	Zn(1) - N(2) - C(21)	133.6(4)	Zn(2) - N(3) - C(31)	130.6(5)	Zn(2) - N(4) - C(41)	130.4(4)				
Zn(1) - N(1) - C(12)	125.9(4)	Zn(1) - N(2) - C(22)	120.1(4)	Zn(2) - N(3) - C(32)	122.0(4)	Zn(2) - N(4) - C(42)	123.1(4)				
C(11) - N(1) - C(12)	105.4(5)	C(21) - N(2) - C(22)	106.0(5)	C(31) - N(3) - C(32)	107.2(6)	C(41) - N(4) - C(42)	105.0(5)				
N(11) - C(12) - C(13)	110.2(6)	N(21) - C(22) - C(23)	110.2(6)	N(31) - C(32) - C(33)	108.4(6)	N(41) - C(42) - C(43)	111.4(6)				
N(11) - C(12) - H(12)	120(4)	N(21) - C(22) - H(22)	119(3)	N(31) - C(32) - H(32)	139(4)	N(41) - C(42) - H(42)	125(4)				
H(12) - C(12) - C(13)	130(4)	H(22) - C(22) - C(23)	131(3)	H(32) - C(32) - C(33)	109(4)	H(42) - C(42) - C(43)	124(4)				
C(12) - C(13) - N(12)	105.4(7)	C(22) - C(23) - N(22)	105.4(6)	C(32) - C(33) - N(32)	107.6(7)	C(42) - C(43) - N(42)	105.7(6)				
C(12) - C(13) - H(13)	133(4)	C(22) - C(23) - H(23)	129(4)	C(32) - C(33) - H(33)	134(3)	C(42) - C(43) - H(43)	135(4)				
H(13) - C(13) - N(12)	121(4)	H(23) - C(23) - N(22)	125(4)	H(33) - C(33) - N(32)	119(3)	H(43) - C(43) - N(42)	119(4)				
C(13) - N(12) - C(11)	108.9(6)	C(23) - N(22) - C(21)	109.4(6)	C(33) - N(32) - C(31)	108.0(6)	C(43) - N(42) - C(41)	107.7(6)				
C(13) - N(12) - H(1)	124(5)	C(23) - N(22) - H(2)	128(5)	C(33) - N(32) - H(3)	144(6)	C(43) - N(42) - H(4)	126(4)				
H(1) - N(12) - C(11)	127(5)	H(2) - N(22) - C(21)	122(5)	H(3) - N(32) - C(31)	106(6)	H(4) - N(42) - C(41)	125(4)				
N(12) - C(11) - N(1)	110.1(6)	N(22) - C(21) - N(2)	108.9(5)	N(32) - C(31) - N(3)	108.7(6)	N(42) - C(41) - N(4)	110.1(6)				
N(12) - C(11) - C(14)	122.3(6)	N(22) - C(21) - C(24)	124.2(6)	N(32) - C(31) - C(34)	124.6(6)	N(42) - C(41) - C(44)	123.6(6)				
C(14) - C(11) - N(1)	127.5(6)	C(24) - C(21) - N(2)	126.9(6)	C(34) - C(31) - N(3)	126.7(7)	C(44) - C(41) - N(4)	126.2(6)				

crystallization: no single crystals could be grown without half a molecule of crystal water.

Initially, it was surprising that the orientation of the 2-methylimidazole ligands in the coordination geometry is *cis*, in stead of *trans* as observed for the water and ammonia compounds<sup>1,2</sup>.

Three main factors can be responsible for this. The first factor might be a particularly-strong hydrogen bonding, with respect to the *trans* arrangement. Packing of the molecules in the chains might be another reason. In case of a *trans* arrangement, large open spaces would occur, possibly hampering the packing of the chains (note, however, that packing of linear chains gives no problem with

TABLE III.2.4. SHORT INTERCHAIN CONTACTS (Å)

DIRECT:	VIA THE WATER MOLECULE
O(141) ..... N(42) 2.796(7)	O(51) ..... N(32) 2.746(8)
O(122) ..... N(22) 2.782(7)	O(51) ..... O(112) 2.771(7)
O(114) ..... N(12) 2.787(7)	O(51) ..... O(121) 3.024(8)

TABLE III.2.4. SHORT INTERCHAIN CONTACTS (Å)

DIRECT:	VIA THE WATER MOLECULE
O(141) ..... N(42) 2.796(7)	O(51) ..... N(32) 2.746(8)
O(122) ..... N(22) 2.782(7)	O(51) ..... O(112) 2.771(7)
O(114) ..... N(12) 2.787(7)	O(51) ..... O(121) 3.024(8)

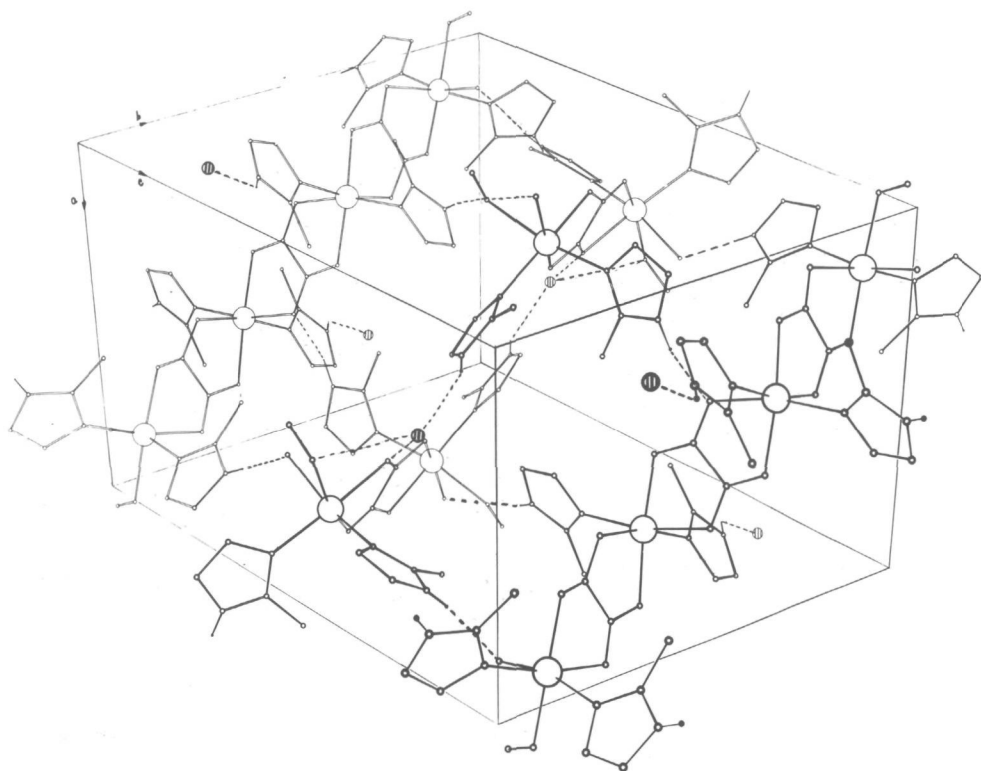


Fig. III.2.2. Packing of the chains in the crystal.

the smaller halogen bridging ligands reported in chapter II). The third and probably most important reason for the *cis* geometry might be the steric requirements of the ligand 2-methylimidazole. The methyl group at the 2-position (besides the N-donor atom) is known to be too bulky for octahedral *trans* geometry (*i.e.* only five-coordinated porphyrin  $\text{Fe}(\text{tpp})(2\text{Miz})$  with Fe displaced from the porphyrin could be obtained<sup>12</sup>). So to prevent steric hindrance between the oxalato anions and the methyl groups, *cis* geometry of the 2-methylimidazole ligands around the  $\text{Zn}(\text{II})$  ion could result.

The angles between the zinc-oxalate planes U, V and W, as defined in figure III.2.1, are 86.4, 76.5 and 17.2° between (U,V), (V,W) and (U,W) respectively.

### III.3. Magnetic Exchange and Spectroscopy in Compounds of Ni(II), Co(II) and Zn(II), with oxalato Anions as symmetric tetradentate bridging Ligands.

#### III.3.1. Experimental

All chemicals were commercially available and used without further purification. Ligands used are: water( $H_2O$ ), 2-methylimidazole(2MIz), 1,2-dimethylimidazole(DMIz) and benzimidazole(BIz). Applied physical measurements are in V.

On mixing solutions of the Ni, Co and Zn metal(II) chlorides (5 mmol) and the ligand (20 mmol) in  $H_2O$  and of sodium oxalate (5 mmol) in  $H_2O$ , very finely-divided powders separated. These powders were filtered and washed with dry ethanol and diethylether and dried *in vacuo* at room temperature.

#### III.3.2. Results and discussion

##### General

Table III.3.1 lists the compounds with their analytical data. All chemical analyses are in good agreement with the listed formulae. The nickel compounds are blue, the cobalt compounds are pink, whereas the zinc compounds are white.

In addition some zinc compounds doped with *ca.* 2% Co(II) were prepared

TABLE III.3.1. CHEMICAL ANALYSES OF COMPOUNDS  $MOxL_2$ , WITH M=Ni, Co for ESR measurements AND Zn, Ox=OXALATO DIANION AND L=WATER OR SUBSTITUTED-IMIDAZOLE (*vide infra*).

COMPOUND	%M		%N		%C		%H	
	cal.	exp.	cal.	exp.	cal.	exp.	cal.	exp.
NiOx(2MIz) <sub>2</sub>	18.9	18.9	18.0	17.5	38.6	38.3	3.9	4.1
CoOx(2MIz) <sub>2</sub>	19.0	18.7	18.0	17.8	38.6	38.0	3.9	4.1
ZnOx(2MIz) <sub>2</sub>	20.6	20.1	17.6	17.7	37.8	37.9	3.8	3.9
NiOx(DMIz) <sub>2</sub>	17.3	17.2	16.5	16.0	42.5	42.0	4.7	4.8
CoOx(DMIz) <sub>2</sub>	17.4	17.6	16.5	16.0	42.5	43.0	4.7	4.9
ZnOx(DMIz) <sub>2</sub>	18.9	19.2	16.2	16.0	41.7	41.7	4.6	4.8
NiOx(BIz) <sub>2</sub>	15.3	15.3	14.6	14.4	50.2	49.2	3.1	3.2
CoOx(BIz) <sub>2</sub>	15.4	15.2	14.6	14.2	50.1	48.8	3.1	3.1
ZnOx(BIz) <sub>2</sub>	16.8	16.7	14.4	14.2	49.3	48.4	3.1	3.3
NiOx( $H_2O$ ) <sub>2</sub>	32.1	32.0	-	-	13.1	13.1	2.2	2.8 <sup>a</sup>
CoOx( $H_2O$ ) <sub>2</sub>	32.2	32.3	-	-	13.1	13.2	2.2	2.5
ZnOx( $H_2O$ ) <sub>2</sub>	34.5	34.3	-	-	12.7	12.9	2.1	2.2

ABBREVIATIONS: 2MIz=2-methylimidazole, DMIz=1,2-dimethylimidazole, BIz= benzimidazole;

<sup>a</sup>=DIFFERENT SAMPLES YIELDED HYDROGEN PERCENTAGES IN THE REGION 2.8-3.0 (SEE TEXT).

X-ray powder diffraction patterns show that compounds with the same ligand but with different metal ions (including Fe(II), to be described in chapter III.4) are powder iso-morphous, except for water where differences occur in the line positions and relative intensities. Probably the strong hydrogen bridges are responsible for these differences.



Another exception is the compound  $\text{NiOx}(\text{2Miz})_2$ , which has a completely different set of lines, although the IR spectra of all 2Miz compounds are almost identical.

For the compound  $\text{NiOx}(\text{H}_2\text{O})_2$ , the water content found by chemical analysis exceeded the theoretical content. This suggests that some additional water molecules are enclosed in the crystal structure. Small differences in the IR spectrum of this compound are observed, compared with the other water compounds. Furthermore, some additional differences in the results of the physical measurements occur (*vide infra*).

### *Infrared and Raman spectra*

Infrared spectra were obtained for all compounds and for the free ligands. In addition, Raman spectra of the zinc compounds have been recorded. The spectra show frequencies due to both ligand vibrations and to oxalate vibrations. The IR spectra of the compounds with the same ligand are almost identical. Comparison with the IR spectra of the free ligands and the Raman spectra of other zinc complexes with these ligands ( $\text{ZnCl}_2\text{L}_2$ ) yields the position of the oxalate vibrations in the spectra of the new compounds. The wavenumbers of the bands for  $\text{ZnOx}(\text{2Miz})_2$ , are listed in table III.3.2. Data for  $\text{Na}_2\text{Ox}$  and  $\text{FeOx}(\text{H}_2\text{O})_2$  are included because, in these compounds, the oxalato anion is crystallographically known to have also  $\text{D}_{2h}$  symmetry<sup>13</sup>. From table III.3.2 it is concluded that in

the new compounds, the oxalato anions also have approximately  $\text{D}_{2h}$  symmetry and must act as tetradentate ligands. Comparison with the data of compounds, whose crystal structure determinations have proved the tetradentate coordination of the oxalato anions, confirms this<sup>14-16</sup>. The only difference is that in the present compounds the asymmetrical C-O stretching vibration

TABLE III.3.2. OXALATE ABSORPTIONS IN THE IR AND RAMAN FREQUENCIES ( $\text{cm}^{-1}$ )

DESCRIPTION			$\text{ZnOx}(\text{2Miz})_2$		$\text{Na}_2\text{Ox}$		$\text{FeOx}(\text{H}_2\text{O})_2$
			RAMAN	IR	RAMAN	IR	IR
$\nu_1$	$\text{A}_g$	C-O STRETCH (SYM)	1465		1455		
$\nu_2$	$\text{A}_g$	C-C STRETCH	915		880		
$\nu_3$	$\text{A}_g$	O-C-O BENDING (SYM)	525		482		
$\nu_4$	$\text{A}_u$	INACTIVE					
$\nu_5$	$\text{B}_{1g}$	C-O STRETCH (SYM)	1630		1642		
$\nu_6$	$\text{B}_{1g}$	C-C-O BENDING (SYM)	585		568		
$\nu_7$	$\text{B}_{2u}$	C-C-O BENDING (ASYM)		485		510	480
$\nu_8$	$\text{B}_{3g}$	OUT OF PLANE	a		220		
$\nu_9$	$\text{B}_{2u}$	C-O STRETCH (ASYM)		1675 1605 <sup>b</sup>	1612 <sup>c</sup>	1630	1630 <sup>d</sup>
$\nu_{10}$	$\text{B}_{1u}$	OUT OF PLANE		a	270 <sup>c</sup>		
$\nu_{11}$	$\text{B}_{3u}$	C-O STRETCH (ASYM)		1320	1355 <sup>c</sup>	1315	1315
$\nu_3 + \nu_{12}$	$\text{B}_{3u}$	COMBINATION BAND		1365		1335	1360
$\nu_{12}$	$\text{B}_{3u}$	O-C-O BENDING (ASYM)		800	800 <sup>c</sup>	780	815

<sup>a</sup>=COULD NOT BE ASSIGNED. BECAUSE OF THE STRONG OVERLAP OF THIS BAND WITH THE M-Ox AND M-L VIBRATIONS THAT OCCUR IN THE SAME REGION; <sup>b</sup>=SPLITTING CAUSED BY A SMALL LOWERING OF THE LATTICE SITE SYMMETRY; <sup>c</sup>=FORBIDDEN LINE; <sup>d</sup>=VERY BROAD ABSORPTION BAND.

at ca.  $1650\text{ cm}^{-1}$  is split into two components. This splitting may be due to a lowering of the lattice site symmetry or a combination band. Another reason may be the differences in C-O distances, as occurs in  $\text{ZnOx}(\text{2MIz})_2 \cdot \frac{1}{2}\text{H}_2\text{O}$  (see chapter III.2). A similar splitting occurs in some dimeric niobium compounds described by Kergoat and Guerschais<sup>17</sup> in which the oxalato anion also serves as a tetradentate bridging ligand.

### Far-infrared spectra

Far-infrared spectra were recorded in order to confirm that all present compounds have similar structures and to see if M-L vibrations could be assigned. In the far-IR region ( $500\text{--}20\text{ cm}^{-1}$ ) the metal-oxygen and metal-ligand vibrations are expected to occur. The absorptions observed in the  $450\text{--}50\text{ cm}^{-1}$  region for the  $\text{MOxL}_2$  compounds with the ligand bands are listed in table III.3.3. In this table some tentative assignments are also included. It is clear that a strong mixing occurs between the M-Ox, M-L and oxalate vibrations. However, all compounds reveal the same pattern, indicating that the same type of structure must be present.

Theoretically, 8 IR-active vibrations ( $2\text{B}_{1u}$ ,  $3\text{B}_{2u}$ ,  $3\text{B}_{3u}$ ) are expected for the  $\text{MO}_4\text{N}_2$  unit under  $\text{D}_{2h}$  symmetry. However, it has to be realized that by taking such a unit to calculate the number of expected bands, vibrations due to

TABLE III.3.3. FAR-INFRARED DATA OF COMPOUNDS  $\text{MOxL}_2$ , WITH  $\text{Ox}=\text{OXALATO DIANION}$ ,  $\text{M}=\text{Ni, Co, Zn}$  AND  $\text{L}=\text{WATER}$ , OR SUBSTITUTED-IMIDAZOLE

COMPOUND	OBSERVED ABSORPTIONS <sup>x</sup> ( $\text{cm}^{-1}$ )										
2MIz			380m	358m		271s		151m	115m	98m	
$\text{NiOx}(\text{2MIz})_2$	<u>427m</u>	<u>405m</u>	385s		<u>296s</u>	273m	<u>252m</u>	220w	195m	175m	74m
$\text{CoOx}(\text{2MIz})_2$	<u>420m</u>	<u>405m</u>	385s		<u>270br</u>			176br			
$\text{ZnOx}(\text{2MIz})_2$	<u>425m</u>	<u>410w</u>	384s		<u>234br</u>			177m	158s		
DMIz	430m					272s					
$\text{NiOx}(\text{DMIz})_2$	450s	<u>429m</u>	<u>411m</u>		<u>300s</u>	272m	<u>259m</u>	215m	181m	163m	
$\text{CoOx}(\text{DMIz})_2$	443s	<u>413m</u>	<u>396m</u>		<u>273s</u>		<u>239m</u>	196m	162m	147m	
$\text{ZnOx}(\text{DMIz})_2$	441s	<u>417m</u>	<u>403m</u>		<u>242s</u>		<u>220w</u>	203m	182m	171w	155m 141m
BIz	416s			270s				241s	227m	155s	106s
$\text{NiOx}(\text{BIz})_2$	432m	<u>423s</u>	<u>403m</u>	292m	<u>300s</u>		<u>273s</u>	254m	225s	170br	
$\text{CoOx}(\text{BIz})_2$	430w	<u>421s</u>	<u>400m</u>	292m	<u>283m</u>		<u>264s</u>	228s	198m	149m	
$\text{ZnOx}(\text{BIz})_2$	432m	<u>424m</u>	<u>408m</u>	288m	<u>245s</u>		<u>230s</u>	195w	148s		
$\text{NiOx}(\text{H}_2\text{O})_2$		<u>450br</u>		<u>358m</u>	<u>332s</u>		<u>285s</u>	252w	203s		
$\text{CoOx}(\text{H}_2\text{O})_2$		<u>445br</u>		<u>355m</u>	<u>306s</u>		<u>282m</u>	182s	153m		
$\text{ZnOx}(\text{H}_2\text{O})_2$		<u>425br</u>		<u>295s</u>	<u>250s</u>		<u>240s</u>	195m	147s		

ABBREVIATIONS: br=BROAD AND STRONG, s=STRONG, m=MEDIUM, w=WEAK;

<sup>x</sup>SINGLE UNDERLINED BANDS HAVE  $\text{Ox-M-Ox}$  AND DOUBLE UNDERLINED BANDS HAVE M-L CHARACTER.

ligand-wagging and ligand-torsion are neglected. Furthermore, one out-of-plane vibration ( $B_{1u}$ ) of the oxalato anion occurs at *ca.*  $270\text{ cm}^{-1}$ , a region where also M-Ox and M-L vibrations are expected, some of which having the same symmetry and giving rise to coupling of vibrations. The theoretically-expected features described here are observed for all compounds by the occurrence of a broad absorption in the  $250\text{--}300\text{ cm}^{-1}$  region. In addition, absorptions of the free ligand are known to occur in the  $200\text{--}300\text{ cm}^{-1}$  region. For reasons outlined above, no attempt was made to give a complete far-IR data assignment; only Ox-M-Ox and M-L vibrations were assigned tentatively.

The sequence of the vibrations Ni-Co-Zn is just as expected from electro-negativity and mass of the metal ions; however, the two highest Ox-M-Ox vibrations do not follow this sequence and it is assumed, that these are C-O-M-O-C ring vibrations.

### *Ligand-field spectra*

The band maxima, and calculated values of Dq and B for the nickel and cobalt compounds are listed in table III.3.4. Dq is the ligand-field splitting and B the Racah parameter for an octahedral environment of the metal ion. These parameters are calculated using published methods, dealing with averaged environment<sup>18,19</sup>.

The observed differences in the Dq values may be due to differences in steric hindrance of the various ligands.

Examination of the position of  $(\text{Ox})^{2-}$  and  $\text{H}_2\text{O}$  in the spectrochemical series<sup>20</sup> shows that the Dq values in the present compounds are unusually high.

TABLE III.3.4. LIGAND-FIELD DATA OF COMPOUNDS  $\text{MOxL}_2$ , WITH  $\text{M}=\text{Ni}$  AND  $\text{Co}$ ,  
L=WATER OR SUBSTITUTED-IMIDAZOLE

COMPOUND <sup>x</sup>	$3T_{1g}(P)^+$	$3T_{1g}(F)^+ 1E_g^+$	$3T_{2g}^+ 3A_{2g}$	Dq	B
	(kK)	(kK)	(kK)	( $\text{cm}^{-1}$ )	( $\text{cm}^{-1}$ )
NiOx(2MIz) <sub>2</sub>	26.0	16.0 13.7sh	9.4	940	878
NiOx(DMIz) <sub>2</sub>	26.0	15.9 13.7sh	9.4	945	871
NiOx(BIz) <sub>2</sub>	25.6	15.6 13.3sh	9.0	900	895
NiOx(H <sub>2</sub> O) <sub>2</sub>	25.6 27.4 <sup>a</sup>	15.7 14.0sh	9.4	935	922
	$4T_{1g}(P)^+$	$4A_{2g}^+$	$4T_{2g}^+ 4T_{1g}(F)$		
CoOx(2MIz) <sub>2</sub>	19.3	16.5sh	8.6	940	785
CoOx(DMIz) <sub>2</sub>	19.4	16.5sh	8.6	935	795
CoOx(BIz) <sub>2</sub>	18.9	16.5sh	8.3	910	775
CoOx(H <sub>2</sub> O) <sub>2</sub>	20.0	17.0sh	8.5	930	840

ABBREVIATION: sh=SHOULDER; <sup>x</sup>=E.S.D. IS 0.1kK; <sup>a</sup>=THIS SPLITTING IS CAUSED BY A LOWERING OF SYMMETRY, PROBABLY DUE TO ADDITIONAL WATER MOLECULES IN THE CRYSTAL LATTICE (SEE TEXT).

This may be due to a lattice effect, as is found in some hydrates or due to a  $\pi$ -back-bonding effect of the symmetrically-bridging oxalato anions, resulting in a lowering of the (partly) filled  $t_{2g}$  orbitals. The B-values occur in the region expected for octahedral Co(II) and Ni(II) compounds.

TABLE III.3.5. ESR PARAMETERS AT X-BAND FREQUENCIES OF COMPOUNDS  $MOxL_2$ , WITH M=98% Zn AND 2% Co (UNCERTAINTIES IN THE g-VALUES ARE 0.01; A-VALUES ARE ACCURATE TO ABOUT 2G IN THE IDEAL SPLITTING CASE)

COMPOUND	$g_1 = g_{//}$	$g_2$	$g_3$	$g_{\perp} = (g_2 + g_3)/2$	$A_1 = A_{//}$	$A_2$	$A_3$
					(G)	(G)	(G)
$MOx(H_2O)_2$	6.28	3.70	2.62	3.16	86	$\approx 51$	$\approx 24$
$MOx(2Miz)_2$	6.29	3.62	2.52	3.07	70 <sup>a</sup>	b	b
$MOx(DMiz)_2$	5.67	3.81	3.81	3.81	70	$\approx 34$	
$MOx(BIz)_2$	5.68	4.20	2.78	3.49	76 <sup>a</sup>	b	b

<sup>a</sup>=THE HYPERFINE STRUCTURE IS NOT COMPLETELY RESOLVED; (IN THE IDEAL CASE THE ABSORPTIONS SPLIT INTO 8 LINES ( $M_I(\text{Co}) = 7/2$  AND ONE EXPECTS  $2I+1=8$  SPLITTINGS)); <sup>b</sup>=NO HYPERFINE STRUCTURE IS OBSERVED

### Electron spin resonance spectra

The ESR spectra of the Co-doped Zn compounds are collected in table III.3.5. Commonly, these parameters can be used to obtain information about the structure of and the bonding in the compounds. The main goal was to confirm the tetragonal geometry and to find out a possible deviation from axial symmetry.

To obtain sufficiently-sharp resonance lines, the samples have to be cooled below *ca.* 20K in order to increase the spin-lattice relaxation time. In this temperature region, high-spin octahedral Co(II) compounds behave as having fic-

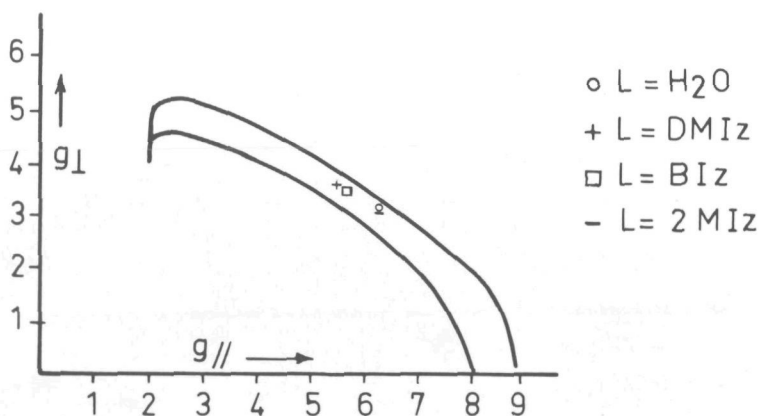


Fig. III.3.1. Experimental values of  $g_{//}$  plotted against  $g_{\perp}$ ; drawn curves are the theoretical ones for weak- (upper) and strong-field (lower-curve).

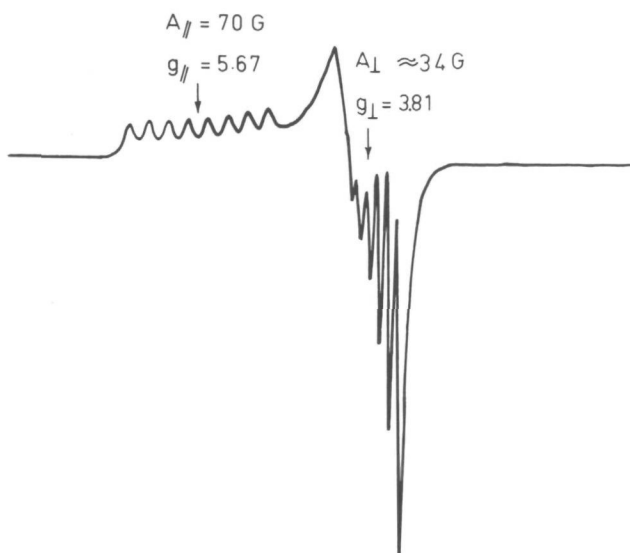


Fig. III.3.2. ESR derivative curve of the 2% Co-doped compound  $\text{ZnOx(DMIz)}_2$  at 4.2K.

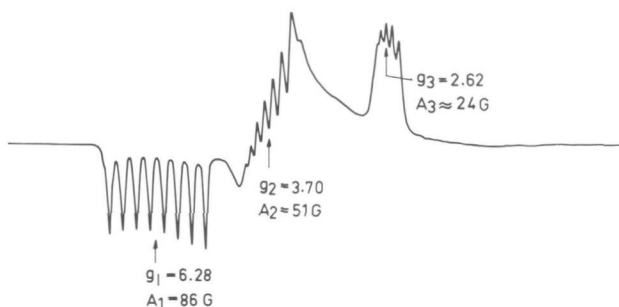
titious  $S=\frac{1}{2}$  spin systems.

Theories about the interpretation of spectral data and the relation with ligand-field parameters were published by Abragam and Price<sup>21</sup>. They described theoretical curves of  $g_{||}$  and  $g_{\perp}$  plotted against each other in the weak- and

strong-field approximations for trigonal symmetry. According to Abragam and Price<sup>21</sup> a relationship exists between structural and spectral parameters. The  $g$ -values are extremely sensitive to small changes in the geometry around the  $\text{Co(II)}$  ion.

In figure III.3.1, the present experimental  $g_{||}$  and  $g_{\perp}$  are plotted against each other and compared with the theoretical plots given by Abragam and Price. Two illustrative spectra are drawn in figure III.3.2 (axial) and figure III.3.3 (rhombic). Most of the spectra show three  $g$ -values, characteristic for rhombic geometry; in those cases the value  $(g_2 + g_3)/2$  was used to calculate  $g_{\perp}$ . Experimental values fall between the two extreme cases of weak-field (upper curve) and strong-field (lower curve).

Fig. III.3.3. ESR derivative curve of the 2% Co-doped compound  $\text{ZnOx(H}_2\text{O)}_2$  at 4.2K.



The observed  $A_{//}$  values for the compounds are all in the region of 70G; this value is frequently found for imidazoles that are octahedrally coordinated to Co(II) and that have  $g_{//} > g_{\perp}^{22}$ .

From the ESR experiment, it is concluded that in the present compounds the  $\text{Co}^{2+}$  ion is octahedrally coordinated; however, only the DMiz compound shows strict axial symmetry, whereas all other compounds reveal a rhombic distortion. It is remarkable that only for the ligand without an acid N-H group, is axial symmetry observed, suggesting that hydrogen bonding between the azole ligands and the oxalato anions is significant. Strong hydrogen bonds indeed occur in the 2Miz compounds, as described in chapter III.2.

### *Magnetic measurements*

Magnetic susceptibility measurements at low temperatures (4.2-100K) were carried out to determine the sign and magnitude of the superexchange coupling between the metal ions and to confirm the chain behaviour. For all compounds the susceptibility vs. temperature curves show a broad maximum, indicating that the metal ions are coupled antiferromagnetically. To describe the experimental susceptibility data, a model is needed. The basic properties of the models can be understood from the spin interaction Hamiltonian as presented in chapter I.

Determination of the thermodynamic functions starting from this general interaction Hamiltonian, gives rise to severe problems. Until now closed-form expressions of the partition function could be derived only for the  $S=\frac{1}{2}$  Ising model<sup>23</sup>, the  $S=\frac{1}{2}$  XY model<sup>24</sup> and for the classical limit  $S \rightarrow \infty$  with arbitrary spin dimensionality<sup>25-27</sup>. Numerical approximations concerning the thermodynamic properties of infinite chain systems are available. Bonner and Fisher<sup>28</sup> and Weng<sup>6</sup> applied the methods of extrapolation from limited chain-length calculations to obtain thermodynamic values for the infinite chain. Weng neglected the influence of zero-field splitting for ions  $S > \frac{1}{2}$  on the thermodynamics of such chains. In fact all ions with  $S > \frac{1}{2}$  (except those in an S-state) may exhibit a large zero-field splitting. Recently, de Neef<sup>7</sup> published some thermodynamic properties of linear chains with Heisenberg exchange and crystal-field anisotropy for  $S=1$  ions. De Neef found that the influence of the zero-field splitting on the specific heat is more pronounced than on the magnetic susceptibility. Since the present data concern only the magnetic susceptibility, in the description of the magnetic data, both Weng's results and de Neef's results for the  $S=1$  systems (Ni(II) chains) are considered. For the  $S=\frac{1}{2}$  system - as is the case for Co(II) at low temperatures - the results of Bonner and Fisher<sup>28</sup> are available for the Heisenberg model.

Within the Ising model, closed-form expressions for the parallel and perpendicular susceptibility are available for the  $S=\frac{1}{2}$  systems<sup>26</sup>. For the  $S=1$  system no expressions for the powder susceptibility are available within the Ising and XY model.

In the present chapter the experimental susceptibility data have been interpreted in the light of the aforementioned calculations and approximations. It should be noted that especially in the isotropic case, much more theoretical work has been done, *i.e.* high temperature series expansions<sup>29</sup>, Green's function approaches<sup>30</sup>, low temperature approximations<sup>31</sup> (spin wave theory). However, using all these available results would lead too far from the present goal of this work, namely to find out if the chain compounds are magnetically one-dimensional and to obtain an indication for the strength of the magnetic superexchange interactions.

In the next section, the experimental magnetic susceptibility data of the Ni and Co chains will be described and discussed.

#### *Nickel compounds*

All susceptibility *vs.* temperature curves show a broad maximum, typical for an antiferromagnetically-coupled spin system. Principally the metal ions can be coupled in three different ways, *i.e.* in dimers, one-dimensional chains and two-dimensional planes. Ginsberg<sup>33</sup> published the theoretical expression for the susceptibility of Ni(II) dimers, but it was not possible to describe the present data with this expression. Furthermore, Hendrickson *et al.*<sup>8</sup> has published magnetic data of crystallographically established dimeric oxalato-bridged nickel compounds. Comparing their data with the present data it is noticed that the susceptibility maxima are much broader and lower, whereas  $T_{\text{max}}$  is of the same order of magnitude. Distinguishing between one- and two-dimensional structures from magnetic measurements on powders is more difficult; however, from the IR spectra of the compounds under discussion and that of *e.g.*  $\text{FeOx}(\text{H}_2\text{O})_2$  and  $\text{ZnOx}(\text{2Miz})_2 \cdot \frac{1}{2}\text{H}_2\text{O}$ , it is clear that chain structures are involved here. Moreover, C-O and C-C-O vibrations will differ for the bis-bidentate (chain) and the tetramonodentate (plane) cases.

From these arguments, it is assumed that in the present compounds the metal ions are coupled in oxalato-bridged chains. This is confirmed by the agreement between calculations according to the infinite chain models and the observed susceptibility data, *vide infra*.

The relevant susceptibility data for the compounds  $\text{NiOxL}_2$  are listed in

table III.3.6, together with the  $J$  and  $g$  parameters obtained for the different one-dimensional models. Within the Heisenberg model, the present susceptibility data were fitted to both Weng's and de Neef's results. Weng<sup>6</sup> has published results obtained from extrapolation of limited chain-length calculations, neglecting zero-field splittings. De Neef<sup>7</sup> did the same, but included an axial zero-field splitting  $D$ , taking an extra term in the Hamiltonian, namely  $-D \sum (S_i^z - \frac{2}{3})$ . Some results according to Weng and de Neef, together with the experimental data of the compound  $\text{NiOx}(\text{2Miz})_2$ , are plotted in figure III.3.4. Within the Ising model no theoretical expressions for the powder susceptibility are available.

From figure III.3.4 it is seen that the present data can be described within the Heisenberg model (for temperatures above *ca.* 40K), with and without a  $D$ -term.

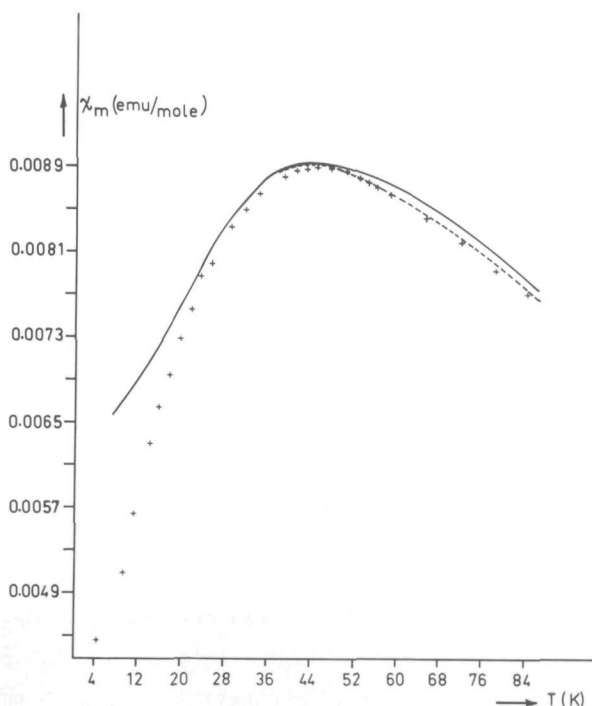


Fig. III.3.4. Molar susceptibility (+) of  $\text{NiOx}(\text{2Miz})_2$  as a function of temperature; The full curve represents the theoretical curve for  $J = -12.0 \text{ cm}^{-1}$ ,  $D = 0 \text{ cm}^{-1}$  and  $g = 2.17$  according to Weng. The dotted curve represents the theoretical curve for  $J = -12.0 \text{ cm}^{-1}$ ,  $D = -12.0 \text{ cm}^{-1}$  and  $g = 2.20$  according to de Neef.

From these experiments and the knowledge that  $\text{Ni}^{2+}$  ions, octahedrally coordinated can exhibit large zero-field splittings and the fact that even at Q-band frequencies no ESR spectra could be obtained, it is reasonable to assume that describing the susceptibility data with a model including a  $D$ -term is



TABLE III.3.6. SUSCEPTIBILITY DATA FOR COMPOUNDS  $\text{NiOxL}_2$ , WITH  $\text{L}=\text{H}_2\text{O}$ ,  $2\text{Miz}$ ,  $\text{DMiz}$ ,  $\text{Biz}$  AND  $\text{Ox}=\text{OXALATO DIANION}$ . UNCERTAINTIES IN THE LAST DIGIT ARE IN PARENTHESES

COMPOUND	$\chi_{\text{M}}^{\text{a}} \cdot 10^2$ max.	$T_{\text{max.}}$	WENG'S RESULTS		DE NEEF'S RESULTS ( $D=- J $ ) <sup>b</sup>	
	(emu/mole)	(K)	$-J(\text{cm}^{-1})$	g	$-J(\text{cm}^{-1})$	g
$\text{NiOx}(\text{H}_2\text{O})_2$	0.928(9)	41(2)	11.0(4)	2.12(4)	11.5(3)	2.22(2)
$\text{NiOx}(2\text{Miz})_2$	0.889(9)	45(2)	12.0(2)	2.17(2)	12.0(2)	2.20(1)
$\text{NiOx}(\text{DMiz})_2$	0.870(9)	47(2)	12.4(2)	2.18(2)	12.5(2)	2.22(2)
$\text{NiOx}(\text{Biz})_2$	0.876(9)	46(2)	12.4(2)	2.19(3)	12.5(2)	2.23(2)

<sup>a</sup>=CORRECTED FOR DIAMAGNETISM OF CONSTITUENT ATOMS USING PASCAL'S CONSTANTS<sup>32</sup>; <sup>b</sup>=HIGH TEMPERATURE REGION.

the most honest approach. However, the value of this axial zero-field splitting parameter,  $D$ , must be regarded only as a rough estimate, because de Neef<sup>7</sup> published results only for values  $D=nx|J|$ , with  $n=-4, -2, -1, 0, +2, +4$ . The best fits for all the compounds were obtained for the curve with  $n=-1$ . The next best fit was obtained by taking the curve with  $n=0$ . (the results of Weng are very close to those of de Neef with  $n=0$ ). The sharp susceptibility decrease at the lowest temperatures can be explained in several ways. A first reason for this decrease could be that the ground state of the  $\text{Ni(II)}$  ion is a non-magnetic singlet caused by the  $D$ -term. A second explanation is that Ising coupling occurs here, but since no expression for the powder susceptibility is known, it is not possible to confirm this. A third explanation could be that anisotropic inter-chain coupling gives rise to the strong decrease in the susceptibility.

For the compound  $\text{NiOx}(\text{H}_2\text{O})_2$  an increase in susceptibility at very low temperatures was found, indicating the presence of a small amount of paramagnetic impurity. Impurity corrections in the 0.5 to 1.0% range (for different samples) of a monomeric nickel compound were necessary in order to describe the data with Weng's results. This correction hardly affected the susceptibility data in the high temperature region, from which the  $D/J$  parameter,  $n$ , was calculated.

To find out to what extent the phenomena of zero-field splitting, inter-chain coupling or anisotropic intra-chain coupling are involved, better theories must be awaited. Especially, a description of the low-temperature region where these phenomena give rise to serious problems in interpretation, is needed. A first step towards obtaining more experimental data could be the measurement of single-crystal susceptibilities; however, so far no large enough single crystals of magnetic compounds have been prepared.

TABLE III.3.7. SUSCEPTIBILITY DATA FOR COMPOUNDS  $\text{CoOxL}_2$ , WITH L=WATER AND SUBSTITUTED-IMIDAZOLE. UNCERTAINTIES IN THE LAST DIGIT ARE IN PARENTHESES

COMPOUND	$\chi_{\text{M max.}}$ (emu/mole)	$T_{\text{max.}}$ (K)	FITTING PARAMETERS (ISING MODEL)						ESR DATA	
			$g_{//}$	$g_{\perp}$	$-J(\text{cm}^{-1})$	$g_{\perp}^y$	$-J(\text{cm}^{-1})$	$C(\text{emu.K/mole})$	$g_{//}$	$g_{\perp}$
$\text{CoOx}(\text{H}_2\text{O})_2$	0.0425(4)	18.0(5)	6.1(1)	3.3(1)	9.3(3)	3.2(1)	9.1(3)	0.004(5)	6.28(1)	3.16(1)
$\text{CoOx}(\text{2MIz})_2$	0.0405(4)	18.5(5)		a		3.0(1)	9.5(5)	0.049(4)	6.29(1)	3.07(1)
$\text{CoOx}(\text{DMIz})_2$	0.0390(3)	19.5(5)		a		3.4(2)	10.6(6)	0.042(4)	5.67(1)	3.81(1)
$\text{CoOx}(\text{BIz})_2$	0.0435(4)	15.0(5)		a		3.3(1)	9.3(4)	0.066(4) <sup>b</sup>	5.68(1)	3.49(1)

<sup>x</sup>=CORRECTED FOR DIAMAGNETISM USING PASCAL'S CONSTANTS<sup>32</sup>; <sup>y</sup>=IMPURITY CORRECTION OF THE FORM C/T INCLUDED; <sup>a</sup>=NO FIT COULD BE OBTAINED; <sup>b</sup>=C-VALUE CORRESPONDING TO ABOUT 1% OF A MONOMERIC  $\text{Co}$  COMPOUND.

### Cobalt compounds

The relevant susceptibility data of the compounds  $\text{CoOxL}_2$ , together with the J and g parameters obtained within the Ising model, are given in table III.3.7. The susceptibility curves again show a broad maximum typical for an antiferromagnetic chain system.

In describing magnetic properties of  $\text{Co}^{2+}$  ions in an octahedral field, one has to bear in mind that, at very low temperatures,  $\text{Co(II)}$  acts as though it had a fictitious spin  $S=\frac{1}{2}$ . In a cubic octahedral field the  $^4\text{F}$  orbital state of the free  $\text{Co(II)}$  ion splits into three levels of which the lowest level  $^4\text{T}_1$  is triply degenerate. Under the action of an axial or rhombic distortion - as is the case in the present compounds - of the crystal field in combination with spin-orbit coupling, the  $^4\text{T}_1$  level splits into six Kramers doublets causing the ground state of the  $\text{Co(II)}$  ion to be a doublet<sup>21</sup>. The same energy level remains lowest for all values of the field strength and the splitting between the two lowest lying doublets is so large, that up to ca. 20-25K the system can be described as having a spin  $S=\frac{1}{2}$ . For higher temperatures, thermal occupation of the higher situated doublets cannot be ignored, resulting in an increase of the susceptibility compared to the fictitious  $S=\frac{1}{2}$  system susceptibility. This would give rise to severe problems in the interpretation of the data. In order to correct for this increase in susceptibility, the energy differences between ground state and the five Kramers doublets must be known and to calculate these energy differences one has to know the crystal-field strength and also the spin-orbit coupling constant. Since these parameters are not known for the compounds under discussion, no description of the high temperature part of the susceptibility curves was attempted and so only the low temperature parts were fitted as being  $S=\frac{1}{2}$  systems in the 4.2-20K region. Within the Heisenberg model, Bonner

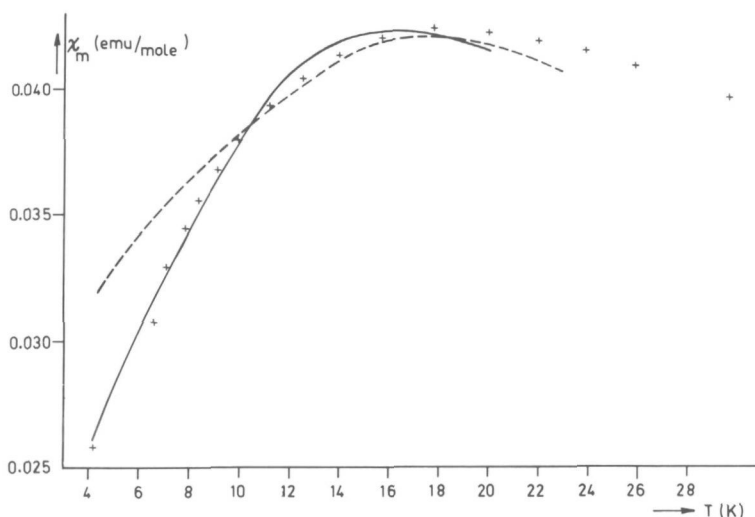


Fig. III.3.5. Molar susceptibility (+) of  $\text{CoOx}(\text{H}_2\text{O})_2$  as a function of temperature; the full curve represents the theoretical curve for  $J=-9.3 \text{ cm}^{-1}$ ,  $g_{\parallel}=6.1$  and  $g_{\perp}=3.3$ . The dotted curve represents the theoretical curve for  $J=-10.1 \text{ cm}^{-1}$  and  $g=4.7$  according to the results of Bonner and Fisher.

and Fisher<sup>28</sup> published the extrapolated curve for  $S=\frac{1}{2}$  ions. Their results, together with Ising and experimental results for  $\text{CoOx}(\text{H}_2\text{O})_2$ , are plotted in figure III.3.5.

By means of the results for the powder susceptibility within the Ising model with  $S=\frac{1}{2}$  (see chapter II.5 ( $J$  is substituted for  $2J$ )), a fit with the experimental susceptibility data was tried.

From figure III.3.5, it is clear that the Ising model describes the susceptibility data best, especially in the low-temperature region where the Heisenberg curve fails. For none of the  $\text{Co}(\text{II})$  compounds a good fit with the experimental data could be obtained with the Heisenberg model. This is in agreement with the ESR results, *i.e.*  $g_{\parallel} > g_{\perp}$  which is indicative of the presence of an Ising type of interaction (see also chapter II.8). Using a least-squares

technique, the data were fitted to the expression for the powder susceptibility from the Ising model in two different ways, yielding the values for the parameters listed in table III.3.7. As mentioned before, the approximation resulting from a fictitious  $S=\frac{1}{2}$  system only holds for temperatures below *ca.* 20K. In this region small amounts of paramagnetic impurity and interchain coupling effects also become important. These effects very strongly affect the  $g_{//}$  and to a lesser extent the  $g_{\perp}$  and J parameters. For these reasons the data were fitted in two ways:

Firstly, the data were fitted without a correction for a small amount of paramagnetic impurity with parameters  $g_{//}$ ,  $g_{\perp}$  and J. Only for the compound with  $L=H_2O$  could a reasonable fit be obtained (*viz.* figure III.3.5). The g-parameters calculated in this way, correlate well with those obtained from the ESR data.

Secondly, the data were fitted with a correction for the presence of a paramagnetic impurity, having a Curie-like susceptibility C/T. Using fixed  $g_{//}$  with  $g_{\perp}$ , J and C as parameters the data were fitted within the Ising model. The values for the fixed  $g_{//}$  were taken from the ESR data, because these could be obtained with great accuracy for all compounds. Examination of these parameters, listed in table III.3.7, reveals that for all compounds the  $g_{\perp}$  results are in good agreement with the ESR data indicating that the  $CoOxL_2$  compounds seem to be good examples of one-dimensional Ising compounds. Differently-prepared samples of one compound yielded data that could be fitted with slightly different C-values and identical  $g_{\perp}$  and J-values.

Finally, it is noticed that one expects the occurrence of long-range order effects below *ca.* 20K for the  $H_2O$  compounds, similar as found in the corresponding Fe(II) compound (see chapter III.4). However since the compounds are not mutually X-ray powder isomorphous and the Co(II) compound could be described down 4.2K with the one-dimensional Ising model, it is likely that either long-range order effects hardly affect the susceptibility or do not occur in the temperature region investigated. Specific heat measurements could give the answer.

### III.4. Magnetic Susceptibility Measurements and Mössbauer Spectroscopy on Fe(II) oxalato-bridged chain Compounds.

#### III.4.1. Experimental

The synthesis of the Fe(II) oxalate compounds  $\text{FeOxL}_2$  is similar to that for the corresponding Ni, Co and Zn compounds, described in chapter III.3.

The compounds were characterized and analyzed as described in chapter V.

#### III.4.2. Results and discussion

##### *General*

All chemical analyses are in agreement with the chemical formula  $\text{FeOxL}_2$ ; the IR spectra resemble those of the corresponding Zn compounds, described in chapter III.3.

The X-ray powder pattern of the compounds  $\text{FeOx}(2\text{Miz})_2$  and  $\text{ZnOx}(2\text{Miz})_2$  (with and without half a molecule of crystal water) are almost identical, meaning that their structures are rather similar (chapter III.2).

##### *Magnetic measurements*

The molar susceptibility *vs.* temperature curves of the present compounds have a broad maximum at *ca.* 20K, just as found for the corresponding Ni and Co compounds (chapter III.3). From the observation of the maxima in these curves it is concluded that the Fe(II) ions exhibit an antiferromagnetic interaction within the chains.

No exact theoretical expressions for the powder susceptibility are available. Weng<sup>6</sup> published the extrapolated results for isotropically-coupled  $S=2$  ions; however, because in the present Fe(II) compounds always a small amount of a Fe(III) impurity seemed to be present (increase of the susceptibility below *ca.* 5-10K) no attempt was made to describe the data in a quantitative way. Furthermore, it is possible that the Fe(II) ions couple anisotropically and since no theoretical powder susceptibility expressions are available for an infinite  $S=2$  chain within the Ising and XY model, the data were not fitted.

##### *Mössbauer-effect measurements*

In order to study the interchain coupling effects, Mössbauer spectrometry has been performed down to 1.7K. In figures III.4.1 and III.4.2 some spectra recorded at 1.7K are shown. It appears that in these compounds the magnetic hyperfine interaction is of the same order as the electric quadrupole interactions.

The positions of the absorption lines are determined from a least-squares

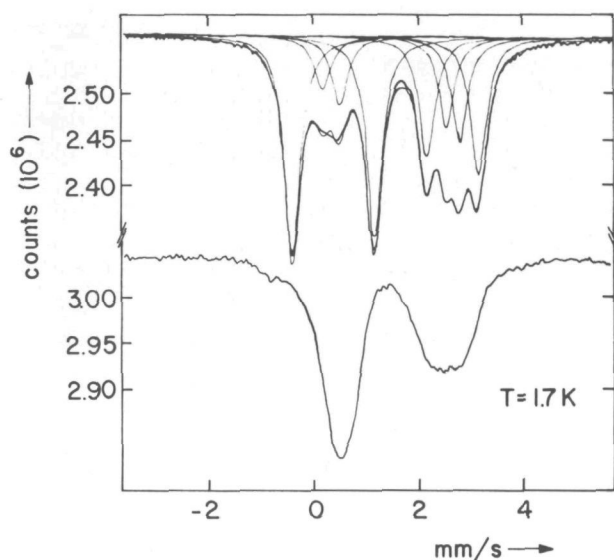


Fig. III.4.1. Mössbauer spectra of the compounds  $\text{FeOx(Iz)}_2$  (upper curve) and  $\text{FeOx(DMIz)}_2$  (lower curve) at 1.7K.

fitting procedure of Lorentzian lines. From the line positions the different interaction parameters have been deduced using the program of van Dongen Torman *et al.*<sup>34</sup> and Kündig<sup>35</sup>. The parameters

deduced are summarized in table III.4.1. The rather complex spectrum of the compound  $\text{FeOx(2MIz)}_2$  (with and without half a molecule of crystal water) at 1.7K (*viz.* figure III.4.2) could only be analyzed by assuming two different Fe(II) sites. Different effective hyperfine fields at these two sites have been found as shown in table III.4.1 and figure III.4.2, while the electric quadrupole splittings are the same. The difference in the effective hyperfine fields is most likely due to the presence of the two different Fe(II) sites (see also chapter III.2).

The small effective hyperfine fields observed in these Fe(II) chain compounds are due to large orbital and anisotropic contributions<sup>36</sup>. The sign of the effective field has been determined by measurements in an external magnetic field of 50 kG. For all the compounds the sign is negative. The hyperfine field in  $\text{FeOx(H}_2\text{O)}_2$  is in agreement with the

TABLE III.4.1. PARAMETERS DEDUCED FROM THE MÖSSBAUER-EFFECT MEASUREMENTS. UNCERTAINTIES IN THE LAST DIGIT ARE WITHIN PARENTHESES

COMPOUND	$T_N$	$H_{\text{eff.}}$	QS	$\theta$	$\phi$	$\eta$	IS
	(K)	(kOe)	(mm/s)	(°)	(°)		(mm/s)
$\text{FeOx(H}_2\text{O)}_2$	26(1)	-155(2)	-1.94(3)	90(5)	0(20)	0.6(2)	+1.43(3)
$\text{FeOx(Iz)}_2$	9.1(1)	-55(2)	+2.21(3)	72(4)	90(30)	0.6(2)	+1.47(3)
$\text{FeOx(2MIz)}_2 \cdot \frac{1}{2}\text{H}_2\text{O}^a$	5(1)	-78(2) -111(2)	+2.99(3)	54(1)	0(15)	0.9(1)	+1.46(3)
$\text{FeOx(DMIz)}_2$	3(1)	-25(5)	+1.79(3)		b		+1.54(3)

<sup>a</sup>= IN THIS COMPOUND TWO SLIGHTLY DIFFERENT Fe(II) SITES OCCUR; <sup>b</sup>=NO COMPLETELY RESOLVED SPECTRUM DOWN 1.7K.

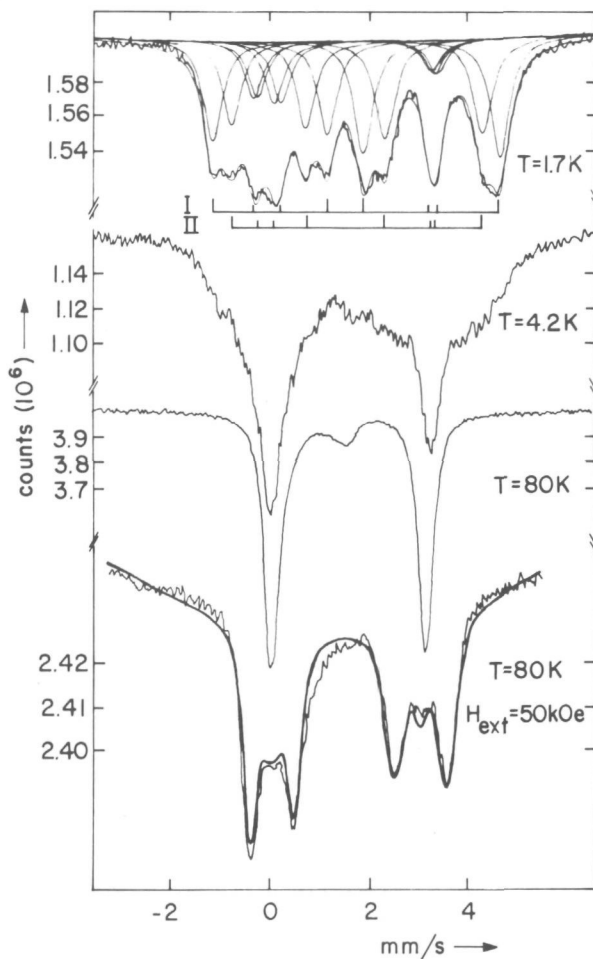


Fig. III.4.2. Mössbauer spectra of  $\text{FeOx}(\text{2Mlz})_2$  at different temperatures and external field. The two hyperfine field spectra at 1.7K are indicated with I and II.

results of Barros *et al.*<sup>37</sup>

The three-dimensional ordering temperature  $T_N$ , due to the interchain coupling has been determined from the vanishing hyperfine splitting of the Mössbauer spectra and they are also given in table III.4.1. From these results it follows that for larger ligands  $T_N$  decreases, which means that the interchain coupling decreases and subsequently the chain

becomes a more "ideal" one-dimensional antiferromagnet. In the vicinity of the transition from a three-dimensional to a one-dimensional magnetic behaviour relaxation effects are observed, as it follows from the shape of the  $\text{FeOx}(\text{2Mlz})_2$  spectrum at  $T=4.2\text{K}$  shown in figure III.4.2. The small peak at the center of the spectrum of this compound at  $T=80\text{K}$  is due to a small  $\text{Fe}^{3+}$  contamination.

The sign of the electric quadrupole splitting has been determined from Mössbauer measurements in an external magnetic field of 50 kG at 80K and is given in table III.4.1. An example of such a measurement is shown also in figure III.4.2. The large electric quadrupole splitting found for  $\text{FeOx}(\text{2Mlz})_2$  compared to the other azole compounds may indicate that the ligands in the

latter are located in a *trans* configuration, although it cannot be proven quantitatively.

From the magnitude and sign of the electric quadrupole splittings the anisotropy contribution to the effective hyperfine field can be calculated<sup>36</sup>. In this way one gets the order of magnitude of the large orbital contribution which yields information about the gS values. However, for a quantitative calculation of these values it is necessary to know the covalency effects on  $\langle r^{-3} \rangle$ <sup>36</sup>.

The occurrence of spin-lattice relaxation effects which in principle can play a rôle at the lowest temperatures could be ruled out by measuring the isomorphous 10% Fe-doped Zn compounds; down to 1.7K no magnetic hyperfine components could be detected, which means that in the present systems the transition temperatures,  $T_N$ , can be correlated with interchain coupling effects.



### III.5. Crystal and Molecular Structure of diaquobis(imidazole)-catena- $\mu$ -((1,3)-squarato)Nickel(II).

#### III.5.1. Experimental

Transparent blue-green single crystals of the title compound, abbreviated NISIA, were slowly grown from a mixture of a solution of  $\text{Ni(II)Cl}_2$  in water (0.01 mol/l) and a solution of imidazole in water and a solution of squaric acid (0.01 mol/l) in water.

#### III.5.2. Crystal and intensity data, structure determination and refinement

From single-crystal diffractometry ( $\text{MoK}\alpha = 0.71069 \text{ \AA}$ ) the following data were obtained:  $a = 7.478(1)$ ,  $b = 11.539(2)$ ,  $c = 8.101(2) \text{ \AA}$ ,  $\beta = 109.27(2)^\circ$ , space group  $\text{P2}_1/c$ ,  $D_m = 1.7 \text{ g/cm}^3$ ,  $D_c = 1.73 \text{ g/cm}^3$ , and  $Z = 2$ .

A specimen showing sharp optical extinctions under crossed polarizers was mounted along the  $c$ -axis. Accurate values of the unit cell parameters and the crystal orientation matrix were determined from a least-squares treatment of the angular settings of 16 reflections, carefully centered on an ENRAF-NONIUS CAD4 computer-controlled diffractometer with Mo-radiation.

The standard deviations in the lattice parameters were obtained from integer values of the indexes, calculated with the orientational matrix, for the angular settings of the orientation reflections as described by Duisenberg<sup>38</sup>.

The crystal selected for data collection was a parallelepiped with two additional facets. The observed crystallographic forms, indexed in accordance with the unit cell determined by X-ray diffraction, were (100), (010), (001), and (10 $\bar{2}$ ). Dimensions were measured under a binocular microscope and were (100) to (100) 0.21 mm, (010) to (010) 0.25 mm, (001) to (001) 0.30 mm, and (10 $\bar{2}$ ) to (10 $\bar{2}$ ) 0.34 mm. The crystal volume amounts to  $1.64 \times 10^{-2} \text{ mm}^3$ .

Intensity data were collected with the CAD4 diffractometer equipped with a scintillation counter in the  $\omega/2\theta$ -scan mode using monochromated  $\text{MoK}\alpha$  radiation ( $2\theta_{\text{mon.}} = 12.8^\circ$ )<sup>39</sup>. The applied scan angle was  $\Delta\omega = 0.60 + 0.35(\tan\theta)^\circ$ . The background was measured in an additional scan area of  $\Delta\omega/4^\circ$  on both sides of the main scan and with the same scan speed. The intensity of every reflection was measured at the highest possible speed and then if necessary, at a speed designed to achieve  $I_{\text{min.}}$  counts above background. A maximum of 120 seconds was placed on the measurement time. The horizontal and vertical detector aperture were both 4 mm. and the distance from the crystal to aperture was 173 mm. An

attenuator would have been automatically inserted if a preliminary scan indicated a count rate greater than 50,000 counts/sec.

The reflections (230), (340), and (151) were used as standard reflections and the intensities were monitored every 30 minutes. There was no indication for decay during the data collection.

Reflection data were collected up to  $\theta < 30^\circ$ . The intensities of a total of 1927 reflections were measured. The net intensity was calculated with

$$I(\text{net}) = (\text{scale})(S - 2(L + R))/npi,$$

where  $(L + R)$  is the total background count,  $S$  the scan count,  $npi$  the ratio of the maximum possible scan speed to the applied scan speed, and  $(\text{scale})$  a function of the time slowly varying around the value 1. To account for short- and long-range fluctuations in the intensity the data were scaled, by interpolation in a polynomial of the third degree through eight neighbouring measurement values of the standard reflection, in order to smooth out very short-term fluctuations in the intensity of the standard reflection. The standard deviation in the net intensity was calculated with

$$\sigma(I) = \frac{\text{scale}}{npi} (S + 4(L + R))^{\frac{1}{2}}.$$

Absorption correction was performed with a Gaussian integration technique using a 8X8X8 grid ( $\mu_{\text{MoK}\alpha} = 15.05 \text{ cm}^{-1}$ ). The observed absorption corrections were in the range from 1.34 to 1.44.

The equivalent reflections were averaged using

$$\bar{I} = \sum_i (I_i / \sigma_i^2) / \sum_i (1 / \sigma_i^2),$$

$$\sigma(\bar{I}) = \{1 / \sum_i (1 / \sigma_i^2)\}^{\frac{1}{2}},$$

where  $I_i$  and  $\sigma_i$  are the intensity and the standard deviation of the  $i$ -th equivalent diffraction. The resulting unique set contained 1708 reflections of which 1576 had intensities above background ( $I > 2.5\sigma(I)$ ).

The data were corrected for Lorentz and polarization factors ( $Lp$ ).

The  $\sigma(I)$ 's were converted to the estimated errors in the relative structure factors  $\sigma(F)$  by

$$\sigma(F) = \{(I + \sigma(I))/Lp\}^{\frac{1}{2}} - (I/Lp)^{\frac{1}{2}}.$$

Direct methods (MULTAN 74<sup>40</sup>) were used to solve the structure. The positions of the non-hydrogen atoms were refined by block-diagonal least-squares procedures to  $R_F = 0.055$  and  $R_{wF} = 0.069^{41}$ . At this stage positions of all hydrogen atoms were determined from a difference Fourier map and weights were introduced based on counting statistics ( $w^{-1} = \sigma(F_O^2) + 0.00002 F_O^2$ ). Refinement was continued using a full-matrix least-squares technique. The structure refinement converged to  $R_F = 0.023$  and  $R_{wF} = 0.032$  for 1576 observed reflections. The positions of all atoms and the anisotropic temperature factors of the non-hydrogen atoms and isotropic temperature factors of the hydrogen atoms were refined. A total of 121 parameters including one scale factor were varied. All shifts were less than 0.2 of their standard deviations when refinement was stopped. The final positional and thermal parameters are tabulated in table III.5.1.

The average deviation in an observation of unit weight, defined by  $\{\Sigma w(|F_O| - |F_C|)^2 / (m-n)\}^{1/2}$ , was 3.80 as compared to the ideal value 1. The function  $\Sigma w(|F_O| - |F_C|)^2$  was not significantly dependent either upon  $F_O$  or upon  $(\sin\theta/\lambda)$ . The final  $R_{wF}$  value for all reflections including the "unobserveds" was 0.032. A final electron density difference Fourier synthesis

TABLE III.5.1. FINAL FRACTIONAL ATOMIC COORDINATES AND THERMAL PARAMETERS<sup>x</sup>. ESTIMATED STANDARD DEVIATIONS ARE WITHIN PARENTHESES

ATOM	x/a	y/b	z/c	100(u <sub>11</sub> or U)	100u <sub>22</sub>	100u <sub>33</sub>	100u <sub>12</sub>	100u <sub>13</sub>	100u <sub>23</sub>
N1	0.0000(0) <sup>a</sup>	0.0000(0) <sup>a</sup>	0.5000(0) <sup>a</sup>	1.88(2)	1.57(1)	1.40(1)	0.03(1)	0.67(1)	0.10(1)
N(1)	-0.2420(2)	-0.0996(1)	0.4587(2)	2.24(7)	2.21(6)	2.51(6)	-0.19(5)	0.90(5)	0.00(5)
N(2)	-0.5430(2)	-0.1455(1)	0.3879(2)	1.98(8)	3.62(7)	3.81(8)	-0.41(6)	0.68(6)	-0.02(6)
O(1)	0.1500(2)	-0.1619(1)	-0.0513(1)	4.46(7)	2.27(5)	2.17(5)	1.55(5)	1.71(5)	0.57(4)
O(2)	0.0492(2)	-0.0692(1)	0.2763(1)	3.05(6)	2.08(5)	1.38(4)	0.51(4)	0.90(4)	0.30(3)
O(3)	-0.1714(2)	0.1348(1)	0.3699(1)	2.77(6)	1.84(5)	1.73(4)	0.35(4)	0.89(4)	0.16(4)
C(1)	-0.4444(3)	-0.2268(2)	0.5043(3)	3.08(11)	3.60(10)	5.36(12)	-0.65(8)	1.46(9)	1.17(8)
C(2)	-0.2603(3)	-0.1987(2)	0.5466(3)	2.64(10)	3.06(8)	4.72(10)	-0.09(7)	1.08(8)	1.34(4)
C(3)	-0.4167(2)	-0.0705(2)	0.3649(2)	2.63(9)	2.82(7)	2.84(7)	-0.15(6)	0.55(6)	0.12(6)
C(4)	0.0679(2)	-0.0731(1)	-0.0243(2)	2.43(8)	1.92(6)	1.47(5)	0.40(5)	0.82(5)	0.24(4)
C(5)	0.0204(2)	-0.0296(1)	0.1259(2)	2.09(8)	1.66(5)	1.56(6)	0.26(5)	0.71(5)	0.10(4)
H(1)	-0.506(4)	-0.280(3)	0.539(4)	4.3(9)					
H(2)	-0.158(4)	-0.239(2)	0.623(3)	1.3(5)					
H(3)	-0.446(4)	-0.006(2)	0.292(4)	2.0(7)					
H(4)	-0.662(4)	-0.138(2)	0.353(3)	1.7(6)					
H(5)	-0.168(3)	0.196(2)	0.423(3)	1.5(6)					
H(6)	-0.168(3)	0.149(2)	0.268(3)	1.3(4)					

<sup>x</sup>=THE ANISOTROPIC THERMAL PARAMETERS ARE IN THE FORM  $\epsilon = \exp \{-2\pi^2 \sum_{i,j} u_{ij} h_i h_j a_i^* a_j^*\}$ ; <sup>a</sup>=PARAMETER WAS HELD FIXED.

revealed no significant residual electron density maxima, higher than  $0.36 \text{ e}/\text{\AA}^3$ .

Scattering factors for all atoms were taken from Doyle<sup>42</sup>, except those for hydrogen which were taken from Stewart<sup>11</sup>. Anomalous dispersion correction for Ni was taken from a compilation by Rietveld<sup>43</sup>.

All computer calculations were performed on a CDC CYBER-73 computer at the computer center of the University of Utrecht. Programs used in this structural analysis included the local programs CAD4 TAPE (for handling of the diffractometer output by D. Kaas), ASYM (averaging to the unique data set by A.L. Spek), MULTAN 74<sup>40</sup> (a direct method procedure), ORTEP (thermal ellipsoid drawings by C.K. Johnson<sup>44</sup>) and an extended version of the XRAY system (by Stewart *et al.*<sup>45</sup>) for most of the other calculations.

### III.5.3. Results and discussion

The crystal structure of diaquobis(imidazole)*catena*- $\mu$ -((1,3)-squarato)-Nickel(II) consists of chains built up by squarato-bridged Ni(II) ions. Contrary to the situation in  $\text{NiSq}(\text{H}_2\text{O})_2$ <sup>46</sup>, where all squarato oxygens are coordinated

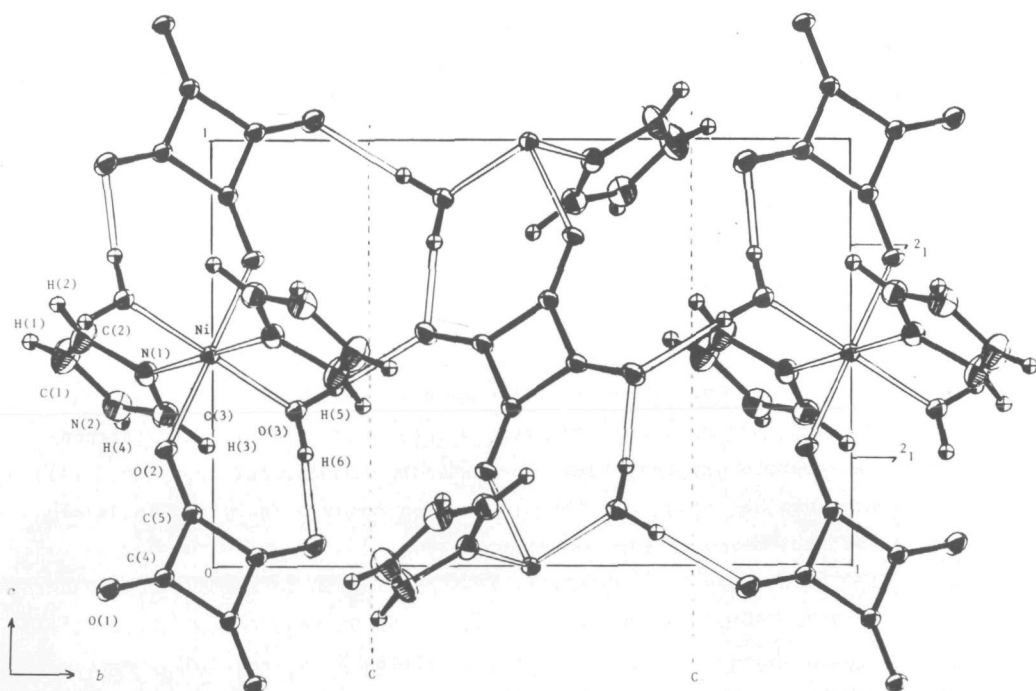


Fig. III.5.1. ORTEP<sup>44</sup> drawing of NISIA.

TABLE III.5.2. INTERATOMIC DISTANCES ( $\text{\AA}$ ) AND ANGLES ( $^\circ$ ). UNCERTAINTIES IN THE LAST DIGIT ARE IN PARENTHESES

DISTANCES															
N1	-	N(1)	2.076(1)	O(2)	-	H(4) <sup>b</sup>	2.19(3)	O(2)	-	C(5)	-	C(4) <sup>a</sup>	137.8(2)		
N1	-	O(2)	2.121(1)	O(1) <sup>a</sup>	-	H(6)	1.81(3)	C(4)	-	C(5)	-	C(4) <sup>a</sup>	89.9(1)		
N1	-	O(3)	2.069(1)	O(1) <sup>c</sup>	-	H(5)	1.93(2)	C(5)	-	C(4)	-	C(5) <sup>a</sup>	90.1(1)		
C(1)	-	N(2)	1.362(3)	O(2)	-	N(2) <sup>b</sup>	3.012(3)	N1	-	O(3)	-	H(5)	118(2)		
C(1)	-	C(2)	1.344(3)	O(1) <sup>a</sup>	-	O(3)	2.657(3)	N1	-	O(3)	-	H(6)	115(2)		
C(2)	-	N(1)	1.377(2)	O(1) <sup>c</sup>	-	O(3)	2.745(3)	H(5)	-	O(3)	-	H(6)	110(2)		
C(3)	-	N(1)	1.320(2)	ANGLES				N(1)	-	C(2)	-	H(2)	124(2)		
C(3)	-	N(2)	1.339(3)	O(2)	-	N1	-	O(3)	95.78(4)	C(1)	-	C(2)	-	H(2)	126(2)
C(4)	-	C(5)	1.463(2)	O(2)	-	N1	-	N(1)	92.37(5)	C(2)	-	C(1)	-	H(1)	134(2)
C(4)	-	C(5) <sup>a</sup>	1.470(2)	O(3)	-	N1	-	N(1)	88.49(5)	N(2)	-	C(1)	-	H(1)	119(2)
C(4)	-	O(1)	1.250(2)	N1	-	N(1)	-	C(2)	127.3(1)	C(1)	-	N(2)	-	H(4)	125(2)
C(5)	-	O(2)	1.252(2)	N1	-	N(1)	-	C(3)	126.6(1)	C(3)	-	N(2)	-	H(4)	127(2)
C(1)	-	H(1)	0.87(4)	N1	-	O(2)	-	C(5)	132.2(2)	N(2)	-	C(3)	-	H(3)	125(2)
C(2)	-	H(2)	0.93(2)	C(1)	-	C(2)	-	N(1)	109.7(2)	N(1)	-	C(3)	-	H(3)	124(2)
C(3)	-	H(3)	0.93(3)	C(2)	-	N(1)	-	C(3)	105.1(1)	C(4) <sup>a</sup>	-	O(1) <sup>a</sup> ...	H(6)	131(2)	
N(2)	-	H(4)	0.84(3)	N(1)	-	C(3)	-	N(2)	111.4(1)	C(4) <sup>c</sup>	-	O(1) <sup>c</sup> ...	H(5)	123(2)	
O(3)	-	H(5)	0.82(2)	C(1)	-	N(2)	-	C(3)	107.2(2)	C(5)	-	O(2)	...	H(4) <sup>b</sup>	104(2)
O(3)	-	H(6)	0.85(3)	C(2)	-	C(1)	-	N(2)	106.6(2)	O(1) <sup>a</sup> ...	H(6)	-	O(3)	174(4)	
				O(1)	-	C(4)	-	C(5)	133.9(1)	O(1) <sup>c</sup> ...	H(5)	-	O(3)	180(4)	
				O(1)	-	C(4)	-	C(5) <sup>a</sup>	136.0(1)	O(2)	...	H(4) <sup>b</sup>	-	N(2) <sup>b</sup>	166(4)
				O(2)	-	C(5)	-	C(4)	132.3(1)						

SYMMETRY OPERATIONS: <sup>a</sup> = -x, -y, -z; <sup>b</sup> = (1+x), y, z; <sup>c</sup> = -x, (y+ $\frac{1}{2}$ ), ( $\frac{1}{2}$ -z).

directly to the Ni(II) ion, forming a chain structure, in the present compound two squarato oxygens bind directly to the Ni(II) ion, whereas the other two coordinate *via* the water molecules by intrachain hydrogen bonds. The water molecules are coordinated directly to nickel and the octahedron around nickel is completed by the imidazole ligands.

The adopted atomic numbering scheme along with the thermal vibrational ellipsoids<sup>44</sup> is shown in figure III.5.1. Interatomic bond distances and angles are given in table III.5.2.

As shown clearly in figure III.5.1, the chains of Ni(II) ions are held together by strong hydrogen bridges between the water molecules and the non-coordinating squarato oxygens, thus forming a two-dimensional array of Ni(II) ions. These planes are hold together by hydrogen bonds between the imidazole hydrogens and the coordinating squarato oxygens.

The Ni-O<sub>w</sub> bond length (2.069(1)  $\text{\AA}$ ) is very similar to the one observed for the compound NiSq(H<sub>2</sub>O)<sub>2</sub><sup>46</sup>, *i.e.* 2.060(9)  $\text{\AA}$ . The Ni-O<sub>s</sub> bond length (2.121(1)  $\text{\AA}$ ) however, is much longer compared with the 2.085(16)  $\text{\AA}$  in NiSq(H<sub>2</sub>O)<sub>2</sub>. Presumably the two strongly-coordinated imidazole ligands are responsible for the larger Ni-O<sub>s</sub> distance. The Ni-N bond length is within the range of values reported for

Ni-N distances<sup>64</sup>. Angles that coordinated atoms subtend at the Ni(II) ion are all near  $90^\circ$  or  $180^\circ$  without notable exception (see table III.5.2).

The squarato anion is almost square planar, the C-C bond lengths (1.463(2) and 1.470(2) Å) are slightly larger than the mean value found in the acid<sup>47</sup> (1.456(12) Å) and close to the value reported for  $\text{NiSq}(\text{H}_2\text{O})_2$ <sup>46</sup> (1.487(16) Å). The O-C-C angles varying between  $132.3(2)$  and  $137.8(2)^\circ$  are similar as observed in squaric acid and  $\text{NiSq}(\text{H}_2\text{O})_2$ . The C-C-C angles are very close to  $90.0^\circ$  ( $89.9(1)$  and  $90.1(1)^\circ$ ) which deviate slightly in squaric acid ( $88.2$  and  $91.8^\circ$ ) and are equal to  $90.0^\circ$  in  $\text{NiSq}(\text{H}_2\text{O})_2$  ( $90.0(1.2)^\circ$ ).

The nickel and water oxygen distances from the least-squares plane through the squarate ligand are rather small ( $+0.15$  and  $-0.18$  Å respectively), therefore the chain structure is almost linear.

The geometry of the imidazole ligand is similar to earlier reported data<sup>48</sup> and will therefore not be discussed in detail here.

The hydrogen-bridge geometries have been included in table III.5.2. It is noticed that the intramolecular hydrogen-bond length is slightly shorter compared to the intermolecular (interchain) hydrogen-bond length (2.657(3) and 2.745(3) Å respectively). The bond strength of the intramolecular hydrogen bridge is almost similar to the bond strength of the intermolecular hydrogen bridge, because of the different O---H-O angles ( $174(4)$  and  $180(4)^\circ$ ). The hydrogen-bond length between the imidazole nitrogen and the coordinating squarato oxygen (3.012(3) Å) (the intersheet hydrogen bridge), and  $\text{O}_s\text{---H-N}$  angle ( $166(4)^\circ$ ) indicate that this latter bond strength is weak compared to the former hydrogen-bond strengths. Comparing this large distance with those observed in the compound  $\text{ZnOx}(\text{2MIz})_2 \cdot \frac{1}{2}\text{-water}$ <sup>49</sup> (2.78-2.80 Å) shows the present intersheet O...H-N hydrogen bridge to be quite weak indeed.

### III.6. Spectroscopy and Magnetism of diaquobis(imidazole)-catena- $\mu$ -((1,3)-squarato)Nickel(II).

#### III.6.1. Experimental

The title compound, abbreviated NISIA, was prepared as described in detail in chapter III.5, in which the results of the X-ray structure analysis have been given.

The compound was characterized using techniques described in chapter V.

#### III.6.2. Results and discussion

##### *Infrared and Raman spectroscopy*

In table III.6.1 the observed IR and Raman frequencies of the squarate molecule have been listed, together with their assignments. To assign the vibrations, the symmetry of the squarato anion was taken as  $D_{4h}$ . The assignment is in agreement with that published by Ito *et al.*<sup>50</sup> The fact that  $\nu_9$  (a C-O stretching vibration) is slightly split and  $\nu_6$  is shifted strongly compared to the corresponding vibration in  $K_2Sq$ <sup>50</sup> suggests that the symmetry of the C-O parts of the molecule is lower than  $D_{4h}$ , as evidenced by the X-ray analysis.

TABLE III.6.1. SQUARATO ABSORPTIONS IN THE IR, AND RAMAN SPECTRA OF NISIA, TOGETHER WITH THE ASSIGNMENT BASED ON  $D_{4h}$  SYMMETRY. THE RESULTS FOR  $K_2C_4O_4$  ARE WITHIN THE BRACKETS. E.S.D. =  $3\text{ cm}^{-1}$

ASSIGNMENT	RAMAN ( $\text{cm}^{-1}$ )	IR ( $\text{cm}^{-1}$ )
$\nu_1$ : C-O STRETCHING	1799w (1794w)	
$\nu_2$ : RING BREATHING	730s (723s)	
$\nu_3$ : INACTIVE		
$\nu_4$ : OUT-OF-PLANE C-O BENDING		243s <sup>b</sup> (259s)
$\nu_5$ : C-C STRETCHING	1135s (1123vs)	
$\nu_6$ : IN-PLANE C-O BENDING	335w (294w)	
$\nu_7$ : INACTIVE		
$\nu_8$ : INACTIVE		
$\nu_9$ : C-O STRETCHING	1595m <sup>a</sup> (1593s)	
$\nu_{10}$ : RING BENDING	655s (647s)	
$\nu_{11}$ : OUT-OF-PLANE C-O BENDING	665w (662w)	
$\nu_{12}$ : C-O STRETCHING		1480br (1530br)
$\nu_{13}$ : C-C STRETCHING		1100s (1090s)
$\nu_{14}$ : IN-PLANE C-O		342m (350m)
$2\nu_2$ : OVERTONE	1450w	
$2\nu_{10}$ : OVERTONE	1300w	

ABBREVIATIONS: br=BROAD AND STRONG, vs=VERY STRONG, s=STRONG, m=MEDIUM, w=WEAK; <sup>a</sup>=SLIGHTLY-SPLIT BAND ; <sup>b</sup>=TENTATIVE ASSIGNMENT, BECAUSE IN THIS REGION N1-O AND N1-L BENDING VIBRATIONS OCCUR.

The deviation of the low frequency bands must also be caused by the difference in the bonding properties of potassium and nickel.

At 3250 and 3050  $\text{cm}^{-1}$  two very broad and intense bands (having a large area of overlap) are observed. On the high energy side a shoulder at *ca.* 3420  $\text{cm}^{-1}$  is observed. The occurrence of these low-lying O-H and N-H stretching vibrations predicts the presence of quite strong hydrogen bridges. Bellamy and Owen<sup>51</sup> published an expression that related the frequency of the O-H stretching vibration and the O-O distance of the hydrogen bridge. It is calculated that for the present O-O distances (2.657 and 2.745 Å) and O-N distance (3.012 Å) (chapter III.5) the O-H stretching and N-H stretching vibrations should occur at 3090, 3320 and 3410  $\text{cm}^{-1}$  respectively; this is in nice agreement with the experimental data (*vide supra*).

In both the far-IR and the low frequency part of the Raman spectrum several well-resolved vibration bands occur, *i.e.* the  $\text{Ni-O}_w$ ,  $\text{Ni-O}_s$ , and Ni-L vibrations.

the metal oxygen vibration bands mostly are more intense compared to the metal nitrogen vibration bands<sup>52</sup>, allowing a tentative assignment, based on the experience with similar oxalato-bridged coordination compounds<sup>53</sup>. The observed bands have been listed in table III.6.2. The bands at 400 and

TABLE III.6.2. FAR-IR AND RAMAN FREQUENCIES IN THE REGION 400-50  $\text{cm}^{-1}$ , TOGETHER WITH SOME TENTATIVE ASSIGNMENTS. E.S.D. = 1  $\text{cm}^{-1}$

DESCRIPTION	FAR-IR( $\text{cm}^{-1}$ )	RAMAN( $\text{cm}^{-1}$ )
$\nu^a_{\text{Ni-O}_{\text{water}}}$	400vs	
$\nu^a_{\text{Ni-O}_{\text{squarate}}}$	369s	
$\nu^b_{\text{Ni-L}}$	269vs 148s	210s 90s
UNASSIGNED AND LIGAND BANDS }	342m 255sh 243s 217vs 182m 176m 126m 115m 99w 77m	370s 335m 240w 180w 135w 105sh 70m 55s

ABBREVIATIONS: sh=SHOULDER, FURTHER AS IN TABLE III.6.1.;

<sup>a</sup>=STRETCHING AND <sup>b</sup>=STRETCHING AND BENDING VIBRATION.

369  $\text{cm}^{-1}$  are assigned to the  $\text{Ni-O}_w$  and  $\text{Ni-O}_s$  stretching vibrations (IR) respectively.  $\text{Ni-O}_w$  vibrations usually occur<sup>52</sup> near 400  $\text{cm}^{-1}$ . The bands at 269 and 148  $\text{cm}^{-1}$  are assigned to the stretching and bending vibrations of the Ni-L bond respectively, in agreement with published data on  $\text{Ni}(\text{imidazole})_6^{2+}$  species<sup>54-56</sup>. In the Raman spectrum these vibrations occur at respectively 210 and 90  $\text{cm}^{-1}$ , just as found in the nitrate compound<sup>54</sup>. The bending Ni-O vibrations are expected to occur below *ca.* 250  $\text{cm}^{-1}$  and because in this region also squarate and imidazole vibrations occur<sup>50, 54</sup>, no attempts were made to assign these vibration bands. Assigning vibrations related to Ni-O bonds in the Raman



spectrum gives rise to problems, because in the  $300\text{--}400\text{ cm}^{-1}$  region also the squarato anion has some Raman frequencies<sup>57</sup>, which could overlap; therefore only the observed vibration bands are listed in table III.6.2.

#### *Ligand-field spectroscopy*

The ligand-field spectrum of NISIA shows three strong absorptions, at 1120, 627 and 376 nm and a shoulder at 708 nm. On the basis of octahedral geometry these bands are assigned to transitions from the  $^3A_{2g}$  ground state to the  $^3T_{2g}$ ,  $^3T_{1g}(F)$ ,  $^3T_{1g}(P)$  and  $^1E_g$  excited states respectively.

The  $Dq$  (ligand-field parameter) and  $B$  (Racah parameter) values are calculated according to published methods dealing with averaged environment<sup>18</sup>. Both  $Dq$  and  $B$  amount to  $890(5)\text{ cm}^{-1}$  and are in the range normally found for octahedrally-coordinated Ni(II) ions, with a ligand set of two N and four O donor atoms.

#### *Magnetic susceptibility measurements*

Magnetic susceptibility measurements at low temperatures (1.2–100K) were carried out to see if exchange coupling between the Ni(II) ions could be observed. The corrected<sup>32</sup> molar susceptibilities *vs.* temperature are plotted in figure III.6.1. In this figure also a theoretical curve for a monomeric Ni(II) compound with an axial zero-field splitting  $D$ , is plotted. It is noticed that below 2K the susceptibility reaches an almost constant finite value, which can be explained in two ways.

Firstly, this behaviour is consistent with the magnetism expected for a spin-triplet state in an axially-distorted environment<sup>58</sup>, with a positive zero-field splitting parameter. Secondly, this behaviour can be expected for antiferromagnetically-coupled Ni(II) ions; in this case the susceptibility should decrease again for temperatures below 1.2K. The only way to find out if the present magnetic data set implies the existence of antiferromagnetically-coupled Ni(II) ions, is to fit the data to theoretical susceptibilities obtained from calculations on one-dimensional models<sup>7</sup> (*vide infra*).

The high-temperature data (above *ca.* 10K) obeyed the Curie-Weiss law, *i.e.*  $\chi_M = C/(T-\theta)$ , yielding  $C$  and  $\theta$  values of  $1.30(2)\text{ emu/K.mole}$  and  $-1.1(8)\text{K}$ , respectively. The calculated  $C$  value lies in the range, that is normally found for octahedrally-surrounded Ni(II) ions. The negative  $\theta$  value is indicative for the presence of an antiferromagnetic interaction.

Least-squares fits to the experimental values of the susceptibility expression of a spin-triplet state in axially-distorted environment<sup>58</sup> yielded good results, however, a fit with unique spin Hamiltonian parameters  $D$ ,  $g_{//}$

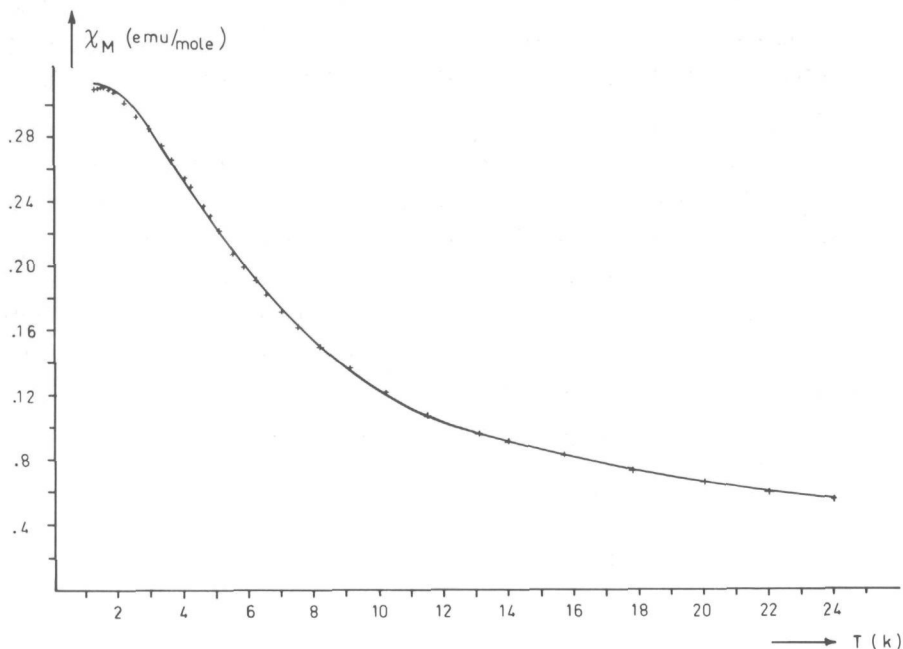


Fig. III.6.1. Molar susceptibility (+) of NISIA as a function of temperature. Full curve represents the susceptibility of a spin triplet which is axially distorted<sup>58</sup>, with parameters  $D=+5.8 \text{ cm}^{-1}$ ,  $g_{//} = g_{\perp} = 2.28$ .

and  $g_{\perp}$  is difficult to obtain<sup>59</sup>; therefore the  $D$ -parameter was calculated from the very low temperature limit equation<sup>59</sup>,  $\chi_M = 4N\beta^2 g_{\perp}^2 / 3D$  ( $kT \ll D$ ). To a first approximation  $g_{//}$  was set equal to  $g_{\perp}$ , since octahedrally-surrounded Ni(II) ions generally show nearly isotropic  $g$ -values<sup>60,61</sup>. From the high-temperature limit equation,  $\chi_M = 2N\beta^2 \bar{g}^2 / 3kT$  ( $kT \gg D$ ) it was calculated that  $\bar{g} = 2.28(3) \approx g_{\perp}$ . Substituting this value for  $g_{\perp}$  in the low-temperature-limit equation, the  $D$ -value was found to be  $+5.8 \text{ cm}^{-1}$ .

As mentioned above, the presence of a one-dimensional exchange interaction cannot be excluded; therefore, the data were also fitted to the results based on calculations on a linear  $S=1$  chain system. Recently, de Neef<sup>7</sup> published several  $\chi$  vs.  $T$  curves for infinite isotropic  $S=1$  systems with antiferromagnetic interactions. Fitting to these curves in principle yield  $g$ ,  $J$  and  $D$  values; however, in the present case no reasonable fit could be obtained. Qualitatively, it was noticed that the larger the ratio  $D/|J|$ , the better the fits became.

Since no results are available for  $D/|J| > 4$  (which curve in fact yielded the best results) it is not possible whether the model is appropriate in the present system. The only conclusion that could be drawn is that it seems as if  $D \gg |J|$ .

Finally, a weak two-dimensional interchain interaction caused by the hydrogen bonds between the water molecules and adjacent squarato anions, might be considered. Because of the fact that exchange *via* hydrogen bonds over long distances (in the present case  $\text{Ni} \dots \text{Ni} = 7.1 \text{ \AA}$ ) is assumed to be very weak and has only a few precedents<sup>62,63</sup>, this possibility was not further considered. Moreover, no theoretical models including a zero-field splitting are known for two-dimensional  $S=1$  systems.

### III.7. Conclusions

The present oxalate compounds appear to be chains, in which the oxalato anion acts as a tetradentate bridging ligand. The metal ions are coupled anti-ferromagnetically, with relatively-large J-values. The magnetism of the Ni(II) compounds was described within the Heisenberg model of isotropic coupling, including a zero-field splitting<sup>7</sup>. The susceptibilities of the Co(II) compounds were described within the Ising model of anisotropic coupling<sup>23</sup>, yielding g-values in agreement with the ESR experiments.

The organic ligands hardly seemed to influence the J-values, in agreement with a superexchange path *via* the O-C-O and/or O-C-C-O bonds of the oxalato anion. Qualitatively such a poly-atomic bridge having a mirror plane perpendicular to the chain, can be regarded as acting like a molecular orbital and because of the symmetry each metal ion will interact identically with this bridge orbital, giving rise to antiferromagnetic interactions<sup>8</sup>.

From the X-ray structure determination of the compound  $\text{ZnOx}(\text{2MIz})_2 \cdot \frac{1}{2}\text{H}_2\text{O}$ , it is seen that the 2MIz compounds form zig-zag chains. For the other azoles it is not clear whether the chains are zig-zag or linear; the oxalate vibrations in the IR and Raman occur at similar frequencies compared to the 2MIz compounds, indicating the presence of a zig-zag chain structure. However, the Mössbauer-effect measurements revealed for the 2MIz compound a much larger quadrupole splitting compared to the others, suggesting a different configuration of ligands for the latter compounds. No definite conclusion can be drawn about the structure in the other azole compounds, because also the ESR experiment confused this problem; only the DMIZ compound revealed an axial ESR spectrum.

The Mössbauer-effect measurements showed that substituting  $\text{H}_2\text{O}$  by an azole ligand indeed increases the one-dimensionality of the chains just as expected. The  $T_N$  temperatures for all compounds were measured.

The results of the X-ray structure analysis on the compound  $\text{NiSq}(\text{Iz})_2(\text{H}_2\text{O})_2$ , showed it to be a squarato-bridged chain, in which only two oxygens of the squarato anion are coordinated directly to Ni(II). The other two oxygens are coordinated indirectly *via* hydrogen bonds with two water molecules to nickel.

The magnetism of the squarate compound could be described with the expression for a monomeric Ni(II) ion, with an axial zero-field splitting, meaning that the superexchange interaction *via* the squarato anion is very small.

Substitution of the oxalate by the squarate bridge apparently gives rise to

very strong reduction of the superexchange interactions in chain compounds, just as observed for dimeric compounds<sup>8</sup>. Presumably the symmetry of the bridge orbitals affects the interaction to a great extent; it is noticed that the plane of the squarate molecule is strongly tipped away from the basal plane of the octahedron around Ni(II), which could result in a different overlap between the  $\pi$ -orbitals of the squarate anion and the unpaired d-electrons of the Ni(II) ions.

Furthermore, from the present studies, it seems that the presence of a bridging unit in which a  $\pi$ -system is operative, does not mean *a priori* that the superexchange will be favoured. This discussion agrees with recent work of Hendrickson *et al.*<sup>65</sup>

### III.8 References

- (1) L. Welo, *Phil. Mag.*, **6**, 481 (1928).
- (2) M. Melnik, H. Langfelderová, J. Garaj and J. Gazo, *Inorg. Chim. Acta*, **7**, 669 (1973).
- (3) C. Mazzi and F. Garavelli, *Periodico Mineral. (Rome)*, **26**, 2 (1957).
- (4) S. Cavid, *Bull. Soc. Franc. Mineral. Cristallogr.*, **82**, 50 (1959).
- (5) S. de S. Barros and S.A. Friedberg, *Phys. Rev.*, **141**, 637 (1966).
- (6) C.Y. Weng, *Ph.D. Thesis*, Carnegie-Mellon Institute of Technology (1968).
- (7) T. de Neef, *Ph.D. Thesis*, Eindhoven University of Technology (1975).
- (8) D.M. Duggan, E.K. Barefield and D.N. Hendrickson, *Inorg. Chem.*, **12**, 985 (1973).
- (9) X-ray system -version of June 1972- technical report TR-192 of the computer science center, University of Maryland, June (1972).
- (10) D.T. Cromer and J.B. Mann, *Acta Crystallogr.*, **A24**, 321 (1968).
- (11) R.F. Stewart, E.R. Davidson and W.T. Simpson, *J. Phys. Chem.*, **42**, 3175 (1965).
- (12) G.B. Jameson, F.S. Molinaro, J.A. Ibers, J.P. Collman, J.I. Brauman, E. Rose and K.S. Suslick, *J. Am. Chem. Soc.*, **100**, 6769 (1978).
- (13) G.A. Jeffrey and G.S. Parry, *J. Am. Chem. Soc.*, **76**, 5283 (1954).
- (14) N.F. Curtis, I.R.N. McCormic and T.N. Waters, *J. Chem. Soc. Dalton*, 1537 (1973).
- (15) F. Le Floch, J. Sala-Pala and J.E. Guerschais, *Bull. Soc. Chim. France*, **120** (1975).
- (16) A.C. Skapski, J.E. Guerschais and J.Y. Calves, *C. R. Hebd. Séances Acad. Sci.*, **C278**, 1377 (1974).
- (17) R. Kergoat and J.E. Guerschais, *Z. Anorg. Allg. Chem.*, **416**, 174 (1975).
- (18) J. Reedijk, P.W.N.M. van Leeuwen and W.L. Groeneveld, *Rec. Trav. Chim.*, **87**, 129 (1968).
- (19) J. Reedijk, W.L. Driessen and W.L. Groeneveld, *Rec. Trav. Chim.*, **88**, 1095 (1969).
- (20) C.K. Jorgensen, "Absorption Spectra and Chemical Bonding in Complexes", Pergamon Press, Oxford (1962).
- (21) A. Abragam and M.H.L. Price, *Proc. Roy. Soc.*, **A206**, 173 (1951).
- (22) J. Reedijk and P.J.J.M. van der Put, *Proc. Int. Conf. Coord. Chem.*, **16**, 2-37b (1974).
- (23) M.E. Fisher, *J. Math. Phys.*, **4**, 124 (1963).
- (24) S. Katsura, *Phys. Rev.*, **127**, 1508 (1962).
- (25) T. Nakamura, *J. Phys. Soc. Japan*, **7**, 264 (1952).
- (26) M.E. Fisher, *Am. J. Phys.*, **32**, 343 (1964).
- (27) H.E. Stanley, *Phys. Rev.*, **179**, 570 (1969).
- (28) J.C. Bonner and M.E. Fisher, *Phys. Rev.*, **A135**, 640 (1964).
- (29) G.S. Rushbrooke, G.A. Baker jr., P.J. Wood, "Phase Transitions and Critical Phenomena", Vol. III, Academic Press, London (1974).
- (30) E. Rhodes and S. Scales, *Phys. Rev.*, **B8**, 1994 (1973).
- (31) F. Keffer, *Handbuch der Physik*, Vol XVIII/2, Springer Verlag, Berlin (1966).
- (32) E. König, "Magnetic Properties of Coordination and Organometallic Transition Metal Complexes", Springer Verlag, Berlin (1966).
- (33) A.P. Ginsberg, R.L. Martin, R.W. Brookes and R.C. Sherwood, *Inorg. Chem.*, **11**, 2884 (1972).
- (34) J. van Dongen Torman, R. Jagannathan and J.M. Trooster, *Hyperfine Int.*, **1**, 135 (1975).
- (35) W. Kündig, *Nucl. Instr. and Meth.*, **48**, 219 (1967).
- (36) W. Marshall and C.E. Johnson, *Le J. de Phys. et Le Rad.*, **23**, 733 (1962).
- (37) S. de S. Barros, P. Zory and L.E. Campbell, *Phys. Letters*, **7**, 135 (1963).
- (38) A.J.M. Duisenberg, Collected Abstracts of the First European Enraf-Nonius CAD4-Users Meeting, Paris, June (1974).
- (39) CAD4-Users Manual, Enraf-Nonius, Delft (1971).

- (40) P. Main, M.M. Woolfson, L. Lessinger, G. Germain, J-P. Declercq, Multan 74, A system of Computer Programs for the automatic solution of crystal structures from X-ray diffraction data.
- (41) The function minimized was  $\Sigma(w(|F_o| - |F_c|))^2$ . The refinement was on  $F$ . The unweighted and weighted residuals are defined as follows:  
 $R_F = (\Sigma|F_o| - |F_c|)/(\Sigma|F_o|)$ ;  $R_{wF} = (\Sigma w(|F_o| - |F_c|)^2)/(\Sigma w|F_o|^2)^{\frac{1}{2}}$ .
- (42) P.A. Doyle and P.S. Turner, *Acta Crystallogr.*, A24, 390 (1968).
- (43) H.M. Rietveld, Fysica Memo 153, RCN Petten, The Netherlands (1966).
- (44) C.K. Johnson, ORTEP, report ORNL-3794 (1965).
- (45) J.M. Stewart, G.J. Kruger, H.L. Ammon, C. Dickinson and S.R. Hall, "XRAY SYSTEM", technical report TR-446, of the computer science center, University of Maryland, implemented and extended by the Dutch X-ray System Group (1976).
- (46) M. Habenschuss and B.C. Gerstein, *J. Chem. Phys.*, 61, 852 (1974).
- (47) D. Semmingsen, *Acta Chem. Scand.*, 27, 3961 (1973).
- (48) L.R. Nassimbeni and A.C. Rodgers, *Acta Crystallogr.*, B32, 257 (1976).
- (49) J.C. Jansen, H. van Koningsveld and J.A.C. van Ooijen, *Cryst. Struct. Comm.*, in press.
- (50) M. Ito and R. West, *J. Am. Chem. Soc.*, 85, 2580 (1963).
- (51) L.J. Bellamy and A.J. Owen, *Spectr. Chim. Acta*, 25A, 329 (1969).
- (52) J.R. Ferraro, "Low-frequency Vibrations of Inorganic and Coordination Compounds", Plenum-Press, New York (1971).
- (53) C.G. van Kralingen, J.A.C. van Ooijen and J. Reedijk, *Transition Met. Chem.*, 3, 90 (1978).
- (54) D.M. Adams and W.R. Trumble, *J. Chem. Soc. Dalton*, 30 (1975).
- (55) J. Reedijk, *Rec. Trav. Chim.*, 88, 1451 (1969).
- (56) J.C. Jansen and J. Reedijk, *Z. Naturf.*, B29, 527 (1974).
- (57) S. Nakashima and M. Balkanski, *Solid State Comm.*, 19, 1225 (1976).
- (58) R.L. Carlin, *J. Chem. Educ.*, 43, 521 (1966).
- (59) P.J. van der Put and A.A. Schilperoord, *Inorg. Chem.*, 13, 2476 (1974).
- (60) F.W. Klaaysen, J. Reedijk and H.T. Witteveen, *Z. Naturf.*, 27A, 1532 (1972).
- (61) J. Reedijk, H.T. Witteveen and F.W. Klaaysen, *J. Inorg. Nucl. Chem.*, 35, 3439 (1973).
- (62) J.A. Bertrand, T.D. Black, P.G. Aller, F.T. Helm and R. Mahmood, *Inorg. Chem.*, 15, 2965 (1976).
- (63) D.M. Duggan, R.G. Jungst, K.R. Mann, G.D. Stucky and D.N. Hendrickson, *J. Am. Chem. Soc.*, 96, 3443 (1974).
- (64) H.C. Freeman and J.M. Guss, *Acta Crystallogr.*, B34, 2451 (1978).
- (65) C.G. Pierpont, L.C. Francesconi and D.N. Hendrickson, *Inorg. Chem.*, 17, 3470 (1978).

## IV. HALOGEN-BRIDGED DIMERIC AND TETRAMERIC COMPOUNDS

### IV.1. Introduction

In previous chapters attention has been given to chain-type compounds, having either small (halogen) or large (oxalate/squarate) bridging ligands.

From literature several examples are known, having the same type of ligands in dimeric (or tetrameric) systems.

In this chapter a few new systems will be discussed having chloride and fluoride as bridging ligands in dimeric and tetrameric systems.

In dimeric hydroxo-bridged copper(II) compounds, Hodgson, Hatfield *et al.*<sup>1</sup> recently found a linear relationship between the value of the exchange integral,  $J$ , and the bridging Cu-O-Cu angle. Although Barraclough and Brookes<sup>2</sup> have postulated a similar relationship for chloride-bridged Ni(II) dimers, such a relationship does not seem to exist, as noticed by Hendrickson and coworkers<sup>3</sup>. Recently, Sinn *et al.*<sup>4</sup>, on the other hand, conclude that a decrease in bridging Ni-Cl-Ni angle coincides with a decrease in the coupling constant from positive  $J$  (ferromagnetic) to negative  $J$  (antiferromagnetic).

Preliminary results on the transition metal compound  $\text{Ni(dmpzm)Cl}_2$ <sup>5</sup>, showed that the magnetic coupling is ferromagnetic in nature, whereas other related compounds, having five-coordinated Ni(II) with a  $\text{Cl}_3\text{N}_2$  core, *i.e.*  $\text{Ni(qnqn)Cl}_2$ <sup>3</sup>,  $\text{Ni(dmp)Cl}_2$ <sup>4</sup>,  $\text{Ni(dmp)Cl}_2 \cdot \text{CHCl}_3$ <sup>4</sup> and  $\text{Ni(biq)Cl}_2$ <sup>4</sup>, show antiferromagnetic superexchange interactions.

To find out the origin of the observed ferromagnetism in  $\text{Ni(dmpzm)Cl}_2$ <sup>5</sup>, a detailed magnetic and structural study was undertaken. The results of the structural study are presented in chapter IV.2, whereas the physical measurements and their interpretation are described in chapter IV.3.

In chapter IV.4, the results of the magnetic susceptibility measurements and magnetization studies on some dimeric and tetrameric fluorine-bridged Co(II) compounds are presented. Only recently, the crystal structures of the unprecedented dimeric and tetrameric species, *i.e.*  $\text{Co}_2\text{F}_2(3,5\text{-dimethylpyrazole})_6(\text{BF}_4)_2$ ,  $\text{Co}_4\text{F}_4(\text{N-ethylimidazole})_{12}(\text{BF}_4)_4$  respectively, have been reported by Reedijk, van Koningsveld and coworkers<sup>6,7</sup>. The superexchange interactions between the Co(II) ions are discussed in relation with the structures of these compounds.



## IV.2. Crystal and Molecular Structure of di- $\mu$ -chlorodichlorobis(bis-(3,5-dimethylpyrazolyl)methane)diNickel(II).

### IV.2.1. Experimental

Orange single crystals of the title compound, abbreviated NIDI, were prepared as described in the literature<sup>5</sup>.

### IV.2.2. Crystal and intensity data, structure determination and refinement

From single-crystal diffractometry ( $\text{MoK}\alpha_1 = 0.70926 \text{ \AA}$ ) the following data were obtained:  $a = 8.944(4)$ ,  $b = 11.015(5)$ ,  $c = 7.864(4) \text{ \AA}$ ,  $\alpha = 75.964(4)$ ,  $\beta = 83.170(5)$ ,  $\gamma = 110.476(6)^\circ$ , space group  $P\bar{1}$ ,  $D_m = 1.6 \text{ g/cm}^3$ ,  $D_c = 1.62 \text{ g/cm}^3$ , and  $Z = 2$  (one dimer).

Intensities of 3249 independent reflections above background ( $I > 2.85\sigma(I)$ ) were collected from a crystal with dimensions  $ca.$   $0.3 \times 0.3 \times 0.1 \text{ mm}$ , using a computer-controlled NONIUS single-crystal diffractometer with a graphite monochromator and Mo-radiation.

The structure was solved by the heavy-atom method and refined by (blocked) full-matrix least-squares calculations, using programs of the XRAY system<sup>8</sup>. The form factors for Ni, Cl, C and N were taken from Cromer and Mann<sup>9</sup> and those for H from Stewart *et al.*<sup>10</sup>. No absorption correction has been applied in the reduction of the intensities to the structure factors ( $\mu_{\text{MoK}\alpha_1} = 16.1 \text{ cm}^{-1}$ ). All non-hydrogen atoms were refined anisotropically; the hydrogen atoms were refined with fixed isotropic temperature factors. The final conventional R-value is 0.035.

Final positional and thermal parameters are shown in table IV.2.1.

### IV.2.3. Results and discussion

Figure IV.2.1 provides an illustration of the dimeric molecule. The dimer is made up by two  $\text{Ni}(\text{bis}-(3,5\text{-dimethylpyrazolyl})\text{methane})\text{Cl}_2$ , abbreviated  $\text{Ni}(\text{dmpzm})\text{Cl}_2$ , units, which are related by the crystallographically imposed-center of symmetry. Each unit consists of a five-coordinated Ni(II) ion surrounded by the bidentate ligand dmpzm, a terminal chloride ion, a bridging chloride ion and a second bridging chloride ion belonging to the other half of the dimer. The bridging chlorides and the Ni(II) ion of each unit interact in a strictly planar bridging system.

The separation between the Ni(II) ions amounts to  $3.587(2) \text{ \AA}$  and the

TABLE IV.2.1. FINAL FRACTIONAL ATOMIC COORDINATES AND THERMAL PARAMETERS<sup>x</sup>. ESTIMATED STANDARD DEVIATIONS ARE IN PARENTHESES

ATOM	$x/a$	$y/b$	$z/c$	$100u_{11}/a^2$	$100u_{22}/b^2$	$100u_{33}/c^2$	$100u_{12}/ab$	$100u_{13}/ac$	$100u_{23}/bc$
N1	0.02293(5)	0.84123(4)	0.07096(5)	2.89(2)	1.90(2)	2.79(2)	1.30(1)	-0.66(1)	-0.88(1)
Cl(1)	0.0888(1)	1.03919(7)	0.1522(1)	4.80(4)	2.57(3)	3.99(4)	2.04(3)	-2.03(3)	-1.62(3)
Cl(2)	-0.1887(1)	0.63912(7)	0.0910(1)	3.96(4)	2.36(3)	5.39(5)	1.11(3)	-1.71(4)	-1.06(3)
Cl	0.1893(4)	0.6395(3)	0.0689(5)	3.9(2)	2.7(1)	4.0(2)	1.9(1)	-0.9(1)	-1.4(1)
Cl1	0.3576(4)	0.9769(3)	-0.2113(5)	3.7(2)	3.2(1)	4.0(2)	1.5(1)	-0.1(1)	-0.8(1)
Cl2	0.4878(4)	0.9411(4)	-0.2616(6)	3.5(2)	4.3(2)	5.1(2)	1.5(1)	0.3(2)	-1.0(2)
Cl3	0.4401(4)	0.8062(3)	-0.1682(5)	3.3(2)	4.4(2)	4.4(2)	2.1(1)	-1.1(1)	-2.1(2)
Cl11	0.3504(6)	1.1143(4)	-0.2760(7)	5.3(2)	3.3(2)	6.8(3)	1.8(2)	1.1(2)	0.2(2)
Cl31	0.5263(5)	0.7125(5)	-0.1728(7)	3.9(2)	5.5(2)	7.4(3)	3.0(2)	-1.3(2)	-2.8(2)
N11	0.2341(3)	0.8704(2)	-0.0935(4)	3.6(1)	2.7(1)	3.6(1)	1.9(1)	-0.6(1)	-1.0(1)
N12	0.2884(3)	0.7656(2)	-0.0693(4)	3.3(1)	3.0(1)	3.6(1)	1.9(1)	-0.7(1)	-1.2(1)
C21	0.1004(4)	0.7322(3)	0.4535(4)	3.8(2)	3.2(1)	3.1(2)	1.2(1)	-1.0(1)	-0.9(1)
C22	0.1807(5)	0.6491(4)	0.5225(5)	4.7(2)	4.2(2)	3.5(2)	1.8(2)	-1.8(2)	-0.8(1)
C23	0.2289(4)	0.6042(3)	0.3880(5)	3.5(2)	3.0(1)	4.2(2)	1.5(1)	-1.4(1)	-0.3(1)
C211	0.0251(6)	0.8055(4)	0.5483(6)	6.8(3)	4.8(2)	3.4(2)	2.7(2)	-1.0(2)	-1.7(2)
C231	0.3231(6)	0.5154(5)	0.3816(7)	5.4(2)	4.9(2)	6.1(3)	3.3(2)	-1.5(2)	-0.2(2)
N21	0.0983(3)	0.7383(2)	0.2830(4)	3.9(1)	2.7(1)	3.3(1)	1.9(1)	-1.1(1)	-1.2(1)
N22	0.1794(3)	0.6596(2)	0.2437(4)	3.9(1)	2.6(1)	3.5(1)	2.0(1)	-0.9(1)	-0.8(1)
H11	0.082(5)	0.604(4)	0.041(5)	4.31 <sup>a</sup>					
H12	0.245(4)	0.582(4)	0.064(5)	4.31					
H121	0.595(5)	1.005(4)	-0.345(6)	5.57					
H1111	0.253(6)	1.108(4)	-0.318(6)	6.46					
H1112	0.437(5)	1.173(4)	-0.371(6)	6.46					
H1113	0.347(6)	1.146(5)	-0.175(7)	6.46					
H1311	0.626(6)	0.757(5)	-0.253(7)	7.09					
H1312	0.465(6)	0.634(5)	-0.214(7)	7.09					
H1313	0.554(6)	0.692(5)	-0.066(7)	7.09					
H221	0.198(5)	0.634(4)	0.636(6)	5.07					
H2111	-0.060(6)	0.806(5)	0.506(7)	6.46					
H2112	-0.018(5)	0.755(5)	0.662(7)	6.46					
H2113	0.103(6)	0.875(5)	0.550(6)	6.46					
H2311	0.426(6)	0.567(5)	0.314(7)	6.84					
H2312	0.324(6)	0.479(5)	0.484(7)	6.84					
H2313	0.284(6)	0.449(5)	0.312(7)	6.84					

<sup>x</sup> = THE ANISOTROPIC THERMAL PARAMETERS ARE IN THE FORM:  $t = \exp \{-2\pi^2 \sum_{i,j} h_i h_j u_{ij}^* \}$ .

<sup>a</sup> = PARAMETER IS HELD FIXED.

Ni-Cl-Ni angle is  $97.36(4)^\circ$ . These values are in the range of values observed in similar structures<sup>3,4</sup> (see also table IV.3.1). Interatomic distances and angles are listed in table IV.2.2 and table IV.2.3 respectively.

The bridging Ni-Cl distances (2.319(1) and 2.456(1) Å) in fact reveal the most asymmetric bridge compared to the other five-coordinated Ni(II) compounds. The reason for this will be discussed below.

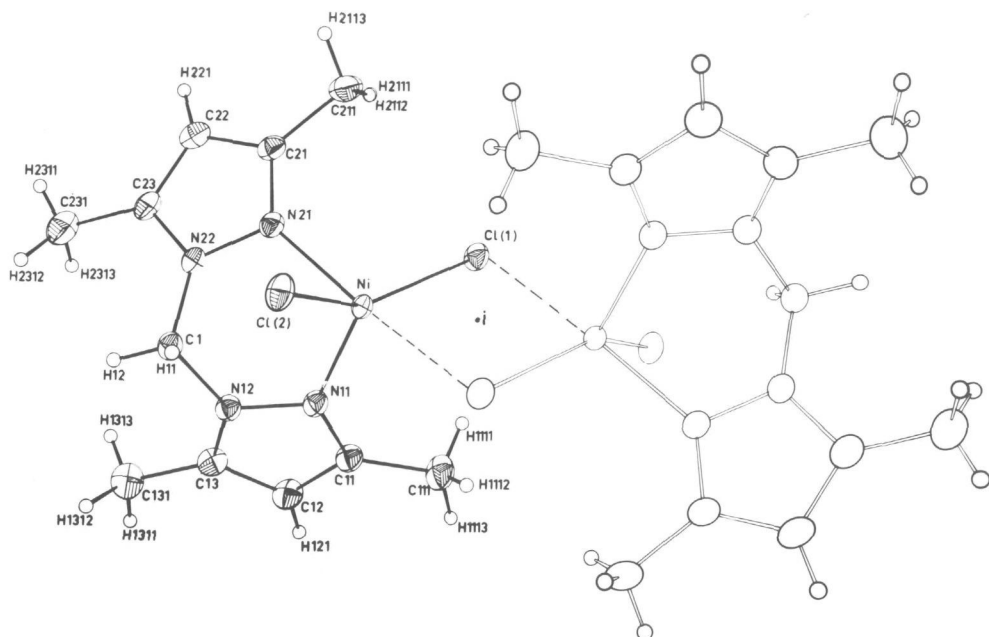


Fig. IV.2.1. ORTEP<sup>11</sup> drawing of NIDI.

Each Ni(II) ion is in a geometry intermediate of a trigonal bipyramid and a square pyramid. The most typical angles of trigonal bipyramidal ( $1 \times 180^\circ + 3 \times 120^\circ$ ) and square pyramidal ( $2 \times \leq 180^\circ + 4 \times \geq 90^\circ$ ) both fit on the present geometry around nickel. The structural differences of the present compound with the four previously reported<sup>3, 4</sup> five-coordinated chlorine-bridged Ni(II)

dimers can be summarized as follows:

- a distortion of the geometry from square pyramidal to trigonal bipyramidal; this is most clearly seen by the N-Ni-Cl angle of  $173.8(3)^\circ$  (compared to  $155-158^\circ$

TABLE IV.2.2. INTERACTOMIC DISTANCES ( $\text{\AA}$ )

N1 - C1(1)	2.319(1)	N11 - C11	1.333(3)	N21 - C21	1.327(5)
N1 - C1(2)	2.318(1)	N11 - N12	1.383(4)	N21 - N22	1.375(5)
N1 - C1(1) <sup>a</sup>	2.456(1)	C11 - C12	1.398(6)	C21 - C22	1.400(6)
N1 - N11	2.033(3)	C11 - C111	1.501(6)	C21 - C211	1.487(7)
N1 - N21	2.099(3)	C111 - H1111	0.96(5)	C211 - H2111	0.86(5)
		C111 - H1112	0.92(4)	C211 - H2112	0.88(5)
C1 - N12	1.439(3)	C111 - H1113	0.94(6)	C211 - H2113	0.84(5)
C1 - N22	1.441(5)	C12 - H121	1.00(3)	C22 - H221	0.91(5)
C1 - H11	0.98(4)	C12 - C13	1.372(5)	C22 - C23	1.357(6)
C1 - H12	0.94(5)	C131 - H1311	0.92(5)	C231 - H2311	0.91(4)
		C131 - H1312	1.00(5)	C231 - H2312	0.81(5)
		C131 - H1313	0.90(6)	C231 - H2313	1.00(6)
		C13 - N12	1.342(4)	C23 - N22	1.352(5)
		C13 - C131	1.493(7)	C23 - C231	1.502(7)

<sup>a</sup> = -x, -y, -z

TABLE IV.2.3. INTERATOMIC ANGLES ( $^{\circ}$ )

Cl(1) - N1 - Cl(2)	144.23(5)	Cl3 - Cl31 - H1313	108(4)
Cl(1) - N1 - N11	103.50(9)	H1311 - Cl31 - H1312	105(4)
Cl(1) - N1 - N21	94.88(9)	H1311 - Cl31 - H1313	103(5)
Cl(1) - N1 - Cl(1) <sup>a</sup>	82.64(4)	H1312 - Cl31 - H1313	117(4)
Cl(2) - N1 - N11	112.08(9)	Cl2 - Cl3 - Cl31	130.2(3)
Cl(2) - N1 - N21	90.26(7)	Cl2 - Cl3 - N12	106.6(4)
Cl(2) - N1 - Cl(1) <sup>a</sup>	88.48(5)	N12 - Cl3 - Cl31	123.1(3)
N11 - N1 - N21	87.6(1)	Cl3 - N12 - N11	111.9(2)
N11 - N1 - Cl(1) <sup>a</sup>	98.56(9)	N11 - N12 - Cl	117.9(3)
N21 - N1 - Cl(1) <sup>a</sup>	173.8(3)	Cl3 - N12 - Cl	129.7(3)
N1 - Cl(1) - N1 <sup>a</sup>	97.36(4)	N1 - N21 - N22	116.8(2)
N12 - Cl - N22	110.6(3)	N1 - N21 - C21	137.7(3)
N12 - Cl - H11	108(2)	C21 - N21 - N22	105.3(3)
N12 - Cl - H12	105(2)	N21 - C21 - C22	109.9(4)
N22 - Cl - H11	113(2)	N21 - C21 - C211	122.3(4)
N22 - Cl - H12	108(3)	C22 - C21 - C211	127.8(4)
H11 - Cl - H12	111(4)	C21 - C211 - H2111	107(4)
N1 - N11 - N12	118.8(2)	C21 - C211 - H2112	109(4)
N1 - N11 - Cl1	135.8(3)	C21 - C211 - H2113	106(4)
Cl1 - N11 - N12	104.5(3)	H2111 - C211 - H2112	103(4)
N11 - Cl1 - Cl2	110.8(3)	H2111 - C211 - H2113	125(5)
N11 - Cl1 - Cl11	122.4(4)	H2112 - C211 - H2113	106(5)
Cl2 - Cl1 - Cl11	126.9(3)	C21 - C22 - C23	107.1(3)
Cl1 - Cl11 - H1111	111(3)	C21 - C22 - H221	124(3)
Cl1 - Cl11 - H1112	112(4)	C23 - C22 - H221	129(3)
Cl1 - Cl11 - H1113	106(3)	C23 - C231 - H2311	109(4)
H1111 - Cl11 - H1112	107(4)	C23 - C231 - H2312	108(4)
H1111 - Cl11 - H1113	108(5)	C23 - C231 - H2313	115(3)
H1112 - Cl11 - H1113	113(4)	H2311 - C231 - H2312	111(5)
Cl1 - Cl2 - Cl3	106.3(3)	H2311 - C231 - H2313	100(4)
Cl1 - Cl2 - H121	125(3)	H2312 - C231 - H2313	113(5)
Cl3 - Cl2 - H121	129(3)	C22 - C23 - C231	131.1(4)
Cl3 - Cl31 - H1311	111(4)	C22 - C23 - N22	106.3(4)
Cl3 - Cl31 - H1312	113(3)	N22 - C23 - C231	122.5(4)
		C23 - N22 - N21	111.3(3)
		N21 - N22 - Cl	118.6(3)
		C23 - N22 - Cl	129.9(3)

<sup>a</sup> = -x, -y, -z

in the other compounds) and by the Cl-Ni-Cl angle of 144.23(5) $^{\circ}$  (compared to 161-169 $^{\circ}$  in the other compounds).

- a quite strong asymmetry in the NiCl<sub>2</sub>Ni bridge; although such an asymmetry was reported before in other dimeric Ni(II) compounds<sup>19</sup> (see also table IV.3.1), this asymmetry could be related to the geometry around Ni(II), making the "axial" Ni-Cl bond (in a trigonal bipyramidal geometry) longer than the "equatorial" Ni-Cl bonds.

- an unusually short distance of 2.6 Å between the terminal chloride (Cl(2)) and a hydrogen (H11) of

the CH<sub>2</sub>-group between the pyrazole fragments of the ligand dmpzm. This is depicted in figure IV.2.2. This distance of 2.6 Å is even a little smaller than the sum of the van der Waals radii of chloride and hydrogen<sup>14</sup>. In fact this CH<sub>2</sub>-group prevents the terminal chloride ion to be located in a position "required" for a square-pyramidal geometry. If this chloride is placed in the mean position as observed in the four other five-coordinated dimeric Ni(II) compounds, the H11 - Cl(2) distance would be as short as *ca.* 2.0 Å.

So, the presence of the CH<sub>2</sub>-group in the dmpzm ligand, in fact hampers the formation of a structure observed in the related compounds and decreases the Cl-Ni-Cl angle to the relatively small value of 144.23(5) $^{\circ}$ . As secondary effects

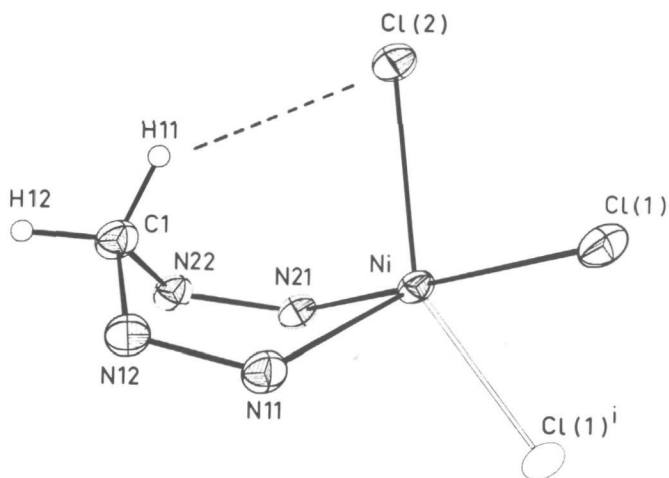


Fig. IV.2.2. Schematic drawing showing the short H11 - Cl(2) distance of 2.6 Å. For clarity the pyrazole carbons have been omitted.

the increase of Cl-Ni-N to  $173.8(3)^\circ$  and the lengthening of Ni-Cl to  $2.456(1)$  Å are observed.

All other intramolecular distances and angles appear normal and will not be discussed in detail.

From the details of the coordination geometry around Ni(II) it is evident that this particular compound is easily transformed to the tetrahedral monomeric species at high temperatures and in solution<sup>5</sup>.

### IV.3. Magnetic Superexchange Interactions in five-coordinated chlorine-bridged dimeric Ni(II) Compounds.

#### IV.3.1. Experimental

Crystals of the compound di- $\mu$ -chlorodichlorobis(bis (3,5-dimethylpyrazolyl)-methane)diNickel(II), abbreviated NIDI, were prepared as described in chapter IV.2, in which the results of the X-ray structure analysis have been given.

The magnetic data were performed as described in chapter V.

#### IV.3.2. Results and discussion

##### *Susceptibility measurements*

Magnetic susceptibility measurements of finely-ground single crystals of NIDI were collected in the 4.2-90K region. The corrected<sup>15</sup> molar susceptibility data set is plotted in figure IV.3.1. In this figure the effective magnetic

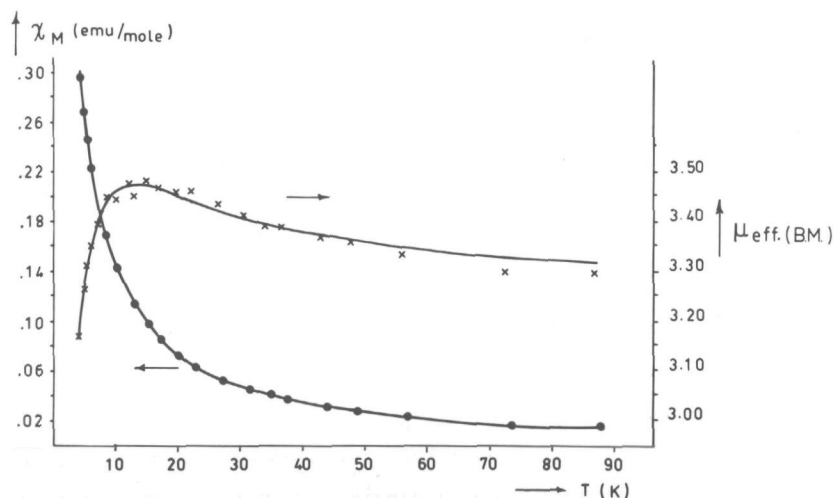


Fig. IV.3.1. Molar susceptibility (●) and effective magnetic moment per Ni(II) ion (x) of NIDI as a function of temperature; the full curves represent the theoretical curves for  $J=+2.58 \text{ cm}^{-1}$ ,  $D=-2.17 \text{ cm}^{-1}$ ,  $zJ'=-0.39 \text{ cm}^{-1}$  and  $g=2.310$ , according to Ginsberg *et al.*<sup>16</sup>

moment per Ni(II) ion, defined as  $\mu_{eff.} = (8\chi_M \cdot T)^{\frac{1}{2}}$  and the results of the fitting procedure are also included. The magnetic susceptibility apparently increases

monotonically down to 4.2K; however, in the curve of the effective magnetic moment *vs.* temperature a maximum is observed, occurring at *ca.* 13K.

A qualitatively similar behaviour has been observed for two other structurally established chlorine-bridged dimers with octahedrally coordinated Ni(II), *i.e.*  $(\text{Ni}(\text{en})_2\text{Cl})_2\text{Cl}_2$ <sup>12</sup> and  $(\text{Ni}(\text{eg})_2\text{Cl})_2\text{Cl}_2$ <sup>13</sup>. For these latter compounds this behaviour could be interpreted assuming ferromagnetic superexchange coupling between the chlorine-bridged Ni(II) ions. The decreasing effective magnetic moment at the lowest temperatures can be explained by antiferromagnetic interdimer interactions, zero-field splitting effects and/or saturation effects. The presence of saturation can be excluded from the measurements by choosing the magnetic field strength below those values for which the susceptibility becomes field dependent. In the present compound the susceptibility was found to be field independent up to *ca.* 6 kG. At higher magnetic fields the measured susceptibility, at 4.2K, decreased.

For the description of the susceptibility data a model has to be chosen, which includes intra- and interdimer exchange, and zero-field splitting. Ginsberg *et al.*<sup>16</sup> have published a susceptibility equation obtained from calculations based on the Hamiltonian

$$H = -2J(\vec{S}_1 \cdot \vec{S}_2) - D(S_{1z}^2 + S_{2z}^2) - 2zJ'(\vec{S}_1 \cdot \vec{S}_1') - g_1 \beta H S_{1z} \dots (1)$$

in which the symbols have their usual meanings<sup>16</sup>. *J* denotes the isotropic intra-dimer superexchange interaction, *D* the axial zero-field splitting and *zJ'* the interdimer interaction parameter (in the molecular-field approximation).

Computer fitting of the theoretical susceptibility equation obtained from (1)<sup>16</sup> to the data, yielded *J*=+2.58 cm<sup>-1</sup>, *D*=-2.17 cm<sup>-1</sup>, *zJ'*=-0.39 cm<sup>-1</sup> and *g*=2.310.

Preliminary results<sup>5</sup> of susceptibility measurements on NIDI were slightly different, since at that time the data were performed at a field strength of *ca.* 18 kG; furthermore, at that time no single crystals were available and the possible presence of small amounts of monomeric impurities could have influenced the experimental data.

#### *Structure-exchange relationship*

About the theories concerning the mechanism of exchange coupling in dimers *via* intermediate diamagnetic ions (superexchange) a large amount of papers has appeared; however, up to now it seems not possible to describe the superexchange interactions in a quantitative way. On the superexchange pathways that occur

in the  $\text{NiCl}_2\text{Ni}$  unit, several papers appeared. Ginsberg<sup>17</sup> and Barraclough and Brookes<sup>2</sup>, using a configuration-interaction method, take into account three ferromagnetic and three antiferromagnetic pathways. The net exchange then, should be largely dependent upon the bridging  $\text{Ni-Cl-Ni}$  angle. More recently, Sinn *et al.*<sup>4</sup> conclude also that the bridging angle mainly determines the magnetic superexchange coupling, saying that a decrease in the  $\text{Ni-Cl-Ni}$  angle is coinciding with a decrease in J-value from positive to negative values.

The structural parameters of NIDI will now be compared with the other known structurally-and magnetically-investigated nickel dimers. In table IV.3.1 some relevant data are listed. The first five compounds listed have structures with five-coordinated  $\text{Ni(II)}$  ions with geometries between square pyramidal and trigonal bipyramidal (sp and tbp respectively), whereas the last two compounds have structures with six-coordinated  $\text{Ni(II)}$  ions. It is noticed that the J-values listed will be only regarded as an estimate of the superexchange interactions, since the J-value can be affected slightly by the other parameters (see above).

It is noticed that no clear correlation exists between the  $\text{Ni-Cl-Ni}$  angle and the J-value; in two cases this angle amounts to  $97.4^\circ$  (dmp and dmpzm com-

TABLE IV.3.1. MAGNETIC AND STRUCTURAL DATA FOR CHLORINE-BRIDGED  $\text{Ni(II)}$  DIMERS

COMPOUND <sup>x</sup>	$\text{Ni-Cl-Ni}$ ( $^\circ$ )	$J^y$ ( $\text{cm}^{-1}$ )	$\text{Ni-Ni}$ ( $\text{\AA}$ )	$\text{Ni-Cl}_{b_1}^z$ ( $\text{\AA}$ )	$\text{Ni-Cl}_{b_2}$ ( $\text{\AA}$ )	$\text{N-Ni-N}$ ( $^\circ$ )	$\text{N-Ni-Cl}_{b_1}$ ( $^\circ$ )
$(\text{Ni}(\text{qnqn})\text{Cl}_2)_2$ <sup>3</sup>	98.2	-4.4 <sup>18</sup>	3.652	2.41	2.42	97.6	158
$(\text{Ni}(\text{dmp})\text{Cl}_2)_2$ <sup>4</sup>	97.4	-5.0 <sup>4</sup>	3.600	2.38	2.41	81.7	155
$(\text{Ni}(\text{biq})\text{Cl}_2)_2$ <sup>4</sup>	96.7	-5 <sup>4</sup>	3.565	2.37	2.40	80.4	158
$(\text{Ni}(\text{dmpzm})\text{Cl}_2)_2$	97.4	+2.6	3.587	2.46	2.32	87.6	174
$(\text{NiCl}_4)_2$ <sup>19</sup>	99.3	-2 <sup>3</sup>	3.669	2.37	2.45		
$(\text{Ni}(\text{en})_2\text{Cl})_2\text{Cl}_2$ <sup>12</sup>	96.6	+5.0 <sup>20</sup>	3.72	2.42	2.51		
$(\text{Ni}(\text{eg})_2\text{Cl})_2\text{Cl}_2$ <sup>13</sup>	93.0	+5.5 <sup>13</sup>	3.458	2.38	2.38		

<sup>x</sup>=REFERENCE OF STRUCTURE PARAMETERS; <sup>y</sup>=REFERENCE OF J PARAMETER; <sup>z</sup>= $\text{Cl}_b$  IS THE BRIDGING CHLORIDE ION.



pounds) whereas the interactions are antiferromagnetic and ferromagnetic respectively. Therefore, the bridging angle does not, *a priori*, determine the value of the exchange parameter,  $J$ . Also the Ni-Ni distance and the Ni-Cl<sub>b</sub> distances do not seem to influence the  $J$ -value greatly.

Another difference between NIDI and the other five-coordinated dimers is the asymmetry in the NiCl<sub>2</sub>Ni unit. If this would influence  $J$  to a great extent, larger differences in  $J$ -value would be expected for the two compounds listed\* at the end of table IV.3.1, *i.e.* (Ni(en)<sub>2</sub>Cl)<sub>2</sub>Cl<sub>2</sub><sup>12</sup> and (Ni(eg)<sub>2</sub>Cl)<sub>2</sub>Cl<sub>2</sub><sup>13</sup>.

The nature of the chelating ligands (all N-N bidentate donors) also is rather similar in all four compounds, so only small differences in charge densities on the Ni(II) ions can be expected for these dimeric compounds; therefore, this effect cannot be responsible for the observed ferromagnetism in NIDI.

In fact the only significant structural difference is the deviation from sp geometry (approaching t<sub>bp</sub> geometry) for NIDI. This geometrical difference is expected to influence the orientation of the d-electron spin densities on the interacting Ni(II) ions. Because the sign and magnitude of the magnetic superexchange is sensitive to the orientation of these spin densities on both metal ions<sup>22,23</sup>, it is likely that such a different orientation of spin densities in NIDI is responsible for the observed ferromagnetism.

Recently, similar observations have been made for hetero-nuclear dimeric compounds<sup>22,23</sup>, tetranuclear Cu(II) compounds<sup>24</sup> and Cu(II) and Co(II) chain compounds (chapter II.11).

#### *Final remarks*

From the present study it is concluded that the prediction of superexchange interactions between paramagnetic ions is not possible even when the compounds have known structures. The main problem seems to be the relative orientation of the d-orbitals (in which the unpaired electrons are) on the chemical bonds surrounding the paramagnetic ions. To study this problem spectroscopic measurements (*e.g.* ESR and ligand-field) on single crystals can be of help.

\*Very recently, Landee and Willett<sup>21</sup> solved the structure of a third dimer of this type, *i.e.* (Ni(H<sub>2</sub>O)Cl<sub>4</sub>)<sub>2</sub>. In this dimer the two Ni-Cl<sub>b</sub> distances are 2.43 and 2.46 Å, the Ni-Ni distance is 3.602 Å and the bridging Ni-Cl-Ni angle is 95.0(1)°. The interaction between the Ni(II) ions is ferromagnetic with  $J = + 7.2 \text{ cm}^{-1}$ .

#### IV.4. Magnetic superexchange Interactions in dimeric and tetrameric fluorine-bridged Co(II) Compounds.

##### IV.4.1. Experimental

Dimeric compounds  $\text{Co}_2\text{F}_2\text{L}_6(\text{BF}_4)_2$ , with L=3,5-dimethylpyrazole (dmpz), 3,4,5-trimethylpyrazole (tmpz) and 4-ethyl-3,5-dimethylpyrazole (edmpz) were prepared as described in the literature<sup>6</sup>.

The tetrameric compound  $\text{Co}_4\text{F}_4\text{L}_{12}(\text{BF}_4)_4$ , with L=N-ethylimidazole, was prepared as described elsewhere<sup>7</sup>.

The compounds were characterized using techniques described in chapter V. Magnetization measurements were performed as described in II.6.1.

##### IV.4.2. Results and discussion

###### Dimeric compounds

The X-ray structure of one of the compounds, *i.e.* di- $\mu$ -fluorohexakis(3,5-dimethylpyrazole)diCobalt(II)bis-(tetrafluoroborate), is described in detail by Reedijk *et al.*<sup>6</sup>. In figure IV.4.1 an ORTEP<sup>11</sup> drawing of the geometry around Co(II) in the dimer is shown.

The bridging unit  $\text{CoF}_2\text{Co}$  is strictly planar. The Co-Co distance within the dimer amounts to 3.092 Å. The two Co-F distances of 1.924 and 2.146 Å make the bridge rather asymmetric. The bridging Co-F-Co angle amounts to 98.8°.

To study the magnetic interaction between the Co(II) ions, magnetic susceptibility measurements and magnetization measurements were carried out. The results of these measurements are plotted in figures IV.4.2 and IV.4.3 respectively.

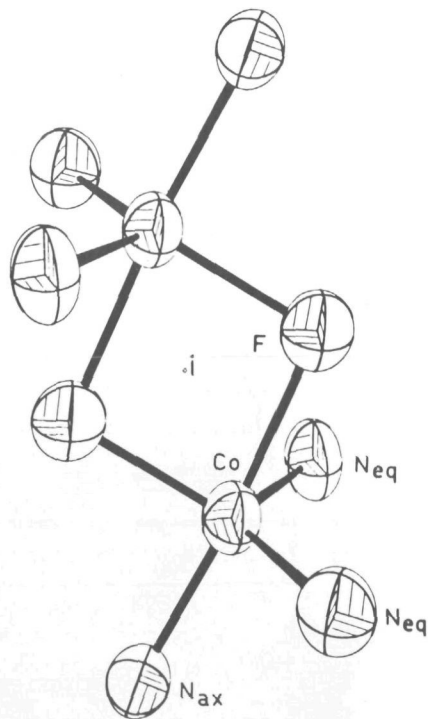


Fig. IV.4.1. ORTEP<sup>11</sup> drawing of the geometry around Co(II) in the compound  $\text{Co}_2\text{F}_2(\text{dmpz})_6(\text{BF}_4)_2$ .

Figure IV.4.2 shows the quadratic effective magnetic moments ( $8\chi_M T$ ) as a function of temperature. It is noticed that the interactions are antiferromagnetic and show an increase in the sequence of ligands, dmpz, edmpz, tmpz.

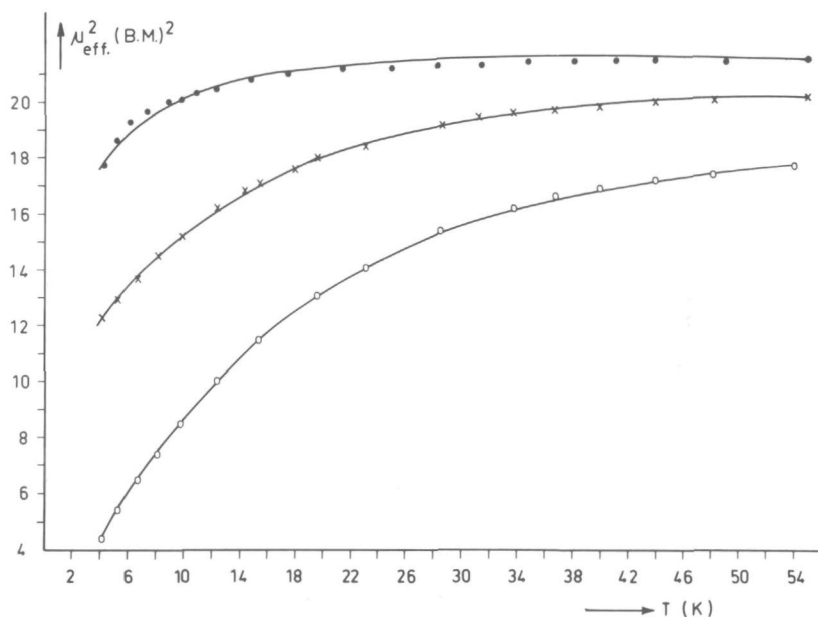


Fig. IV.4.2.  $8\chi_M T$  ( $g^2 S(S+1)$  B.M.<sup>2</sup>) as a function of temperature for the dimeric Co(II) compounds, with L=dmpz (●), edmpz (x) and tmpz (o).

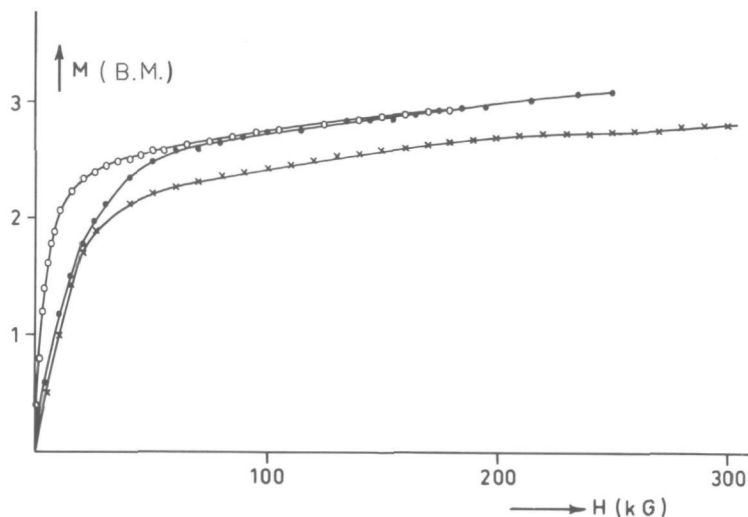
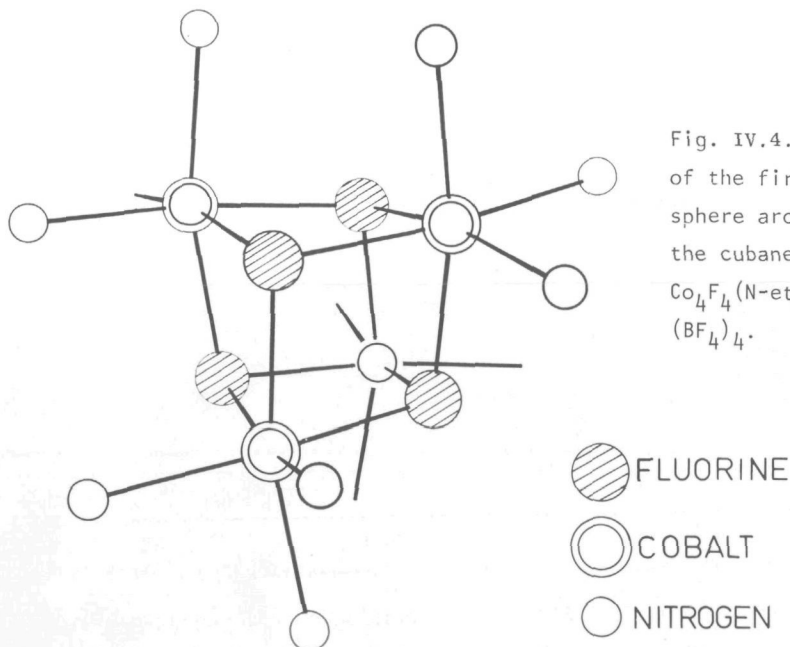


Fig. IV.4.3. Magnetization (g S B.M.) as a function of the magnetic field for the dimeric Co(II) compounds, with L=dmpz (●), edmpz (x) and tmpz (o); T=1.2K.

In the magnetic susceptibility *vs.* temperature curves no maximum was observed down to 4.2K.

For the description of the magnetic data a model has to be chosen. Since octahedrally-coordinated Co(II) ions behave as fictitious  $S=\frac{1}{2}$  spins at low temperatures (see *e.g.* chapter III.3), the low-temperature data were fitted to the equation for dimeric  $S=\frac{1}{2}$  ions (chapter II.5). However, no fit could be obtained. One of the possible reasons is that the five-coordinated Co(II) ions does not behave as  $S=\frac{1}{2}$  ions at low temperatures. To calculate the energy gap between the ground-state doublet and the first excited doublets, angular overlap calculations<sup>25</sup> were carried out. The results of these calculations<sup>26</sup> indicated that the energy gap presumably amounts to only *ca.* 30  $\text{cm}^{-1}$ ; also the *g*-values for the ground state and first-excited state doublet were very different, depending mainly on the choice of the angular overlap parameters.

For the reasons outlined above, no further attempts were made to describe the magnetic data quantitatively. Furthermore, the magnetic data of the tmpz compound seemed to be dependent on the time between preparation and measurement; the older the sample, the stronger the coupling (*viz.* fig. IV.4.2 : old sample (one month) and fig. IV.4.3 : fresh sample). Presumably the contamination of ethylformate during crystallization, which slowly evaporates from the sample, is the origin of this effect.



Finally, in figure IV.4.3 the magnetization at 1.2K is shown. All compounds saturate at rather low fields, indicating the rather weak interaction (ca.  $-1 \text{ cm}^{-1}$ ) that occurs between the cobalt ions.

#### *Tetrameric compounds*

Preliminary results of the X-ray structure determination of the compound tetra- $\mu$ -fluoro-dodeca(N-ethylimidazole)tetraCobalt(II)tetra (tetrafluoroborate) showed<sup>7</sup> the compound to consist of tetranuclear fluorine-bridged Co(II) units, in which the Co(II) ions are arranged in a cubane-type cluster. In figure IV.4.4 the first coordination sphere around the Co(II) ions is shown. The mean Co-F and Co-Co distances are 2.14 and 3.29 Å respectively. The mean Co-F-Co angle is  $100.5^\circ$ .

To study the magnetic superexchange interactions within the tetrameric unit, magnetic susceptibility measurements and magnetization measurements were carried out.

In figure IV.4.5 the magnetic susceptibility is plotted against the temperature. The observed maximum is indicative for the presence of antiferromagnetic interactions. Because of theoretical problems that occur for the des-

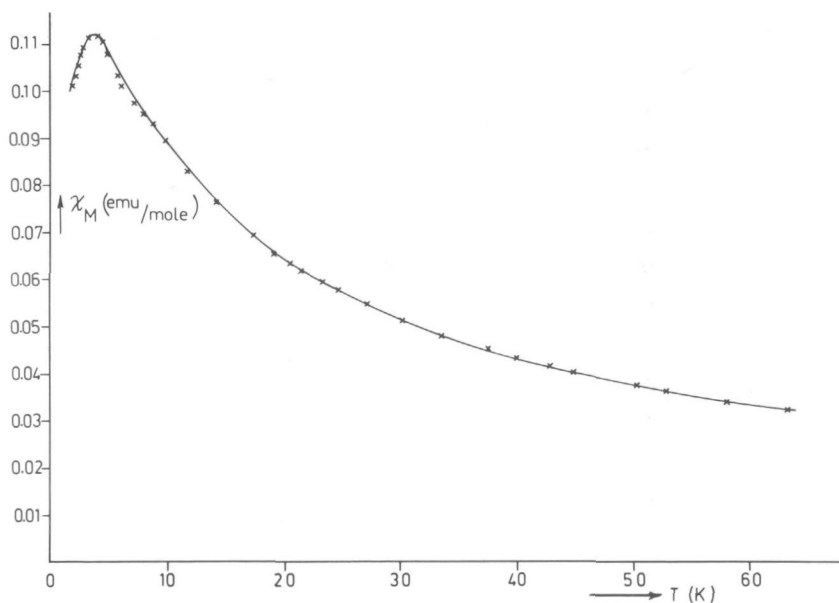


Fig. IV.4.5. Molar susceptibility ( $\chi$ ) as a function of temperature for the compound  $\text{Co}_4\text{F}_4(\text{N-ethylimidazole})_{12}(\text{BF}_4)_4$ .

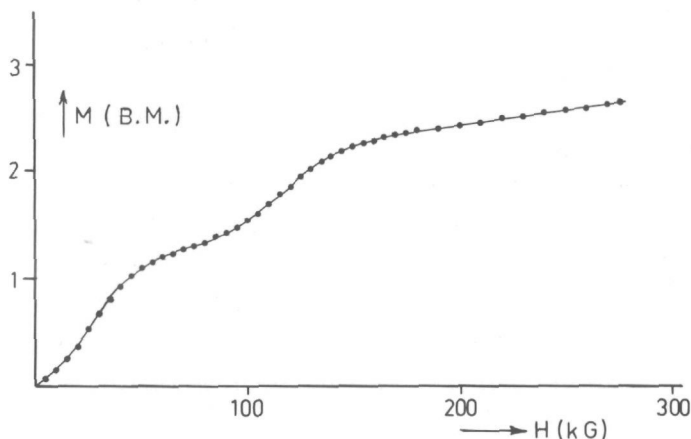


Fig. IV.4.6. Magnetization (gS B.M.) as a function of the magnetic field for the compound  $\text{Co}_4\text{F}_4(\text{N-ethylimidazole})_{12}(\text{BF}_4)_4$ ;  $T=1.2\text{K}$ .

cription of magnetic data on  $\text{Co(II)}$  ions (see above) the results were interpreted only in a qualitative manner.

In figure IV.4.6 the magnetization curve at 1.2K is shown. Saturation is reached in two steps; qualitatively, this can be explained by assuming that at first the dimeric interactions are saturated, followed by the interdimer interactions (or *vice versa*). Bonner *et al.*<sup>27</sup> published some theoretical results of calculations on competing superexchange interactions in a linear array of four  $\text{Co(II)}$  ions. They explain the two-steps magnetization by stating that the ground state changes with increasing magnetic field, *i.e.*  $S_z$  varies from 0 *via* 1 to 2. However, this behaviour is expected for single-crystal magnetization with the field in the  $z$ -direction for all ions. In the present compound it is expected from the point-symmetry of the  $\text{Co(II)}$  ions, that the crystal-field axes would be different for each of the four ions in the cluster, namely that the crystal-field axes would lie along the body-diagonals of the cube, formed by the cobalt and fluoride ions. In that case there would be a strong field needed to overcome the crystal-field anisotropies of the individual ions in the cluster, in order to saturate the moments in the direction of the field. The two steps in the  $M$  *vs.*  $H$  curve may therefore not be simply related to magnetic superexchange effects alone. In order to make any further progress

in the quantitative analysis of the experimental susceptibility and magnetization curves, a knowledge of the g-tensors for the Co(II) ion is indispensable. Unfortunately, attempts to grow single crystals of the  $\text{Co}^{2+}$ -doped non-magnetic isomorphous cadmium compound, in order to measure the g-tensor with ESR spectroscopy, have so far met with no success. Also, the inability to grow single crystals large enough for magnetization studies inhibits a further analysis at this moment.

Clearly, however, the superexchange interactions are again rather small ( $\text{ca. } -5 \text{ cm}^{-1}$ ). This observed exchange of a few  $\text{cm}^{-1}$  can be compared with  $J = \text{ca. } -1 \text{ cm}^{-1}$  found for the dimeric compounds, with  $J = \text{ca. } -10 \text{ cm}^{-1}$  found for fluorine-bridged Co(II) chains<sup>28</sup> and with  $J = \text{ca. } -70 \text{ cm}^{-1}$  found for the  $180^\circ$  Co-F-Co superexchange path in  $\text{KCoF}_3$ ,  $\text{K}_2\text{CoF}_4$  and  $\text{Rb}_2\text{CoF}_4$ <sup>29</sup>.

#### IV.4.3. Final remarks

The magnetic properties of new types of compounds, *i.e.* the dimeric and tetrameric fluorine-bridged Co(II) compounds, are investigated. For all compounds the interactions are antiferromagnetic. More work must be carried out to relate quantitatively the structural and magnetic parameters. Especially the theories concerning the interpretation of magnetic data on Co(II) ions need much more attention.

#### IV.5. References

- (1) V.H. Crawford, H.W. Richardson, J.R. Wasson, D.J. Hodgson and W.E. Hatfield, *Inorg. Chem.*, **15**, 2107 (1976).
- (2) C.G. Barraclough and R.W. Brookes, *J. Chem. Soc. Faraday II*, 1364 (1974).
- (3) E.J. Laskowski, T.F. Felthouse, D.N. Hendrickson and G.J. Long, *Inorg. Chem.*, **15**, 2908 (1976).
- (4) R.J. Butcher and E. Sinn, *Inorg. Chem.*, **16**, 2334 (1977).
- (5) J. Reedijk and J. Verbiest, *Transition Met. Chem.*, **3**, 51 (1978).
- (6) J. Reedijk, J.C. Jansen, H. van Koningsveld and C.G. van Kralingen, *Inorg. Chem.*, **17**, 1990 (1978).
- (7) J.C. Jansen, H. van Koningsveld and J. Reedijk, *Nature*, **269**, 318 (1977).
- (8) X-ray system -version of June 1972- technical report TR-192 of the computer science center, University of Maryland, June (1972).
- (9) D.T. Cromer and J.B. Mann, *Acta Crystallogr.*, **A24**, 321 (1968).
- (10) R.F. Stewart, E.R. Davidson and W.T. Simpson, *J. Phys. Chem.*, **42**, 3175 (1965).
- (11) C.K. Johnson, ORTEP, report ORNL-3794 (1965).
- (12) G.A. Bottomley, C.G. Glossop, C.L. Raston, A.H. White and A.C. Willis, *Aust. J. Chem.*, **31**, 285 (1978).
- (13) D. Knetsch, *Ph. D. Thesis*, Leiden University (1976).
- (14) A. Bondi, *J. Phys. Chem.*, **68**, 441 (1964).
- (15) E. König, "Magnetic Properties of Coordination and Organometallic Transition Metal Complexes", Springer Verlag, Berlin (1966).
- (16) A.P. Ginsberg, R.L. Martin, R.W. Brookes and R.C. Sherwood, *Inorg. Chem.*, **11**, 2884 (1972).
- (17) A.P. Ginsberg, *Inorg. Chim. Acta Rev.*, **5**, 45 (1971).
- (18) G.J. Long and E.O. Schlemper, *Inorg. Chem.*, **13**, 279 (1974).
- (19) F.K. Ross and G.D. Stucky, *J. Am. Chem. Soc.*, **92**, 4538 (1970).
- (20) Y. Journaux, O. Kahn, B. Chevalier, J. Etourneau, R. Claude and A. Dworkin, *Chem. Phys. Letters*, **55**, 140 (1978).
- (21) C.P. Landee and R.D. Willett, Washington State University, unpublished results.
- (22) O. Kahn, R. Claude and H. Coudanne, *J. Chem. Soc. Chem. Comm.*, 1012 (1978).
- (23) O. Kahn, P. Tola, J. Galy and H. Coudanne, *J. Am. Chem. Soc.*, **100**, 3931 (1978).
- (24) L. Merz and W. Haase, *J. Chem. Soc. Dalton*, 1594 (1978).
- (25) C.E. Schäffer, *Structure and Bonding*, **5**, 68 (1968).
- (26) P.J. van der Put, unpublished results.
- (27) J.C. Bonner, H. Kobayashi, I. Tsujikawa, Y. Nakamura and S.A. Friedberg, *J. Chem. Phys.*, **63**, 19 (1975).
- (28) M.A. Guichelaar, J.A.M. van Hest and J. Reedijk, *Inorg. Nucl. Chem. Letters*, **10**, 999 (1974).
- (29) L.J. de Jongh and A.R. Miedema, *Adv. Phys.*, **23**, 1 (1974).



## V. EXPERIMENTAL PROCEDURES

### V.1. Spectroscopy and chemical Analyses

As said in chapter I, the experimental details of the synthetical work are reported in the appropriate chapters. The details of the more generally used techniques throughout this thesis are described below.

Infrared spectra of the solid compounds were recorded on a Beckman Acculab 6 spectrometer as a suspension in nujol, sandwiched between potassium bromide windows in the  $4000\text{--}400\text{ cm}^{-1}$  region.

Far-infrared spectra were recorded on a Beckman IR-720 Fourier spectrofotometer, in pressed polyethylene plates in the spectral range  $500\text{--}20\text{ cm}^{-1}$ .

Ligand-field spectra were performed on a Beckman DK-2 ratio-recording spectrometer, furnished with a reflectance attachment ( $35,000\text{--}4,000\text{ cm}^{-1}$ ).  $\text{BaSO}_4$  was taken as the reference material.

Raman spectra of solid samples were obtained using a JEOL Raman spectrometer using Ar and Ne excitation (Free University, Amsterdam).

X-ray powder diagrams were obtained with a Guinier camera using  $\text{CuK}\alpha$  radiation; the samples were mounted with vaseline.

Electron spin resonance (ESR) spectra were recorded with a Varian E-9 X-band (9.5 GHz) and a Varian V4500 Q-band (35 GHz) spectrometer. The field was calibrated using a AEG Proton NMR apparatus, whereas the frequency was calibrated indirectly using DPPH as a calibrant. X- and Q-band spectra at liquid-nitrogen temperature were recorded using a standard liquid-nitrogen dewar. X-band spectra at liquid-helium temperature were performed using a flow cryostat of Air Products.

The Mössbauer spectra of the samples were obtained using a  $^{57}\text{Co}$  source (10 mCurie) in a Rh foil mounted on a constant acceleration drive system. Details of the technical equipment are described in the thesis of van der Kraan<sup>1</sup>. The velocity scale of the Mössbauer spectrometer is calibrated by measuring the hyperfine field of  $\alpha\text{-Fe}_2\text{O}_3$  at room temperature ( $H_{\text{eff.}} = 515\text{ kG}$ ). The isomer shift is determined relative to the standard reference material  $\text{Na}_2\text{Fe}(\text{CN})_5\text{NO}\cdot 2\text{H}_2\text{O}$  (N.B.S. no. 725). The Mössbauer spectra of the samples were measured from  $T=1.7\text{K}$  up to room temperature; from  $1.7\text{K}$  up to  $78\text{K}$ , a helium gas flow cryostat and from  $78\text{K}$  up to room temperature a nitrogen-bath cryostat have been used respectively.

Chemical analyses (C/H/N/Cl) have been carried out by Mr. J. Cornelisse in our laboratory and also at the Organic Chemistry Institute TNO in Utrecht. The metal content has been measured using standard EDTA titrations<sup>2</sup>.

## V.2. Magnetic Susceptibility

Magnetic susceptibility measurements in the temperature region 4.2-100K, were carried out by means of a commercial Princeton Applied Research (PAR) vibrating-sample magnetometer Model 155. This type of magnetometer was first described by Foner<sup>3</sup>. The mechanical system of the instrument used, is mounted on a liquid-helium dewar. A small sample of the compound (ca. 100 mgr) is placed in a closed teflon sample holder located at the end of a rod that is vibrated perpendicular to the field direction of the magnet. This induces an AC voltage in a set of stationary pick up coils, located at the center of the external magnetic field. The associated electron system measures this induced voltage from which the magnetic properties of the sample are deduced.

By means of a throttle valve a continuous flow of liquid helium is transferred from the helium bath of the cryostat to the sample chamber. At the bottom of the sample holder a small heat exchanger is located that controls the temperature of the helium gas stream emerging from this heat exchanger. The helium vapor stream evades at the top of the sample chamber. With this system the temperature in the sample zone can be maintained at any temperature between 4.2 and 100K.

The temperature in the sample zone was measured indirectly from potassium chromium alum, whereas the field was calibrated with a pure nickel sample. The susceptibility measurements were carried out at field strengths between 0.15 and 18.00 kG.

## V.3. References

- (1) A.M. van der Kraan, *Ph.D. Thesis*, Delft University of Technology (1974).
- (2) E. Wänninen, "Essays on Analytical Chemistry", Pergamon Press, Oxford (1977).
- (3) A. Weiss and H. Witte, "Magnetochemie", Verlag Chemie, Weinheim (1973).

## VI. APPENDIX

### VI.1. Magnetism and Structure of Copper(II) coordination Compounds. Crystal and Molecular Structure of *trans*-dichlorobis(N-methylimidazole)Copper(II).

#### VI.1.1. Abstract

Two modifications of the compound *trans*-dichlorobis(N-methylimidazole)-Copper(II) have been synthesized and the crystal and molecular structure of one has been determined by a single-crystal X-ray analysis using three-dimensional X-ray data. The compound crystallizes in the triclinic space group  $P\bar{1}$  with two formula units in a unit cell of dimensions  $a = 7.632(3)$ ,  $b = 8.166(9)$ ,  $c = 10.232(3)$  Å,  $\alpha = 87.84(5)$ ,  $\beta = 82.77(2)$ ,  $\gamma = 76.12(5)^\circ$ . The structure was determined by direct methods and refined by least-squares techniques to  $R_F = 0.041$  and  $R_{wF} = 0.049$  for 2307 reflections. The structure consists of discrete monomeric  $\text{CuCl}_2(\text{NMIz})_2$  units with tetrahedrally-distorted *trans*-square-planar geometries around copper(II). The Cu-Cl distances (2.260(3) and 2.256(2) Å) are normal for terminal Cu-Cl bonds. The Cu-N distances (1.962(4) and 1.975(5) Å) are in the range expected for this type of compound. The two different crystal forms appear to have only slightly different spectroscopic and magnetic properties, but totally different X-ray powder patterns.

#### VI.1.2. Introduction

Several compounds in the series  $\text{CuX}_2\text{L}_2$ , with  $\text{X}=\text{Cl}$ ,  $\text{Br}$  and  $\text{L}=(\text{substituted})\text{-pyridine}$ , *imidazole* and *pyrazole*, have been investigated in recent years<sup>1-8</sup>. All of the structurally-established  $\text{CuCl}_2(\text{py})_2$ -like series of compounds show antiferromagnetic superexchange interactions which result in the observation of broad maxima in the susceptibility *vs.* temperature curves, at low temperatures.

Much effort has been undertaken to predict the structure from magnetic and spectroscopic data, however, until now, it is not possible to predict structural data in a quantitative way. One of the reasons for this failure is that, up to date, it is not clear which factors govern the kind and magnitude of the magnetic superexchange interactions in this class of one-dimensional transition-metal coordination compounds.

Recently, some compounds were reported in which only very weak superex-

change interactions occur<sup>8</sup>. One of these compounds,  $\text{CuCl}_2(\text{N-methylimidazole})_2$ , abbreviated  $\text{CuCl}_2(\text{NMiz})_2$ , showed a very small interaction between the copper(II) ions and because the geometry of a chain with an exchange constant,  $J$ , near zero is highly interesting, an X-ray investigation was undertaken.

In addition some other compounds, which could not be prepared as single crystals suitable for a complete structure determination, have been investigated by powder diffraction techniques and/or Weissenberg photographs, in order to obtain information about the shortest crystal axis. For the chain compounds that have been investigated structurally, always one short crystal axis in the vicinity of 4.0 Å (equal to the M-M distance along the chain) was found<sup>1-5,9-12</sup>.

#### VI.1.3. Experimental

Green single crystals of the title compound were slowly grown from a mixture of a solution of  $\text{CuCl}_2$  in ethanol (0.01 mol/l) and a solution of NMiz (0.02 mol/l) in ethanol.

Repeated synthesis resulted in two different species with chemical formula  $\text{CuCl}_2(\text{NMiz})_2$  (*vide infra*).

#### VI.1.4. Crystal and intensity data, structure determination and refinement

From single-crystal diffractometry ( $\text{MoK}\alpha = 0.71069 \text{ \AA}$ ) the following data were obtained:  $a = 7.632(3)$ ,  $b = 8.166(9)$ ,  $c = 10.232(3) \text{ \AA}$ ,  $\alpha = 87.84(5)^\circ$ ,  $\beta = 82.77(2)^\circ$ ,  $\gamma = 76.12(5)^\circ$ , space group  $\text{P}\bar{1}$ ,  $D_m = 1.6 \text{ g/cm}^3$ ,  $D_c = 1.62 \text{ g/cm}^3$ , and  $Z=2$ .

A suitable specimen, a rectangular parallelepiped measuring 0.11 X 0.21 X 0.29 mm, was mounted on an ENRAF-NONIUS CAD4 diffractometer and X-ray intensity data were measured in the  $\omega/2\theta$ -scan mode, by use of monochromated  $\text{MoK}\alpha$  radiation ( $2\theta_{\text{mon.}} = 12.8^\circ$ ).

Accurate unit-cell parameters and the orientational matrix were determined from a least-squares treatment of the angular settings of 8 reflections.

The standard deviations in the lattice parameters were obtained from the comparison of the deviations from integer values of the indices, calculated with the orientation reflections as described by Duisenberg<sup>13</sup>.

Intensity data were collected for a redundant set of 2993 reflections to  $\theta_{\text{max.}} = 27.5^\circ$ . A standard reflection was measured every 30 minutes of X-ray exposure time. A smooth function through these measurement values has been used to correct for fluctuations in the intensity data (3%). Averaging of equivalent data resulted in a set of 2810 unique reflections of which 2307 had intensities above background ( $I > 2.5\sigma(I)$ ). Intensities were corrected for Lorentz and polar-

ization effects. No absorption correction has been applied ( $\mu_{\text{MoK}\alpha} = 22.5 \text{ cm}^{-1}$ ).

The data were converted to normalized structure magnitudes and the structure solved by direct methods for the heavy atoms. The other atoms have been found by application of Fourier techniques. The positions and anisotropic temperature factors were refined by block-diagonal least-squares techniques to a final  $R_F = 0.041$  and  $R_{wF} = 0.049^{14}$ . Unit weights were used throughout the refinement. A final difference-Fourier map only showed possible hydrogen positions, however, no attempts were made to include them in the calculations. At the end of refinement all parameter shifts were  $< 0.6\sigma$ . Programs used in this structure determination include MULTAN 77<sup>15</sup>, XRAY76-SYSTEM<sup>16</sup> and ORTEP<sup>17</sup>.

Final positional and thermal parameters are listed in table VI.1.1. Atomic scattering factors for Cu, Cl, N and C were taken from Doyle<sup>18</sup>. Observed and calculated structure factors are listed elsewhere<sup>19</sup>.

## VI.1.5. Results and discussion

### *Description and discussion of the structure*

The structure of *trans*-dichlorobis(N-methylimidazole)Copper(II) consists of two discrete monomeric  $\text{CuCl}_2(\text{NMiz})_2$  units. In figure VI.1.1 a molecular unit is drawn. The geometry about each copper ion is best described as tetra-

TABLE VI.1.1. FINAL FRACTIONAL ATOMIC COORDINATES AND THERMAL PARAMETERS<sup>x</sup> FOR THE NON-HYDROGEN ATOMS. ESTIMATED STANDARD DEVIATIONS ARE IN PARENTHESES

ATOM	$x/a$	$y/b$	$z/c$	100 $u_{11}$	100 $u_{22}$	100 $u_{33}$	100 $u_{12}$	100 $u_{13}$	100 $u_{23}$
Cu	0.3212(1)	0.2645(1)	0.2184(1)	4.66(3)	3.62(3)	4.22(3)	-1.09(1)	-1.50(2)	0.80(2)
Cl(1)	0.1972(2)	0.5179(2)	0.1312(1)	7.56(9)	3.46(6)	6.05(8)	-0.46(6)	-3.11(7)	0.60(5)
Cl(2)	0.2808(2)	0.0824(2)	0.3843(1)	7.9(1)	7.25(9)	5.67(8)	-3.75(8)	-2.31(7)	2.86(7)
N(11)	0.2599(5)	0.1308(5)	0.0830(4)	4.3(2)	3.6(2)	4.7(2)	-1.0(2)	-1.1(2)	0.4(2)
N(12)	0.1939(5)	0.0576(5)	-0.1063(4)	4.4(2)	4.2(2)	5.1(2)	-0.9(2)	-0.7(2)	-0.5(2)
C(11)	0.2038(7)	0.1871(6)	-0.0314(5)	4.7(3)	4.0(2)	4.5(3)	-1.1(2)	-1.1(2)	0.1(1)
C(12)	0.2452(7)	-0.0896(6)	-0.0349(5)	5.3(3)	3.9(3)	6.0(3)	-1.1(2)	-0.2(2)	-0.3(2)
C(13)	0.2859(7)	-0.0442(6)	0.0816(5)	5.2(3)	3.5(2)	6.2(3)	-0.8(2)	-0.5(2)	0.6(2)
C(14)	0.1411(9)	0.0716(8)	-0.2403(6)	8.0(4)	6.3(3)	5.0(3)	-1.3(3)	-2.0(3)	-1.1(3)
N(21)	0.5049(5)	0.3484(5)	0.2984(4)	4.7(2)	3.9(2)	4.1(2)	-1.1(2)	-1.1(2)	0.3(2)
N(22)	0.7164(5)	0.3634(5)	0.4205(4)	4.6(2)	4.9(2)	5.1(2)	-1.0(2)	-1.3(2)	-0.6(2)
C(21)	0.5779(6)	0.2920(6)	0.4081(5)	4.2(2)	4.2(2)	4.5(3)	-0.5(2)	-1.1(2)	-0.3(2)
C(22)	0.7327(9)	0.4702(8)	0.3155(6)	7.2(4)	6.9(4)	6.1(3)	-3.4(3)	-1.6(3)	0.7(3)
C(23)	0.6013(8)	0.4618(7)	0.2391(6)	6.8(4)	6.0(3)	5.5(3)	-3.0(3)	-1.2(3)	1.0(3)
C(24)	0.8302(8)	0.3309(8)	0.5302(6)	6.4(4)	7.7(4)	6.5(4)	-1.8(3)	-3.4(3)	-0.3(3)

<sup>x</sup>THE ANISOTROPIC THERMAL PARAMETERS ARE IN THE FORM:  $t = \exp \{-2\pi^2 \sum_{i,j} u_{ij} h_i h_j\}$ .

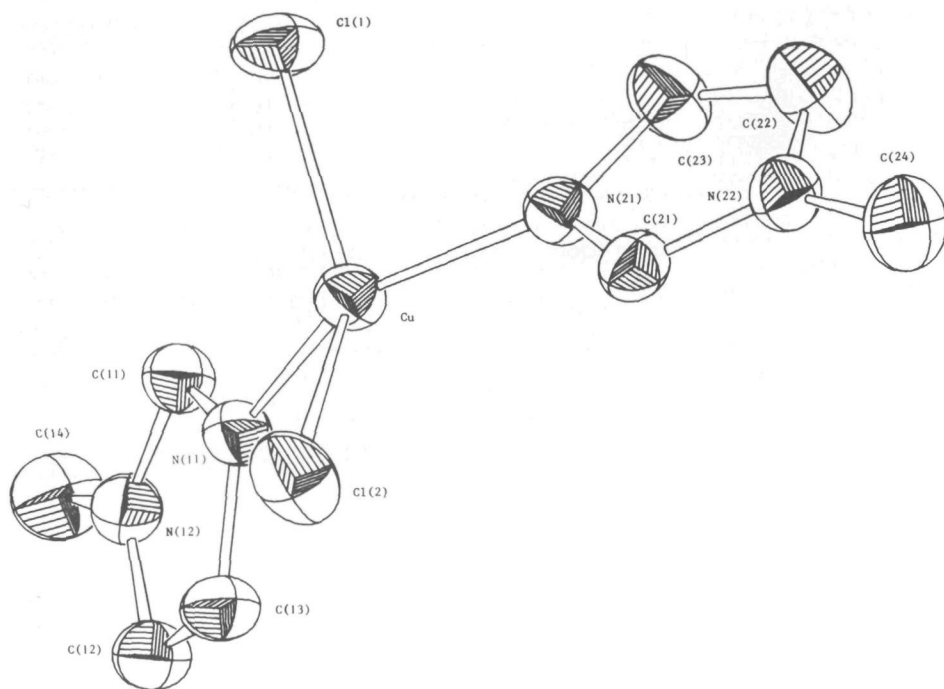


Fig. VI.1.1. ORTEP<sup>17</sup> drawing of  $\text{CuCl}_2(\text{NMiz})_2$ .

hedrally-distorted square-planar. The ligands are in the *trans* position.

The interatomic distances, angles and planes of interest in  $\text{CuCl}_2(\text{NMiz})_2$  are given in tables VI.1.2 and VI.1.3.

The two independent Cu-Cl distances (2.260(3) and 2.256(2) Å) are typical for terminal Cu-Cl bonds. The shortest intermolecular separations are much greater than the sum of the van der Waals radii of the two atoms involved. From this fact it is evident that  $\text{CuCl}_2(\text{NMiz})_2$  does not belong to the  $\text{CuCl}_2(\text{py})_2$ -like series of compounds. The Cu-N distances (1.962(4) and 1.975(5) Å) are very close to the Cu-N bond length of 1.953(5) Å in  $\text{CuBr}_2(\text{NMiz})_2$ <sup>4</sup>.

The *cis* angles (94.0(1) - 95.4(1)°) and *trans* angles (143.57(6) and 149.7(1)°) of all ligands around the copper ion are intermediate between the expected values for tetrahedral (109.3°) and square-planar geometries (90/180°) respectively. Comparable angles, deviating slightly more from the angles expected for tetrahedral geometries, occur in  $\text{CuCl}_2(\text{DMAEP})$ <sup>20</sup>. In this latter compound the geometry is described as pseudo-tetrahedral, as concluded from the electronic spectrum; initially, in the present case this conclusion could not be

TABLE VI.1.2. INTERATOMIC DISTANCES ( $\text{\AA}$ ) AND ANGLES ( $^\circ$ ). UNCERTAINTIES IN THE LAST DIGIT ARE IN PARENTHESES

DISTANCES				N(22) - C(24) 1.482(8)				C(11) - N(11) - C(13) 106.4(4)				
Cu	-	C1(1)	2.260(3)	C(22)	-	C(23)	1.363(9)	N(11)	-	C(11)	- N(12) 110.6(4)	
Cu	-	C1(2)	2.256(2)	C(23)	-	N(21)	1.392(8)	C(11)	-	N(12)	- C(12) 107.6(4)	
Cu	-	N(11)	1.962(4)	ANGLES				C(11)	-	N(12)	- C(14) 125.9(4)	
Cu	-	N(21)	1.975(5)					C(12)	-	N(12)	- C(14) 126.5(5)	
N(11)-	C(11)	1.325(6)	C1(1)	-	Cu	-	C1(2)	143.57(6)	N(12)	-	C(12)	- C(13) 106.6(4)
C(11)-	N(12)	1.351(7)	C1(1)	-	Cu	-	N(21)	94.0(1)	N(11)	-	C(13)	- C(12) 108.8(4)
N(12)-	C(12)	1.382(6)	C1(2)	-	Cu	-	N(11)	94.9(1)	C(21)	-	N(21)	- C(23) 107.1(5)
N(12)-	C(14)	1.470(7)	C1(2)	-	Cu	-	N(21)	94.4(1)	N(21)	-	C(21)	- N(22) 109.7(4)
C(12)-	C(13)	1.356(8)	N(11)	-	Cu	-	N(21)	149.7(1)	C(21)	-	N(22)	- C(22) 108.4(5)
C(13)-	N(11)	1.395(6)	Cu	-	N(11)	-	C(11)	126.5(3)	C(21)	-	N(22)	- C(24) 125.1(4)
N(21)-	C(21)	1.333(6)	Cu	-	N(11)	-	C(13)	126.7(3)	C(22)	-	N(22)	- C(24) 126.5(5)
C(21)-	N(22)	1.345(7)	Cu	-	N(21)	-	C(21)	127.2(4)	N(22)	-	C(22)	- C(23) 107.0(6)
N(22)-	C(22)	1.371(7)	Cu	-	N(21)	-	C(23)	125.1(3)	N(21)	-	C(23)	- C(22) 107.9(5)

drawn from the spectroscopic measurements. (see chapter II.5).

The interatomic angles and distances within the two different NMiz ligands are similar, furthermore the observed values are very close to those reported for  $\text{CuBr}_2(\text{NMiz})_2$ <sup>4</sup>, *cis*- $\text{PtCl}_2(\text{NMiz})_2$ <sup>21</sup> and other metal compounds containing this ligand.

Least-squares planes through the ring atoms of NMiz are shown in table VI.1.3. The methyl groups are almost within the plane, but the copper ion is

TABLE VI.1.3. LEAST-SQUARES PLANES THROUGH THE RING ATOMS

PLANE	ATOMS IN PLANE	OTHER ATOMS	DISTANCE <sup>x</sup>
I (0.003) <sup>a</sup>	N(11)	Cu	0.19
	N(12)	Cl(1)	-0.16
	C(11)	Cl(2)	-0.76
	C(12)	N(21)	1.33
	C(13)	C(14)	0.03
II (0.002) <sup>a</sup>	N(21)	Cu	-0.25
	N(22)	Cl(1)	1.04
	C(21)	Cl(2)	-0.27
	C(22)	N(11)	-1.39
	C(23)	C(24)	0.001

<sup>x</sup>=DISTANCE FROM THE CALCULATED PLANE IN  $\text{\AA}$ ; <sup>a</sup>=STANDARD DEVIATION IN  $\text{\AA}$ .

although, it might be related to the crystal packing.

displaced by 0.19 and 0.25  $\text{\AA}$  out of the least-squares planes, defined by NMiz(I) and NMiz(II) respectively.

Another typical feature of the structure is, that the chloride ions lie very close to the planes through the NMiz rings; Cl(1) has a distance to plane I of 0.16  $\text{\AA}$  and Cl(2) has a distance to plane II of 0.27  $\text{\AA}$ . The origin for this is not clear,

### *Spectroscopy and Magnetism*

Two modifications of  $\text{CuCl}_2(\text{NMiz})_2$  were found ( $\alpha, \beta$ ), which have only slightly-different IR spectra (*vide infra*) and magnetic susceptibilities. The  $\alpha$ -form of which the X-ray structure is presented here, could be isolated in a pure form. The  $\beta$ -form could not be prepared pure, since the compound crystallizes contaminated to some extent by the  $\alpha$ -form. On recrystallization of both forms from alcohol, the compound  $\text{CuCl}_2(\text{NMiz})_2$  decomposed. Despite of careful investigations no conditions could be found to prepare one of the modifications in a predictable pure form.

The NMiz ligand has shown to yield four different crystal modifications in the compound *cis*- $\text{PtCl}_2(\text{NMiz})_2$ <sup>21</sup>. This could be concluded from the totally-different X-ray powder patterns and IR spectra. The IR spectra of the present  $\text{CuCl}_2(\text{NMiz})_2$  compounds show small differences, occurring at ca.  $875\text{ cm}^{-1}$  and  $3150\text{ cm}^{-1}$ . In the  $\alpha$ -modification the band at  $3150\text{ cm}^{-1}$  (C-H stretching vibration<sup>21</sup>) is split, whereas in the  $\beta$ -modification this band does not split. In the  $\beta$ -modification the band at  $875\text{ cm}^{-1}$  (a C-H out-of-plane bending<sup>21</sup>) is very weak, whereas in the  $\alpha$ -modification this band is very strong. From these data it is concluded that the NMiz ligands may have different orientations in the crystal structures. The X-ray powder diffraction patterns of the two modifications are completely different. A possible reason for the occurrence of the different modifications could be the absence of hydrogen bonding, which results in only very weak (only van der Waals interactions) intermolecular forces and therefore, small differences in packing energy between different ligand orientations.

The ligand-field and ESR spectra are very similar for both modifications and have been described previously<sup>8</sup> (see also chapter II.5).

The magnetic susceptibility measurements carried out on the  $\beta$ -modification showed very weak magnetic superexchange interactions between adjacent copper(II) ions<sup>8</sup>. Magnetic susceptibility measurements on the  $\alpha$ -modification in the 4.2-100K region did not show any magnetic interaction down to 4.2K, i.e. the effective magnetic moment per Cu(II) ion was temperature independent even at the lowest temperatures.

### *Magnetism-structure relationship*

Preliminary results from Weissenberg photographs of very thin needle-like single crystals and powder diffraction data, on the compounds  $\text{CuCl}_2(\text{Pz})_2$  and  $\text{CuCl}_2(4\text{-Mepy})_2$  show that these compounds all have a short axis in the vicinity of  $4.0\text{ \AA}$ . The existence of this short crystal axis in  $\text{CuCl}_2(\text{Pz})_2$  ( $3.76(5)\text{ \AA}$ )



is very promising, because the observed exchange is very small<sup>8</sup>. The structural data should yield the parameters responsible for a superexchange interaction being almost zero. These data will give further insights into the problem of understanding structure-superexchange relations in one-dimensional copper(II) chain compounds. However, single crystals of  $\text{CuCl}_2(\text{Pz})_2$  needed for a detailed structure analysis could not be prepared.

The magnetic susceptibility vs. temperature curve of the compound  $\text{CuCl}_2(4\text{-Mepy})_2$  deviates strongly from the other chains within the  $\text{CuCl}_2(\text{py})_2$ -like series of compounds<sup>6,7</sup>. Hatfield *et al.*<sup>6</sup> suggested from the susceptibility data that the structure of this compound exists of linear  $\text{CuCl}_2$  chains with alternating long and short Cu-Cu distances. However, from the  $4.0(1) \text{ \AA}$  crystal axis presently observed it is evident that in this compound no alternating Cu-Cu distances occur at room temperature, since this short crystal axis is equal to the Cu-Cu distance within the chain<sup>1-5,12</sup>.

Finally, it is noticed that from this structure determination of the compound  $\text{CuCl}_2(\text{NMIz})_2$  and the fact that the ESR g-values are very close to those observed for other geometries around Cu(II) it is evident that ESR measurements on copper(II) compounds must be handled with great care if one tries to correlate them with structure details. For example, three structurally-investigated copper(II) compounds, having almost identical powder g-values are known, *i.e.*  $\text{CuCl}_2(4\text{-Vipy})_2$ <sup>3</sup> (g-values 2.26, 2.08, 2.04<sup>7</sup>),  $\text{CuCl}_2(\text{Iz})_2$ <sup>22</sup> (g-values 2.24, 2.09, 2.03<sup>8</sup>) and  $\text{CuCl}_2(\text{NMIz})_2$  (g-values 2.27, 2.09, 2.04<sup>8</sup>). For these compounds the geometries around the Cu(II) ions are best described as pseudo-elongated octahedral, distorted square-pyramidal, tetrahedrally-distorted square-planar, respectively. From these data it is evident that from ESR powder data only, it is not possible to predict the geometry around the Cu(II) center. Recently, Hatfield *et al.*<sup>12</sup> published a "reversed" ESR spectrum for the compound  $\text{CuCl}_2(\text{thiazole})_2$ , which structure is very similar to the structure of  $\text{CuCl}_2(\text{py})_2$ . This unexpected ESR spectrum can be explained by assuming exchange narrowing between different Cu(II) sites, which could be confirmed only by the crystal structure determination<sup>12</sup>.

#### VI.1.6. References

- (1) B. Morosin, *Acta Crystallogr.*, B31, 632 (1975).
- (2) M. Laing and G. Carr, *J. Chem. Soc. A*, 1141 (1971).
- (3) M. Laing and E. Horsfield, *J. Chem. Soc. Chem. Comm.*, 735 (1968).
- (4) J.C. Jansen, H. van Koningsveld and J.A.C. van Ooijen, *Cryst. Struct. Comm.*, 7, 637 (1978).
- (5) J.A.C. van Ooijen, J. Reedijk, E.J. Sonneveld and J.W. Visser, *Transition Met. Chem.*, in press.

- (6) V.H. Crawford and W.E. Hatfield, *Inorg. Chem.*, **16**, 1336 (1977).
- (7) J.A.C. van Ooijen and J. Reedijk, *Inorg. Chim. Acta*, **25**, 131 (1977).
- (8) J.A.C. van Ooijen and J. Reedijk, *J. Chem. Soc. Dalton*, 1170 (1978).
- (9) P.J. Clarke and H.L. Milledge, *Acta Crystallogr.*, **B31**, 1543 (1975).
- (10) S. Gorter, A.D. van Ingen Schenau and G.C. Verschoor, *Acta Crystallogr.*, **B30**, 1867 (1974).
- (11) H. Paulus, *Z. Anorg. Allg. Chem.*, **369**, 38 (1969).
- (12) W.E. Estes, D.P. Gavel, W.E. Hatfield and D.J. Hodgson, *Inorg. Chem.*, **17**, 1415 (1978).
- (13) A.J.M. Duisenberg, Collected Abstracts of the First European Enraf-Nonius CAD4-Users Meeting, Paris, June (1974).
- (14) The function minimized was  $\Sigma(w(|F_o| - |F_c|))^2$ . The refinement was on  $F$ . The unweighted and weighted residuals are defined as follows:  

$$R_F = (\Sigma|F_o| - |F_c|)/(\Sigma|F_o|); \quad R_{wF} = (\Sigma w(|F_o| - |F_c|)^2)/(\Sigma w|F_o|^2)^{\frac{1}{2}}.$$
- (15) P. Main, M.M. Woolfson, L. Lessinger, G. Germain, J-P. Declercq, Multan 77, A system of Computer Programs for the automatic solution of crystal structures from X-ray diffraction data.
- (16) J.M. Stewart, G.J. Kruger, H.L. Ammon, C. Dickinson and S.R. Hall, "XRAY SYSTEM", technical report TR-446, of the computer science center, University of Maryland, implemented and extended by the Dutch X-ray System Group (1976).
- (17) C.K. Johnson, ORTEP, report ORNL-3794 (1965).
- (18) P.A. Doyle and P.S. Turner, *Acta Crystallogr.*, **A24**, 390 (1968).
- (19) J.A.C. van Ooijen, J. Reedijk and A.L. Spek, *J. Chem. Soc. Dalton*, in press.
- (20) R.B. Wilson, J.R. Wasson, W.E. Hatfield and D.J. Hodgson, *Inorg. Chem.*, **17**, 641 (1978).
- (21) B.J. Graves, D.J. Hodgson, C.G. van Kralingen and J. Reedijk, *Inorg. Chem.*, **17**, 3007 (1978).
- (22) B.K.S. Lundberg, *Acta Chem. Scand.*, **26**, 3977 (1972).

## VI.2. Acoustic Emission during the Preparation of dichloro(pyrazine)Zinc(II).

As part of an investigation on linear chain compounds, having potentially bridging ligands, an unusual acoustic effect was noticed during the synthesis of the title compound. Upon addition of a solution of  $\text{Zn(II)Cl}_2$  (1 mol/l) in water to a solution of pyrazine (1 mol/l) in water, immediately a precipitate is formed. This precipitation is accompanied by a rather strong cracking sound. This cracking is heard again when the mixture is shaken after some hours.

The intensity of this acoustic emission appeared to be proportional to the concentrations of both the reactants; the higher the concentration, the louder the cracking. A temperature increase accompanies these crackings, which is stronger than the rise in temperature observed upon dilution of concentrated  $\text{ZnCl}_2$  solutions.

In trying to understand this unusual effect, the reaction was carefully followed visually and it was noticed that, immediately after mixing, a very finely-divided white-colored powder is formed, directly followed by the fast formation of bright white crystals, looking like a flash of lightning; the cracking is observed during this latter process.

The solid product has been analyzed by chemical analysis and IR and far-IR spectroscopy, and it was found that the compound is  $\text{ZnCl}_2(\text{pyr})$  (pyr=pyrazine), identical with the compound prepared first by Stoehr<sup>1</sup>. However, the cracking was neither mentioned in this early report, nor in subsequent reports describing the spectroscopic properties and structure of this compound<sup>2</sup>. The IR and far-IR data of the final product are identical with those reported by other investigators<sup>3</sup>. From these data it has been concluded that the  $\text{Zn(II)}$  ion can be considered as hexacoordinated, with an octahedrally-based geometry in which both halide and pyrazine are bridging between the metal ions.

On searching the literature, no other examples were found that show a similar effect, making an explanation of this phenomenon very difficult and presently only some effects that may be responsible for the cracking can be suggested<sup>4,6</sup>. A possible explanation may be a phase transition in the crystal that damages the original crystal. Such a phase transition may be caused by a change in coordination geometry from initially formed, tetrahedrally-coordinated  $\text{Zn(II)}$ , with bridging pyrazines and terminal chloride ions, to octahedrally-coordinated  $\text{Zn(II)}$  with bridging pyrazines and chloride ions (the final product). A second possibility is the initial formation of relative short chains or dimers, followed by

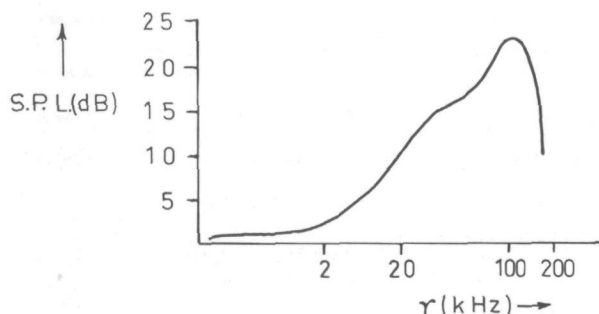


Fig. VI.2.1. Sound pressure level (S.P.L.) as a function of the frequency for one "crack" of the acoustic emission of crystallizing  $\text{ZnCl}_2(\text{pyr})$ .

a rapid polymerization into infinite polymers. To investigate the nature of the acoustic emission, a frequency-intensity analysis has been performed. The sound pressure level (S.P.L.) of a single "crack" has been plotted as a function of the frequency in figure VI.2.1. It is observed that the most intense sound emission is outside the region of the human hearing (which is up to *ca.* 16 kHz). The maximum in the S.P.L. curve at *ca.* 100 kHz is not accurately determined, owing to the use of a low-pass filter in the fast Fourier transform analysis. No measurements at all were possible above 160 kHz.

#### References

- (1) C. Stoehr, *J. Prakt. Chem.*, **51**, 449 (1895).
- (2) J.R. Ferraro, W. Wozniak and G. Roch, *Ric. Sci.*, **38**, 433 (1968).
- (3) J.R. Ferraro, "Low Frequency Vibrations of Inorganic and Coordination Compounds", Plenum Press, New York (1970).
- (4) The authors are indebted to one of the referees pointing our attention to a paper<sup>5</sup> describing the crystalloluminescence of  $\text{Ba}(\text{ClO}_3)_2$  and of  $\text{KNa}_3(\text{SO}_4)_2$ . Acoustic signals registered by a hydrophone placed into the solution coincided with the luminiscence.
- (5) L.M. Belyaev, V.V. Nabatov and Y.N. Martyshev, *Soviet Phys. Crystallogr.*, **7**, 464 (1963).
- (6) A relationship with the well-known phenomenon of triboluminescence<sup>7</sup> was initially supposed. However, we were unable to detect any luminescence during or after the cracking.
- (7) See *e.g.* J.I. Zink, *Inorg. Chem.*, **14**, 555 (1975); G.E. Hardy, J.C. Baldwin, J.I. Zink, W.C. Kaska, P.H. Liu and L. Dubois, *J. Am. Chem. Soc.*, **99**, 3552 (1977).
- (8) After the appearance of this note (*J. Am. Chem. Soc.*, **100**, 5569 (1978)) the authors were informed<sup>9</sup> that diastereoisomers of compounds  $\text{SiR}_1\text{R}_2\text{R}_3\text{R}_4$  show simultaneously acoustic emission and luminescence during recrystallization from organic solvents.
- (9) J. Fleming, work done at Massachusetts Institute of Technology, private communication.

## SUMMARY

This thesis describes an investigation on the relations between structural and magnetic properties of low-dimensional systems, showing magnetic superexchange interactions. Special attention has been given to the bridge geometry in

chains and dimers having  and  bridges with

M = a transition metal ion, X = Cl, Br, F or a large ligand, like oxalate and squarate. Therefore, new chain and dimeric compounds have been synthesized and their spectroscopic and magnetic properties studied.

After an introduction and survey, describing the main goal and possibilities to find the above-mentioned relations, in chapter II, the double-halogen bridged chain compounds  $MX_2L_2$ , with M = Cu, Co, Fe, X = Cl, Br and L = (substituted)-pyridine, -pyrazole, -imidazole are discussed. The results of two X-ray structure analyses of compounds belonging to this type are reported. The infrared, far-infrared, ligand-field and electron spin resonance spectra are in agreement with the supposed chain structure for most compounds. The magnetic susceptibilities of the Cu(II) compounds are described using different models. The isotropic coupling model (*Heisenberg*) yields the best description for most of the compounds, whereas the anisotropic coupling model (*Ising*) only yields good fits for the Co(II) compounds which are all ferromagnetic, just as found for the corresponding Fe(II) compounds. One of the Cu(II) compounds, *i.e.*  $CuBr_2(N\text{-methylimidazole})_2$ , seems to be a very good example of a rare alternating  $S=\frac{1}{2}$  system. During the ESR experiments on Cu(II)-doped Cd(II) chains, a compound has been prepared in which the Cu(II) ions occur in a tetragonally-compressed geometry, which has been found only in a few other compounds. In addition, in this chapter the magnetic properties of some single-chlorine bridged Cu(II) compounds are described. A relationship with the structures of these compounds is not as simple as suggested by previous investigators, and the superexchange seems to be built up from different factors, like d-electron spin density, bridge geometry and bridge ions.

Chapter III, describes the synthesis and physical properties of some new chain compounds with Ni(II), Co(II), Zn(II) and Fe(II) and oxalate and squarate as bridging ligands. The X-ray structures of two compounds are described. It is shown that for zinc oxalate and 2-methylimidazole ligands zig-zag chains occur, in which the ligands are *cis* coordinated. A nickel compound with

squarato dianions and imidazole ligands appears to be built up of linear squarato-bridged chains, in which strong intra-molecular hydrogen bridges occur. The IR, far-IR, Raman, ligand-field and ESR spectra are in agreement with the structures, whereas from Mössbauer-effect spectroscopy, the one-dimensionality of the oxalato-bridged chains has been determined. The corresponding Néel temperature seems to be strongly dependent upon the organic ligand. The magnetic susceptibilities of the nickel oxalate compounds could be described with the isotropic coupling model, including a zero-field splitting. The cobalt chains seem to be good examples of Ising systems. When the oxalato dianion is substituted for the squarato dianion as the bridging ligand, the superexchange interactions decrease dramatically. Finally, changing the organic ligand in the oxalate compounds does not seem to influence the intrachain coupling, in agreement with the supposed rigidity of the oxalato dianion.

Even in dimeric systems, described in chapter IV, the superexchange interactions do not seem to be simply related to the structure parameters, like bridging angle and metal-metal distance. Five-coordinated chlorine-bridged dimeric Ni(II) compounds have been investigated, for which several X-ray structure determinations are reported in literature, and which all have antiferromagnetically-coupled Ni(II) ions. For a new compound of this type, which shows ferromagnetic interactions, the X-ray structure determination is carried out. As a possible reason for the occurrence of ferromagnetism, a different orientation of the unpaired d-electrons on the Ni(II) ions, indirectly caused by a steric effect of the ligands, is suggested. In this chapter also some recently found dimeric and tetrameric fluorine-bridged Co(II) compounds are described. These compounds all exhibit weak antiferromagnetic interactions. The number of systems is still too small, however, to relate the magnetic and structure parameters.

In appendix VI.1, the X-ray structure determination of a Cu(II) compound is described, which - according to spectroscopic results - was thought to be also a chain compound. The observed monomeric structure gives evidence for the fact that the interpretation of ESR spectra can easily result in wrong structure proposals, especially when different Cu(II) sites occur in the unit cell, which are exchange coupled.

That syntheses in coordination chemistry not always proceed quietly, is shown in appendix VI.2. During an investigation on pyrazine-bridged oxalate chains, a compound was prepared, whose crystallization was accompanied by a cracking sound. Up to now, no clear explanation could be given.

## SAMENVATTING

In dit proefschrift is een onderzoek beschreven naar de relaties tussen structurele en magnetische eigenschappen van laag-dimensionale systemen, waarin een magnetische wisselwerking tussen paramagnetische metaalionen voorkomt. Het gaat hierbij vooral om een studie van de bruggeometrie in de volgende typen

verbindingen:  $\begin{array}{c} \diagup \quad \diagdown \\ \text{M} \quad \text{X} \quad \text{M} \\ \diagdown \quad \diagup \end{array}$  en  $\text{M}-\text{X}-\text{M}-\text{X}-\text{M}$ , met M = een over-

gangs-metaalion en X = Cl, Br, F, of een groot ligand, zoals oxalaat en squaaraat. Hiertoe zijn de synthese en spectroscopische en magnetische eigenschappen van een aantal nieuwe ketens en dimere coördinatieverbindingen bestudeerd.

Na introductie en overzicht, waar doel en mogelijkheden om bovengenoemde relaties te vinden worden beschreven, wordt in hoofdstuk II vooral ingegaan op de dubbel-halogenen gebrugde ketenverbindingen  $\text{MX}_2\text{L}_2$ , met M=Cu, Co, Fe, X=Cl, Br en L=(gesubstitueerd)-pyridine, -pyrazool, -imidazool. Twee molekuul- en kristalstructuren van dit type verbinding werden bepaald met behulp van röntgendiffractie aan een éénkristal en aan een poeder. De waargenomen infrarood, ver-infrarood, ligand-veld en elektronen spin resonantie spectra zijn in overeenstemming met de veronderstelde ketenstructuur in vrijwel alle verbindingen. De magnetische susceptibiliteit van de Cu(II) complexen kan beschreven worden met verschillende modellen. Het isotrope koppelingsmodel (*Heisenberg*) blijkt voor de meeste verbindingen het best toepasbaar, terwijl het anisotrope koppelingsmodel (*Ising*) alleen opgaat voor de Co(II) verbindingen, welke overigens ferromagnetisch zijn, evenals de overeenkomstige Fe(II) verbindingen. Eén van de Cu(II) complexen,  $\text{CuBr}_2(\text{N-methylimidazool})_2$ , blijkt een goed voorbeeld te zijn van een zelden gevonden alternerend  $S=\frac{1}{2}$  systeem. Tijdens de ESR experimenten aan de met Cu(II) gedoteerde Cd(II)verbindingen is een verbinding bereid, waarin de Cu(II) ionen een ingedeukte tetragonale geometrie bezitten, hetgeen tot nu toe nog nauwelijks was gevonden. Ook worden in dit hoofdstuk de magnetische eigenschappen van door één chloor gebrugde Cu(II) verbindingen beschreven. De gezochte relaties blijken niet zo eenvoudig te zijn als door andere onderzoekers gesuggereerd werd en de exchange blijkt opgebouwd te zijn uit verschillende bijdragen, zoals d-electron spindichtheid, bruggeometrie en soort brugionen.

Hoofdstuk III beschrijft de synthese en fysische eigenschappen van enkele nieuwe ketenverbindingen met Ni, Co, Zn en Fe als metaalionen, en oxalaat en

squaraat als brugliganden. De molekuul- en kristalstructuren van twee complexen worden beschreven. Het blijkt dat in geval van zink en 2-methylimidazool als liganden een zig-zag oxalaatketen voorkomt, waarbij de imidazool liganden *cis* gecoördineerd zijn. Een nikkelverbinding met squaraationen en imidazool liganden blijkt opgebouwd uit lineaire door squaraat gebrugde ketens, waarin sterke intramoleculaire waterstofbruggen voorkomen. De IR, ver-IR, Raman, ligandveld en ESR spectra zijn in overeenstemming met de gevonden structuren, terwijl met behulp van Mössbauer-effect spectroscopie de mate van één-dimensionaliteit van de oxalaatketens is bepaald; deze blijkt afhankelijk te zijn van het organisch ligand. De magnetische susceptibiliteit van de Ni(II) oxalaatketens blijkt beschreven te kunnen worden m.b.v. het isotrope koppelingsmodel, inclusief een nulveld-splittings. De Co(II) ketens blijken goede voorbeelden van Ising systemen te zijn. Wanneer het oxalaat vervangen wordt door het squaraat als brugligand, neemt de super-exchange drastisch af. Verder blijkt het gebruikte organisch ligand op de intraketenkoppeling geen effect te hebben, in overeenstemming met de veronderstelde starheid van het oxalaat ion.

In dimere systemen, welke in hoofdstuk IV worden behandeld, blijkt de waargenomen exchange interactie evenmin eenvoudig te relateren met de structuurparameters, zoals brughoek of M-M afstand. In het bijzonder is aandacht gegeven aan de vijfomringde door chloor gebrugde dimere Ni(II) systemen, waarvan in de literatuur reeds enkele kristalstructuren bekend waren en die alle antiferromagnetisch zijn. Van een nieuwe verbinding behorend tot deze klasse, welke echter ferromagnetisch blijkt te zijn is de kristalstructuur bepaald. Als mogelijke reden voor het optreden van ferromagnetisme in deze verbinding wordt genoemd de mogelijk afwijkende d-electronen dichtheden op de Ni(II) ionen, indirect veroorzaakt door sterische effecten van het ligand. In dit hoofdstuk wordt ook kort ingegaan op recent gevonden, door fluor gebrugde dimere en tetramere systemen. De Co(II) ionen blijken zwak antiferromagnetisch gekoppeld te zijn. Het aantal systemen is echter nog te gering om gedetailleerde conclusies betreffende relaties tussen exchange en structuur toe te staan.

In appendix VI.1 wordt de kristalstructuur beschreven van een Cu(II) verbinding welke op grond van spectroscopische gegevens tot de ketenverbindingen zou kunnen behoren; de monomere structuur bewijst dat ESR spectra gemakkelijk aanleiding kunnen geven tot foutieve structuurvoorstellen, vooral wanneer er in het kristal meerdere magnetisch gekoppelde Cu(II) sites aanwezig zijn.

Dat de synthese in de coordinatiechemie niet altijd geruisloos hoeft te verlopen blijkt uit appendix VI.2. Tijdens een deelonderzoek naar pyrazine-gebrugde oxalaatketens werd een verbinding bereid, welke onder gekraak uitkristalliseerde. Tot op heden is hiervoor geen duidelijke verklaring gevonden.



# FREQUENTLY USED ABBREVIATIONS, SYMBOLS AND UNITS

## Abbreviations

py	:pyridine
3-Mepy	:3-methylpyridine
4-Mepy	:4-methylpyridine
3,4-diMepy	:3,4-dimethylpyridine
3,5-diMepy	:3,5-dimethylpyridine
4-Etpy	:4-ethylpyridine
4-Vipy	:4-vinylpyridine
3,5-diClpy	:3,5-dichloropyridine
4-Mison	:4-methylisonicotinate
4-Acpy	:4-acetylpyridine
Iz	:imidazole
NMIz	:N-methylimidazole
2MIz	:2-methylimidazole
DMIz	:1,2-dimethylimidazole
BIZ	:benzimidazole
pyr	:pyrazine
Pz	:pyrazole
Indz	:indazole
DMSO	:dimethylsulphoxide
CAF	:1,3,7-trimethyl-2,6-purinedione (caffeine)
MAEP	:2-(2-methylaminoethyl)-pyridine
Ox	:oxalato dianion
Sq	:squarato dianion
tpp	:tetraphenylporphyrin
qnqn	: <i>trans</i> -2-(2'-quinolyl)-methylene-3-quinuclidinone
dmp	:2,9-dimethyl-1,10-phenanthroline

DMAEP	:2-(2-dimethylaminoethyl)-pyridine
biq	:2,2'-biquinolyl
dmpzm	:bis(3,5-dimethylpyrazolyl)-methane
en	:ethylene diamine
eg	:ethylene glycol
dmpz	:3,5-dimethylpyrazole
edmpz	:4-ethyl-3,5-dimethylpyrazole
tmpz	:3,4,5-trimethylpyrazole
IR	:infrared
far-IR	:far-infrared
NMR	:nuclear magnetic resonance
ESD	:estimated standard deviation
ESR	:electron spin resonance
EPR	:electron paramagnetic resonance
DPPH	:diphenylpicrylhydrazyle
AC	:alternating current
S.P.L.	:sound pressure level
CPC	:CuCl <sub>2</sub> (pyridine) <sub>2</sub>
CPB	:CuBr <sub>2</sub> (pyridine) <sub>2</sub>
CNIMB	:CuBr <sub>2</sub> (N-methylimidazole) <sub>2</sub>
CLB	:CuBr <sub>2</sub> (3,5-dimethylpyridine) <sub>2</sub>
NISIA	:NiSq(Iz) <sub>2</sub> (H <sub>2</sub> O) <sub>2</sub>
NIDI	:NiCl <sub>2</sub> (dmpzm) <sub>2</sub>
CCCP	:Cu <sub>0.02</sub> Cd <sub>0.98</sub> Cl <sub>2</sub> (Pz) <sub>2</sub>

*Symbols and units (conversion factors to SI units are in parentheses)*

## Magnetism and ESR spectroscopy

J	:superexchange interaction parameter in cm <sup>-1</sup> (1.99 x 10 <sup>-23</sup> Joule)
χ <sub>m</sub> , χ <sub>M</sub>	:corrected molar susceptibility in emu/mole (4π x 10 <sup>-6</sup> m <sup>3</sup> /mole)
χ <sub>powder</sub>	:is (χ <sub>//</sub> + 2χ <sub>⊥</sub> )/3 in emu/mole
χ <sub>//</sub> , χ <sub>⊥</sub>	:principal molar susceptibilities parallel and perpendicular to the principal magnetic axis
χ <sub>Mmax.</sub>	:maximum molar susceptibility in emu/mole
T <sub>max.</sub>	:temperature at the maximum molar susceptibility in Kelvin
μ <sub>eff.</sub>	:effective magnetic moment in B.M. defined as √8χ <sub>M</sub> T
β, μ <sub>B</sub> , B.M.	:Bohr magneton (9.27 x 10 <sup>-24</sup> Joule/Tesla)

t.i.p.	:temperature independent paramagnetism in emu/mole
$M_{I(n)}$	:spin quantum number of nucleus n
G	:Gauss (0.0001 Tesla)
kG	:kilo Gauss (0.1 Tesla)
$\vec{S}$	:spin angular momentum operator
$S_i, S^i$	:components of spin angular momentum operator; $i=x,y,z$
S	:electron spin quantum number
D	:axial zero-field splitting parameter in $\text{cm}^{-1}$
H	:magnetic field strength in Gauss
$H_{c1}, H_{c2}$	:first and second critical magnetic field strength in Gauss
M	:magnetization in B.M. or relative magnetization
C	:Curie constant in emu.K/mole
$\theta$	:Curie-Weiss temperature in Kelvin or bridging M-X-M angle in $^\circ$
$g_{\text{fit}}$	:g-value obtained from susceptibility fit
$g_i$	:spectroscopic splitting factor parallel to the i axis; $i=1/x, 2/y, 3/z$
$g_{//}, g_{\perp}$	:spectroscopic splitting factor parallel and perpendicular to the principal magnetic axis
$\bar{g}$	:average spectroscopic splitting factor
Hz	:hertz ( $6.63 \times 10^{-34}$ Joule)
kHz, GHz	:kilo and giga hertz
$A_n$	:hyperfine splitting parameter due to ligand nucleus n (super-hyperfine structure) in G or $\text{cm}^{-1}$
$A_i$	:i-th component of the hyperfine splitting; $i=1,2,3$
$\nu$	:frequency in hertz
P	:is $g_e \cdot g_n \cdot \beta_n \langle r^{-3} \rangle$
$g_e, g_n$	:electron and proton nuclear g-value (2.0023 and -5.5855 respectively)
$\beta_n$	:nuclear magneton ( $5.05 \times 10^{-27}$ Joule/Tesla)
$\langle r^{-3} \rangle$	:one electron average of $r^{-3}$
$\kappa$	:dimensionless parameter, characterizing the contact hyperfine interaction

#### Mössbauer-effect spectroscopy

$T_N$	:magnetic transition/three-dimensional ordering temperature in Kelvin
QS, $\Delta E_q$	:electric quadrupole splitting in mm/s
IS	:isomer shift in mm/s
$\theta, \phi$	:angles specifying the direction of $H_{\text{eff}}$ with respect to the electric field gradient tensor

$\eta$  : asymmetry parameter defined as  $(|V_{xx}| - |V_{yy}|) / |V_{zz}|$   
 $V_{xx}, V_{yy}, V_{zz}$  : principal components of the electric field gradient tensor  
 $H_{\text{eff.}}$  : effective hyperfine field in kG/kilo Oersted (0.1 Tesla)

#### X-ray diffraction

$a, b, c$  : lengths of the unit cell edges in Å  
 $a^*, b^*, c^*$  : reciprocal cell constants in Å<sup>-1</sup>  
 $h, k, l$  : Miller's indices  
 $\text{Å}$  : Angstrom ( $10^{-10}$  m)  
 $\alpha, \beta, \gamma$  : angles between the axes of the unit cell in °  
 $D_m$  : measured density in g/cm<sup>3</sup> ( $10^3$  kg/m<sup>3</sup>)  
 $D_c$  : calculated density in g/cm<sup>3</sup>  
 $Z$  : number of formula units in the unit cell  
 $I_i, I_{\bar{i}}$  : intensity of the  $i, \bar{i}$ -th reflection  
 $\sigma$  : standard deviation  
 $F_o, F_c$  : observed and calculated structure factor  
 $R, R_F$  : unweighted residual  
 $R_{wF}$  : weighted residual  
 $\mu_{\text{MoK}\alpha_1}, \mu_{\text{MoK}\alpha}$  : linear absorption coefficient for MoK $\alpha_1$ /MoK $\alpha$  radiation in cm<sup>-1</sup>  
 $U_{ij}, u_{ij}$  : anisotropic temperature factors in Å<sup>2</sup>  
 $L/R$  : number of background counts on the left/right side  
 $m/n$  : number of reflections/parameters  
 $\theta$  : limit of measurement in °  
 $\theta_{\text{mon.}}$  : monochromator angle in °  
 $\lambda$  : wavelength in Å  
 $U$  : isotropic temperature factor in Å<sup>2</sup>  
 ORTEP : Oak Ridge Thermal Ellipsoids Plot, scaled to include 40% probability

#### General

$T$  : temperature in Kelvin ( $1.38 \times 10^{-23}$  Joule)  
 $K$  : Kelvin  
 $k$  : Boltzmann constant ( $1.38 \times 10^{-23}$  Joule/Kelvin)  
 $\text{dB}$  : decibel  
 $\text{kK}$  : kilo Kaiser ( $10 \text{ m}^{-1}$ )  
 $H, \hat{H}$  : Hamiltonian  
 $\mu\text{F}$  : micro Farad ( $\text{A}^2 \cdot \text{s}^4 / \text{kg} \cdot \text{m}^2$ )  
 $\text{kV}$  : kilo Volt ( $\times 10^3 \text{ kg} \cdot \text{m}^2 / \text{A} \cdot \text{s}^3$ )

nm	:nano meter ( $10^{-9}$ m)
B	:Racah parameter in $\text{cm}^{-1}$
$\text{pK}_a$	:negative logarithm of acid-base equilibrium constant
$\nu$	:frequency in $\text{cm}^{-1}$
N	:Avogadro constant ( $6.02 \times 10^{23}$ /mole)
Dq	:cubic ligand-field splitting parameter in $\text{cm}^{-1}$

*Curriculum Vitae van J.A.C. van Ooijen*

1952 : 19 april geboren te Leerdam

1968 : eindexamen MULO-B, Koningin Juliana School te Leerdam

1970 : eindexamen HBS-B, Koningin Wilhelmina College te Culemborg

1973 : kandidaatsexamen Natuurkunde, Rijks Universiteit te Utrecht

1974 : kandidaatsexamen Scheikunde, Rijks Universiteit te Utrecht

1975 : doctoraal examen Scheikunde, Rijks Universiteit te Utrecht

1975 - 1979 : wetenschappelijk medewerker in ZWO-verband (SON) aan  
de Technische Hogeschool te Delft

## STELLINGEN

1. Een promotieonderzoek waarvan de duur niet wordt bepaald door het resultaat maar alleen door de maximaal beschikbare tijd, zoals tegenwoordig gebruikelijk is bij 4-jarige contracten, kan aanleiding geven tot het trekken van wetenschappelijk nog niet verantwoorde conclusies.
2. Het zou nuttig zijn een eventuele opvolger op een promotieplaats een overlap van tenminste een half jaar met zijn/haar voorganger te geven en niet, zoals vaak gebruikelijk is, de opvolger pas enige tijd na het vertrek van zijn/haar voorganger aan te stellen.
3. Reinen hanteert een onjuiste uitdrukking voor de g-waarden in antiferrodistortieve koperverbindingen.  
D. Reinen, *Solid State Comm.*, 21, 137 (1977)  
B.J. Hathaway and D.E. Billing, *Coord. Chem. Rev.*, 5, 143 (1970)
4. Bij de interpretatie van verschuivingen in bindingsenergieën in mangaancarbonylen is ten onrechte geen rekening gehouden met relaxatie, waardoor onjuiste gevolgtrekkingen zijn gemaakt.  
D.F. van de Vondel, L.F. Wuyts, G.P. van der Kelen and L. Bevernage, *J. of Electr. Spectr. and Related Phenomena*, 10, 389 (1977)
5. De methode voor de berekening van de nulveldsplitsing in  $\text{CoCl}_4^{2-}$  ionen van Horrocks en Burlone is onjuist.  
W. DeW. Horrocks, Jr. and D.A. Burlone, *J. Am. Chem. Soc.*, 98, 6512 (1976)
6. Bij de verklaring van de opsplitsing van proton NMR lijnen van tetrabutylammonium tolueendithiocobaltaat(III) is onvoldoende rekening gehouden met de mogelijkheid van liganduitwisseling.  
P.J. van der Put and A.A. Schilperoord, *Inorg. Chem.*, 13, 2476 (1974)
7. De door Engelter en medewerkers voorgestelde interpretatie van ver-infrarood spectra van verbindingen met formule *trans*- $\text{PtX}_2(\text{pyridine})_2$ , met  $\text{X}=\text{Cl}, \text{Br}, \text{I}$  en  $\text{SCN}$ , is onjuist.  
C. Engelter, A.T. Hutton and D.A. Thornton, *J. Mol. Struct.*, 44, 23 (1978)
8. Het valt te betreuren dat in een tijd van toenemende werkloosheid, man en vrouw uit één gezin samen aan het arbeidsproces deelnemen en daardoor een dubbel inkomen genieten.

9. Het is onaanvaardbaar dat een ambtenaar zelf niet mag beslissen of hij wel of niet wordt opgenomen in het Algemeen burgerlijk pensioenfonds.
10. De emancipatie van de vrouw gaat niet toevallig gepaard met de schrikbarende toename van het aantal echtscheidingen.

Dagblad *Trouw*, 27 januari 1979

11. Het zogenaamde "doordraaien" van fruit en groenten op veilingen en de vastgestelde melkprijs voor boeren, bewijzen dat de beginselen van een gezonde economie in Nederland ver te zoeken zijn.
12. Dat het nog steeds niet verplicht is voor de levensmiddelenfabrikant om toegevoegde chemische stoffen, b.v. geur-, kleur-, smaak-, conserveringsmiddelen e.d., te vermelden op de productverpakking is een grove nalatigheid van de overheid.
13. Grootschaligheid in de land- en tuinbouw leidt tot een intensiever gebruik van bestrijdingsmiddelen hetgeen een gevaar is voor de gezondheid van de mens.
14. De kinderdoop, welke bij de meeste religies nog steeds wordt toegepast, wijst er op dat de kerkhervorming, begonnen door Luther, nog niet voltooid is.

J.A.C. van Ooijen

18 april 1979